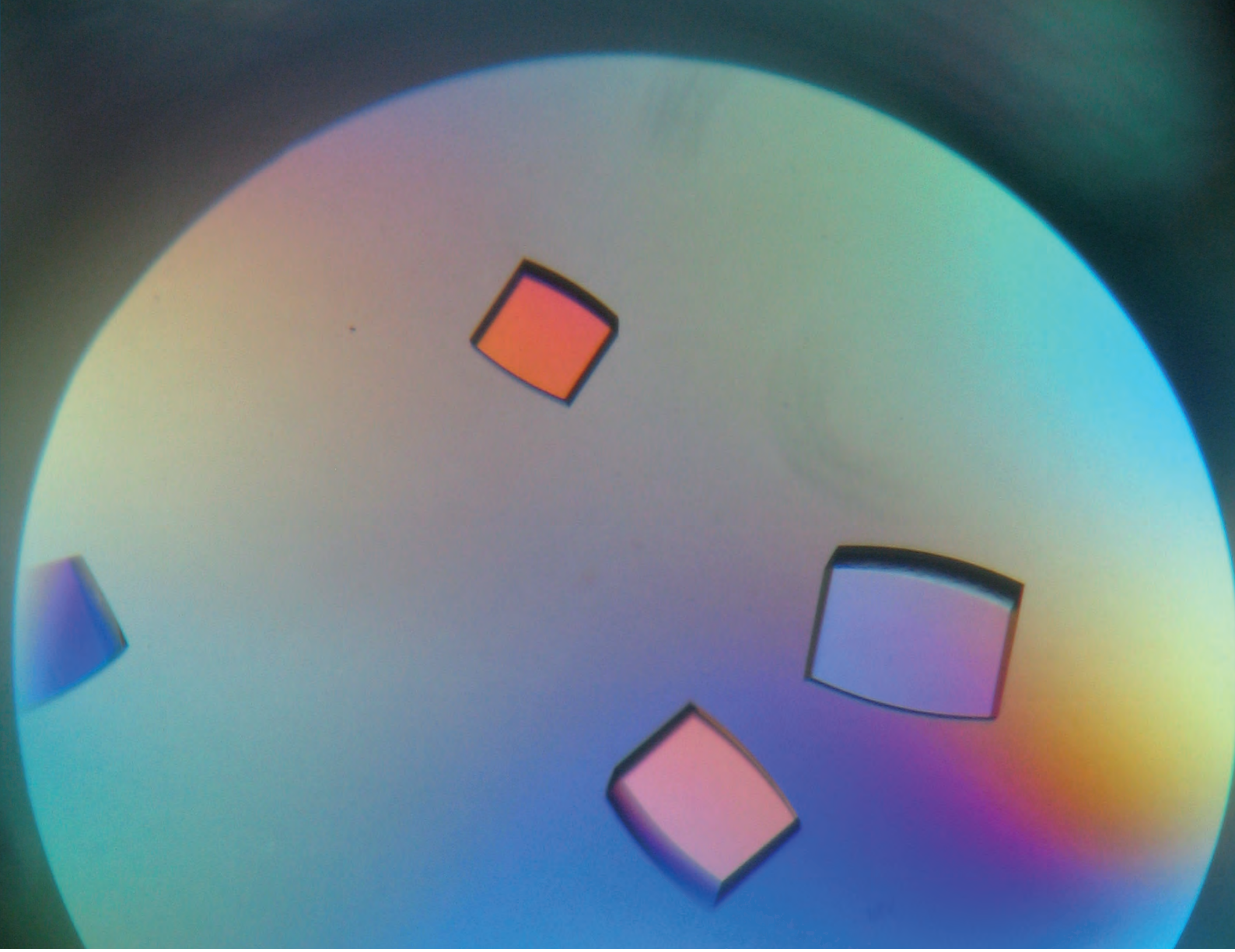

PHOTON SCIENCE 2012.

Highlights and Annual Report

Accelerators | Photon Science | Particle Physics

Deutsches Elektronen-Synchrotron
A Research Centre of the Helmholtz Association

Cover

Protein crystals containing a calcium pump/calmodulin complex. The structure of this complex has been solved by X-ray crystallography and small-angle X-ray scattering (SAXS). Using an interdisciplinary approach, this structure together with further *in vitro* and *in vivo* characterisation and mathematical modelling led to the identification of a bimodular regulation mechanism of the calcium pump, which contains a previously unknown “turbo gear”. More information about this measurement can be found in the contribution ‘Turbo switch of calcium pump in biological cells’ on page 38.

PHOTON SCIENCE 2012.

Highlights and Annual Report

User Contributions to the Annual Report.

DESY Photon Science

A deeper insight into the photon science activities at DESY is provided by the several hundred annual user experiment and development reports. Formerly published in the “HASYLAB Jahresbericht”, they are now available online:

http://photon-science.desy.de/annual_report/

A search function and an authors’ index are also provided.

The users’ reports present all activities/experiments performed by user groups and in-house research at the DESY light sources DORIS III, PETRA III and FLASH and are published online every year in May.
Furthermore, a list of publications concerning work done at DESY is accessible online:

http://photon-science.desy.de/publications
http://pubdb.desy.de (search function in the left frame)

DESY tries to keep the list as complete and as updated as possible, but relies on the cooperation of all users to achieve this goal.

Contents.

The year 2012 at DESY.

Chairman's foreword

Hundred years ago, in 1912, two major discoveries have dramatically influenced the scientific world: the discovery of X-ray diffraction by Max von Laue and the observation of cosmic rays by Victor Hess. Both physicists were pioneers in their respective fields. While the study of cosmic radiation stimulated many developments in particle and astroparticle physics, X-ray diffraction opened a new gateway into the world of molecules and atoms.

DESY´s light sources PETRA III and FLASH as well as the European X-ray laser XFEL are the most advanced X-ray facilities built on Max von Laue´s heritage. These modern research facilities enable leading-edge research ranging from physics, chemistry, biology to materials and life sciences, and support application-driven research for our society's needs, for instance in energy, environment, key technologies and health.

PETRA III is the world´s most brilliant high-energy X-ray source serving national and international researchers. The number of beam time proposals is rising exponentially and I am excited to see the many wonderful results which have become possible. In honour of the 100 years of X-ray diffraction the PETRA III experimental hall was recently named after "Max von Laue" – in a dedication ceremony with the presence of German Chancellor Angela Merkel.

The European XFEL is DESY´s priority project. DESY contributes significant resources to this international prestige project in Germany. As major cooperation partner we are responsible for the superconducting accelerator which supplies in a 2 km long tunnel the tailored 17.5 GeV electron bunches for the X-ray lasing process. The construction of the XFEL accelerator is well underway and will be finished in the second half of 2015. This is a huge effort for our laboratory, in particular for the machine division, the administration and the DESY infrastructure. Together with our partners we are currently working out the best conditions and appropriate governance frame for the future operation of the European XFEL. Moreover, DESY is currently working on the construction of FLASH II and on the two PETRA III extension halls which will host ten state-of-the-art beamlines for our users and for our international partners in Sweden, Russia and India who invested substantial resources into this extension project.

In October we ended the user operation of the DORIS III synchrotron radiation facility. DORIS was a unique research infra-

The grand naming ceremony of the PETRA III experimental hall to "Max von Laue" took place on 19 September 2012 in the presence of Chancellor Angela Merkel, the First Mayor of Hamburg Olaf Scholz and Nobel Laureate Ada Yonath.

structure: It served as a European workhorse for synchrotron radiation and was also a notable particle physics collider facility. Over its entire lifespan of almost four decades an immense scientific output was produced. Many experimental techniques and methods relevant for X-ray synchrotron radiation science and for particle physics applications have been pioneered at DORIS, opening up new research opportunities and exploring novel technologies and their industrial applications. It is quite important to clearly demonstrate to our policy-makers and funding agencies the profound impacts that research infrastructures make on science, economy and society. We will therefore launch a dedicated DORIS socio-economic study covering the complete lifetime of DORIS.

DESY is striving to further enhance its collaboration with German universities. DESY is the national hub for two Helmholtz alliances in particle and astroparticle physics thereby establishing an

Chairman Helmut Dosch presenting Chancellor Angela Merkel with the reproduction of a superconducting cavity.

interactive network between all major German universities and Helmholtz research centres which are active in these fields. DESY´s role herein has been further strengthened. The two key projects, LHC at CERN and IceCube at the South Pole are producing highlighting scientific results which are boosting such research. DESY´s future weight at the LHC will critically hinge on its role in the LHC detector upgrade program. In turn, DESY is currently organizing the necessary resources for its contribution to the ATLAS and CMS upgrades of the LHC.

The new partnership with the University of Hamburg, PIER, is taking up momentum: end of October the new PIER-Helmholtz Graduate School has been launched with strong support by the Helmholtz association and the Joachim Herz Foundation. DESY is also preparing joint appointments with the University of Kiel in the frame of the “Ruprecht Haensel-Laboratory” and with the University of Göttingen.

In order to assure that DESY research remains at the forefront of science, it is mandatory to promote young talents and to offer equal opportunities at DESY. Ten young investigator groups are currently carrying out research at DESY in close collaboration with our partner universities. Four of the young investigators are women such as Kerstin Tackmann, for instance. She has been significantly involved in the discovery of the Higgs-like boson at the LHC and just recently earned the Hertha-Sponer Award 2013 of the Deutsche Physikalische Gesellschaft DPG. I am sure that others will follow her example.
I would like to thank all collaborators and colleagues for their fruitful work. ●

Helmut Dosch.

Helmut Dosch
Chairman of the DESY Board of Directors

Photon Science at DESY.

Introduction

In the morning of Monday 22 October 2012 the synchrotron operation at DORIS III was shut down. This ended the very successful 38 years lasting era of research with synchrotron radiation at DORIS. Many experimental techniques being standard today have been pioneered at DORIS. Being a second generation synchrotron radiation source, the wiggler beams of DORIS III provided a quite high flux for millimetre size samples. But they were not able to compete with the extremely high flux densities that modern high energy third generation sources do provide. Nevertheless, until the final shutdown DORIS III served very successfully a wide user community in many disciplines and produced almost every year more than 600 publications in refereed journals. In order to celebrate the scientific achievements at DORIS, DESY will organize a scientific symposium from 14 to 15 May 2013, to which all users are cordially invited.

By the end of the year 2012 all PETRA III beamlines are in user operation. The PETRA III storage ring has achieved all major design goals. Meanwhile more than 600 user experiments have already been carried out. The very small beams at PETRA III enabled several exciting achievements like ptychographic reconstructions of non-periodic objects at 10 nm resolution from coherent diffractive imaging data as well as nano focussed beams down to 20 or even 10 nm resolution for spatially resolved element analysis and in-line holography experiments, respectively. The very small beams at PETRA III pose very stringent requirements on the quality and the stability of X-ray optical elements in order to exploit these beam properties to their full potential. To meet these challenges in mechanical and X-ray optical design continued research and development will be required for some time. Meanwhile also the first publications derived from work at PETRA III appeared in highly ranked journals. Some examples for scientific experiments carried out at PETRA III can be found in this brochure. Since there were quite a number of heavily used experimental techniques at DORIS III that are not yet available at PETRA III, an extension project for PETRA III has been initiated. The extension consists of two smaller experimental halls adjacent to the present experimental hall Max von Laue, each providing space for 5 additional beamlines. The extension project will start mid-2013, and we hope to be able to provide beam again in the experimental hall Max von Laue at the beginning of 2014. Highest priority for the beamlines in the extension will have those for absorption spectroscopy that should get first beam in autumn 2014. After completion of the extension project there will be more than 40 experimental stations at PETRA III from which 27 can be operated in parallel, 26 of them will receive beams from undulators.

At present, FLASH undergoes a major transformation with the FLASH II project being in full swing. The FLASH II project will add another FEL undulator called ‘FLASH2’ and a second experimental hall to the FLASH facility. Linac and electron beam transport tests for distributing different portions of a bunch train on different undulators have already been carried out successfully. Meanwhile the construction work for the tunnel of the second FEL is progressing. We expect the tunnel to be finished by end of January 2013. The second experimental hall will be finished by mid-2013. We expect first user experiments in the new experimental hall in 2014. On the one hand FLASH2 will effectively almost double the capacity for user experiments at FLASH where overbooking continues to be about a factor of four and experimental time is scarce. On the other hand FLASH2 will serve as a testbed for various seeding schemes like direct seeding with High Harmonic Generation (HHG) generated laser radiation and for High Gain Harmonic Generation (HGHG) seeding schemes. Since the timing and the photon energy of the seed laser will determine the temporal and spectral properties of the seeded FEL radiation pulses we expect a significantly improved stability for these parameters. Several major results in view of FEL performance were achieved during 2012 at FLASH. During several experimental periods long bunch trains with up to 5000 bunches per second were delivered to user experiments. Because of a careful control of the low level radio frequency phases of the accelerating cavities of the FLASH linac and a closed feedback loop it is now possible to reduce the FEL bunch arrival jitter to something close to 20 femtosecond (fs) RMS in user operation mode with respect to an external master clock. Finally the sFLASH project led by the University of Hamburg in close collaboration with DESY scientists was able to show for the first time direct HHG seeding at FLASH at 38 nm wavelength. All these results were critical milestones for the further development of the FLASH facility towards more routine operation for few fs timing experiments. Also in this year scientists at FLASH continued to achieve exciting scientific results as you will see later in this brochure.
Heavy construction and related planning work is not only taking

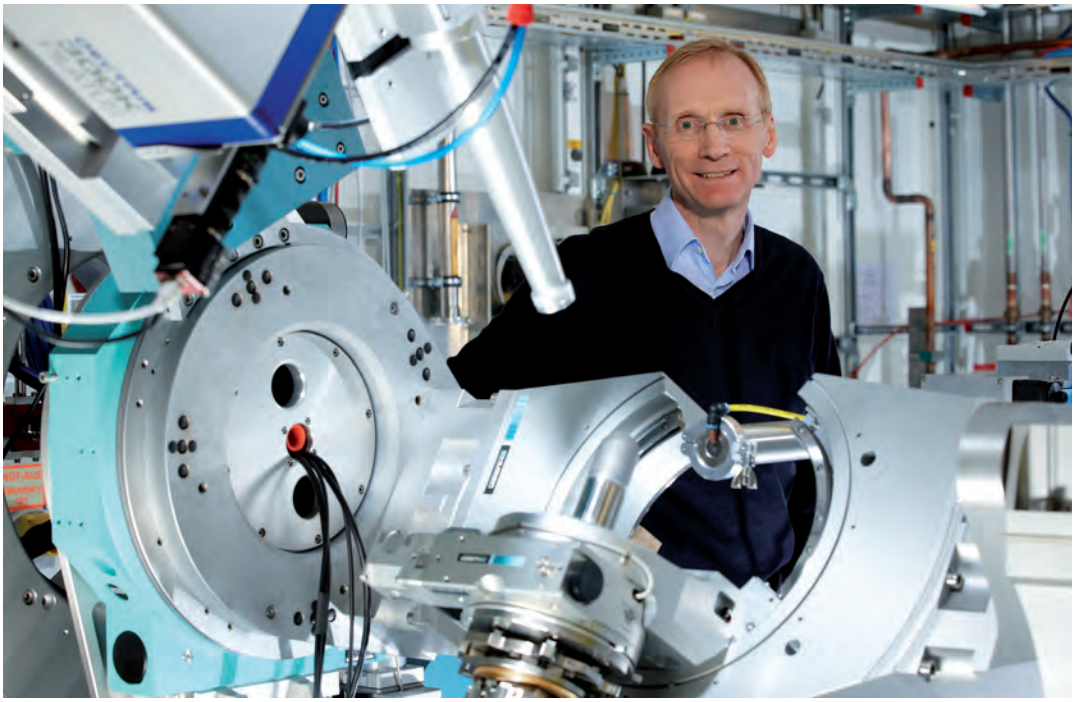

Edgar Weckert at an experimental station at the most brilliant X-ray source worldwide PETRA III.

place for the DESY photon science facilities PETRA III extension and FLASH, but also for a number of laboratory buildings on site. The architects have been selected for the new Photon Science building that will also house a NanoLab. This building will be constructed close to the present buildings between the PETRA III and FLASH experimental halls. The NanoLab will support users of PETRA III and FLASH to prepare and pre-characterize their samples as well as to foster our in-house research activities in that area. The NanoLab is headed by Prof. Andreas Stierle, who joined DESY from the University of Siegen in March 2012. The beginning of the construction of the new Photon Science building is expected for the middle of 2013.

After three years of construction scientists from DESY, Max Planck Society and the University of Hamburg were finally able to move into the new building for the Center for Free-Electron Laser Science (CFEL) built by the city of Hamburg in September 2012. This move was impatiently awaited by all CFEL colleagues, since suitable laboratory space is extremely short. The success of all CFEL scientists during the last years is certainly one of the reasons for the Max Planck Society to establish a new Max Planck Institute with three further directors in addition to the two already working here at the Bahrenfeld campus.

The activities towards the realization of the Centre for Structural Systems Biology (CSSB) made major steps forward in 2012. The nine partners have signed a memorandum of understanding in the beginning of 2012. In a first phase of hiring of group heads three W3 and a number of W2 and junior professor positions had been advertised, selected and in part offers have been made or candidates have been appointed already. Last but not least, the architect for the new CSSB building to be situated close to the PETRA III hall and the EMBL premises has been selected and the detailed planning is ongoing right now. Start of the construction work is expected for the middle of 2013. The successful operation and further developments of instrumentation and experimental methods depends to a large extend on strong in-house research activities at the facilities. In this brochure you will find several examples for in-house research and cutting edge instrumentation developments. Especially the newly established method for serial fs nano-crystallography promises to change the field of structural biology for those compounds that cannot be grown to crystals larger than micrometre size as it is often the case for membrane proteins and large macromolecular complexes. The success of these activities paved the way to the establishment of an international user consortia led by H. Chapman (CFEL/DESY) and a proposal for a dedicated end station for this technique at the European XFEL.
After the establishment of the Partnership for Innovation, Education and Research (PIER) between DESY and the University of Hamburg the collaboration between DESY and colleagues from University of Hamburg, Max Planck Society, EMBL and European XFEL enters a new era with the successful proposal for the “Hamburg Centre for Ultrafast Imaging (CUI)” within the Excellence Initiative of the German federal and state governments.

These years of transition of our facilities impose a very heavy load on many people at DESY. Without their dedication this all would not be possible. Let me take this opportunity to thank all of them for their effort and continuous support. Also our user community will have some inconvenience due to longer shutdowns. We hope for your understanding and we look forward for a brilliant future.
Finally, let me wish all of you a personally and scientifically most successful year 2013.

Edgar Weckert
Director Photon Science

News and Events.

News and Events.

A busy year 2012

January

25 January:
Joint European XFEL and HASYLAB Users' Meeting

The European XFEL Users' Meeting and the Annual Users' Meeting of HASYLAB were held at DESY on January 25-27. Following a successful tradition, a joint 3-day program was organized. The first day was dedicated to the European XFEL. The morning of the second day featured reports on the status of FLASH and on commissioning of new FEL facilities as well as scientific talks on experiments using soft X-ray radiation at FELs. In the afternoon satellite meetings were organized which focused on various instruments and science applications. On the third day the photon science activities at DESY were presented in the morning, while the afternoon gave room for a joint poster session with nearly 300 contributions and a vendors exhibition of more than 60 commercial suppliers of synchrotron and FEL instrumentation. The joint meeting and its satellite meetings had a record high participation of more than 680 scientists, staff, and policy makers from as many as 28 countries. Participation of 23 young scientists was afforded with support of European XFEL bursaries. Presentations and posters gave a broad overview of activities at the operating DESY facilities, the storage rings DORIS III and PETRA III, and at the XUV free-electron laser FLASH, and were complemented by reports on progress achieved at other places, like the FEL facilities LCLS, SACLA and FERMI. Much interest was raised by the presentation of activities related to FLASH II and the European XFEL, facilities which are presently under construction at DESY.

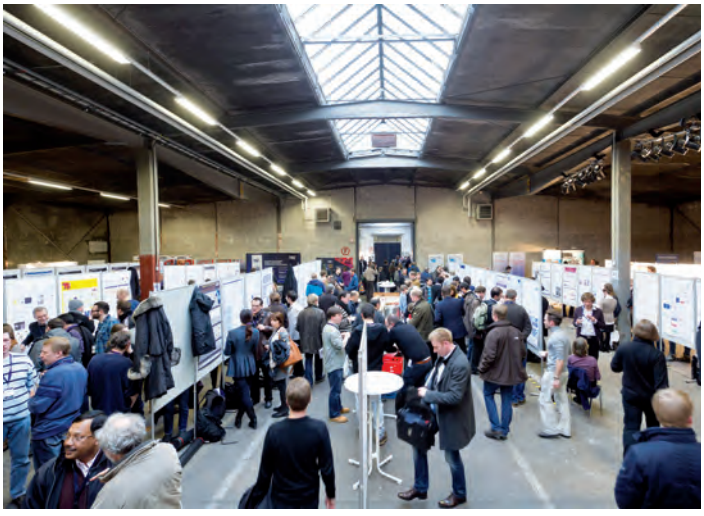

The very well-attended poster session on the third day of the Users' Meeting.

Especially notable highlights were a session on life science applications using hard X-ray FELs on the first day and a report by T. Ishikawa (Riken, Japan) about first lasing at the Japanese SACLA facility on the second day.

The accompanying satellite meetings and workshops were intended to discuss more specific issues. Four meetings were held by the European XFEL which included a consortium meeting, a workshop on photon beam diagnostics and meetings on two of the experiments planned at the European XFEL (SQS and FXE). Satellite events of the DESY photon science community were the "Peak Brightness Collaboration Meeting on FLASH experiments" and meetings on "X-ray nano-imaging of biological and chemical systems", "High energy X-ray diffraction at BW5 and P07", "Status and perspectives of small angle scattering at DESY", and on the PETRA III beamline P04.

Fully occupied DESY Auditorium during the presentations.

February

15 February:
Olaf Scholz visits DESY

Olaf Scholz, First Mayor of the Free and Hanseatic City of Hamburg, visited DESY. Olaf Scholz, who knows DESY well, informed himself about current plans and projects of Hamburg's largest research centre.

Olaf Scholz and Karen Ong performing a vacuum experiment.

After detailed discussions with the DESY directorate, the Mayor paid a visit to the DESY school laboratory "Physik begreifen", where he witnessed the good atmosphere and the commitment and concentration of fourth-graders doing vacuum experiments, and of upper secondary school pupils doing electron experiments. He personally performed some vacuum experiments together with Karen Ong, head of the school lab.
Later, Mayor Scholz visited the PETRA III experimental hall. During discussions with staff scientists, he declared himself impressed by the sophisticated technologies and the wide range of research that is possible at modern synchrotron light sources like PETRA III. He also emphasized his appreciation that top level research at DESY is not kept in the ivory tower but also includes an active communication with the city of Hamburg, its citizens and the local companies.
In his reply Helmut Dosch, Chairman of the DESY Board of Directors, said that DESY develops and runs X-ray microscopes with highest resolution for the analysis of high-performance materials and new agents, which in the future will be better accessible particularly for high-tech industries in our metropolitan region. Moreover, Helmut Dosch thanked the City of Hamburg for supporting these new developments and for the reliable funding of research at DESY.

27 February:
Joint PNI-HDRI and PaNdata workshop

The first joint PNI-HDRI and PaNdata ODI workshop took place at DESY in Hamburg on February 27-28. The workshop was attended by 52 participants from 14 different facilities and institutions from all over Europe.
PNI-HDRI is a high data rate project of the German Photon, Neutron and Ion-Facilities of the Helmholtz-Society. PaNdata ODI is the Open Data Infrastructure project of the PaNdata collaboration, which includes all major European Photon and Neutron research infrastructures. Both projects have closely co-operated on specific topics related to scientific data management, in particular on the development and implementation of a standard data format (NeXus/HDF5). Since there are many more themes of common interest, ranging from GPU-accelerated analysis tools via data management issues to global user authentication, the workshop was organized as a joint workshop to intensify and broaden the co-operation.

March

2 March:
Workshop on Inelastic X-ray Scattering activities at PETRA III

DESY is currently building a new inelastic X-ray scattering instrument at the high brilliance beamline P01 of PETRA III. The two-days international workshop was organized at the early stage of the project to present the current design parameters of the beamline, to connect with the potential user community, to share ideas with the experts of the field, and to discuss the matter with members of the designated beamline advisory committee. About 40 participants came from main synchrotron radiation facilities in U.S. (APS, CHESS, SSRL), Europe (DESY, European XFEL, ESRF), and Asia (SPring-8) and from other research institutes. User demands were discussed and a beamline review was prepared for submission to the advisory committee. A PETRA III tour completed the event.

21 March:
XI. Research Course on X-Ray Science

The annual DESY Research Course on X-ray science provides basic knowledge about new directions of X-ray research. It addresses Diploma, Master, and PhD students and young research fellows. The 11th course took place on March 21-23 in the FLASH seminar hall and was dedicated to applications of X-ray scattering and spectroscopy in biological systems. 13 international speakers presented new results and applications with special attention to the impact of new synchrotron and FEL light sources such as PETRA III, FLASH, and European XFEL on the study of biological systems. 120 participants from all over Europe attended the course. During a poster session the participants presented and discussed own research work. Guided tours of FLASH and PETRA III were also well received.

April

13 April:
DESY cooperates with CAN GmbH - Hamburg

DESY has been admitted as a participating member of the Nanotechnology Sponsors' Association which is the holder of the Center for Applied Nanotechnology (CAN) GmbH. CAN is a Hamburg based nanotechnology enterprise providing nanotechnology products to be used for example in medicine and food industry, as well as custom nanotechnology research. Nanotechnology will have a considerable impact on future developments, from fuel cells to solar panels. The broad range of analysis methods available at DESY, e.g. tomography and small angle scattering, ideally meets the nanotechnology research needs and makes an important contribution to this future-oriented technology. DESY and CAN GmbH will deal with issues in the field of life sciences, energy research and materials science. In a next step, expert teams will specifically define the common research topics.

May

28 April:
First seeding at FLASH

Worldwide, researchers are looking for methods to initiate the process of light production in a Free-Electron Laser (FEL) by means of a well-defined radiation pulse, generated by an external laser source and superimposed to the electron bunch at the undulator entrance. This method is called “seeding” and promises FEL pulses which are more stable and better reproducible in both pulse duration and frequency spectrum. Moreover, the time resolution of pump-probe experiments is improved if the seeding laser simultaneously initiates a dynamic process in the investigated sample. One of the possible seeding methods using so-called High Harmonic Generation pulses (HHG) was now successfully verified at FLASH by a team of scientists from DESY and the University of Hamburg. In the sFLASH experiment, the scientists guided the light of a high-order harmonic generated by an accelerator-synchronised laser into the electron beam of FLASH and superimposed it with the electron bunches in an undulator. Stimulated by the seeding pulse the electron bunches generated an intense FEL flash with a wavelength of 38 nanometres. This is the shortest wavelength ever obtained with this “direct seeding” method – a new world record for FLASH and an important milestone on the way to FLASH II, which will be equipped with variable-gap undulators as were used with the sFLASH experiment.

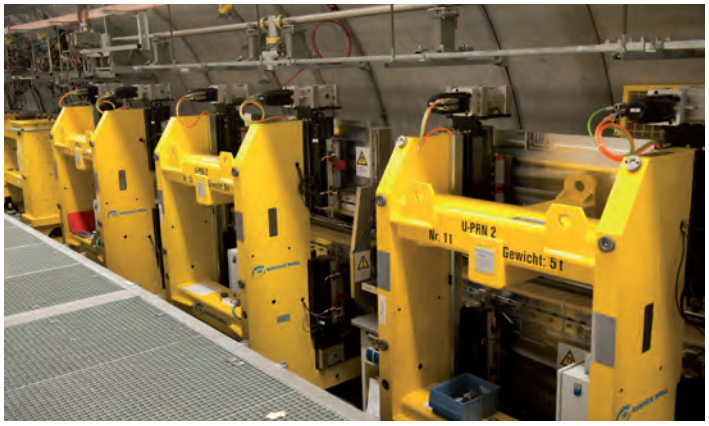

Undulators at FLASH.

22 May:
Russian and German partners collaborate on data management and analysis

European XFEL, DESY, Forschungszentrum Jülich, and the Kurchatov Institute in Moscow will cooperate in developing IT solutions for large scientific facilities. A memorandum of understanding on a collaboration to find new data management and data analysis solutions was signed in Berlin during the closing event of the German–Russian Year of Education, Science, and Innovation 2011–2012. Experiments at new large research facilities, such as the European XFEL, produce enormous amounts of data that need to be stored, maintained, and made available for analysis. This challenging task requires new ways to manage data and to provide computing infrastructure that will support scientists during and after their experiments. The European XFEL can serve as a pilot project for further collaboration between the involved partners in this area.

Signature of the “Memorandum of Understanding on collaboration to develop data management and data analysis solutions for large-scale scientific experimental facilities” on 22 May 2012 in Berlin. From left to right: Mikhail V. Rychev (Deputy Director, Special Representative of Kurchatov Centre in European International Organisations), Annette Schavan (Federal Minister of Education and Research), Andrei A. Fursenko (Minister of Education and Science of the Russian Federation), Massimo Altarelli (Chairman of the Management Board, European XFEL), Christian Scherf (Director of Administration, DESY), Inna Bilenkina (Deputy Minister of Education and Science of the Russian Federation), Serguei Molodtsov (Scientific Director, European XFEL), Sebastian M. Schmidt (Member of the Board of Directors, Forschungszentrum Jülich), Thomas Lippert (Head of Jülich Supercomputing Centre). (Photo: BMBF)

30 May:
Workshop on a German-Russian beamline at the PETRA III extension

In the frame of the German-Russian collaboration a new beamline is planned at the PETRA III extension. With the start of operation being foreseen in 2015, the new beamline is mainly intended to investigate low-dimensional and nanoscaled sample systems by means of X-ray diffraction and accompanying methods. A two-day workshop was organized to discuss the science case of the new experimental infrastructure, to clarify technical issues, and to arrange further co-operation steps. The workshop was attended by about 50 participants, 15 coming from Russia, and featured 17 talks.
The planned beamline will be financially supported by the German Ministry of Education and Research (BMBF).
On occasion of the workshop, a Russian delegation of journalists also visited DESY with the intention to present PETRA III and the bilateral collaboration to the Russian public.

31 May
Establishment of European Free-Electron Laser Collaboration

Ten European research centres, including DESY and the European XFEL, agreed on a close long-term collaboration in the field of Free-Electron Lasers and accelerator based short-pulse sources. With combined efforts, the technologies and methods for operation and use of these novel research facilities will be further developed and implemented, thus creating a unique top level research infrastructure for science in Europe, offering optimal experimental conditions for a wide range of applications. An agreement was signed at DESY by representatives of all institutes on the occasion of the ERF workshop “Socio-economic Relevance of Research Infrastructures”.

Helmut Dosch who signed the agreement for DESY together with Edgar Weckert stated that the fantastic experiments at the first free-electron lasers FLASH and LCLS, with more than 200 scientific publications, demonstrate the enormous potential of these new facilities in an impressive way. The agreement to cooperate more closely will be a basis to exploit this scientific potential to full extent and to continue playing a leading role in Europe. The partner institutions who signed the agreement are DESY (Germany), European XFEL (Germany), INFN (Italy), Helmholtz Centre Berlin (Germany), MAX IV Laboratory (Sweden), National Centre for Nuclear Research (Poland), Paul Scherrer Institute (Switzerland), Science and Technology Facilities Council (Great Britain), Sincrotrone Trieste (Italy), and SOLEIL (France). The representatives of the partners nominated Josef Feldhaus (DESY) as first chairman of the collaboration’s steering committee.

14 June:
Tunnel construction completed: European X-Ray Free-Electron Laser reaches important milestone

The European X-Ray Free-Electron Laser reached an important milestone: the construction of the network of tunnels, which totals nearly 5.8 kilometres in length and extends 3.4 kilometres from the DESY site to Schenefeld in Schleswig-Holstein, is finished. With an investment volume of more than a billion euro, including 240 million euro for the construction of the tunnels and other underground buildings, the new international research facility is one of the largest scientific projects on German territory. As of 2015, laser-like X-ray flashes that enable completely new insights into the nanoworld will be generated in these tunnels. The tunnel completion was celebrated in a festive event with more than 400 participants including guests from politics and science as well as staff from collaborating companies. Following tradition, the patron saint of miners and tunnel builders, Saint Barbara, was thanked in a short ceremony. Speakers at the event were Massimo Altarelli, Managing Director of European XFEL, Beatrix Vierkorn-Rudolph, German Federal Ministry of Education and Research, Robert Feidenhans’l, Chairman of the European XFEL Council, Helmut Dosch, Chairman of the DESY Board of Directors, and Ullrich Reinke, member of the Executive Board of Hochtief Solutions AG.
Massimo Altarelli stated that the tunnel construction was considered one of the most difficult building phases of the whole project. Finally this task could be completed according to plan and costs could be kept within the tight budget targets set when the contract was awarded. He thanked the personnel of the participating construction companies for their good work. Their commitment helped to take a big step forward to reach the envisaged scientific goals.

The tunnel boring crew in front of their large tool.

Tunnel construction began in July 2010 with the main accelerator tunnel using the tunnel boring machine TULA (“TUnnel for Laser”). In January 2011, the second machine, AMELI (the German acronym for “At the end there will be light”), started to excavate the five photon tunnels leading into the experiment hall. This was a difficult mission: given the special layout of the tunnel system, the 160-tonne colossus had to be repeatedly relocated and prepared for the next action. TULA completed its work in August 2011. With the completion of the last section, the mission of AMELI has come to an end.

July

15 June:
DESY participates in a new Cluster of Excellence

Physics in Hamburg achieved a major success in the excellence initiative of the federal and state governments: as from November 2012, funds will be granted to the "Hamburg Centre for Ultrafast Imaging – Structure Dynamics and Control of Matter at the Atomic Scale (CUI)". The University of Hamburg submitted this project proposal which was developed in cooperation with DESY, CFEL, and the European XFEL. In Northern Germany, many of the world's leading scientists in nanostructure research are currently gathering around the new Free-Electron Lasers FLASH and European XFEL.
Research in the CUI cluster will focus on real-time observation of atomic movements. Central aim is to investigate and understand in detail the dynamics of fundamental physical and chemical processes at all relevant length and energy scales. These investigations will be made possible due to the development of the extremely brilliant electron and X-ray sources. To see atoms in action at physical, chemical and biological processes is the ultimate dream of any natural scientist. Beginning with the most elementary processes of electron excitation in the attosecond range, the research programme includes the investigation of structure and dynamics of protein molecules, the formation of crystals and the order formation of collective electron systems which manifest themselves in properties like magnetism or superconductivity.
The excellence initiative was initiated by the federal and state governments to strengthen top-level university research in Germany. The current funding round involves 2.5 billion euros, 75 % thereof are financed by the federal government and the remaining part by the corresponding states.

6 July:
Workshop on achievements at DORIS beamline A2 and future perspectives

With the final shutdown of DORIS III the small angle X-ray scattering instrument at beamline A2 will come to its end after almost 30 years of successful operation. The workshop, which was attended by about 30 users of A2 was an occasion to recall the early days of small angle X-ray scattering at DESY and the history of beamline A2, which was built 1985 by the group of Professor H. G. Zachmann (University of Hamburg) as an instrument dedicated to polymer science. Talks by long term users of A2 on their projects were followed by a lively discussion about the requirements for future experiments at PETRA III.

15 July:
SRI2012 Satellite Meeting: Science at FELs

A Satellite Meeting to the 11th International Conference on Synchrotron Radiation Instrumentation (SRI) in Lyon, France, was held July 15 to 18 at DESY. It was jointly organized by European XFEL and DESY and attended by about 200 researchers. Science at FELs 2012 was the world's first major international conference dedicated exclusively to science with X-ray Free-Electron Lasers. Scientific experiments and approaches offering new insights into the nanoworld were discussed and speakers from around the world presented a number of highlights achieved in the first seven years of operation of short-wavelength free-electron lasers: FLASH in Hamburg (since 2005), LCLS in the USA (since 2009), SACLA in Japan (since 2012), and FERMI in Italy (since 2012). The scientific topics covered a large variety of scientific areas such as atomic and molecular physics, chemistry, life science, condensed matter physics, and matter under extreme conditions as well as new enabling developments in FEL science. Participants came from over 20 countries in Europe, America, and Asia. In addition to well-known researchers and long-time experts in science with FELs, many young scientists attended the conference. A sizeable number of presentations were given by young researchers indicating that a new generation of young scientists educated for and trained in using this new class of light sources is actively exploiting the wide spectrum of research opportunities offered by FEL facilities. In total 30 oral and 96 poster contributions were complemented by an industry vendor exhibition and by visits of the European XFEL site in Schenefeld and the FLASH and PETRA III facilities.

Coffee break during the SRI2012 Satellite Meeting "Science at FELs".

August

17 July:
Start of DESY Summer Student Program 2012

The DESY summer student program started on 17 July. The part of the program related to Photon Science was attended by 33 undergraduate students from Great Britain, Armenia, Italy, Moldavia, Austria, Poland, Russia, Spain, Sweden, United States, Brazil, and Germany. They were selected from 116 applicants, graduating in various fields of natural sciences, who had named “research with synchrotron radiation” as the first priority in the application. The selected students were distributed among the different photon science research groups at DESY, CFEL, and EMBL, where they participated in the everyday work and were assigned a small project of their own to work on. As every year, this was accompanied by a series of common lectures about DESY activities in general, including accelerator and particle physics and a series of lectures on research with synchrotron radiation introducing the different experimental techniques in greater detail. The lecture series was followed by an exercise week, in which the students had the possibility to perform experiments in small groups at eight selected DORIS III and PETRA III experimental stations. The stay of all DESY summer students ended on September 6 with a final student session during which selected participants gave brief presentations of their projects during the stay. The program was again a great success and very well received by the students who especially appreciated the international atmosphere at DESY and the good mixture of practical work and lectures on topics which are usually not presented in such a comprehensive manner in university courses. Many participants consider coming back to DESY as a PhD student or postdoc. Education and promotion of young scientist is a central part of DESY’s mission with the summer student program being an essential part of it.

The students of the photon science related part of the DESY summerstudent program 2012.

23 August:
Start of construction work for FLASH II main tunnel

Construction of the FLASH II extension has started with the main tunnel section. In 2013, the technical system for a second X-ray laser beam will be installed in this 110-metre-long tunnel to serve light for a second experimental hall. The unique light of the existing FLASH facility is in high demand among scientists. With the x-ray laser it is possible to take snapshots of the world of molecules and to follow ultrafast processes in the nanocosmos. The existing FLASH experimental stations are completely overbooked. With FLASH II, DESY will not only extend the number of experimental stations, the facility will also become more flexible. FLASH II will allow changing the wavelength of the emitted light during operation which is not possible with the existing facility.

The FLASH II main tunnel starts to take shape.

In order to keep on-going research activities as undisturbed as possible, the construction of the extension tunnel was subdivided into three sections. The front section – the connection to the existing FLASH accelerator tunnel – is already completed. At the rear end, the tunnel crosses DESY’s accelerator ring PETRA III which must also run mostly unaffected. The rear tunnel sector which connects the future experimental hall has been completed as well.
The main tunnel also includes two new buildings with technical installations for operation and research. And there are already plans providing a further expansion in the future. The 15-metre-wide and 9-metre-high tunnel offers enough space for an optional third undulator line.

September

27 August:
DESY extends cooperation with Thailand

DESY strengthens cooperation with scientists in Thailand with the aim to extend the exchange of knowledge, experience, equipment, employees, and students. In the presence of HRH Princess Maha Chakri Sirindhorn, DESY Director Helmut Dosch and representatives of the Thai Synchrotron Light Research Institute SLRI, of the Thailand Center of Excellence in Physics, and of the Thai National Science and Technology Development Agency signed a corresponding Memorandum of Understanding. The extension of cooperation involves all research fields of DESY: accelerator physics, photon science, particle-, and astro-particle physics. It will consolidate the traditionally good relations between DESY and research institutes in Thailand. Helmut Dosch stated that Thailand is a dynamic country with a very high scientific potential in research with synchrotron radiation. Cooperation between DESY and its Thai partners was already agreed upon earlier, e.g. at the photo injector test facility PITZ in Zeuthen or for the support of young Thai students in the DESY Summer Student Program which will now be upgraded.

The framework agreement on an extended cooperation of DESY with scientists in Thailand was signed in Bangkok.

6 September:
Visit of the 4th Russian-German "Travelling Seminar" at DESY

The "travelling seminar" is an initiative started a few years ago by the University of Erlangen-Nürnberg and funded by the German Ministry of Education and Research (BMBF) in the framework of the German-Russian Cooperation. Every year, alternatively in Germany and Russia, a group of Russian and German PhD student and young scientists, selected by a bilateral commission, participate in a two-week summer school in photon science, of which one week is dedicated to visiting synchrotron radiation and FEL facilities in the hosting country. In 2012, the travelling seminar took place in Germany, and comprised a two day visit of DESY. The group of about 20 students, accompanied by four faculty members from Erlangen and Ekaterinburg, attended talks held by the accompanying as well as by DESY scientists especially addressing research on nanoparticles using large photon sources. The students could also present their own research results. On the second day, the group had ample opportunity to visit the facilities PETRA III and FLASH. According to the students, the two days were a very interesting and fruitful experience. We wish the participants good luck for their work and hope to see them again in the future!

Participants of the 4th Russian-German "Travelling Seminar".

13 September:
New CFEL building comes to life

The newest architectural landmark on DESY campus has opened its doors to the scientists. After more than three years of construction, the new building of the Center for Free-Electron Laser Science (CFEL) was handed over to Hamburg University. The eye-catching facility – located in the close neighbourhood of the PETRA III experimental hall – comes with four thousand square metres of office space for over four hundred employees, approximately the same amount for laboratories, four hundred square metres for scientific meetings, and its own cafeteria. Scientists at CFEL, a scientific collaboration between DESY, the Max Planck Society, and Hamburg University, pursue research with modern light sources such as free-electron lasers to utilize its ultra-short and ultra-intense light pulses for research in physics, biology, chemistry, material science, and several other areas. CFEL groups have been working at DESY in temporary offices since early 2008.

The atrium of the new CFEL building.

CFEL's new home has been designed by the Stuttgart architects hammeskrause. The building's impressive transparent roof creates a vast open space at the centre of the building with the offices arranged around it in a concentric fashion to create synergies between the various research groups and to foster communication among scientists as the architects state. The new facility provides 21 state-of-the-art laser laboratories, which are strictly vibration-cushioned and temperature-controlled. Large air conditioning installations keep the temperature on the experimentalists' optical tables constant within half a degree. Laboratory space is complemented with a clean room, workshops for detector development, chemistry and biochemistry laboratories, and a spacious experimental hall for the assembly of large-scale synchrotron radiation and free-electron laser setups. The construction costs of approximately forty million euros have been predominantly covered by the City of Hamburg with additional funds coming from the German federal government.

19 September:
PETRA III experimental hall named after Nobel Laureate Max von Laue

Calling it simply "PETRA III hall" is not appropriate for the 300 m long building that hosts the experimental stations at the currently most brilliant storage ring based synchrotron radiation source in the world. 2012 is the Max-von-Laue year, which reminds us of the first X-ray crystal diffraction experiment carried out by Max von Laue in 1912. Already two years later he was awarded the Nobel Prize in Physics for this ground breaking discovery which laid the foundation for the exciting developments which lead to many of the activities performed at PETRA III today. PETRA III brings the scientific heritage of Max von Laue to new frontiers and limits, thus, experimental hall Max von Laue is definitely an appropriate name.

Federal Chancellor Angela Merkel, DESY Director Helmut Dosch and Hamburg's First Mayor Olaf Scholz (left) in the PETRA III experimental hall Max von Laue.

For the naming ceremony on 19 September DESY Director Helmut Dosch could welcome prominent support: Federal Chancellor Angela Merkel, Hamburg's First Mayor Olaf Scholz, and Nobel Prize Laureate in Chemistry Ada Yonath attended the ceremonial act in front of 1215 visitors, including external guests from science and politics and as special guests grand- and great-grandchildren of Max von Laue.
In her celebratory speech, Chancellor Merkel emphasised the importance of progress in basic research as the breeding ground for tomorrow's technologies and innovations. "They pave the way for economic and social progress. This, of course, is extremely important for a nation lacking in raw materials like Germany. This is why it is crucial for us to do basic research. It is the key for Germany's prosperity in the future." DESY offers the best conditions for global research cooperation. "In the field of basic research in natural sciences, DESY plays a leading role in the world. And it is an attractive location for state-of-the-art large-scale facilities," Chancellor Merkel said.

October

26 September:
Workshop on Transient and Ultrafast Processes in X-ray Excited Matter

Experiments at FLASH and LCLS have started to exploit the fact that intense XUV and X-ray FEL pulses can drive matter significantly out of equilibrium. Due to the extremely short duration of the pulses, much shorter than the involved relaxation timescales, matter can be brought to a transient state. The scope of the meeting was to discuss, on one side, the underlying physical processes of XUV/X-ray excitation of matter and on the other side, possible experiments for studying properties of matter in a semi-equilibrium or transient state. For this purpose, the description of radiation-matter interaction and the discussion of new experimental techniques for probing matter were in the focus of the meeting. Theorists and experimentalists shared their views on the development of new ideas, future experiments, and the identification of challenging "open questions".
The workshop program comprised contributions by ten invited speakers. The number of participants was limited to 60 in order to have a good discussion forum. Each of the three main sessions was followed by a dedicated discussion session. Theoretical approaches included macro- and microscopic description of X-ray excitation in the quantum and in the classical regime. Various experimental methods for generation and diagnosis of XUV/X-ray excited matter were reported. The discussion made clear that a vast amount of experimental data from laser experiments already exists which allows testing the performance of new simulation codes. At the same time it became obvious that an accurate description of some transient states, following interaction of samples with intense and ultrafast XUV/X-ray beams is still missing. The joint development of theory and experiment will be important to achieve a better understanding of states of matter which are expected to be exploited in the coming years at FLASH, the European XFEL, and at other X-ray FEL sources world-wide.

18 October:
Workshop on "Science beyond 4 Mbar and using Dynamic Compression"

The workshop brought together a group of about 30 scientific experts from six countries to discuss scientific questions and to propose related experiments that are relevant for simultaneous high-pressure and high-temperature condensed matter physics and which currently cannot be studied by using conventional static compression methods like diamond anvil cells. The workshop aimed particularly at exploring science that will emerge or benefit from new and enabling techniques such as the combination of intense pulsed X-ray sources with pulsed sample excitation by means of high-energy optical lasers. Key scientific questions addressed at the workshop were: Understanding planetary bodies (solid and gaseous), understanding materials and their driven dynamics, and obtaining quantitative data from dynamic compression experiments. In particular the last subject emphasized that the physics of dynamic compression itself is still not well understood.

In summary, the workshop indicated that there is a huge demand for experimental data of a variety of physical properties of materials relevant to planetology and materials science. In order to gain access to these data the physics of dynamic compression needs to be better understood, so that one can obtain quantitative data (static and dynamic). The application of bright X-ray sources in combination with high energy lasers creating dynamic compression was identified as the most promising pathway to obtain structural and equation-of-state data as well as many of the other physical properties discussed during the workshop. Hence, FEL light sources with their very short, bright and highly coherent X-ray pulses will be ideal for collecting quantitative data on relevant physical properties. Currently there is no facility that offers the combination of a large optical laser system for ramped compression and a 4^{th} generation light source and thus it would be very desirable to establish such capabilities at the HED instrument of the European XFEL.

22 October:
"Tschüüüs DORIS": Farewell celebration on occasion of the last DORIS III synchrotron radiation run

In the morning of 22 October at 8 a. m. the very last synchrotron radiation run of DORIS III came to an end. This marks the end of the extremely successful operation of DORIS for photon science which started with the commissioning of the machine in 1974. DORIS III is still running until the end of 2012, but the last experiments are done with the detector OLYMPUS to study effects in elastic electron scattering. In the afternoon of this memorable day a ceremony was held in the DESY auditorium which was attended by many present and former users and staff members. It was entitled "Tschüüüs DORIS". "Tschüs" is a local word originally used in the Hamburg (northern German) area and means "goodbye, farewell". Eventually it made its way into the German vocabulary. After a talk given by Edgar Weckert about the future perspectives of Photon Science at DESY and the reasons to close DORIS operation Volker Saile (KIT, Karlsruhe), one of the former heads of HASYLAB, gave a comprehensive historical overview of 38 years research with synchrotron radiation at DORIS. The session was completed by a round table moderated by Jochen R. Schneider in which Karen Appel, Robert Feidenhans'l, Ken Holmes, Gerhard Materlik, Bernd Sonntag, and Ernst-Werner Weiner talked about impressions remembered from their work at DORIS.
A great farewell event to appreciate the merits of DORIS in the fields of particle physics and photon science is planned in spring 2013.

Round table chat about DORIS. From the left: J.R. Schneider, K. Holmes, R. Feidenhans'l, B. Sonntag, K. Appel, G. Materlik, E.W. Weiner.

31 October:
PhD thesis prize for Arik Willner

This year's PhD thesis prize of the Association of the Friends and Sponsors of DESY is shared by Katarzyna Anna Rejzner und Arik Willner.
Arik Willner was born in Lübeck and studied in Kassel and later in Hamburg, where he graduated with his PhD work entitled „A High Repetition Rate XUV Seeding Source for FLASH II". It addresses the possibilities for seeding of Free-Electron Laser sources. FELs like FLASH at DESY are able to produce extremely short and intense X-ray pulses but the quality of the consecutive pulses is statistically fluctuating. Seeding is a means to eliminate these fluctuations and is presently in the focus of research worldwide. Its basic idea is to initially excite the lasing process with a weak laser pulse of the desired wavelength. In the wavelength range from 100 nm to 10 nm these so-called seeding pulses are very difficult to produce, especially with the desired repetition rate in the kHz-range as needed in the case of FLASH. With his PhD work Arik Willner could demonstrate a way to solve this problem which means a significant step forward for the technological development of seeded Free-Electron Lasers (see also the Research Highlight article 'Bright XUV laser source with dual-gas high harmonic generation', DESY Photon Science Report 2011, p. 32-33).

Katarzyna Anna Rejzner was born in Poland and studied first in Krakau. She got her PhD in Hamburg for her work on gauge theories, which form a basis in particle physics.

The PhD thesis award of the Association of the Friends and Sponsors of DESY includes 3000 euros prize money. Every year, the association presents this prize for one or two outstanding PhD theses.

Arik Willner

Katarzyna Anna Rejzner

31 October:
EPDIC Young Scientist Award for DESY Scientist

The European Powder Diffraction Conference (EPDIC) held in Grenoble, France, honoured DESY scientist Dr. Kenneth Beyerlein with the 2012 Young Scientist Award. Beyerlein is post-doctoral scientist in the group of Henry Chapman at the Center for Free-Electron Laser Science (CFEL) and received the highly competitive and prestigious award in recognition of his outstanding graduate research work on modelling and interpreting powder diffraction patterns from nanoparticles.

Kenneth Beyerlein receiving the EPDIC Young Scientist Award 2012.

As a graduate student, Beyerlein studied under Professors Bob Snyder and Mo Li at the Georgia Institute of Technology (Atlanta, USA) as well as Professor Paolo Scardi at the University of Trento (Italy), where he developed new approaches to determine the shapes and sizes of nanoparticles from powder diffraction data. Furthermore, the award-winning research led to an improved understanding of the effects that heat-induced vibrations, surface structure, and structural imperfections have on the diffraction signals of nano-sized crystals. At CFEL, Beyerlein transfers the results of his graduate research to the emerging field of protein nano-crystallography using X-ray free-electron lasers. Although structural biologists have been using diffraction techniques for many years, challenging proteins forming only nano-sized crystals have not been accessible in previous studies. The work of the Chapman group has shown that a protein structure can be solved with the patterns from a few thousand nanocrystals. The same idea that Beyerlein used to characterize the size and shapes of nanomaterials can be applied to studying small protein crystals. Biomedical and pharmaceutical applications greatly benefit from a detailed knowledge of protein structures. Hence, nanocrystallography is expected to provide a new impetus for these research areas.

EPDIC recognizes the outstanding scientific achievements by a young researcher in the field of powder diffraction once every two years.

Research Highlights.

The battle of ground states.

Charge density waves versus superconductivity in the high-temperature superconductor $YBa_2Cu_3O_{6.67}$

A high energy X-ray diffraction study probing symmetry breaking states in the high temperature superconductor $YBa_2Cu_3O_{6.67}$ is presented. A charge density wave is found to emerge in the normal state above the transition temperature of the superconducting phase and persists in the superconducting state. Application of an external magnetic field enhances the intensity of the charge ordering reflection and suppresses superconductivity. These results provide a mechanism for the Fermi surface reconstruction observed by quantum oscillation experiments in high magnetic fields.

The determination of the ground state from which high-temperature superconductivity emerges is at the heart of this fascinating phenomenon. One approach to access this state is to suppress superconductivity by introducing defects into the crystal lattice. Several of these non-superconducting materials show tendencies spin density waves in the underdoped phase, with hole-doping concentrations p of about 1/8. In the single layer compound $La_{1.58}Nd_{0.4}Sr_{0.12}CuO_4$ so-called stripe order has been found, where one-dimensional rivers of charges are separated by antiferromagnetic domains [1]. More recent studies on $La_{2-x}Ba_xCuO_4$ showed that this stripe order is strongest at p = 1/8 where superconductivity is suppressed down to T_c = 2 K, but persists well into the doping regime where superconductivity becomes strong [2]. However, the question whether this state is generic to high-temperature superconductivity or whether it is a consequence of structural distortions due to the ion replacement remains. Another approach to suppress superconductivity is the application of a high magnetic field. $YBa_2Cu_3O_{6+x}$ (YBCO) is considered as one of the superconductors with highest purity, since hole-doping proceeds not by ionic replacement, but via the introduction of oxygen, which forms relatively well ordered chains. In addition it exhibits very high transition temperatures of T_c = 92 K at optimal doping. In the underdoped state quantum oscillations of various physical properties have been observed at high magnetic fields, which are indicative for the existence of small hole pockets at the Fermi surface [3,4]. A possible origin for such hole pockets could be a charge density wave (CDW). This could also be the cause for the line splitting originating from one of the Cu sites at magnetic fields above H = 9 T in a nuclear magnetic resonance (NMR) study [5], which is an indication for the presence of two distinct Cu valence states.

Using high energy X-ray diffraction we are able to study structural distortions related to charge ordering. Surprisingly, we find that signatures of charge order appear already at zero magnetic field and temperatures well above the transition into the superconducting phase. The intensity associated with this CDW reflection increases with decreasing temperature until the transition temperature into the superconducting phase, T_c, is reached. Below T_c the intensity decreases. Applying a high magnetic field the CDW intensity is enhanced below T_c, whereas no field effects are observed above this temperature.

The experiment was performed at the high-energy X-ray beamline BW5 at DORIS using 100 keV X-rays. The $YBa_2Cu_3O_{6.67}$ sample with a doping concentration of p = 1/8 and a size of 1.5 x 1.5 x 0.8 mm^3 was studied in transmission geometry, thus probing bulk properties. High field studies were performed with a 17 Tesla superconducting magnet, which was newly developed by University of Birmingham for beamline use.
Signatures of a charge density wave order are observed by the appearance of diffuse scattering reflections at ordering wave

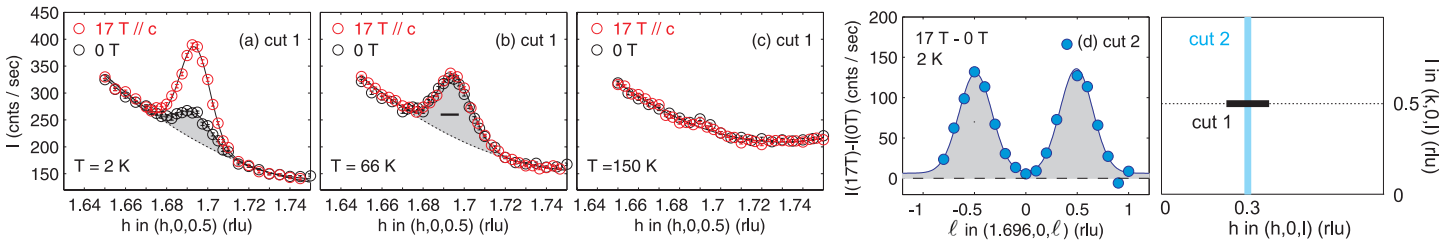

Figure 1

Charge density wave reflection at (1.695, 0, 0.5). Scans along (h, 0, 0.5) and T = 2 K show a clear difference between H = 17 T and 0 T (a), at T_c = 66 K no field dependence is found (b) and the intensity is of the order 2 x 10^{-6} weaker than the (2, 0, 0) reflection. CDW order disappears above 135 K (c). The field induced intensity scaned along (0, k, 0.5) shows peaks at l = ±0.5 (d). Scan directions in reciprocal space (e).

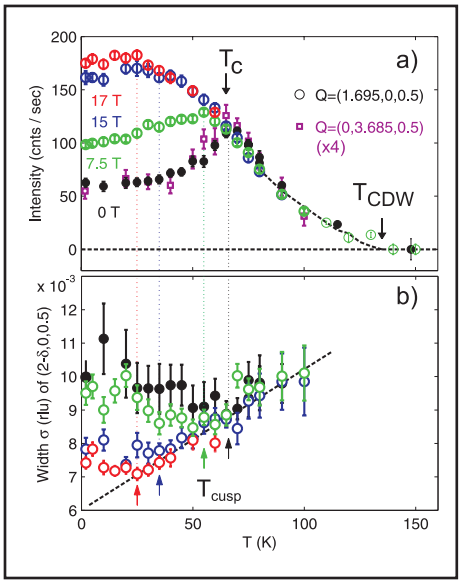

Figure 2

Temperature dependence of the charge density wave reflections at (1.695, 0, 0.5) and (0, 3.685, 0.5) at different magnetic fields (a). The square data points have been multiplied by a factor of four. Peak widths along a* are shown in (b). Vertical lines mark the temperatures at which the intensity reaches a maximum and below which the correlation length freezes in.

vectors (0.3, 0, 0.5) and (0, 0.3, 0.5) as shown in Fig. 1a. The intensity of this charge density wave reflection grows below 135 K and reaches a maximum at T_c = 67 K, the transition temperature into the superconducting phase. The competition of superconductivity and CDW order is well observed by the sharp drop in intensity of the CDW reflection below T_c, as shown in Fig. 2a. Furthermore, the drop is converted into a strong intensity increase by the application of a magnetic field that suppresses superconductivity (Fig. 2b). At the same time the correlation length increases reaching a maximum of 95 Å at 17 T. The strongest contribution to the scattering cross section is coming from atomic displacements associated with the charge order. The electronic origin of the ordering process has been shown in an independent study using the resonant scattering technique at the Cu L-edges [6].

The observation of a charge density wave at zero field and temperatures up to 135 K seems to contradict NMR data, where CDW order appears only below T = 67 K and H > 9 T. This discrepancy might be resolved by the different timescales of the two probes. X-rays take snapshots of the structure on timescales of fs, which are averaged by the integration time, whereas NMR probes on timescales of the Lamor frequency which is ~ 3 ns. Thus it might require a higher field and lower temperature to freeze the CDW on NMR timescales.

An interesting question is whether the CDW observed in YBCO and the stripe order in the single layer compounds are of common origin. Like the CDW wave in YBCO, the charge stripes are competing with superconductivity and are enhanced by a magnetic field applied parallel to the c-axis [7]. Translational symmetry is broken along c in a similar way by both kinds of orders. However, the in-plane ordering wave vectors of (0.31, 0) and (0, 0.32) could suggest that Fermi surface nesting gives rise to the CDW in YBCO and no magnetic order is involved, as found in the NMR and resonant scattering studies [5,6]. In contrast, stripe order exhibits a very intimate relation between charge and magnetic order and it is the separation of spin and charge that leads to this particular order [1].

This study shows that charge density wave order is competing with superconductivity. Thus, one route to push T_c towards higher temperatures might be to artificially supress CDW order. Such a route might be promising as demonstrated in a recent study on non-superconducting $La_{1.675}Eu_{0.2}Sr_{0.125}Cu_{O4}$ where stripe order was destroyed by an intense laser pulse and a transient superconducting state obtained on timescales of ps [8].

Contact: Johan Chang, johan.chang@epfl.ch
Martin von Zimmermann, martin.v.zimmermann@desy.de

Authors

J. Chang[1,2], E. Blackburn[3], A.T. Holmes[3], N.B. Christensen[4], J. Larsen[4,5], J. Mesot[1,2], Ruixing Liang[6,7], D.A. Bonn[6,7], W.N. Hardy[6,7], A. Watenphul[8], M. v. Zimmermann[8], E.M. Forgan[3], and S.M. Hayden[9]

1. Institute de la Matière Complexe, Ecole Polytechnique Férderale de Lausanne (EPFL), CH-1015 Lausanne, Switzerland
2. Paul Scherrer Institut, Swiss Light Source, CH-5232 Villigen PSI, Switzerland
3. School of Physics and Astronomy, University of Birmingham, Birmingham B15 2TT, United Kingdom
4. Department of Physics, Technical University of Denmark, DK-2800 Kongens Lyngby, Denmark
5. Laboratory for Neutron Scattering, Paul Scherrer Institut, CH-5232 Villigen PSI, Switzerland
6. Department of Physics & Astronomy, University of British Columbia, Vancouver, Canada
7. Canadian Institute for Advanced Research, Toronto, Canada
8. Deutsches Elektronen-Synchrotron DESY, 22603 Hamburg, Germany
9. H. H. Wills Physics Laboratory, University of Bristol, Bristol, BS8 1TL, United Kingdom

Original publication

"Direct observation of competition between superconductivity and charge density wave order in $YBa_2Cu_{3O6.67}$", Nature Physics 8, 871-876 (2012).

References

1. **J. M. Tranquada, et al., "Evidence for stripe correlations of spins and holes in copper oxide superconductors", Nature 375, 561-563 (1995).**
2. **M. Hücker et al., "Stripe order in superconducting $La_{2-x}Ba_xCuO_4$ (0.095 < x < 0.155)", Phys. Rev. B 83, 104506 (2011).**
3. **N. Doiron-Leyraud et al., "Quantum oscillations and the Fermi surface in an underdoped high-Tc superconductor", Nature 447, 565-568 (2007).**
4. **D. LeBoeuf et al., "Electron pockets in the Fermi surface of underdoped high-Tc superconductors", Nature 450, 533-536 (2007).**
5. **T. Wu, et al., "Magnetic-field-induced charge-stripe order in the high-temperature superconductor $YBa_2Cu_3O_y$", Nature 477, 191-194 (2011).**
6. **G. Ghiringhelli, et al., "Long-range incommensurate charge fluctuations in (Y,Nd)$Ba_2Cu_3O_{6+x}$", Science 337, 821 (2011).**
7. **J. Wen et al., "Uniaxial linear resistivity of superconducting $La_{1.905}Ba_{0.095}CuO_4$ induced by an external magnetic field", Phys. Rev. B 85, 134513 (2012).**
8. **D. Fausti et al., "Light-Induced Superconductivity in a Stripe-Ordered Cuprate", Science 331, 189-191 (2011).**

Superconductivity under cover.

Charge stripes near the surface of $La_{1.88}Sr_{0.12}CuO_4$

Most of present day's understanding of high-temperature superconductors (high-T_c) is based on experiments that either probe the bulk of the material or the topmost surface layer. Making use of the wide range of X-ray energies available at modern synchrotron facilities we found clear differences in the properties of the bulk and near-surface region of the prototypical high-T_c material $La_{1.88}Sr_{0.12}CuO_4$ (LSCO): While near the surface doped charges arrange in one-dimensional stripes, such order is not found in the bulk. These results show that the material is sufficiently close to stripe formation and that small perturbations like strain or reduced dimensionality near the surface stabilize this order. It also tells us that bulk and surface properties in such materials can be very different.

The basic building blocks of cuprate high-temperature superconductors are CuO_2 planes (Fig. 1a). It has been predicted early [1] that doped holes may arrange as lines in these planes forming charged anti-phase domain walls for the antiferromagnetic order on the hole-poor sites (Fig. 1b). Such patterns, called stripes, can be detected via their characteristic additional superstructure reflections (Fig. 1c) in neutron [2] and X-ray experiments [3]. Two sets of reflections, one set due to the magnetic stripe order and the other set due to the charge stripes were indeed found in various high-T_c materials [4]. Interestingly, for the prototypical material LSCO only the magnetic stripe peaks could be found [5], while the charge stripe signal was missing [6]. This has been puzzling, because both are supposed to be closely linked together.

Over the last years, two X-ray based methods have been developed that both are extremely sensitive to charge stripe order. Resonant soft X-ray diffraction (RSXD) employs excitations from either a copper 2*p* core level to the unoccupied copper 3*d* states or from an oxygen 1*s* to an unoccupied oxygen 2*p* state to create a spectroscopic sensitivity to the local hole density. The corresponding resonances are in the soft X-ray range where the probing depth is of the order of a few nanometers. The other method, high-energy X-ray diffraction, has a probing depth of the order of millimeters. Since so many lattice planes contribute to the scattering signal, extremely well-defined diffraction peaks are generated [3]. Charge order is probed in this experiment via small lattice distortions caused by local variations of the Coulomb interaction. Despite the very different contrast mechanisms, both techniques have comparable sensitivities to charge stripes.

The high-energy experiments were carried out at Beamline BW5 at DORIS using 100 keV X-rays; the soft X-ray experiments at

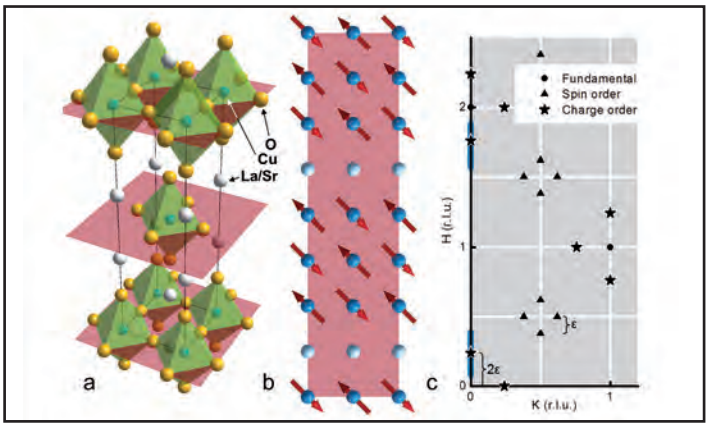

Figure 1

Stripe order and the observed charge order peaks. a) Crystal structure of the layered perovskite cuprates, b) a model picture of site-centred stripe order in the CuO planes (red planes in a) where only the Cu sites are shown. Light blue denotes hole-rich, dark blue hole-poor sites; the arrows indicate the spin direction. c) Reciprocal space map with fundamental Bragg peaks and superstructure reflections related to the stripe phase. The blue lines denote the direction of the scans presented in Fig. 2.

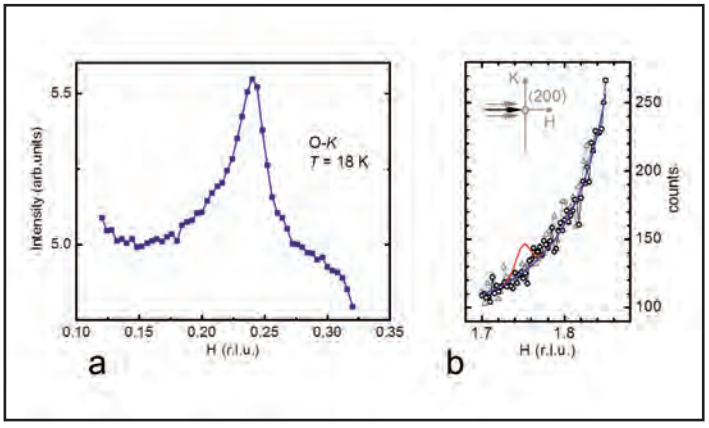

Figure 2

Reciprocal space scans through charge-order positions. a) Scans along [100] *(H)* through the (0.24 0 0) superstructure peak of LSCO. b) Example for high-energy X-ray scans through an expected charge-order satellite position near (200) (symbols and blue line) and slightly offset in *K* (grey symbols) to be sure not to miss any signal. The red line is a simulation of a charge order peak with the same width as the one in Fig. 2a and an intensity of 10^{-8} times the intensity of a strong nuclear reflection.

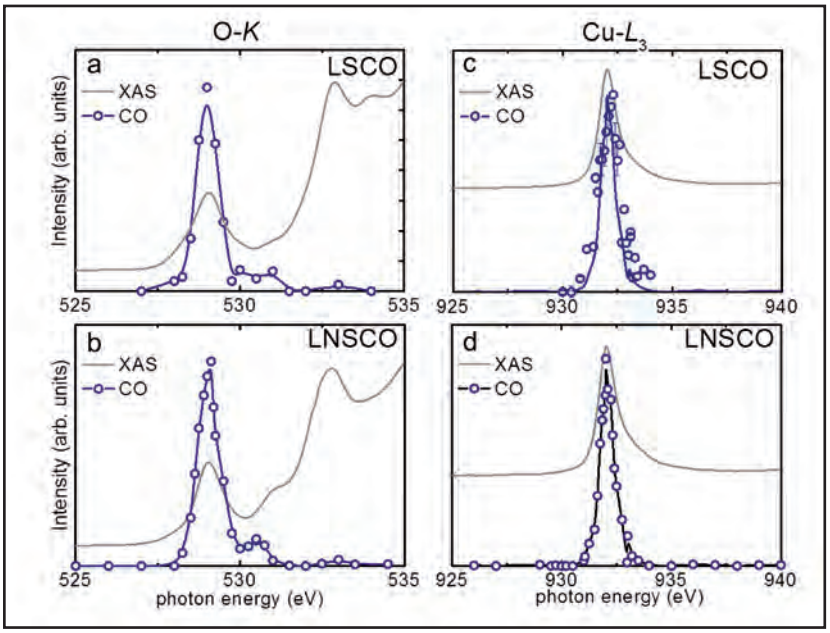

Figure 3

Resonance spectra from LSCO and LNSCO. Energy dependence of the (0.24 0 0) RSXD signals (symbols) as observed at the oxygen *1s* → *2p* (a) and copper *2p* → *3d* resonances (c) in comparison to the same signal from LNSCO (b,d). The lines through the symbols are guides to the eye. The respective X-ray absorption signals are shown as energy reference.

UE46-PGM1 of BESSY II; for both experiments pieces of the same single crystal were used. With soft x-rays a clear peak is found at the position where a charge-stripe signal is expected (Fig. 2a). We compared its energy dependence with that from the charge-stripe peak in $La_{1.48}Nd_{0.4}Sr_{0.12}CuO_4$ (LNSCO). LNSCO is the cuprate material, in which charge stripes were first observed experimentally [2], and served as a reference. The agreement between the spectra recorded from the two materials (Fig. 3) clearly shows that the peak found in LSCO has the same origin in charge stripes as the peak in LNSCO. This assignment is further confirmed by the temperature dependence of the peak intensity. Remarkably, no charge stripe signal is found in the high-energy diffraction experiment. As an illustration we show a set of scans through a position where a charge-stripe peak should show up (Fig. 2b). The red line is a simulation for a charge stripe peak that is eight orders of magnitude weaker than a strong nuclear reflection, which is what we regard as our detection limit. Clearly no such signal exists.

From the peak width found in the soft x-ray diffraction experiment we know that charge-stripe order exists in a near-surface region of at least 4 to 6 nanometers thickness. The order is hence not a property of the topmost surface layer. In order to check the effect of surface preparation, we compared samples that were polished ex-situ with those that were cleaved in vacuum. Charge stripes can be found near surfaces prepared with both methods; they are hence an intrinsic property of the material.

From these findings we conclude that LSCO at 12% doping level is so close to stripe formation that small perturbations like strain fields near the surface or the reduced dimensionality is sufficient to stabilize them, while in the bulk this stabilizing effect is either missing or not strong enough. We further learn that materials like LSCO can develop different properties near the surface than deeper in the bulk. This has to be taken into account when results from surface-sensitive experiments shall be interpreted in terms of bulk properties.

Contact: Christian Schüßler-Langeheine, christian.schuessler@helmholtz-berlin.de

Authors

Hsueh-Hung Wu[1,2], Marcel Buchholz[1], Christoph Trabant[1,3], Chun-Fu Chang[1,4], Alexander C. Komarek[1,4], Franziskus Heigl[5], Martin v. Zimmermann[6], Matthias Cwik[1], Fumihiko Nakamura[7], Markus Braden[1] and Christian Schüßler-Langeheine[1,3]

1. II. Physikalisches Institut, Universität zu Köln, Zülpicher Str. 77, 50937 Köln, Germany
2 National Synchrotron Radiation Center, Hsinchu 30076, Taiwan
3. Helmholtz-Zentrum Berlin für Materialien und Energie GmbH, Albert-Einstein-Str. 15, 12489 Berlin, Germany
4 Max-Planck Institute CPfS, Nöthnitzer Str. 40, 01187 Dresden, Germany
5. ALBA Synchrotron Light Facility, 08290 Cerdanyola del Vallès, Barcelona, Spain
6. Deutsches Elektronen-Synchrotron DESY, 22603 Hamburg, Germany
7. Department of Quantum Matter, ADSM, Hiroshima University, Higashi-Hiroshima 739-8530, Japan

Original publication

"Charge stripe order near the surface of 12-percent doped $La_{2-x}Sr_xCuO_4$", Nature Communications 3, 1023 (2012).

References

1. **J. Zaanen, O. Gunnarsson, "Charged magnetic domain lines and the magnetism of high-T_c oxides", Phys. Rev. B 40, 7391-7394 (1989).**
2. **J. M. Tranquada, B. J. Sternlieb, J. D. Axe, Y. Nakamura, S. Uchida, "Evidence for stripe correlations of spins and holes in copper oxide superconductors" Nature 375, 561-563 (1995).**
3. **M. v. Zimmermann, A. Vigliante, T. Niemöller, N. Ichikawa, T. Frello, J. Madsen, P. Wochner, S. Uchida, N. H. Andersen, J. M. Tranquada, D. Gibbs, J. R. Schneider, "Hard–X-ray diffraction study of charge stripe order in $La_{1.48}Nd_{0.4}Sr_{0.12}CuO_4$", Europhys. Lett. 41, 629 (1998).**
4. **M. Vojta, "Lattice symmetry breaking in cuprate superconductors: stripes, nematics, and superconductivity", Advances in Physics 58, 699-820 (2009).**
5. **T. Suzuki, T. Goto, K. Chiba, T. Shinoda, T. Fukase, H. Kimura, K. Yamada, M. Ohashi, Y. Yamaguchi, "Observation of modulated magnetic long-range order in $La_{1.88}Sr_{0.12}CuO_4$", Phys. Rev. B 57, R3229-R3232 (1998).**
6. **M. Fujita, H. Goka, K. Yamada, M. Matsuda, "Competition between Charge- and Spin-Density-Wave Order and Superconductivity in $La_{1.875}Ba_{0.125-x}Sr_xCuO_4$", Phys. Rev. Lett. 88, 167008 (2002).**

Cut and paste zeolites.

Design of zeolite by inverse sigma transformation

Zeolites are highly crystalline microporous materials. Their unique properties let them stand out in many applications such as adsorption, catalysis and separation. Inserting heteroelements often improves their desired properties. Germanium is known to direct towards extra-large pore zeolites but decreases stability. We managed to fully remove germanium from a germanosilicate zeolite by acid leaching while preserving the silicate layers. These layers are used as building units to generate new zeolite frameworks in a one-step synthesis. This structural transformation is the first practical example of an inverse sigma transformation, which up to now was an entirely theoretical concept. We found germanium to be present in a germanate four-ring in the parent zeolite which is first shifted into the pores before its full removal.

In the last 50 years, the interest in zeolite structures has gone beyond pure academic curiosity. The impact of zeolites in the field of science and technology is immense. Nowadays it's hard to imagine catalysis, petrochemistry and separation techniques without these crystalline microporous materials. Up to date, 200 zeolite frameworks have been synthesized, mostly relying on trial and error, and only very few topologies are really applied in industry [1]. The now practically achieved inverse sigma transformation allows a rational approach to zeolite synthesis: building units from existing zeolites can be harvested and re-arranged into new zeolite frameworks.

As starting material served the IM-12 zeolite with UTL framework topology [2], which can be described as dense silicate layers interconnected by double four-rings that contain tetrahedral germaniumoxide units next to silica [3,4]. Like many germanosilicate zeolites, UTL zeolite is unstable towards hydrolysis. Contact to even small amounts of water has to be avoided. Due to this instability, the UTL framework can be exploited as a source for structured silicate layers, serving as building units for new framework topologies. A new highly crystalline and stable phase is obtained by directly reconstructing connectivity of UTL layers in a one-step synthesis. An acid treatment, eliminating germanium from the framework before reconnection of the remaining layers, led to the new zeolite topologies, called –COK-14 and COK-14.

Laboratory diffraction experiments indicated that –COK-14 retained some reflections of the parent structure. Indexing of the powder pattern resulted in a unit cell of a = 24.64 Å, b = 13.92 Å, c = 12.26 Å and a monoclinic angle of 109.20° compared to a = 29.00 Å, b = 13.98 Å, c = 12.45 Å and β = 104.91° for the parent UTL. This clearly marked it as a new phase structurally related to UTL zeolite. Since the *bc* planes in UTL zeolite are parallel to the layers, the new material should contain the same layers but stacked in a different way. Nitrogen adsorption measurements revealed that a zeolite with 10- and 12-membered rings was obtained, and chemical analysis indicated that it contained only a very small amount of germanium. ^{29}Si-NMR revealed the framework was not fully connected as indicated by the large concentration of silanol groups. To allow a structure solution, a Rietveld refinement of synchrotron data was per-

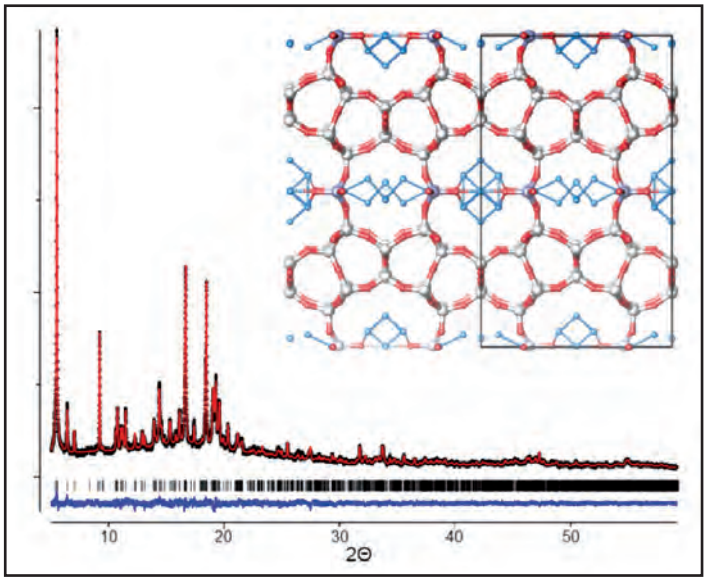

Figure 1

Rietveld refinement of –COK-14 equilibrated with ambient humidity, recorded using synchrotron radiation (λ = 1.1172 Å). Experimental (black) and calculated (red) XRD patterns as well as their difference profile are shown (blue). The short tick marks below the patterns give the position of the Bragg reflections. The inset shows the refined structure (grey silicon, red framework oxygen, blue water oxygen).

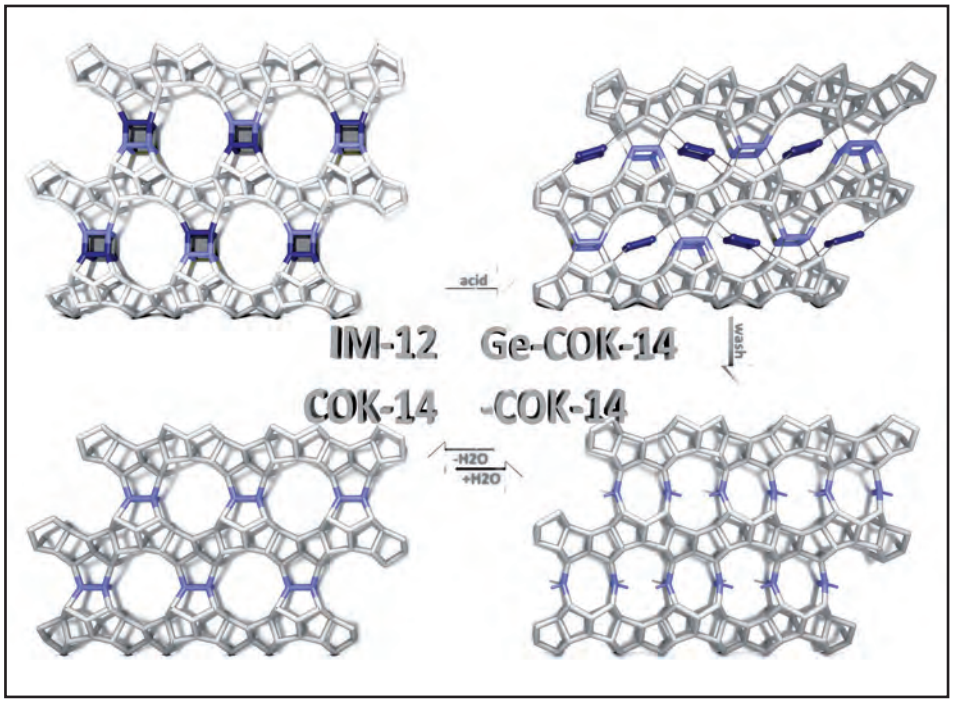

Figure 2

Acid leaching of IM-12 zeolite can dislodge the germanate four-ring (dark blue) and shift it into the channels of the contracted framework of Ge-COK-14. Further acid leaching fully eliminates the germanate four-ring resulting in the interrupted (–COK-14) or fully condensed framework (COK-14) depending on the conditions.

formed (Fig. 1). X-ray powder diffraction experiments on –COK-14 equilibrated with ambient humidity were performed at the B2 beamline at DORIS/DESY in Hamburg at the germanium K-edge (11.1 keV) in transmission geometry. This data revealed –COK-14 as new all-silica interrupted framework presenting a two-dimensional channel system with interconnecting 8-, 10- and 12-membered rings (Fig. 1, Fig. 2).

By further drying while excluding all humidity, silanol condensation takes place, resulting in the formation of the fully connected framework (COK-14) (Fig.2). An inverse sigma transformation, only known as a theoretical concept used for simulation of new frameworks, perfectly describes this transformation. Topologically, two T-atoms of the TO_4 tetrahedra unit along the edges of the double four-rings merge, reducing the cube-like double four-rings to single four-rings (Fig. 2). This transformation can be seen as the reverse process compared to well-known swelling and pillaring procedures.

The occurrence of a true inverse sigma transformation of UTL type zeolite into COK-14 was further investigated. An intermediate state, named Ge-COK-14, was captured where the layers already were disconnected but the detached fragment was not yet removed. In this sample, germanium occurred as germanate four-ring in the position that would later become the 12-membered ring of COK-14 (Fig. 2).

The COK-14 zeolite family is a valuable addition to the all-silica large-pore zeolite types. More new zeolites with attractive pore architectures could be obtained from zeolites containing heteroatoms like germanium allowing a rational design of zeolite topologies.

Contact:
Christine Kirschhock, christine.kirschhock@biw.kuleuven.be

Authors

Elke Verheyen[1], Lennart Joos[2], Kristof Van Havenbergh[3], Eric Breynaert[1], Nataliia Kasian[1,4], Elena Gobechiya[1], Kristof Houthoofd[1], Charlotte Martineau[5], Manuel Hinterstein[6], Francis Taulelle[5], Veronique Van Speybroeck[2], Michel Waroquier[2], Sara Bals[3], Gustaaf Van Tendeloo[3], Christine E. A. Kirschhock[1] and Johan A. Martens[1]

1. Center for Surface Chemistry and Catalysis, KU Leuven, 3001 Heverlee, Belgium
2. Center for Molecular Modeling, Ghent University, 9052 Zwijnaarde, Belgium
3. Electron Microscopy for Materials Science, University of Antwerp, 2020 Antwerp, Belgium
4. L.V. Pisarzhevsky Institute of Physical Chemistry, National Academy of Sciences of Ukraine, 03028 Kyiv, Ukraine
5. Tectospin, Institut Lavoisier, UMR 8180 Université de Versailles ST Quentin en Yvelines, 45 Avenue des Etats Unis, 78035 Versailles Cedex, France
6. Institut für Werkstoffwissenschaft, Technische Universität Dresden, 01062 Dresden, Germany

Original publication

"Design of zeolite by inverse sigma transformation", Nat. Mater. DOI: 10.1038/NMAT3455

References

1. **W. Vermeiren, J.P. Gilson, "Impact of zeolites on the petroleum and petrochemical industry" Top. Catal. 52, 1131–1161 (2009).**
2. **url: http:// izasc-mirror.la.asu.edu/fmi/xsl/IZA-SC/ft.xsl**
3. **A. Corma, M.J. Díaz–Cabañas, F. Rey, S. Nicolopoulus, K. Boulahya, "ITQ-15: The first ultralarge pore zeolite with a bi-directional pore system formed by intersecting 14- and 12-ring channels, and its catalytic implications" Chem. Commun. 12, 1356-1357 (2004).**
4. **J. Paillaud, B. Harbuzaru, J. Patarin, H. Bats, "Extra-large-pore zeolites with two-dimensional channels formed by 14 and 12 rings" Science 304, 990-992 (2004).**

A new route to creating amorphous metallic alloys.

$Sc_{75}Fe_{25}$ metallic nanoglass

Amorphous metallic glasses have improved magnetic and/or mechanical properties compared to their crystalline counterparts, but they are often fragile, like single crystals. We have found improved mechanical properties for the nano-counterpart of bulk metallic glass, a nanoglass, created via consolidation of amorphous nanoparticles. Using temperature annealing, the properties of these nano-structured metallic glasses can be tuned. We followed the growth of lower density interface areas inside the $Sc_{75}Fe_{25}$ nanoglasses as a function of temperature using small- and wide-angle X-ray scattering and observed a nearly perfect transformation of the nanoglass to a bulk metallic glass.

"Nanoglass" or "nanograined metallic glass" is a new kind of material which differs from the glasses available today by its microstructure. Normal glassy materials have an atomic structure of the melt frozen-in at the glass transition temperature, while nanoglasses consist of nanometer-sized amorphous regions that are connected by glass-glass interfaces analogously to intercrystalline boundaries connecting the crystals in a polycrystal. We call these amorphous nanograined materials nanoglasses even though they are not formed by quenching the material from a melt but via consolidation of amorphous nanoparticles. The special nanostructure of nanoglasses gives an opportunity for materials scientists to design amorphous alloys with interesting physical, e.g. mechanical or magnetic, properties. Nanoglasses were introduced for the first time a couple of decades ago [1], but direct information about the sizes of the glass-glass interface regions and the density difference between the glassy core regions and the interfaces has been lacking. Thanks to advances in modern analysis techniques, especially small-angle X-ray scattering (SAXS), we can now study the interfaces more accurately than before.

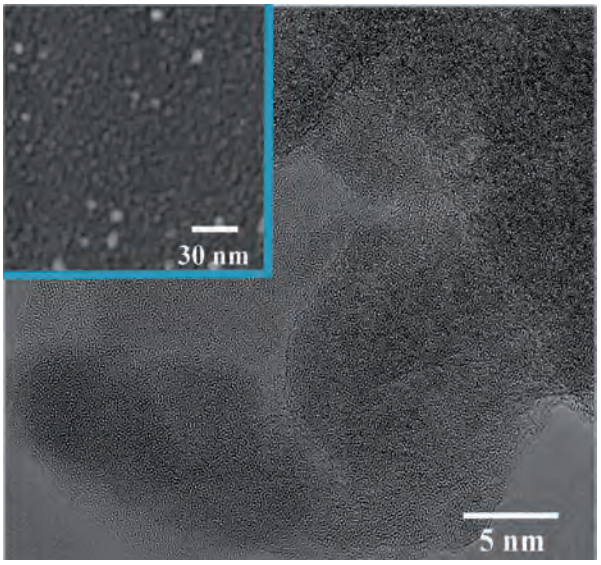

Figure 1

HRTEM image of $Sc_{75}Fe_{25}$ nanoglass powder compacted with 4.5 GPa pressure. Inset in upper left corner shows a TEM image of loose $Sc_{75}Fe_{25}$ nanoparticle powder, similar to the one that was used to produce the consolidated nanoglass.

The possibility to tune the structure of a nanoglass by annealing at temperatures well below the glass transition as well as the crystallization temperatures is an interesting aspect of the new material. The diffusion of atoms from the cores to the interface area would allow for the structure of the nanoglass to slowly approach that of a bulk metallic glass, resulting in a new way of creating amorphous metallic alloys in bulk. Until now, bulk metallic glasses have only been made using the rapid cooling of the melt. The effect of temperature annealing on the nanoglass structure has already been studied via molecular dynamics [2]. To study experimentally the possibilities of altering the glass-glass interface size and density via temperature annealing, we created $Sc_{75}Fe_{25}$ nanoglasses via inert gas condensation and further consolidation with 4.5 GPa pressure with a setup that is described in refs. [3] and [4]. The samples had a diameter of 8 mm and their thickness was 200–400 μm.

Characterization of the prepared $Sc_{75}Fe_{25}$ nanoglass samples was made first with differential scanning calorimeter (DSC), positron annihilation spectroscopy (PAS), elemental mapping, and transmission electron microscopy (TEM). Inset in Fig. 1 shows electron microscopy images of the powder created via condensation, showing particles of a radius of about 7 nm. After consolidation with 4.5 GPa pressure, the nanoglass is formed, but even from the high resolution TEM image in Fig. 1 it is difficult to say where the glass-glass interfaces are and what size they have. To study in more detail the glass-glass interfaces, simultaneous *in situ* small-angle and wide-angle X-ray scattering (SAXS/WAXS) experiments were made at the beamline B1 at the DORIS III synchrotron storage ring. During the

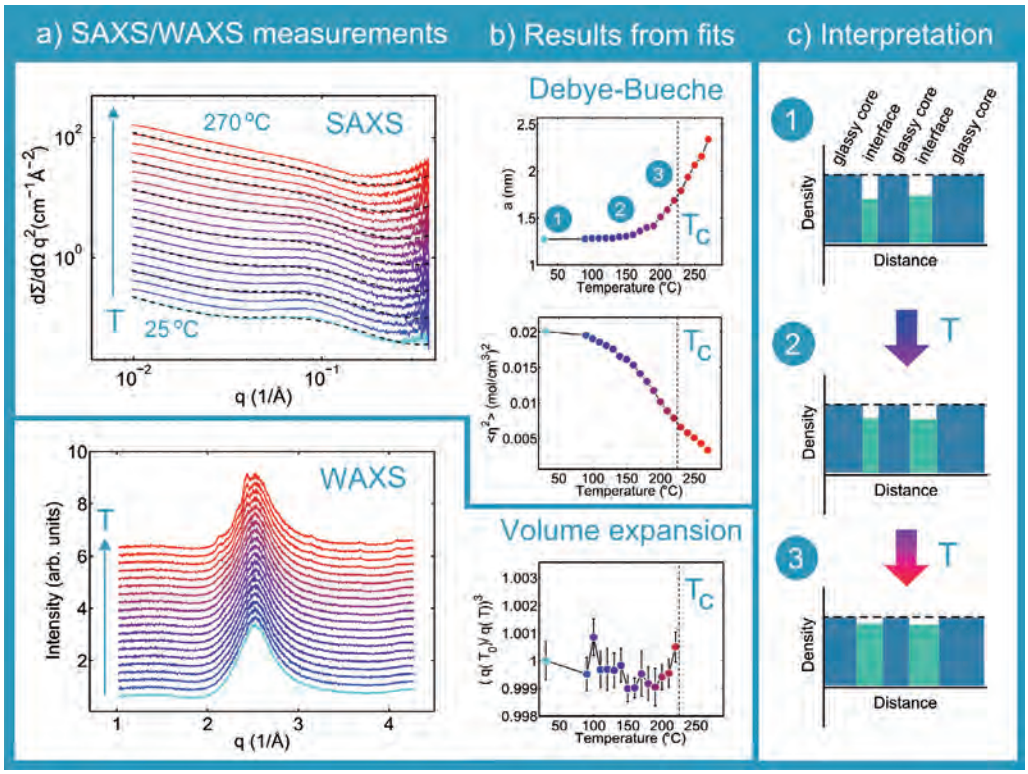

Figure 2

a) SAXS curves have been multiplied by scattering vector length q squared to represent better the small hump related to the electron density difference between the cores and the interfaces. The dashed lines show some of the fits to the data. Except for the room temperature measurement, the SAXS and WAXS curves have been shifted for clarity. b) The fitting results: correlation length a and mean square fluctuation in electron density $<\eta^2>$ from the SAXS curves, and volume expansion $(q(T_0)/q(T))^3$ from the position q of the main peak in the WAXS curves. T_c marks the temperature where crystallization was first observed. c) A schematic model of the density for a cross section of the studied nanoglass showing the delocalization of the voids in the interface towards the cores.

SAXS/WAXS experiment the samples were placed in a heating cell in a vacuum chamber ($P \approx 10^{-4}$ mbar) and heated step-wise up to 270 °C. The onset of crystallization occurred at about 230 °C.

The X-ray experiments in Fig. 2 give us an overview of the growth of the interface areas and the reduction in density difference between the glassy cores and the interfaces while heating. The SAXS data was fitted using the analytical Debye-Bueche random phase model equation [5] with which we can determine a correlation length related to the size of the nanograined structure as well as the mean square fluctuation in electron density.

From the SAXS results, we estimate that before temperature annealing the interface area is about 17 % less dense (in mass) than the core. Approximating the system to be composed of core-shell particles, the total volume fraction of interface areas was estimated to be about 31 %, which is in accord with PAS measurements which gave a volume fraction of about 35 %. Furthermore, we can use the same approximation to attain an average interface width from the correlation length. The analysis indicates that the interface width was exponentially increasing from about 0.8 to 1.2 nm as a function of temperature in the range from 25 to 230 °C, while the density of the interface increased continuously, reaching a density very close to that of the cores.

Microcompression experiments showed more plasticity for the nanoglass specimens than for bulk metallic glass specimens of the same composition. Even after annealing the nanoglass specimens at 200 °C for two hours, the plasticity remained better than in the bulk counterpart. This study shows that it is possible to create monolithic amorphous metallic materials via temperature annealing of nanoglass with improved mechanical properties compared to bulk metallic glasses. These results open the way to a new technique for creating amorphous metallic glasses, a technique similar to powder metallurgy, where improved properties of alloys can be achieved via sintering of crystalline metal powder.

Contact: Herbert Gleiter, herbert.gleiter@kit.edu

Authors

Jixiang Fang[1,2], Ulla Vainio[3], Werner Puff[4], Roland Würschum[4], Xiaolei Wang, Di Wang[1], Mohammad Ghafari[1], Feng Jiang[2], Jun Sun[2], Horst Hahn[1,5] and Herbert Gleiter[1]

1. Institute for Nanotechnology, Karlsruhe Institute of Technology (KIT), Karlsruhe 76021, Germany
2. State Key Laboratory for Mechanical Behavior of Materials and MOE Key Laboratory for Nonequilibrium Synthesis and Modulation of Condensed Matter, Xi'an Jiaotong University, Shann Xi, 710049, People's Republic of China
3. Deutsches Elektronen-Synchrotron DESY, Notkestr. 85, D-22607 Hamburg, Germany
4. Institut für Materialphysik, Technische Universität Graz, Petersgasse 16, A-8010 Graz, Austria
5. Joint Research Laboratory Nanomaterials, Technische Universität Darmstadt, Petersenstr. 32, 64287 Darmstadt, Germany

Original publication

"Atomic Structure and Structural Stability of $Sc_{75}Fe_{25}$ Nanoglasses", Nano Letters 12, 5058-5058 (2012).

References

1. **H. Gleiter, "Our thoughts are ours, their ends none of our own: Are there ways to synthesize materials beyond the limitations of today?", Acta Materialia 56, 5875–5893 (2008).**
2. **D. Sopu, K. Albe, Y. Ritter, H. Gleiter, "From nanoglasses to bulk massive glasses", Appl. Phys. Lett. 94, 191911 (2009).**
3. **J. Jing, A. Kramer, R. Birringer, H. Gleiter, U. Gonser, "Modified atomic-structure in a Pd-Fe-Si nanoglass – A mossbauer study", J. Non-Cryst. Solids 113, 167–170 (1989).**
4. **J. Weissmüller, R. Birringer, H. Gleiter, "Nanostructured crystalline and amorphous solids", Key Eng. Mater. 77, 161–170 (1992).**
5. **P. Debye, H.R. Anderson, Jr., H. Brumberger, "Scattering by an Inhomogeneous Solid. II. The correlation function and its application" J. Appl. Phys. 28, 679–683.**

X-raying protein solutions at deep sea conditions.

Protein interactions studied in osmolyte solutions at high pressures

In deep sea habitats, organisms are exposed to pressures of up to 1000 bar. Such harsh environmental conditions affect both protein stability and metabolism. For instance, in order to cope with hydrostatic pressure stress at deep sea conditions, the level of protecting solutes, compatible osmolytes, is increased intracellularly. A molecular level understanding of the stabilizing effect of such osmolytes under high pressure conditions is still lacking. X-ray scattering experiments on concentrated protein solutions under high pressure conditions allowed to identify the complex interplay between proteins and cosolvents of different nature. These studies shed new light on the stabilization of proteins, ensuring their biological functions also under extreme environmental conditions.

Proteins are very sensitive to environmental conditions such as high and low temperatures or high hydrostatic pressures. Changes to the three-dimensional structure of proteins under high pressure conditions are accompanied by the loss of their biological function. In nature, living organisms are able to compensate for extreme environmental conditions and hence rescue proteins from denaturation, for example, by using osmolytes. Organic osmolytes are accumulated under thermal and pressure stresses. Among these substances are methylamines such as trimethylamine-*N*-oxide (TMAO), which has been found to enhance protein folding and ligand binding most efficiently. On the other hand, urea, a highly concentrated waste product in organisms, is a perturbant which is increasingly concentrated under high pressure conditions. It is also a major organic co-solute in marine elasmobranch fishes. Interestingly, TMAO has been found to counteract perturbations imposed by urea and hydrostatic pressure in deep-sea animals, most effectively at a 2:1 urea:TMAO ratio [1]. The term "piezolyte" has even been coined for this osmolyte. The cytosol of the biological cell is a highly concentrated solution containing many types of biomacromolecules, including proteins at concentrations up to 200 – 300 mg/mL. Hence, in order to reveal the influence of both TMAO and urea, concentrated protein solutions under high pressures conditions served as model system in this study.

We employed small-angle X-ray scattering at BW4 at DORIS III under high hydrostatic pressures to investigate the influence of both osmolytes, TMAO and urea as well as mixtures thereof, on the intermolecular interaction in concentrated solutions of the protein lysozyme. In order to relate the structure factor

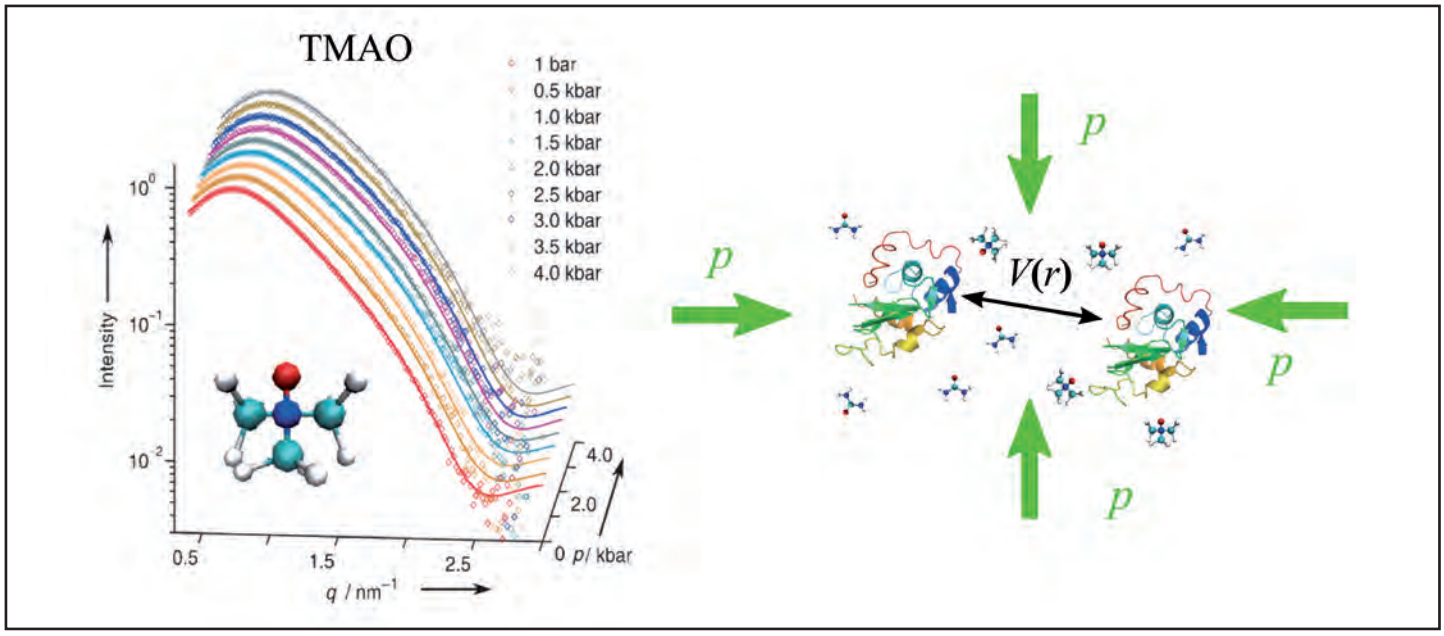

Figure 1

SAXS curves of 100 mg mL^{-1} lysozyme solutions in the presence of 1 M TMAO at different pressures (T = 25°C).

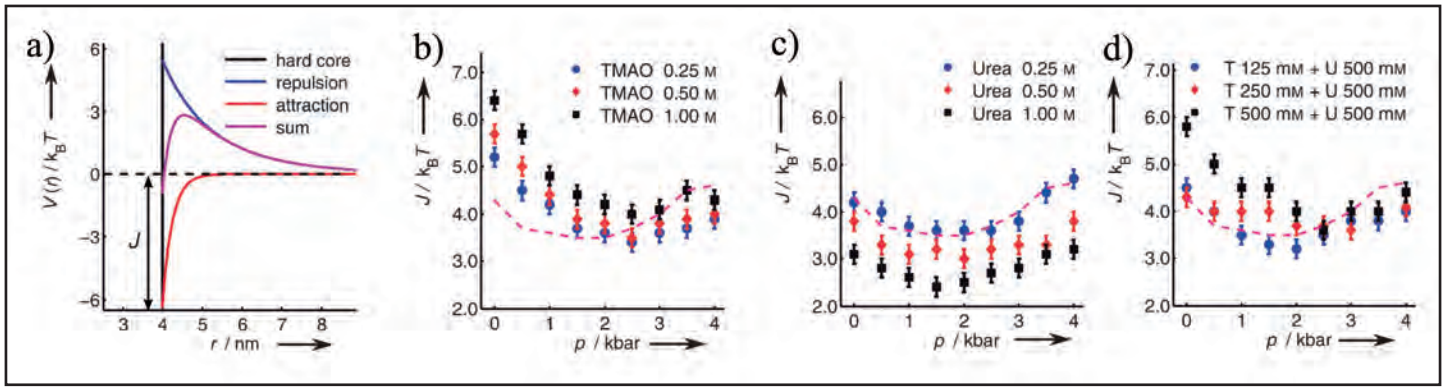

Figure 2

Pressure-dependence of the protein-protein interaction potential $V(r)$ of a concentrated lysozyme solution in the presence of TMAO and urea. a) Different contributions to $V(r)$. The meaning of attraction strength, J, is displayed. b) - d) Pressure dependence of J for TMAO, urea and TMAO-urea mixtures. The dashed line shows the result for the protein in pure buffer solution [2].

to the protein-protein interaction potential, a statistical mechanical model based on the mean-spherical approximation in combination with a DLVO type of potential has been used.

We show (Fig. 1) scattering curves obtained for lysozyme dissolved in water with 1 M TMAO. Fitting the theoretical model to the experimental data allows the extraction of the protein-protein interaction potential $V(r)$ (Fig. 2), which can be described by three contributions: a hard core repulsion, a screened repulsive Coulomb interaction and an attractive van der Waals-like interaction. Taking the pressure dependence of all the parameters involved into account, the central parameter for refining the data is the attraction strength, J.

In the absence of osmolytes we recently observed a nonlinear pressure dependence of the protein-protein interaction $J(p)$ which is largely independent of temperature and salt concentration [2, 3]. This effect is probably related to a collapse of the second hydration shell of water upon pressurization. A similar result is observed in the presence of urea as seen in Fig. 2c which exhibits a minimum of $J(p)$ at 2 kbar. Increasing the urea concentration leads to a decrease of the attraction. Conversely upon addition of TMAO an enhancement of the attractive part of $V(r)$ is observed (Fig. 2b). For mimicking the conditions met in deep-sea organisms SAXS data of mixtures of TMAO and urea were measured. The results for a 0.5 M urea solution with different amounts of TMAO are shown in Fig. 2d and reveal that even in the presence of TMAO concentrations as low as 0.125 M the tendency of urea on $V(r)$ is largely compensated by the addition of TMAO.

The pronounced influence of TMAO on the pressure dependent interaction can be explained by its property as a "water structure maker" as proposed recently [4, 5]: TMAO increases the amount of strong H-bonds in water leading to a strengthening of the H-bond network structure. This in turn moves the second hydration shell of water slightly outwards which is counterbalancing the compression due to the high pressure [6].

In summary, we observe for urea-TMAO mixtures a large counteracting effect on the intermolecular interaction which is qualitatively similar to the mixtures influence on the protein stability. Hence, indirect solvent mediated effects seem to play a major role in protein stabilisation under high pressure conditions. Our findings may thus be of importance for understanding the compensatory effect of urea-TMAO mixtures in deep-sea organisms.

Contact: Martin Schroer, martin.schroer@desy.de, Roland Winter, roland.winter@tu-dortmund.de

Authors

Martin A. Schroer[1], Yong Zhai[2], D. C. Florian Wieland[1], Christoph J. Sahle[1], Julia Nase[1], Michael Paulus[1], Metin Tolan[1] and Roland Winter[2]

1. Fakultät Physik/DELTA, TU Dortmund, Maria-Goeppert-Mayer-Str. 2., 44227 Dortmund, Germany
2. Fakultät Chemie/Physikalische Chemie - Biophysikalische Chemie, Otto-Hahn Str. 6, 44227 Dortmund, Germany

Original publication

"Exploring the Piezophilic Behavior of Natural Cosolvent Mixtures", Angewandte Chemie Intern. Ed. 50, 11413-11416 (2011).

References

1. **P. H. Yancey, "Organic osmolytes as compatible, metabolic and counteracting cytoprotectants in high osmolarity and other stresses", J. Exp Biol. 208, 2819-2830 (2005).**
2. **M. A. Schroer, J. Markgraf, D. C. F. Wieland, Ch.J. Sahle, J. Möller, M. Paulus, M. Tolan, R. Winter,"Nonlinear pressure dependence of the interaction potential of dense protein solutions", Phys. Rev. Lett.106, 178102 (2011).**
3. **J. Möller, M.A. Schroer, M. Erlkamp, S. Grobelny, M. Paulus, S. Tiemeyer, F.J. Wirkert, M. Tolan, R. Winter, "The effect of ionic strength, temperature and pressure on the interaction potential of dense protein solutions: From nonlinear pressure response to pressure-induced protein crystallization", Biophys. J. 102, 2641-2648 (2012).**
4. **S. Paul, G.N Patey, "Structure and interaction in aqueous urea-trimethylamine-N- oxide solutions", J. Am. Chem. Soc., 129, 4476-4482 (2007).**
5. **A. Panuszko, P. Bruzdziak, J. Zielkiewicz, D. Wyrzykowski, J. Stangret, "Effects of urea and trimethylamine-N-oxide on the properties of water and the secondary structure of hen egg white lysozyme", J. Phys. Chem. B 113, 14797-14809 (2009).**
6. **F. Meersman, D. Bowron, A. K. Soper, M. H. J. Koch. Counteraction of urea by trimethylamine N-oxide is due to direct interaction. *Biophys. J.* 97, 2559-2566 (2009).**

Dragonflies and mayflies are sister groups.

Unravelling insect evolution

The early evolution of winged insects (Pterygota) is a longstanding problem in evolutionary biology. Previous studies, focusing on the wings and the genital apparatus, suffered from the fact that the closest relatives of Pterygota - silverfish (Zygentoma) - are wingless and transmit their sperm externally. Therefore, they could not be compared to the winged insects in these regards. We circumvented these problems by studying the insect head using SR-microCT to accomplish the detailed anatomic analysis of a wide range of specimens in a reasonable timeframe. Our results indicate a sister group relationship between a clade Palaeoptera (dragonflies + mayflies) and the mega diverse insect lineage Neoptera (comprising all remaining winged insects) for the first time using head morphology as the data base.

When trying to hypothesize the earliest branching events within winged insects (Pterygota), i.e. the relationships between dragonflies (Odonata), mayflies (Ephemeroptera) and all remaining winged insects (Neoptera), fundamental problems become apparent. As a consequence of the flight apparatus evolution a drastic redesign of the thoracic morphology took place. This makes reliable homology hypotheses of several thoracic elements between wingless (apterygote) and winged (pterygote) lineages very problematic. In a phylogenetic context, the definition of characters (primary homology hypotheses) is impossible. A similar dilemma exists with characters related to the reproductive system due to the drastically different mode of sperm transfer, i.e. externally deposited spermatophores (silverfish) versus internal fertilization using an intromittent organ (winged insects). Again, this hampers the homologisation between wingless and winged insect lineages and character state polarisation. Nonetheless, these character systems have been used for decades to reconstruct the early evolution of winged insects [2,3]. Basically, our approach is to infer the evolution of the early winged insect lineages by choosing another body region. The head is perfectly suitable as it is not directly affected by the evolution of the flight apparatus or the modified sperm transfer. The homologisation of head structures between bristletails (Archaeognatha), silverfish (Zygentoma) and the winged lineages of insects (Pterygota) is straightforward and unproblematic.

To contribute to a resolution of the persistent problem of early insect evolution, we studied the complex head anatomy of representatives of all major insect lineages including a bristletail, a silverfish, eight species of mayflies, seven species of dragonflies, and 30 representatives of all major neopteran lineages. Eighteen taxa were represented by original data.

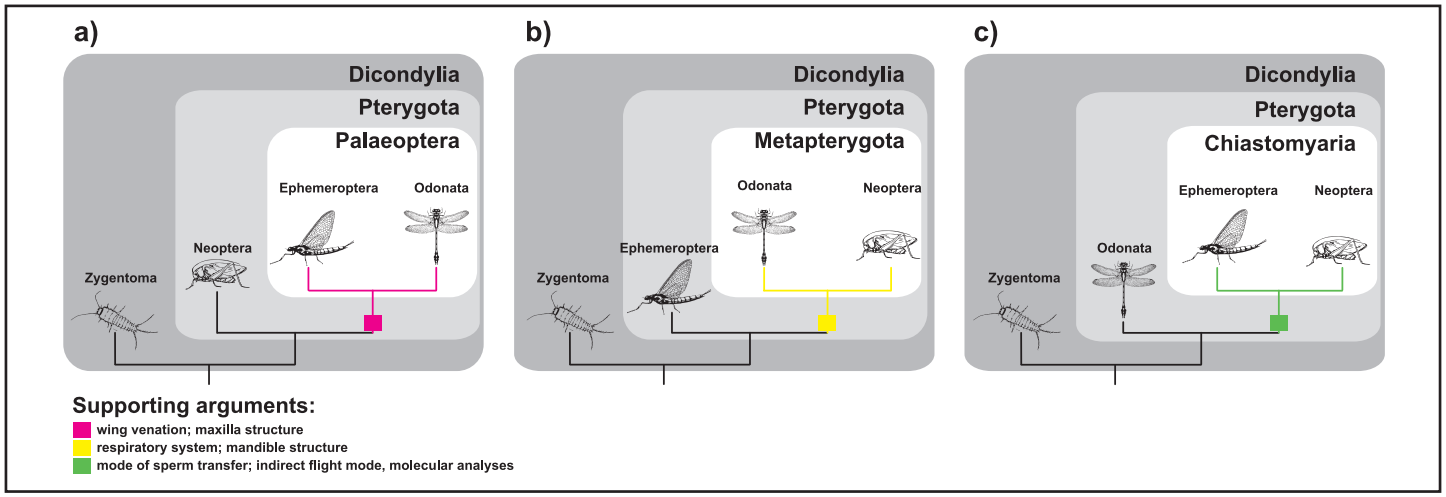

Figure 1

The most frequently encountered hypotheses and the supporting arguments concerning relationships of mayflies (Ephemeroptera), dragonflies (Odonata), and all remaining winged insects (Neoptera). a) Palaeoptera (Odonata + Ephemeroptera); b) Metapterygota (Odonata + Neoptera); c) Chiastomyaria (Ephemeroptera + Neoptera).

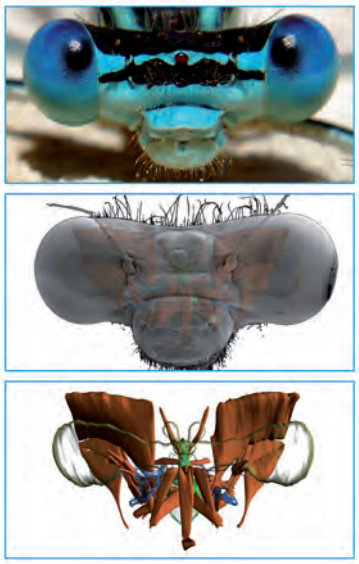

Figure 2

The outer and inner anatomy of Coenagrion puella in frontal view. A part of the muscle equipment (orange), the brain (yellow), pharynx (green), and some endoskeletal features (blue) are shown. From top down: photo of the head; scanning-electron microscopy image with an overlay of the anatomic features to show the spatial distribution; pure 3D reconstruction of anatomic features based in SR-microCT data.

The anatomy was investigated using synchrotron micro-Computer Tomography (SR-microCT). Prior to scanning, samples were dried at the critical point and mounted on specimen holders. Except for *Siphlonurus lacustris* (Ephemeroptera) and *Thermobia domestica* (Zygentoma), all specimens were scanned at the beamline BW2/DORIS III using a monochromatic X-ray beam at 8 keV photon energy. The tomography station at this beamline operated by Helmholtz-Zentrum Geesthacht (HZG, Geesthacht, Germany) is optimized for performing high-density resolution microtomography [1] . *T. domestica* and *S. lacustris* were scanned at the Swiss Light Source (SLS, Villigen, Switzerland).
External and internal morphological characters comprise 19 characters of the head capsule, six labral characters, 22 characters of the antennae, 13 tentorial characters, 13 mandibular characters, 17 characters of the maxillae, 33 labial characters and 16 characters of the hypopharynx, salivarium and oesophagus. Our morphological investigation clarified many seemingly ambiguous features described in earlier studies.

Analyses support a sister group relationship between a clade Palaeoptera (dragonflies + mayflies) and the mega diverse insect lineage Neoptera (comprising all remaining winged insects) for the first time using head morphology.

A sister group relationship between the two most ancestral pterygote lineages, dragonflies and mayflies, was up to now not supported by any character of the head. Features of the mandibular articulation and muscle equipment strongly pointed towards a clade Metapterygota. In the present study, all characters potentially supporting alternative concepts (e.g., Metapterygota, Chiastomyaria) are taken into account. Nevertheless, a clade Palaeoptera (Odonata + Ephemeroptera) is consistently supported.

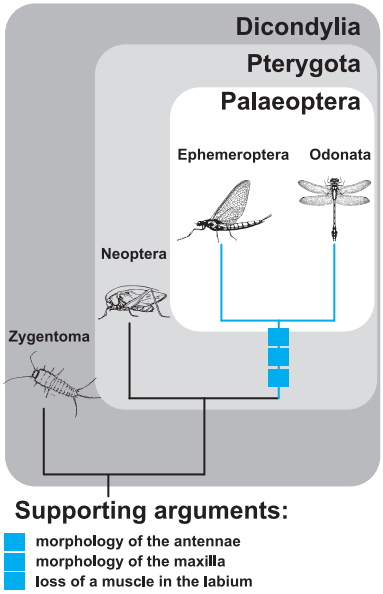

Figure 3

The resulting hypothesis concerning relationships of the early winged lineages of insects.

Past morphological studies gave the impression that the basal splitting events of winged insects are based on robust theories derived from mandible anatomy [4]. The present study shows that this is by no means true. Even though the phylogenetic hypothesis presented here may be preliminary, the well-documented SR-microCT data will allow a better understanding of character transformations in the early evolution of Pterygota. A stepwise progress in this direction will also reveal possible interconnections of different characters and character systems and features, which require more detailed investigations. This process will very likely lead to a well-founded and detailed evolutionary scenario of the winged insects, arguably the most successful group of organisms.

Contact: Alexander Blanke, blanke@uni-bonn.de

Authors

Alexander Blanke[1], Benjamin Wipfler[2], Harald Letsch[3], Markus Koch[4], Felix Beckmann[5], Rolf Beutel[2] and Bernhard Misof[1]

1. Forschungsmuseum Alexander Koenig, Adenauerallee 160, 53113 Bonn, Germany
2. Entomology Group, Institut für Spezielle Zoologie und Evolutionsbiologie, Friedrich-Schiller-Universität Jena, Erbertstraße 1, 07743 Jena, Germany
3. Department für Tropenökologie und Biodiversität der Tiere, Universität Wien, Rennweg 14, A-1030 Vienna, Austria
4. Institute of Evolutionary Biology and Animal Ecology, University of Bonn, An der Immenburg 1, 53121 Bonn, Germany
5. Institute of Materials Research, Helmholtz-Zentrum Geesthacht, Max-Planck-Str. 1, 21502 Geesthacht, Germany

Original publication

„Revival of Palaeoptera – head characters support a monophyletic origin of Odonata and Ephemeroptera (Insecta)“ Cladistics 1 – 22 (2012). DOI: 10.1111/j.1096-0031.2012.00405.x.

References

1. **F. Beckmann, J. Herzen, A. Haibel, B. Müller, and A. Schreyer. “High density resolution in synchrotron-radiation-based attenuation-contrast microtomography”. Proceedings of SPIE 7078, Devlopments in X-Ray Tomography VI, 70781D (2008).**
2. **N. P. Kristensen, “The phylogeny of hexapod “orders”. A critical review of recent accounts”. Journal of Zoological Systematics and Evolutionary Research 13, 1-44 (1975)**
3. **J. Kukalová-Peck, “Phylogeny of higher taxa in Insecta: Finding synapomorphies in the extant fauna and separating them from homoplasies”. Evolutionary Biology 35, 4-51 (2008).**
4. **A. H. Staniczek, “The mandible of silverfish (Insecta: Zygentoma) and mayflies (Ephemeroptera): Its morphology and phylogenetic significance”. Zoologischer Anzeiger 239, 147-178 (2000).**

Transport of matter by aqueous fluids in the deep Earth.

The case of zirconium

Aqueous fluids are important agents in the deep Earth that are responsible for large-scale transport of matter, even into the Earth's atmosphere through volcanic activity. The conditions controlling mineral dissolution and element transport by supercritical aqueous fluids are still poorly understood, which partially stems from the difficulty in obtaining reliable data on fluid-mineral interaction at high pressure and temperature. Valuable insights are gained by combining diamond anvil pressure cells with synchrotron radiation. We used X-ray fluorescence analysis and X-ray absorption spectroscopy to investigate *in situ* the solubility of the mineral zircon and the complexation of Zr in the aqueous fluid.

Oceanic crust steadily forms from the Earth's mantle by magmatism at mid-ocean ridges. After emplacement, interaction with the water of the overlying ocean leads to formation of OH-bearing minerals throughout the oceanic lithosphere. At convergent plate boundaries this hydrated lithosphere descends back into the mantle in a process termed "subduction". Subduction leads to formation of aqueous supercritical fluids and fluid-induced magmatism with abundant volcanism (Fig. 1). Fluids and melts are responsible for large-scale chemical redistribution and mass transfer in this "subduction factory" and as such, these processes are fundamental to the Earth's evolution. They mediate global cycling of elements and over time produced the continental crust [1].

High-field-strength elements (e.g. Ti, Zr, Hf, Nb, Ta) in natural rocks are important petrogenetic indicators providing insight into chemical processes in the deep Earth. Zr and Hf are predominantly hosted by the accessory mineral zircon $(Zr,Hf)SiO_4$, which occurs in nature as a Zr-rich solid solution (~98 - 99 wt% $ZrSiO_4$). Dissolution and re-crystallization of zircon therefore strongly controls the mobility of Zr and Hf in the deep Earth. However, little is known about the solubility of zircon in aqueous solutions at high pressures and temperatures, or the incorporation mechanism of Zr and Hf in aqueous fluids.

We studied the dissolution of zircon at *in situ* conditions in aqueous fluids. We added Na-Al silicate components to the aqueous solution to model fluids that had equilibrated with silicate minerals of subducting oceanic crust. We used a hydrothermal diamond cell (HDAC, Fig. 2a) to determine the Zr contents in aqueous fluids *in situ* by X-ray fluorescence (XRF) spectroscopy. With the same apparatus, the complexation of Zr in fluids was constrained by *in situ* X-ray absorption near edge structure (XANES) measurements at the Zr K-edge, performed on fluids in equilibrium with zircon. *In situ* micro-XRF analysis was performed at beamline L of DORIS III with a confocal XRF setup in order to enhance the signal to noise ratio [2]. Resolution-enhanced Zr XANES spectra were acquired in fluorescence mode at ID 26 of the ESRF using a high-resolution wavelength dispersive spectrometer in Rowland geometry [3].
Zircon solubility is strongly enhanced by addition of $Na_2Si_3O_7$ (NS3) to H_2O (Fig. 2b). The degree of enhancement varies with $Na_2Si_3O_7$ concentration. Zircon solubility in these fluids decreases considerably with pressure and increases slightly with temperature. Addition of Al_2O_3 decreases the zircon solubility. In H_2O-NaAlSi$_3O_8$ fluids, Zr concentrations are in the sub-ppm to ppm range, still orders of magnitude above contents expected for pure H_2O at similar conditions. Zr contents in NaOH solutions in equilibrium with monoclinic ZrO_2 increase with pressure and temperature.

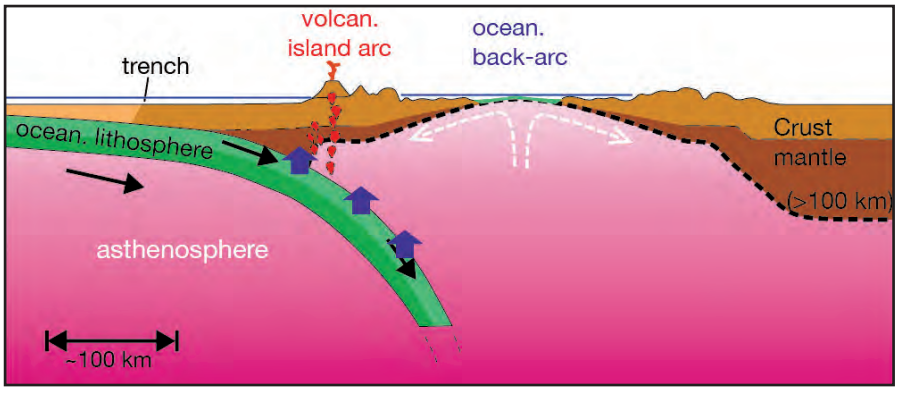

Figure 1

Schematic depth profile of the Earth at subduction zones. Hydrated dense oceanic lithosphere is subducted into the mantle (black arrows). During subduction, increase of pressure and temperature leads to decomposition of OH-bearing minerals and produces aqueous fluids (blue arrows). Aqueous fluids will hydrate the overlying asthenosphere/mantle. Hydration lowers the melting temperature, leading to magma formation and ultimately to volcanic eruptions at the Earth's surface. (Figure courtesy of R. Bousquet. Modified after [4].)

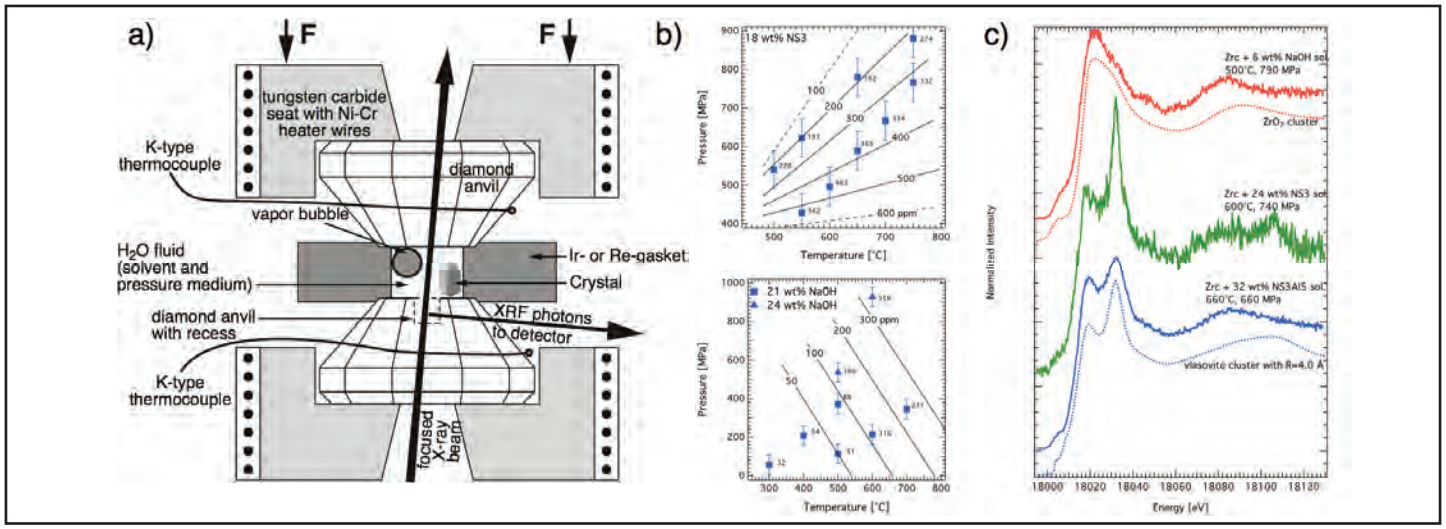

Figure 2

a) Sketch of externally heated hydrothermal diamond anvil cell. The aqueous fluid present in the recess of one diamond represents the volume probed by XRF analysis. Concentrations are determined by comparison of XRF intensities to those measured on standard solutions loaded into the HDAC. Modified after [4]. b) (top) Solubility of zircon in aqueous fluid containing 18 wt% $Na_2Si_3O_7$ (NS3) as a function of pressure and temperature; (bottom) solubility of monoclinic ZrO_2 in NaOH-solution. Tags indicate Zr concentrations in the fluid and lines indicate isopleths of Zr content. c) Experimental and calculated by Feff [7] XANES spectra at the Zr K-edge of aqueous fluids at P and T for various compositions as indicated.

The different dependence of the Zr contents on pressure and temperature in silicate-H_2O fluids and in NaOH-solutions points to different complexation of Zr. In Na-Al silicate-bearing fluids, Zr likely complexes with silicate components in the fluid.

In situ XANES spectra collected on Zr in H_2O + $Na_2Si_3O_7$, H_2O + $Na_2Si_3O_7$ + Al_2O_3, H_2O + NaOH, and H_2O + HCl fluids in equilibrium with zircon provide evidence for strong differences in the Zr complexation between these fluids. Comparison of XANES spectra to those of model compounds and ab-initio simulations of XANES spectra revealed $^{[7]}$Zr for the NaOH solution (Fig. 2c). $^{[6]}$Zr is found for the Na-Al-silicate-bearing solutions. Formation of alkali zircono-silicate complexes is indicated by the similarity of XANES spectra to spectra simulated based on the local structure around Zr in the alkali zircono-silicates such as vlasovite ($Na_2ZrSi_4O_{11}$). For zircon dissolved in HCl-solution (not shown), our data indicate that Zr is coordinated by both O and Cl.

Zirconium complexation by alkali zircono-silicate complexes has not previously been identified as a mechanism for enhancement of Zr concentrations in natural aqueous fluids. In nature, aqueous fluids will equilibrate with silicate minerals and thus will contain substantial silica, alumina and alkalis at high pressure and temperature. Therefore, the enhancement of solubility by alkali zircono-silicate complexes is likely to occur also in natural systems.

This study highlights that combination of experiments at high pressure and temperature with *in situ* analysis based on synchrotron radiation provides unique insights to fundamental processes in geological systems. The results imply that interactions between aqueous fluid and rock matrix in the deep Earth will have a strong effect on its capability in mobilizing Zr or high-field strength elements in general. Significantly, incongruent dissolution of common minerals like feldspar or mica will result in aqueous fluids with high alkali-aluminium ratios, for which our data suggests substantial concentrations of Zr. Positive correlation between signs of zircon crystallization and abundance of phyllosilicates observed in nature [6] further support this idea.

Contact: Max Wilke, max@gfz-potsdam.de

Authors

Max Wilke[1], Christian Schmidt[1], Julien Dubrail[1], Karen Appel[2], Manuela Borchert[2], Kristina Kvashninia[3] and Craig E. Manning[4]

1. Deutsches GeoForschungsZentrum GFZ, Telegrafenberg, 14473 Potsdam, Germany
2. Deutsches Elektronen-Synchrotron, Notkestr. 85, 22607 Hamburg, Germany
3. European Synchrotron Radiation Facility, 6 rue Horowitz, 38043 Grenoble, France
4. Department of Earth and Space Sciences, University of California, Los Angeles, 90025-1567, USA

Original publication

"Zircon solubility and zirconium complexation in H_2O + Na_2O + SiO_2 ± Al_2O_3 fluids at high pressure and temperature", Earth and Planetary Sciences Letters 349-350, 15-25 (2012).

References

1. **C. Manning, "The chemistry of subduction-zone fluids", Earth Planet. Sci. Lett. 223, 1-16 (2004).**
2. **M. Wilke, K. Appel, L. Vincze, C. Schmidt, M. Borchert, S. Pascarelli, "A confocal set-up for micro-XRF and XAFS experiments using diamond-anvil cells", J. Synchr. Rad. 17, 669-675 (2010).**
3. **P. Glatzel, U. Bergmann, "High resolution 1s core hole X-ray spectroscopy in 3d transition metal complexes—electronic and structural information", Coord. Chem. Rev. 249, 65-95 (2005).**
4. **R.D. Hyndman, S.M. Peacock "Serpentinization of the forearc mantle", Earth Planet. Sci. Let. 212, 417-432 (2003).**
5. **C. Schmidt, K. Rickers, R. Wirth, L. Nasdala, J. Hanchar, "Low-temperature Zr mobility: An in situ synchrotron-radiation XRF study of the effect of radiation damage in zircon on the element release in H_2O + HCl ± SiO_2 fluids", Am. Mineral. 91, 1211-1215 (2006).**
6. **D.C. Hay, T.J Dempster, "Zircon behaviour during low-temperature metamorphism", J. Petrol. 50, 571-589 (2009).**
7. **J.J. Rehr, R.C. Albers, "Theoretical approaches to x-ray absorption fine structure", Rev. Modern Phys. 72, 621-654 (2000)**

Turbo switch of calcium pump in biological cells.

Unexpected mechanism of calcium pump

In eukaryotes, calmodulin-stimulated calcium pumps, including plasma-membrane Ca^{2+}-ATPases (PMCA), are key regulators in intracellular Ca^{2+} concentration. These pumps contain an on-off switch, however the precise mechanism of how they are regulated remained elusive. We determined the structure of a PMCA regulatory domain in complex with calmodulin by X-ray crystallography and small-angle X-ray scattering (SAXS). Using an interdisciplinary approach combining biochemical and biophysical data with mathematical modelling we found that the on-off switch of the pump has a previously unknown third position, in which the pump changes into the turbo gear.

The element calcium plays a central role in many processes of life, such as cell division and the communication of cells [1]. The decisive factor is a gradient in the calcium concentration, which is normally high outside the cell and low inside it. For example, under stress the calcium concentration in the cell increases and triggers a corresponding reaction. Afterwards, the concentration must be lowered again. The calcium gradient is maintained among others through a calcium pump, known as PMCA (plasma-membrane calcium-ATPase), which occurs in all higher organisms (eukaryotes). PMCAs are high-affinity calcium pumps that export Ca^{2+} from the cytosol to the extracellular environment of eukaryotic cells and thus are fundamental for the control of overall Ca^{2+} homoeostasis and local intracellular Ca^{2+} signalling [2].

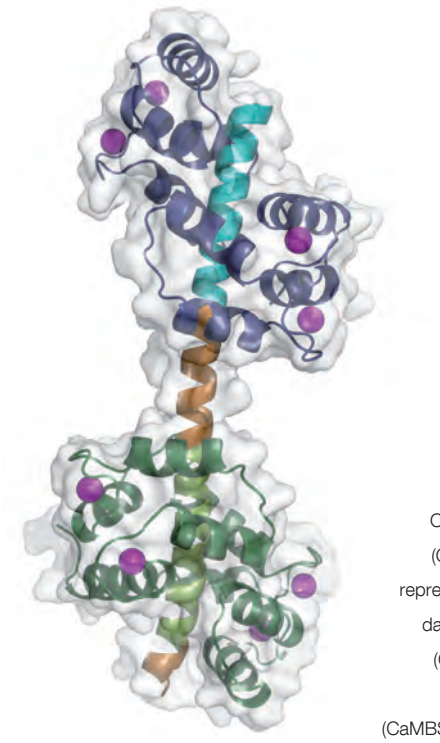

Figure 2

Overall structure of the *A. thaliana* $(CaM)_2$/ACA8R complex. Cartoon representation with CaM molecules in darkgreen (CaMBS1) and darkblue (CaMBS2) and ACA8R in orange, lightgreen (CaMBS1) and cyan (CaMBS2). Ca^{2+} are shown in magenta.

Because the export of calcium out off the cell requires a lot of energy, it is important that the pump is only activated when needed. The pump thus has a switch, which is actuated by the protein calmodulin. When calcium binds to calmodulin, the latter changes its shape so that it can dock onto a binding site of the cell's calcium pump, thereby activating the pump. When the calcium concentration in the cell increases, more and more pumps are thus switched on, however, the detailed mechanism of this regulation was unknown.

We determined the structure of the complex between a PMCA regulatory domain and calmodulin by X-ray crystallography and small-angle X-ray scattering (SAXS). Crystallised samples of the calcium pump complex are shown in Fig. 1. The structure shows an overall dumbbell shape and reveals an unexpected 2:1 stoichiometry (Fig. 2). To our great surprise, we found that the calcium pump has two binding sites for calmodulin and not just one as previously thought. While the first site (CaMBS1) had been previously mapped by mutational studies [3], the second binding site (CaMBS2) was unknown and unexpected.

SAXS data of the complex in solution agree with the 2:1 complex crystal structure. The distance distribution function shows two separated peaks indicating the presence of two subdomains, and the *ab initio* SAXS model superimposes with the crystal structure (Fig. 3). This indicates that the 2:1 complex is indeed the favoured, stable complex in solution.

We next determined whether the newly discovered second CaM-binding site has a biological significance. *In vivo* yeast complementation tests and activity assays indeed revealed that pumps in which one site was disabled could not run at full power. These results show that the calcium pump is controlled in three steps. Under low Ca^{2+} concentrations the pump is inactive. If the concentration rises, binding of calmodulin to one site within the regulatory domain leads to a basal activity state,

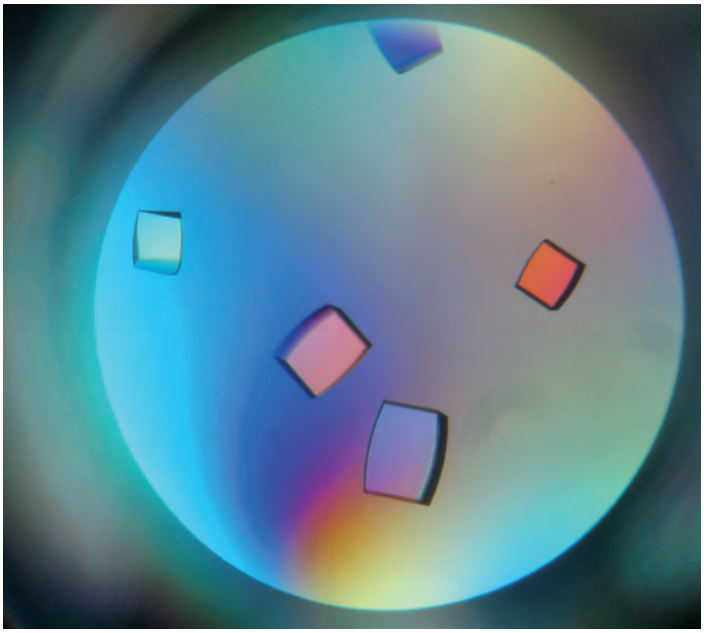

Figure 1
Crystals of the $(CaM)_2$/ACA8R complex from *A. thaliana*. Crystals were obtained by the sitting-drop vapor diffusion method and grew to max. dimensions of 0.7 x 0.35 x 0.2 mm.

while even higher Ca^{2+} concentration will cause full pump activity via binding of calmodulin to both sites.
The pump is thus activated step by step, depending on how much calcium is present in the cell. When the calcium concentration increases, the pump first operates in an energy-efficient way at moderate speed. If the calcium threatens to reach an amount that is dangerous for the cell, the pump changes into the turbo gear, which enables it to very quickly reduce the concentration.

Figure 3
Comparison between crystal and solution structure of $(CaM)_2$/ACA8R complex. *Ab initio* shape reonstruction based on SAXS data superimposed on crystal structure of $(CaM)_2$/ACA8R complex. The results show good agreement between crystal and solution structure.

Mathematical modelling indicates that the role of the second calmodulin-binding site is to maintain a stable, basal level at a threshold Ca^{2+} concentration, where steep activation occurs. This mechanism is present in plants and mammals despite the lack of sequence similarity and different location of their regulatory domains (N-terminus in plants, C-terminus in mammals).

In conclusion, we have developed a general structural model for calmodulin-mediated regulation of calcium pumps involving a turbo switch and allowing a stringent and highly responsive control of intracellular calcium concentration in eukaryotes. This discovery not only improves our understanding of a fundamental mechanism in the biology of all higher organisms, but could one day allow for better treatment of certain diseases in which the calcium balance is disturbed.

Contact: Henning Tidow, het@mb.au.dk

Authors

Henning Tidow[1,2], Lisbeth R. Poulsen[1,3], Antonina Andreeva[4], Michael Knudsen[1,5], Kim L. Hein[1,2], Carsten Wiuf[6], Michael G. Palmgren[1,3] and Poul Nissen[1,2]

1. Centre for Membrane Pumps in Cells and Disease – PUMPKIN, 8000 Aarhus C, Denmark
2. Department of Molecular Biology, Aarhus University, Gustav Wieds Vej 10c, DK - 8000 Aarhus C, Denmark
3. Department of Plant Biology and Biotechnology, University of Copenhagen, Thorvaldsensvej 40, DK - 1871 Frederiksberg C, Denmark
4. MRC Laboratory of Molecular Biology, Hills Road, Cambridge CB2 0QH, UK
5. Bioinformatics Research Centre, Aarhus University, C.F. Møllers Allé 8, DK - 8000 Aarhus C, Denmark
6. Department of Mathematical Sciences, University of Copenhagen, Universitetsparken 5, DK - 2100 Copenhagen, Denmark

Original publication

"A bimodular mechanism of calcium control in eukaryotes", Nature, doi:10.10138/nature11539 (2012).

References

1. **D. E. Clapham, "Calcium signaling", Cell 131, 1047-1058 (2007).**
2. **M. Brini and E. Carafoli, "Calcium pumps in health and disease", Physiol. Rev. 89, 1341 - 1378 (2009).**
3. **L. Baekgaard et al., "The plant plasma membrane Ca^{2+} pump ACA8 contains overlapping as well as physically separated autoinhibitory and calmodulin-binding domains", J. Biol. Chem., 281, 1058 - 1065 (2006).**

Superhelical architecture of myomesin.

Unravelling the secret of muscle elasticity

The process by which active muscles can generate substantial mechanical forces and still remain elastic and keep their overall organisation presents an interesting problem and one that is still not fully understood. Using a hybrid structural approach we have been able to determine the architecture of a section of the muscle filament linking protein myomesin. The data show that myomesin is folded into a superhelical coil arrangement and acts as a highly elastic ribbon that can be stretched up to 2.5 times its original length. This mechanism has never been observed before and could explain how muscles can behave elastically while still keeping their overall structural organisation.

Active muscles are capable of generating extensive mechanical forces by cycles of contraction and relaxation. These processes rely on molecular structures of extreme stability that ensure the muscle fibres resume and maintain an ordered state despite being subjected to these extreme forces. Striated muscle, found in skeletal and cardiac muscle cells, is a sophisticated and highly efficient machinery which transforms chemical energy into movement. It represents a highly organized cellular system for studying and understanding just how active forces can be generated while the overall structural organization of the underlying sarcomeric units is maintained.

The fundamental unit of the muscle cell, the sarcomere, is a highly ordered assembly consisting of filament systems (namely the thick filament composed of myosin, the thin of actin and the elastic of titin) and a number of bands or discs associated with these filaments making up the cytoskeleton. This cytoskeleton consists of three basic structural elements – alpha-actinin, which anchors the thin filaments in the so-called Z-discs at the periphery of the sarcomere, myomesin, which crosslinks the thick filaments in the central M-band, and titin. The M-band ensures the packing regularity of the thick filaments and the uniform distribution of the tension across the myosin filaments during contraction (Fig. 1).

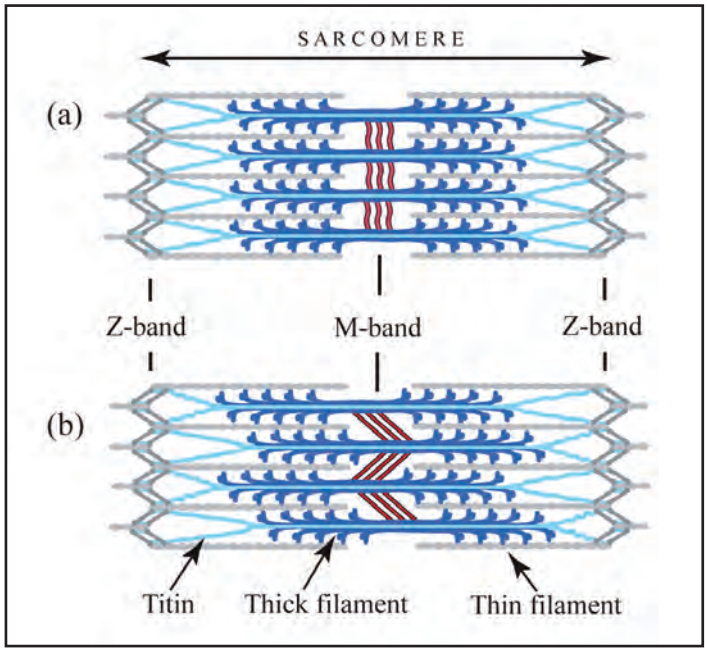

Figure 1

Diagram showing the assembly of the sarcomere. (a) Relaxed sarcomere, (b) after isometric contraction causing tension in the M-band and sliding between thick filaments (from Tskhovrebova and Trinick [7]).

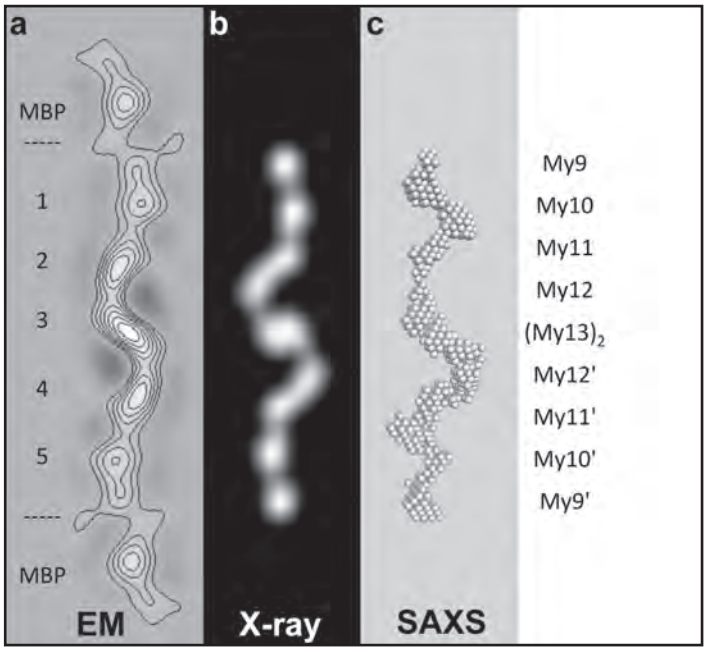

Figure 2

Cross-validation of the overall structure of the dimeric tail-to-tail My9–My13 filament as shown by electron microscopy, X-ray crystallography (low pass filtered to 30Å resolution) and small angle X-ray scattering.

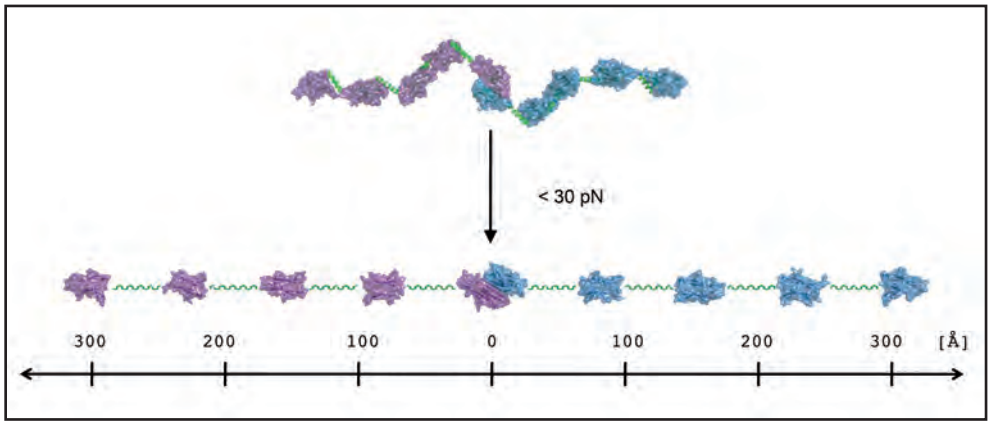

Figure 3

Representation of the C-terminal part of myomesin tail-to-tail filament structure.The alpha helical linkers are shown in green. A ruler, providing an overall length estimate of the extended filament is shown below. The lower image shows the extended filament at 2.5 times its original length.

Upon activation of the muscle cell, both substantial axial and radial forces are generated within the overall sarcomere structure [1]. To maintain a constant sarcomere volume under defined physiological conditions, these forces can lead to changes in both radial and longitudinal contour dimensions of the sarcomere. Under typical tension conditions, M-band-associated thick filaments can substantially move away from the sarcomeric center by 0.1 µm or more, which can lead to M-band-induced instability of the sarcomere [2]. Due to the presence of a stiff Z-disk architecture at the sarcomeric periphery, the amount of movement decreases with the overall sarcomere length so that the resting tension stays constant. In cardiac muscles, elastic M-band motions are thought to correlate with heart beat rate [3], rendering investigations of the underlying molecular parameters highly relevant to heart and skeletal muscle research.

To ensure that the sarcomere retains its shape and form, there are two principal structural compartments with elastic properties. One of these two sites for molecular elasticity is within the M-band, in which so-called M-bridges transversely connect thick filaments with each other and with titin filaments [4]. At the molecular level, M-bridges are thought to be primarily composed of myomesin (*MYOM1*), which is universally expressed, and two related isoforms, *MYOM2* and *MYOM3*, which show tissue-specific expression [5]. However, in the absence of ultrastructural data at a molecular resolution, the overall organisation of M-bridges, and any associated requirements for molecular elasticity, has remained largely unknown to date.

To address this we have made use of a previous prediction suggesting that the entire C-terminal part of the myomesin filament consists of an array of repetitive Ig domains followed by exposed α-helical linkers [6]. By using a number of structural biology methods such as X-ray crystallography, electron microscopy and small angle X-ray scattering, we were able to determine the architecture of the C-terminal immunoglobulin domain array of myomesin (Fig. 2). The data reveal a dimeric tail-to-tail filament structure of about 360 Å in length which is folded into an irregular superhelical coil arrangement of virtually identical α-helix/domain modules (Fig. 2,3). Additional atomic force microscopy studies show that this part of myomesin can be stretched to ca. 2.5 times its original length by reversible unfolding of the α-helical linkers (Fig. 3). The findings demonstrate that the protein can adapt its overall length to dimensions that match those observed in working myofibrils. The data also demonstrate how repetitive domain modules may generate highly elastic protein structures, and future studies will determine whether this mechanism is unique to myomesin or whether it also occurs in other filament systems.

Contact: Matthias Wilmanns, matthias.wilmanns@embl-hamburg.de

Authors

Nikos Pinotsis[1,2], Spyros D. Chatziefthimiou[2,4], Felix Berkemeier[5], Fabienne Beuron[3], Irene M. Mavridis[4], Petr V. Konarev[2], Dmitri I. Svergun[2], Edward Morris[3], Matthias Rief[5] and Matthias Wilmanns[2]

1. Max F. Perutz Laboratories, University of Vienna, Campus Vienna Biocenter 5, A-1030 Vienna, Austria
2. European Molecular Biology Laboratory Hamburg, Hamburg, Germany,
3. Section of Structural Biology, The Institute of Cancer Research, Chester Beatty Laboratories, London, United Kingdom,
4. Institute of Physical Chemistry, National Centre for Scientific Research Demokritos, Athens, Greece,
5. Institute for Biophysics and Munich Center for Integrated Protein Science, Physics Department, Technical University of Munich, Garching, Germany

Original publication

"Superhelical Architecture of the Myosin Filament-Linking Protein Myomesin with Unusual Elastic Properties". PLoS Biol 10(2): e1001261. doi:10.1371/journal.pbio.1001261

References

1. **B. M. Millman, "The filament lattice of striated muscle", Physiol. Rev. 78, 359–391 (1998).**
2. **R. Horowits, R. J. Podolsky, "The positional stability of thick filaments in activated skeletal muscle depends on sarcomere length: evidence for the role of titin filaments", J. Cell Biol. 105, 2217–2223 (1987).**
3. **H. T. Pask, K. L. Jones, P. K. Luther, J. M. Squire, "M-band structure, M-bridge interactions and contraction speed in vertebrate cardiac muscles", J. Muscle Res. Cell. Motil. 15, 633–645 (1994).**
4. **I. Agarkova, J. C. Perriard, "The M-band: an elastic web that crosslinks thick filaments in the center of the sarcomere", Trends Cell Biol. 15, 477–485 (2005).**
5. **R. Schoenauer, S. Lange, A. Hirschy, E. Ehler, J. C. Perriard et al. "Myomesin 3, a novel structural component of the M-band in striated muscle". J. Mol. Biol. 376, 338–351 (2008)**
6. **N. Pinotsis, S. Lange, J. C. Perriard, D. I. Svergun, M. Wilmanns, "Molecular basis of the C-terminal tail-to-tail assembly of the sarcomeric filament protein myomesin", EMBO J. 27, 253–264 (2008).**
7. **L. Tskhovrebova, J. Trinick, "Making Muscle Elastic: The Structural Basis of Myomesin Stretching". PLoS Biol 10(2): e1001264. doi:10.1371/journal.pbio.1001264**

Discovering viral tricks to influence the human immune response.

Decoy protein of a herpes virus at work

The Epstein Barr Virus (EBV), a member of the herpes virus family, is a global human pathogen causing a diverse range of diseases. A multidisciplinary study using synchrotron radiation, electron microscopy, biophysical and cellular methods revealed at the molecular level how the virus can deactivate the alert system of the body's immune defence by using a molecular decoy. The EBV secrets a protein called BARF1 that neutralizes a human colony-stimulating factor 1 (hCSF-1). The latter is a growth factor which plays an essential role in the immune defence by stimulating the growth of white blood cells (leucocytes). We showed that the flexible BARF1 protein locks the dimeric hCSF-1 into an inactive conformation, rendering it unable to perform its signalling function. The novel mechanisms have implications on the development of therapies and drug compounds.

The Epstein Barr Virus (EBV), also known as the Human Herpes Virus 4 (HHV4), is a member of the herpes virus family and is a global human pathogen known for a diverse range of diseases [1] including fever (mononucleosis), also known as "kissing disease". Moreover, it plays a role in at least one type of cancer. The pathogen HHV4 is extremely widespread, although the infection is often asymptomatic. In 90 – 95 % of the population, once the initial infection and viral production cycle has been brought under control, the virus remains latent in the host cells for the rest of the individual's life.

EBV has co-evolved with its host by developing sophisticated interactions with host cells with the aim of evading detection and subsequent elimination by the human immune system. One of the possible strategies employed by EBV to subvert the human immune system is to secret a protein named BARF1 that blocks the protein hCSF-1 in the human body [2]. The hematopoietic cytokine hCSF-1 is a so-called growth factor which plays an essential role in the immune defence by stimulating the growth of white blood cells (leucocytes). hCSF-1 is therefore highly essential for innate and adaptive immunity against viral and microbial infections and cancer.

An international team coordinated by Prof. Savvas Savvides from Ghent University studied the molecular mechanisms of the deactivation of the human immune defence system using a multidisciplinary approach. The high resolution structures of BARF1, hCSF-1 and their complex in the crystal were revealed by macromolecular crystallography at the European Synchrotron Radiation Facility ESRF and the Swiss Light Source SLS. At the EMBL beamline X33 of the DORIS III storage ring (DESY) [3] the structure of the proteins and complexes was elucidated in solution, i.e. in conditions close to their natural environment, using small-angle X-ray scattering (SAXS). The SAXS data collected at X33 were processed and interpreted using the ATSAS program suite developed at the EMBL [4]. The synchrotron X-ray analyses were complemented by electron microscopy, surface plasmon resonance, biophysical and cellular studies.

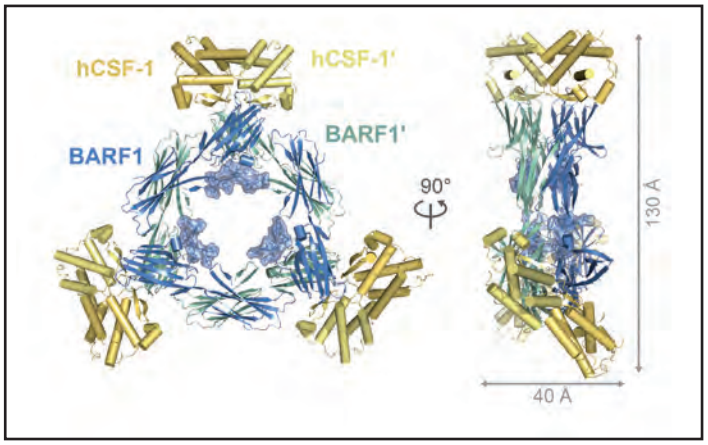

Figure 1

High resolution crystal structure of the BARF1–hCSF-1 assembly. Hexameric BARF1 (blue ribbons) binds three hCSF-1 (yellow) dimers. The oligomannose-type glycan structures lining the inner circle of the BARF1 toroid are shown in stick-and-surface representation. Prime symbols refer to the second hCSF-1 and BARF1 subunits in their respective oligomers.

The crystallographic studies revealed that BARF1 inactivates hCSF-1 by capturing three copies of hCSF-1 to establish a long-lived complex with ultra-high affinity (Figure 1). The SAXS pattern computed from the crystallographic model agreed well with the experimental scattering data indicating that the crystallographic structure of the complex is preserved in solution (Figure 2A). The BARF1 protein in the complex showed a toroidal trimeric structure, similar to the crystal structure of the unliganded BARF1 [5]. Very interestingly, however, the crystal structures of the BARF1 alone did not give good fits to the experimental

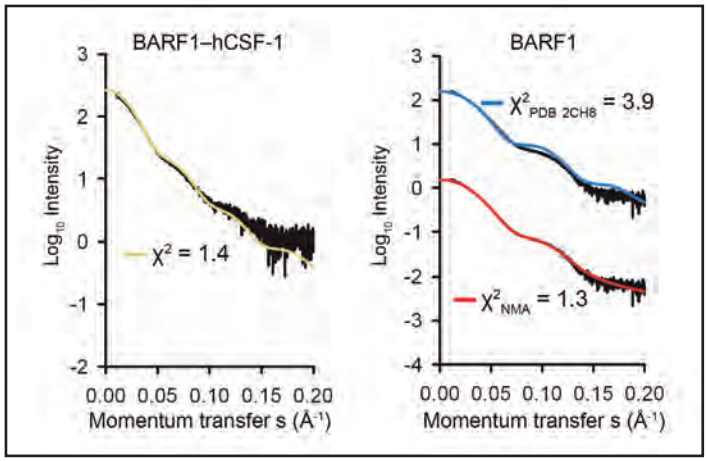

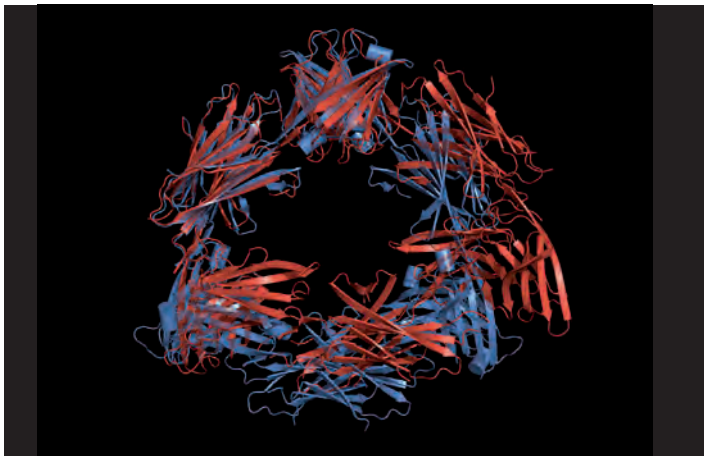

Figure 2

SAXS analysis of the BARF1–hCSF-1 complex and of unbound BARF1. (A) The experimental scattering patterns and fits from the models. Left panel, experimental data of the BARF1–hCSF-1 complex is well fitted by the computed scattering from the model with discrepancy $\chi^2 = 1.4$. The right panel displays the scattering from free BARF1 in solution and fits from the unbound BARF1 crystal structure (PDB code 2CH8 [4]) with discrepancy $\chi^2 = 3.9$ and from the NMA-refined asymmetric model ($\chi^2 = 1.3$). The logarithm of the scattering intensity is displayed as a function of momentum transfer $s = 4\pi\sin(\theta)/\lambda$, where 2θ is the scattering angle and λ is the X-ray wavelength. The fits from the two models are displaced along the logarithmic axis for better visualization. (B) The unbound BARF1 crystal structure (blue) overlapped with the NMA-refined model (red).

scattering from the free BARF1 in solution (Figure 2A). A refinement of the crystal structure of BARF1, by normal mode analysis (NMA) based on an iterative protocol [6] yielded a model with a squashed ring structure fitting the SAXS data (Figure 2A, B). Thus, unbound BARF1 may display some flexibility manifested as alternative conformations, and this flexibility seems to play a significant role in its function. Indeed, in the crystal BARF1 manages to lock dimeric hCSF-1 into an inactive conformation so that it is unable to activate its own receptor. This, in turn, is preventing monocyte maturation into macrophages, a key cell type in the immune response against viral and microbial infections.

The discovered mechanism of modulating the immune response suggests a new viral strategy paradigm where an allosteric decoy receptor efficiently sequests and inactivates a host growth factor to abrogate cooperative assembly of the cognate signalling complex. As the secretion of BARF1 is highly associated with types of carcinomas, understanding how BARF1 may interfere with the human immune response is crucial for shedding light on the process of the diseases and developing possible therapies. This study also revealed a new functional role for hCSF-1 cooperativity in signalling. Interestingly, monomeric hCSF-1 was unable to bind to BARF1, confirming that the hCSF-1 dimer interface is the actual target for BARF1 and that the plasticity of the dimeric cytokine is linked to extracellular signalling complex formation. This has profound implications for the development of therapeutic approaches against CSF-1 signalling as such, an area of great clinical importance in its own right. Overall, the study is a vivid demonstration of the power of hybrid approaches in modern molecular biology, where the methods providing information at different resolution scales are integrated to yield a comprehensive picture of a biological process.

Contact: Dmitri Svergun, svergun@EMBL-Hamburg.de
Savvas Savvides, savvas.savvides@ugent.be

Authors

Jonathan Elegheert[1], Nathalie Bracke[1,5], Philippe Pouliot[2], Irina Gutsche[3], Alexander V. Shkumatov[4,5], Nicolas Tarbouriech[3], Kenneth Verstraete[1], Anaïs Bekaert[1,5], Wim P. Burmeister[3], Dmitri I Svergun[4], Bart N Lambrecht[2], Bjorn Vergauwen[1] and Savvas N. Savvides[1]

1. Unit for Structural Biology, Laboratory for Protein Biochemistry and Biomolecular Engineering, Department of Biochemistry & Microbiology, Ghent University, Ghent, Belgium.
2. Laboratory of Immunoregulation and Mucosal Immunology, Department of Molecular Biomedical Research, VIB and Ghent University, Ghent, Belgium.
3. Unit for Virus Host-Cell Interactions, Université Joseph Fourier, European Molecular Biology Laboratory and Centre National de la Recherche Scientifique, Grenoble, France.
4. Biological Small Angle Scattering Group, European Molecular Biology Laboratory, Hamburg Unit, Deutsches Elektronen-Synchrotron, Hamburg, Germany.
5. Present addresses: Laboratory of Drug Quality and Registration, Department of Pharmaceutical Analysis, Ghent University, Ghent, Belgium (N.B.); Department of Biological Chemistry and Molecular Pharmacology, Harvard Medical School, Boston, Massachusetts, USA (A.V.S.); Oxyrane, Ghent, Belgium (A.B.).

Original publication

"Allosteric competitive inactivation of hematopoietic CSF-1 signaling by the viral decoy receptor BARF1", Nat Struct Mol Biol. 19, 938-947 (2012).

References

1. **J.L. Kutok, F.Wang, "Spectrum of Epstein-Barr virus-associated diseases." Annu. Rev. Pathol. 1, 375–404 (2006).**
2. **L.D. Strockbine, J.I. Cohen, T. Farrah, S.D. Lyman, F. Wagener, R.F. DuBose, R.J. Armitage, M.K. Spriggs. "The Epstein-Barr virus BARF1 gene encodes a novel, soluble colony-stimulating factor-1 receptor." J. Virol. 72, 4015–4021 (1998).**
3. **C.E. Blanchet, A.V. Zozulya, A.G. Kikhney, D. Franke, P.V. Konarev, W. Shang, R. Klaering, B. Robrahn, C. Hermes, F. Cipriani, D.I. Svergun, and M. Roessle "Instrumental setup for high-throughput small- and wide-angle solution scattering at the X33 beamline of EMBL Hamburg." J. Appl. Cryst., 45, 489-495 (2012).**
4. **M.V. Petoukhov, , D. Franke, A.V. Shkumatov, G. Tria, A.G. Kikhney, M. Gajda, C. Gorba, H.D.T. Mertens, P.V. Konarev, and D.I. Svergun, New developments in the ATSAS program package for small-angle scattering data analysis. Journal of Applied Crystallography, 45(2): p. 342-350 (2012).**
5. **N. Tarbouriech, F. Ruggiero, M. de Turenne-Tessier, T. Ooka, W.P. Burmeister "Structure of the Epstein-Barr virus oncogene BARF1." J. Mol. Biol. 359, 667–678 (2006).**
6. **C. Gorba, O. Miyashita, F. Tama, "Normal-mode flexible fitting of high-resolution structure of biological molecules toward one-dimensional low-resolution data." Biophys. J. 94, 1589–1599 (2008).**

Moving spins in a labyrinth of magnetic domains.

Probing the spatial response during ultrafast magnetization

When a magnetized material is bombarded by a femtosecond infra-red laser pulse, the magnetization of the material drops within a few hundreds of femtoseconds. In a study using ultrashort X-ray pulses delivered by FLASH we investigate the process of ultrafast demagnetization in a sample exhibiting nanometer-sized magnetic domains. In the pump-probe experiment the evolution of the magnetization is monitored with femtosecond time resolution and nanometer spatial resolution. The results together with simulations suggest that superdiffusive spin transport between adjacent magnetic domains contributes to the ultrafast demagnetization and significantly changes the spin structure at the domain walls.

In 1996 Beaurepaire *et al.* reported on an experiment [1] which opened a new field of magnetism research. It was observed that the magnetization of a nickel film after being pumped by an optical femtosecond laser pulse drops on a timescale of a few hundred femtoseconds. This magnetization change is orders of magnitude faster than expected by classical magnetization dynamics typically taking place on the nano- and picosecond timescale. Since the discovery of the ultrafast demagnetization process, its mechanism has been intensely debated. So far, most experimental as well as theoretical work has focused on homogeneous samples in order to understand the intrinsic demagnetization mechanisms. In particular, the transport of energy and angular momentum between the light pulse used for excitation, the electrons, their spin configuration and the crystal lattice with its phonon excitations have to be addressed. The electron spin is intimately linked to the samples magnetization.

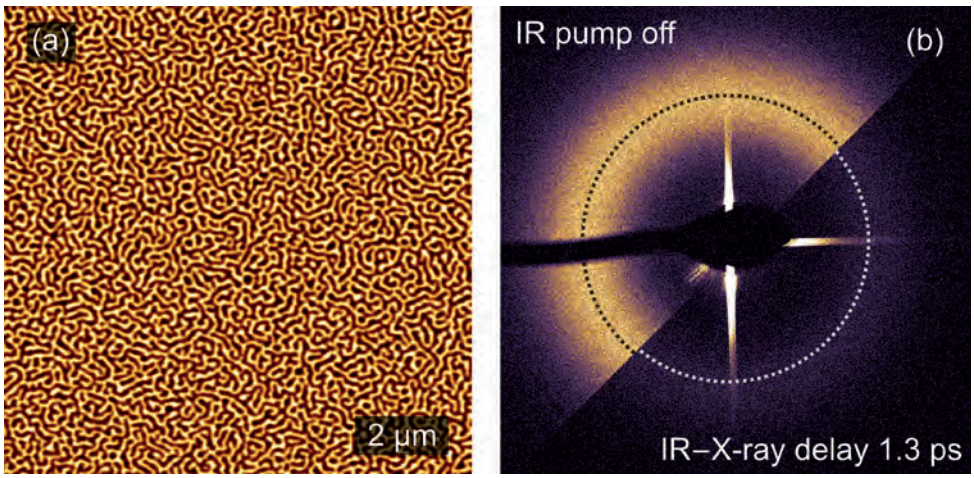

Figure 1

(a) Magnetic force microscopy (MFM) image of the magnetic labyrinth domain pattern exhibited by the thin-film Co/Pt multilayer structure. The magnetization of the domains is alternately pointing up or down, perpendicular to the magnetic film. (b) Related magnetic small-angle X-ray scattering pattern of the domains. The image shows a comparison of the pattern in the equilibrium (unpumped) state and after the sample was pumped by an IR laser. The dotted lines highlight the peak radius.

Additional extrinsic demagnetization channels due to a heterogeneous sample structure and resulting interfaces have been considered so far only for layered thin-film samples with interfaces between ferromagnetic and paramagnetic layers [2]. Recently, it was proposed in a theoretical study, that superdiffusive spin transport could significantly contribute to the ultrafast demagnetization [3]. This concept is based on the notion that the lifetimes, velocities and, consequentially, the mean free paths for hot electrons in metals are spin dependent if the electrons move in a magnetized region. As electrons carrying the majority spin possess a much higher mobility than the minority electrons, the majority electrons may preferentially leak from a ferromagnetic layer into an adjacent layer leading to a demagnetization of the ferromagnetic layer. Moreover the effective transport of spin may even change the magnetization in the destination layer [4].

In our study we investigate ultrafast demagnetization in a thin-film Co/Pt multilayer sample which is magnetized in the out-of-plane direction. In the remanent equilibrium state the magnetic film exhibits a nanoscale labyrinth-like pattern of magnetic domains with the magnetization pointing either “up” or “down” (Fig. 1a). The boundaries between the domains, the domain

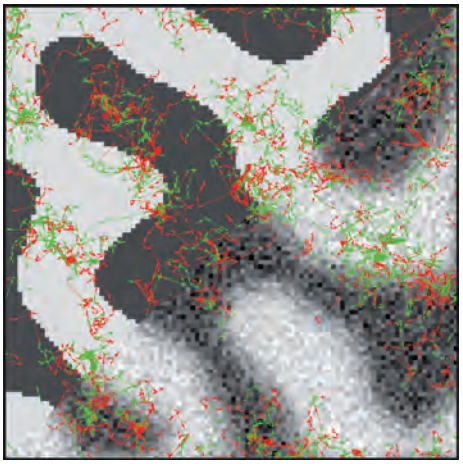

Figure 2

Detail (488 × 488 nm^2) of the magnetization matrix used in the Monte-Carlo simulations of the lateral superdiffusive spin-transport. In the background the magnetization of the simulated film is shown as it is initialized at the beginning of the simulation (top-left) and as it has evolved after 300 fs (bottom-right). The magnetization of the light areas is pointing up and in the dark areas it is pointing down. On top the electron trajectories of electron cascades initialized by 40 selected excited electrons are drawn. The green arrows correspond to spin-up electrons while the red arrows indicate spin-down electrons. In the domains with the magnetization pointing up, the mobility of the spin-up electrons is enhanced compared to the spin-down electrons and vice versa.

walls, are purely magnetic in nature as the sample is laterally homogeneous with respect to elemental composition.

The pump-probe experiment has been performed at the free-electron laser FLASH. The sample was pumped by a 70 fs long infra-red (IR) laser pulse and after a certain delay time (0-15 ps), the magnetic state of the sample was probed by a 100 fs long soft X-ray pulse. The ultrashort pump and probe pulses allow to investigate the evolution of the magnetization on a sub-ps timescale. The magnetic sensitivity is obtained via the X-ray magnetic circular dichroism effect. This effect gives rise to a magnetization-dependent X-ray absorption if the wavelength of the radiation is tuned to a suitable absorption edge of the magnetized material. Due to the alternating arrangement of oppositely magnetized domains, the magnetic layer acts as a diffraction grating and intensity maxima on the side of the directly transmitted radiation are observed in the diffraction pattern of the sample. Changes in the shape of this diffraction ring can be used to identify modifications in the domain arrangement with nanometer resolution.

As depicted in Fig. 1b, the intensity of the diffraction ring drastically reduces after the sample is pumped by the IR pulse. This finding is directly explained by the ultrafast demagnetization of the magnetic material. In addition, we observe a reduction of the scattering ring radius by about 4 %, which must be directly related to spatial changes in the magnetic domain pattern.

In order to explain our observation, we have performed Monte-Carlo simulations of the spin-dependent lateral motion of hot electrons in the magnetic film characterized by the presence of magnetic domains (Fig. 2). The simulations reveal that hot majority electrons which diffuse in the domain pattern get trapped when they have crossed a domain wall. The reason for this behaviour is their reduced mobility once they have become a minority electron by entering the adjacent domain. The accumulation of minority spin at the walls leads to a magnetic softening of the boundaries. A simulation of the scattering experiment shows that this domain wall softening explains the reduction of the diffraction ring radius.

We anticipate that it will be possible to tailor time constants of optical demagnetization by variation of the domain size or by specific nanostructuring [5]. Given the tremendous advances in the use of magnetic interfaces for electronic and spintronic applications in the past decades, one may envision the utilization of superdiffusive spin transport across ferromagnetic domain walls for ultrafast magneto-optical devices in the future.

Contact: Stefan Eisebitt, eisebitt@physik.tu-berlin.de

Authors

Bastian Pfau[1], Stefan Schaffert[1], Leonard Müller[2], Christian Gutt[2], Alaa Al-Shemmary[2], Felix Büttner[1,3,4,5], Renaud Delaunay[6], Stefan Düsterer[2], Samuel Flewett[1,4], Robert Frömter[7], Jan Geilhufe[8], Erik Guehrs[1], Christian M. Günther[1], Ranjit Hawaldar[6], Matthias Hille[7], Nicolas Jaouen[9], Aandré Kobs[7], Kaigong Li[6], Jyoti Mohanty[1], Harald Redlin[2], William F. Schlotter[10], Daniel Stickler[7], Rolf Treusch[2], Boris Vodungbo[6,11], Mathias Kläui[3,4,5], Hans Peter Oepen[7], Jan Lüning[6], Gerhard Grübel[2], Stefan Eisebitt[1,8]

1. TU Berlin, Institut für Optik und Atomare Physik, 10623 Berlin, Germany
2. Deutsches Elektronen-Synchrotron DESY, 22607 Hamburg, Germany
3. Johannes Gutenberg-Universität Mainz, Institut für Physik, 55099 Mainz, Germany
4. SwissFEL, Paul Scherrer Institut, 5232 Villigen PSI, Switzerland
5. École Polytechnique Fédérale de Lausanne, 1015 Lausanne, Switzerland
6. Université Pierre et Marie Curie, Laboratoire de Chimie Physique – Matière et Rayonnement – CNRS UMR 7614, 75005 Paris, France
7. Universität Hamburg, Institut für Angewandte Physik, 20355 Hamburg, Germany
8. Helmholtz-Zentrum Berlin für Materialien und Energie, 14109 Berlin, Germany
9. Synchrotron SOLEIL, L'Orme des Merisiers, Saint-Aubin, 91192 Gif-sur-Yvette Cedex, France
10. Linac Coherent Light Source, SLAC National Accelerator Laboratory, Menlo Park, California 94025, USA
11. Laboratoire d'Optique Appliquée, ENSTA ParisTech – CNRS UMR 7639 – École polytechnique, Chemin de la Hunière, 91761 Palaiseau, France

Original publication

"Ultrafast optical demagnetization manipulates nanoscale spin structure in domain walls", Nature Communications 3, 1100 (2012).

References

1. **E. Beaurepaire, J.-C. Merle, A. Daunois, J.-Y. Bigot, "Ultrafast spin dynamics in ferromagnetic nickel." Phys. Rev. Lett. 76, 4250–4253 (1996).**
2. **G. Malinowski, et al., "Control of speed and efficiency of ultrafast demagnetization by direct transfer of spin angular momentum." Nat. Phys. 4, 855–858 (2008).**
3. **M. Battiato, K. Carva, P.M. Oppeneer, "Superdiffusive spin transport as a mechanism of ultrafast demagnetization." Phys. Rev. Lett. 105, 027203 (2010).**
4. **D. Rudolf et al., "Ultrafast magnetization enhancement in metallic multi-layers driven by superdiffusive spin current", Nat. Commun. 3, 1037 (2012).**
5. **B. Vodungbo et al., "Laser-induced ultrafast demagnetization in the presence of a nanoscale magnetic domain network", Nat. Commun. 3, 999 (2012).**

Snapshots of fireworks in nanoparticles in X-ray pulses.

Beyond conventional ultrafast spectroscopy

A Holy Grail of ultrafast science and technology is to image the changing structure of matter at the nanometer length scale with femtosecond time resolution. We used intense laser pulses delivered by the FLASH free-electron laser for X-ray scattering from nanoparticles. The goal was to look into ultrafast electronic processes during the nanoplasma formation where conventional spectroscopy techniques are inherently blind. These experiments open up new routes for the investigation of transient electronic configurations of highly excited states of matter such as the interior of stars which can now be created in the laboratory.

Ultrafast X-ray scattering opens the door for unprecedented insight into the structure and dynamics of matter with atomic resolution [1]. However, any sample in the focus of an intense X-ray laser flash will be converted into a highly excited, non-equilibrium plasma hotter than the sun [2]. The scattering signal is affected by the changes in the electronic structure of the sample, leading to modifications of the scattered light even though the particle geometry remains the same on the time scale of the interaction with the laser pulse. Conversely, the information carried by the scattering signal can be exploited to gain insight into transient electronic states on the femtosecond time scale.

In our work we performed single-shot single-particle scattering experiments on xenon clusters to investigate the interplay between excitation and scattering in nanoscale objects with femtosecond X-ray pulses. Because of their finite size and simple electronic structure, atomic clusters are ideal objects for investigating the interaction between intense light pulses and matter. The conventional way to analyse the interaction is to detect the cluster fragments with ion time-of-flight (TOF) spectrometers. An inherent limitation of this technique is that only the final products of the reaction – in other words, the charge states of the cluster fragments microseconds after the reaction took place – are detected. This leaves plenty of time for higher charge states to be created and to recombine, never to be seen in ion TOF spectroscopy.

The experiments were performed with 20 fs long soft X-ray pulses at 90 eV from the FLASH free-electron laser [3] with power densities up to 5 x 10^{13} W/cm^2. The experimental set-up is shown in Fig. 1. In the present work the scattering signal is used to track ultrafast changes in the electronic structure of the clusters. The clusters are produced by expanding Xe gas through a cooled, pulsed nozzle. From fits of the scattering patterns with Mie theory [4] cluster radii up to 200 nm are deduced. In

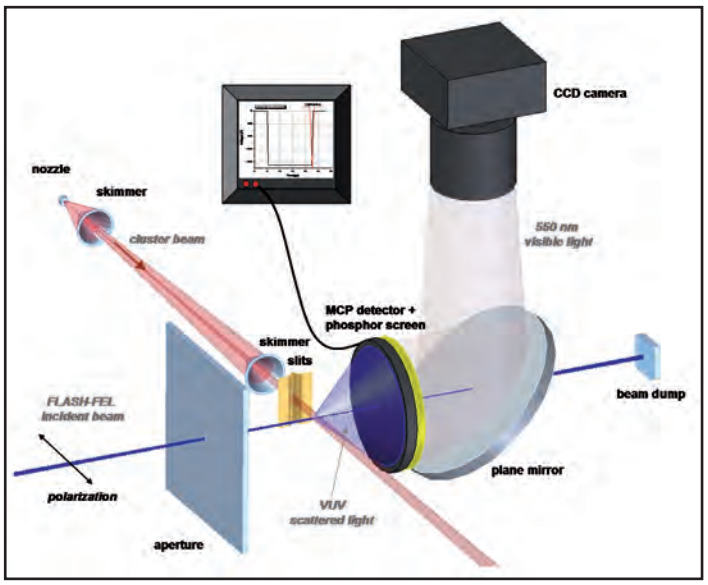

Figure 1

Experimental setup for single-shot single-particle scattering experiments on xenon nanoclusters. X-ray photons are detected, converted into optical photons, and digitized.

Fig. 2 a representative single-shot single-particle image is shown. The ring structure of the diffraction patterns reflects the shape of the clusters to be almost spherical. To extract the scattering profiles, i.e., the scattering intensity as a function of scattering

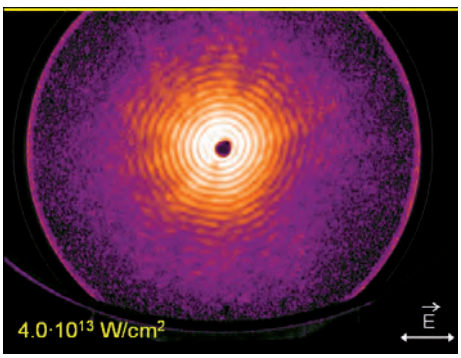

Figure 2

Scattering image for a high-power-density X-ray beam.

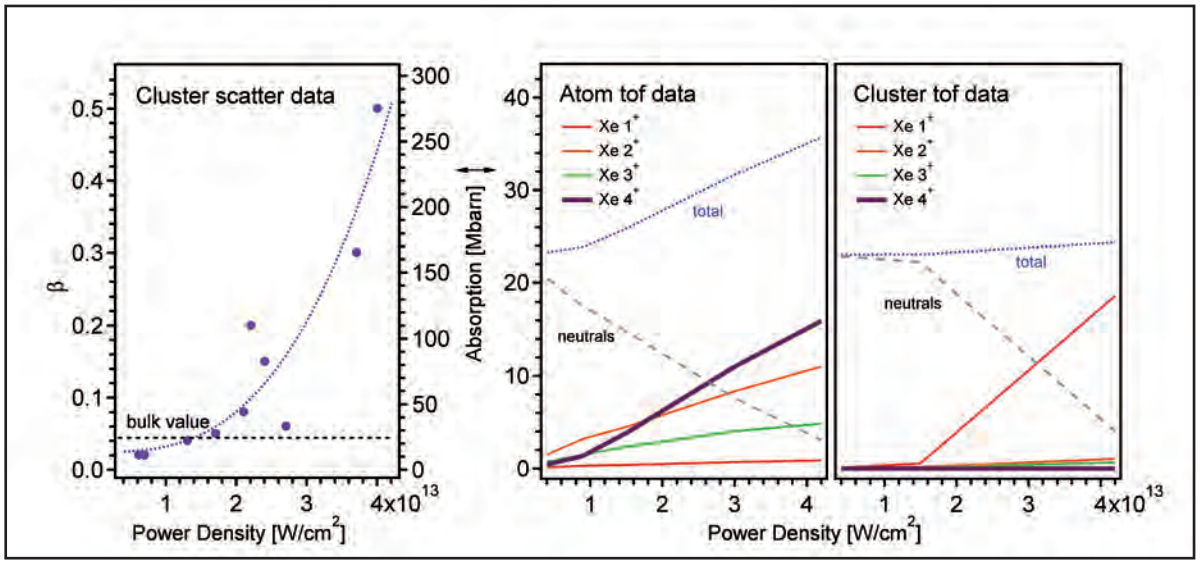

Figure 3

Particle absorption parameter β deduced from the scattering patterns. Right: Modelled relative absorption contribution, i.e., relative abundance times cross section, of the dominant ions based on atom and cluster target TOF spectra recorded with similar laser conditions.

angle, a slice of 20 degrees is cut out of the two-dimensional scattering pattern perpendicular to the polarization axis of the incoming light and averaged radially, i.e., over intensities at constant values of the momentum transfer q of the photon during the scattering process. The resulting scattering profiles are analysed using Mie theory and yield information on the real (δ) and the imaginary (β) part of the index of refraction [4]. The imaginary part β is a measure for the light absorption. It strongly increases with power density as can be seen in Fig. 3. While at low power densities β is close to the value of bulk xenon, for high power densities it exceeds the bulk value by more than a factor of 10, corresponding to an absorption cross section exceeding 200 Mbarn. The unexpectedly strong changes in the scattering pattern as a function of power density can be correlated to the ionization processes in the particle during the laser pulse. The scattering pattern is only generated during the pulse and therefore it is susceptible to the X-ray pulse-induced transient changes in the particle electronic structure. A comparison with theoretical work [5] indicates that strongly absorbing Xe ions with a charge state of 4+ are formed during the X-ray pulse. Such ions can also be detected with a TOF mass spectrometer several microseconds after the light pulse, but it turned out that their abundance is very small (only a few per cent of the total ion yield), as shown in the right part of Fig. 3. On the other hand, the strong enhancement of the scattering signal gives strong evidence that during the light pulse these highly charged ions are formed with a high probability. The small percentage of Xe^{4+} long after the pulse indicates that very efficient electron-ion recombination takes place on a fs to ns time scale.

In summary, the data show that single-shot single-particle scattering yields insight into ultrafast processes in highly excited systems where conventional spectroscopy techniques such as TOF mass spectroscopy are inherently blind. There, the particles are detected long after the light – matter interaction took place and they are subject to secondary processes such as plasma recombination. Therefore, scattering experiments with intense ultrashort X-ray pulses open up new opportunities for the investigation of transient electronic configurations of highly excited states of matter, nonequilibrium plasmas, and dense exotic systems, in addition to being key for solving structural information problems.

Contact: Thomas Möller, thomas.moeller@physik.tu-berlin, Christoph Bostedt, bostedt@slac.stanford.edu

Authors

C. Bostedt[1,2], Eremina[1], D. Rupp[1], M. Adolph[1], H. Thomas[1], M. Hoener[1], A.R.B. de Castro[3], J. Tiggesbäumker[4], K.-H. Meiwes-Broer[4], T. Laarmann[5], H. Wabnitz[5], E. Plönjes[5], R. Treusch[5], J. R. Schneider[5], and T. Möller[1]

1. Institut für Optik und Atomare Physik, Technische Universität Berlin, Eugene-Wigner-Building EW 3-1, Hardenbergstrasse 36, 10623 Berlin, Germany
2. SLAC National Accelerator Laboratory, P.O. Box 20450, Stanford, California 94309, USA
3. Laboratorio Nacional de Luz Sincrotron, 13084-971 Campinas SP, Brazil and Instituto de Fisica Gleb Wataghin, Universidade Estadual de Campinas, 13083-970 Campinas SP, Brazil
4. Institut für Physik, Universität Rostock, 18051 Rostock, Germany
5. Deutsches Elektronen-Synchrotron DESY, 22603 Hamburg, Germany

Original publication

"Ultrafast X-Ray Scattering of Xenon Nanoparticles: Imaging Transient States of Matter", Physical Review Letters 108, 093401 (2012)

References

1. **K. Gaffney and H. Chapman, Science 316, 1444 (2007).**
2. **C. Bostedt, H. Thomas, M. Hoener, E. Eremina, T. Fennel, K.-H. Meiwes-Broer, H. Wabnitz, M. Kuhlmann, E. Plönjes, and K. Tiedtke et al., Phys. Rev. Lett. 100, 133401 (2008).**
3. **W. Ackermannet al., Nature Photon. 1, 336 (2007).**
4. **G. Mie, Ann. Phys. (Leipzig) 330, 377 (1908).**
5. **J. Nilsen, W. Johnson, and K. Cheng, Proc. SPIE Int. Soc. Opt. Eng. 6702, 67020N (2007).**

Watching the quantum race of electrons.

Chirped Auger electron emission

When a photon of sufficiently high energy hits an atom it may kick out an electron. Quantum mechanics predicts that the electron behaves like a wave that runs away from the atom. If the photon energy was chosen right then a second electron (Auger electron) may be liberated from the atom, racing behind the first one. We were able to detect how this second electron overtakes the first one within only a few femtoseconds (1fs = 10^{-15} seconds) and to observe the dynamic exchange of energy between the two electrons when they are passing each other.

The Auger effect, i.e. the emission of a secondary electron after a non-radiative decay of a deeply bound electronic core-hole is often used as a spectroscopic tool in modern analytical instruments. It derives its capabilities from the fact that the electron's kinetic energy is an intrinsic property of the electronic structure of the excited atom and does not rely on the energy of the exciting photon, electron or ion. The electron emission is not mono-energetic, though; the fast – attosecond to femtosecond – decay times imply corresponding spectral widths in a range of a few tens of meV to a few eV. This time-energy correspondence suggests a uniform distribution of all energy components over time. In this work, we demonstrate that for specific, but spectroscopically relevant conditions, this presumption is wrong. Instead, our time-resolved experiments show evidence of an energetic chirp, i.e. a pronounced time-dependent variation of the Auger electrons´ kinetic energy. It appears as a consequence of the correlated motion of both photo- and Auger electrons in the Coulomb field of the remaining ion. The basic principle is shown in Fig. 1. First an XUV photon liberates a photo-electron from an inner shell which is followed by an Auger electron (a). The photo- and Auger electron wave packets run away from the ionic core (b). After some time the later Auger electron reaches the earlier but slower photo-electron and both electrons exchange energy (c). In a classical picture the energy gain of the Auger electron ΔE_{Auger} is inversely proportional to the distance r from the ionic core at the moment of the interaction: $\Delta E_{Auger} \sim 1/r$. Thus, for an Auger electron emitted immediately after the photo-electron the energy gain is large, since it overtakes the photo-electron close to the ionic core while later Auger electrons gain less energy. In a quantum mechanical picture the head of the Auger electron wave packet is blue shifted with respect to the tail of the wave packet (d). Such time-energy relation is called "chirp", but was so far mostly used in connection with light- rather than matter waves. While the underlying mechanism – also known as 'post-collision interaction' (PCI) – has extensively been discussed in the literature, no attention has so far been paid to the consequence of the effect for the temporal properties of the escaping electron wave packets.

We visualize this temporal energy variation by using an ultra-fast terahertz-field-driven streak camera [1, 2] where the ultra-short (~20 fs) FLASH XUV pulses are superimposed with linearly polarized far-infrared (terahertz, THz) light pulses from the FLASH THz undulator [3] in a gas target (Fig. 2). The gas atoms are ionized by the XUV radiation and the resulting photo- and Auger electrons are immediately accelerated by the electromagnetic THz field. The final kinetic energies of the electrons are measured with time-of-flight (TOF) spectrometers parallel and perpendicular to the THz polarization. The oscillating electric field of the THz pulses accelerates the electrons in the direction of the THz polarization. The resulting momentum change depends on the phase of the THz field at the moment of ionization. Thus, the temporal profile of the electron wave packets is mapped onto electron energy changes. A chirp of the electron wave packet leads to an asymmetry in the line widths at ascending and descending slopes of the kinetic energy shift.

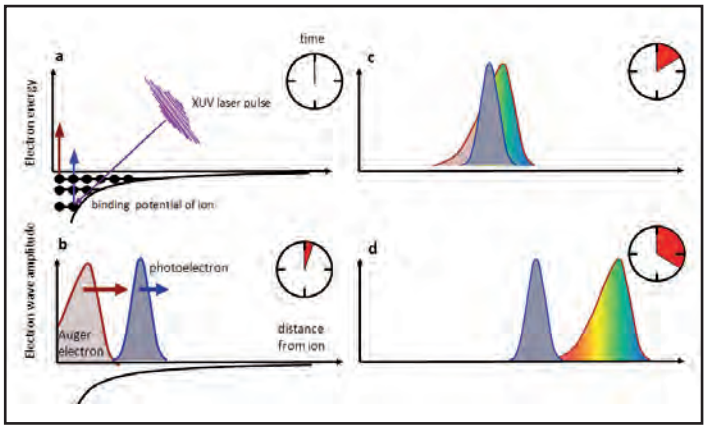

Figure 1

An XUV photon liberates two electrons from an atom (a). The two electron wave packets run away from the ionic core (b). The later Auger electron reaches the earlier but slower photo-electron (c). Interaction of electrons leads to a time dependent energy exchange between the electrons (d).

This technique is intensively used in attosecond metrology utilizing a near infrared streaking field [4, 5]. By scaling the oscillation period of the streaking field by two orders of magnitude into the THz range we have adapted it for the analysis of processes in the femtosecond range [1, 2].

Fig. 3 shows a series of kinetic energy spectra of Xenon NOO Auger electrons measured in the direction of the THz polarisation for different XUV THz-delay times. The XUV wavelength was 13.5 nm (92 eV) while the THz wavelength was 92 µm. The oscillating kinetic energy shift of the electrons is proportional to the vector potential of the THz field. The spectral widths of the Auger electrons are significantly smaller on the ascending slopes of the kinetic energy shift than on the descending slopes (white arrows in fig. 3). This is a clear indication for a spectral chirp.

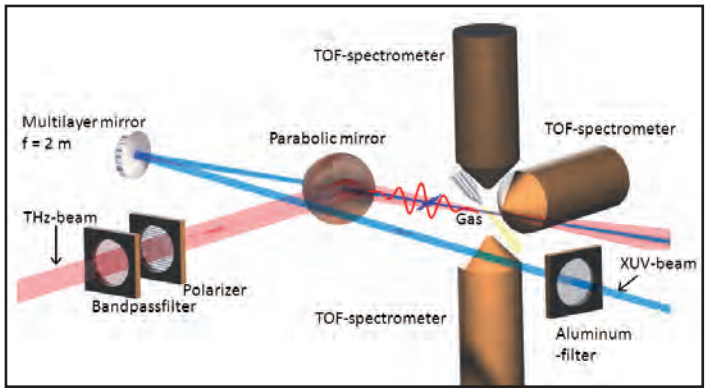

Figure 2

Schematic of the THz-streak camera. The FLASH XUV pulses (blue beam) are superimposed with vertically polarized THz pulses (red beam) in a gas target. Photo- and Auger electrons are detected with time-of-flight (TOF) spectrometers oriented parallel and perpendicular to the THz polarization.

The observed spectral modulations are readily reproduced with semi-classical as well as quantum simulations of the dynamics of two well-timed electrons in the presence of both a static and a time-varying electric field [6]. It turns out that the time-dependent observation of field-assisted electron-electron collision reveals details of the electronic correlation with much higher sensitivity than the mere energy-domain approach. In fact, our analysis shows that a significant contribution to the observed mechanism is due to an electron-electron collision taking place at many atomic radii – much more than typically considered in strong-field rescattering experiments.

The experimental findings were reproduced using laser-based XUV and THz sources [2]. Here, also the XUV pulses could be chirped in a controlled way and it was confirmed that the observed chirp of the Auger electrons is independent of a chirp of the XUV pulses. At the used photon energy of 91 eV, the Xe 4d electron energy is above 20 eV, such that the process of the Auger electron overtaking the photo-electron occurs relatively far from the ion. In order to further support our interpretation, the photon energy was increased to 97.5 eV at a laser based XUV source [2] and Krypton was used as the target medium. In this case the kinetic energy of the 3d photo-electrons is only 2.5 and 3.7 eV while the Auger kinetic energy is increased. Thus, in comparison to Xenon the Krypton Auger electrons overtake the photo-electrons closer to the ionic core which leads to a larger PCI effect and an increased chirp of the Auger lines. Well in accordance with our model, the observed line width asymmetry of spectra recorded at the ascending and the descending slope is now found to be considerably larger than before.

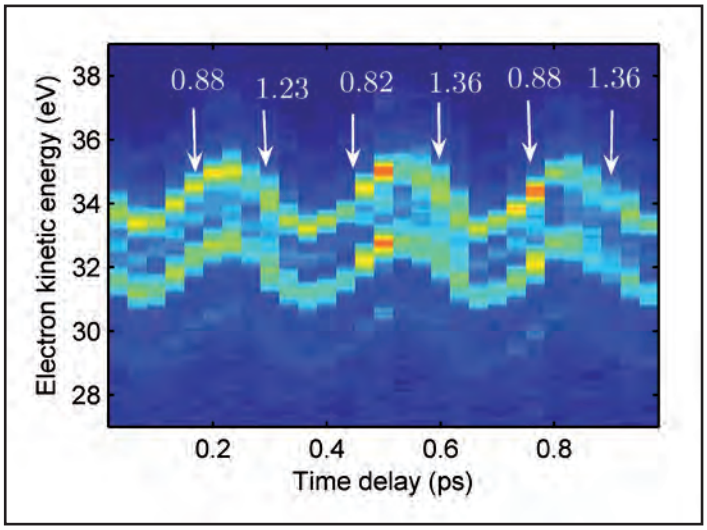

Figure 3

Series of Xe Auger electron spectra taken for different XUV/THz delay times. The electron energies are modified by the electric field of the THz pulses whereby the energy gain depends on the THz phase at ionization time. Thus the oscillation of the THz field becomes visible. The widths of the Auger electron spectra is smaller on the ascending than on the descending slopes of the energy shift (marked with white arrows). This is an indication of an energy chirp. The white numbers indicate the widths of the Auger lines in eV.

Contact: Markus Drescher, markus.drescher@desy.de

Authors

B. Schütte[1,3], S. Bauch[2], U. Frühling[1], M. Wieland[1], M. Gensch[4,5], E. Plönjes[4], T. Gaumnitz[1], A. Azima[1], M. Bonitz[2] and M. Drescher[1]

1. Institut für Experimentalphysik, Universität Hamburg, Luruper Chaussee 149, 22761 Hamburg, Germany
2. Institut für Theoretische Physik und Astrophysik, Christian-Albrechts-Universität, Leibnizstraße 15, 24098 Kiel, Germany
3. Max-Born-Institut, Max-Born-Straße 2A, 12489 Berlin, Germany
4. Deutsches Elektronen-Synchrotron DESY, Notkestr. 85, 22607 Hamburg, Germany
5. Helmholtz-Zentrum Dresden Rossendorf, Bautzner Landstraße 400, 01328 Dresden, Germany

Original publication

"Evidence for Chirped Auger-Electron Emission", Physical Review Letters 108, 253003 (2012).

References

1. **U. Frühling et al., "Single-shot terahertz-field-driven X-ray streak camera", Nature Photonics 3, 523 (2009).**
2. **B. Schütte et al., "Electron wave packet sampling with laser-generated extreme ultraviolet and terahertz fields", Optics Express 19, 18833 (2011).**
3. **M. Gensch et al., "New infrared undulator beamline at FLASH", Infrared Physics Technology 51, 423 (2008).**
4. **M. Drescher et al., "Time resolved atomic inner-shell spectroscopy", Nature 419, 803 (2002).**
5. **R. Kienberger et al., "Atomic transient recorder", Nature 427, 817 (2004).**
6. **S. Bauch and M. Bonitz , "Theoretical description of field-assisted post-collision interaction in Auger decay of Atoms", Phys. Rev. A 85, 053416 (2012).**

Self-reinforcement of rubber.

Crystallization under dynamic strain

Tailoring the properties of polymers by tuning crystallinity and orientation is common practice. Natural rubber has the astonishing ability to crystallize under strain. In regions of high strain and stress, the crystallites locally reinforce the material, while in the remainder of the rubber part the excellent elastic properties of the amorphous rubber are preserved. These properties still make natural rubber the material of choice for high-demanding applications like truck tires. Since the rubber is subjected to dynamic loads, it is critical to understand the time dependence of crystallization. By applying a steplike strain, we followed the crystallization over time in wide angle X-ray scattering (WAXD) with an unprecedented time resolution of 7 ms and derived a new kinetic law. Direct observation of crystallization during cyclic dynamic loading at 1 Hz gave insight into the structural processes under realistic loading conditions.

It has recently been pointed out, that natural rubber is a unique material "where one pulls […] a little bit and it snaps, but pull twice as hard and it holds together" [1]. Strain-induced crystallization is the reason behind these outstanding mechanical properties. Especially tear fatigue is significantly enhanced due to the reinforcing ability of highly oriented crystallites that form around the crack tip and reduce crack growth. The relation between strain and crystallinity for differently filled natural rubber composites is well established (Fig. 1a-c), but almost all of these studies are limited to quasistatic conditions [2, 3]. However, given that the majority of the world's yearly natural rubber production goes into the tire industry, the dynamic behaviour is more important than the quasistatic. While the dynamic mechanical properties are routinely measured, the establishment of structure property relations is hampered by the difficulty to characterize the structure under dynamic loading conditions. The classic method to quantify crystallinity is WAXD, the time resolution of which is limited by photon flux and detector readout times. Owing to the brilliance of the MiNaXS beamline P03 at PETRA III and the progress made in detector development, these limitations could be overcome and the strain-induced crystallization in natural rubber was studied with a time resolution of 7 ms while the rubber was subjected to dynamic load.

To elucidate the fundamentals of the kinetics of strain-induced crystallization, a fast tensile machine was developed to perform impact tensile tests in the beamline, stretching the sample by several hundred percent within less than 10 ms. Over a period of 60 s, WAXD patterns were acquired with a frame rate of 140 frames per second. Already 10 ms after the strain step, a significant amount of crystallinity was detected. So far, most studies reported longer incubation times [4]. During the following seconds, a distinct evolution of the crystallinity was observed, suggesting that the mechanism is different from thermal crystallization (Fig. 1d, e). The most widely used model for thermal crystallization, the Avrami model, was not able to fit the data with a physically meaningful set of parameters. This is due to the different morphologies, mobilities and driving forces in thermal crystallization and strain-induced crystallization of a cross-linked elastomer. The crystallites observed in our studies

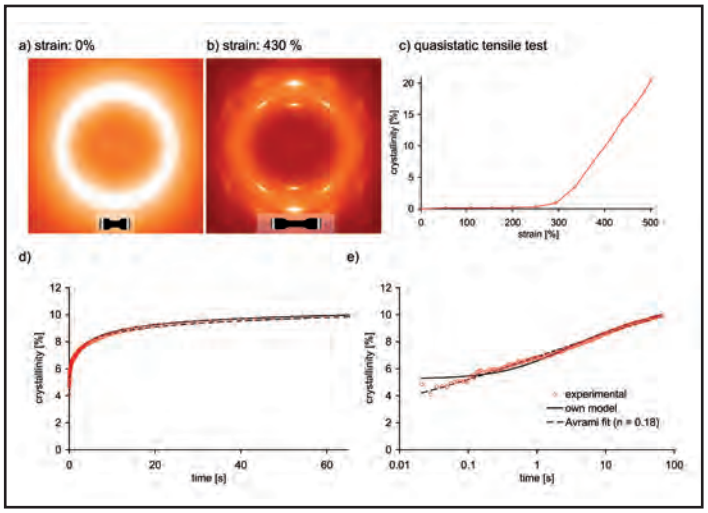

Figure 1

a, b) WAXD patterns of unstretched and stretched natural rubber.

c) In unfilled natural rubber under uniaxial quasistatic strain, crystallization sets in at around 300 % strain.

d) Crystallinity vs. time curves obtained from strain-step experiments. Initial strain 0 % (t < 0), final strain 410 % (t > 0). Crystallinity grows in an exponential manner, approaching the quasistatic level after > 10 s.

e) Same data as in d) in a semi-log representation. Fitting the data with the Avrami equation yields unphysically small exponents. Our model predicts a crystallization rate $\frac{d\Phi}{dt}$ proportional to the crystallizable material to the n^{th} power, where n describes the propensity of the amorphous chain segments to undergo crystallization: $\frac{d\Phi}{dt} = (k\,(\Phi_f - \Phi))^n$.

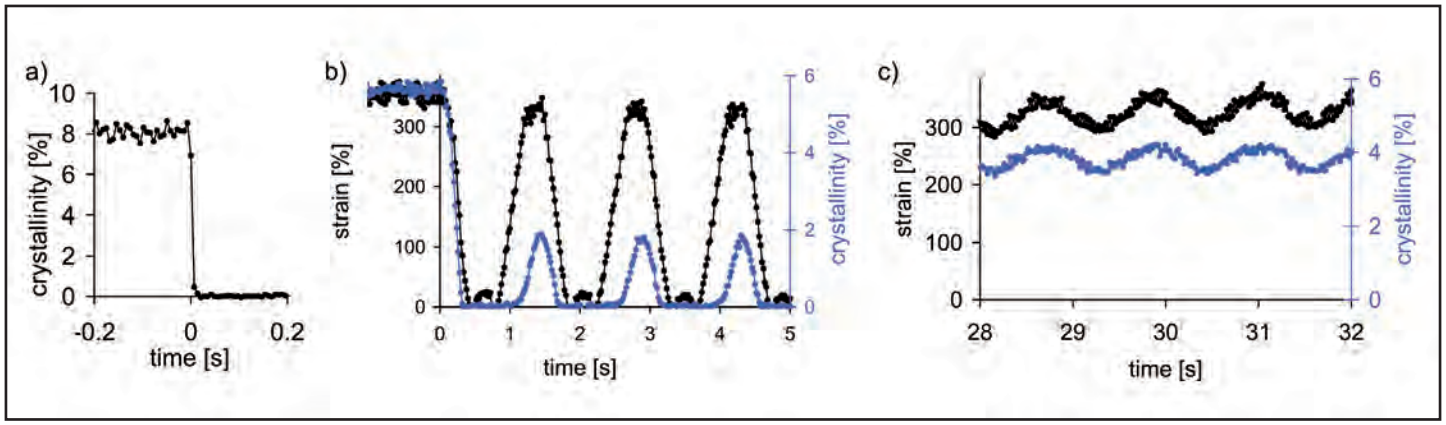

Figure 2

a) Crystallinity over time after steplike unloading. The time between two consecutive points is 7 ms. Crystallinity disappears instantaneously.

b) Suppression of crystallization during dynamic loading: While in the quasistatic state, crystallinity is 6 % (t < 0), it drops to 2 % during cyclic loading despite the same maximum strain of 365 %.

c) Subjecting the sample to non-relaxing dynamic load (between 290 % and 365 % strain) increases the crystallinity over the fully relaxing conditions in b).

were of sizes well below 50 nm, derived from the WAXD data and from electron microscopy.

A new kinetic law was developed to describe the crystallinity depending on strain and time. We propose that strain-induced crystallization is a two-step process, consisting of, first, nucleation by an instantaneous coil-stretch transition, and, second, a growth step. In analogy to flow-induced crystallization and shish formation, the crystallites are supposedly arranged in strands which make up the fibrils observed in SEM and give rise to the high orientation of the crystallites, as observed in WAXD. The growth of the strands is restricted to the radial direction, as derived from the Scherrer equation.

In contrast to the crystallization, the dissolution of the crystallites upon removal of the load is much faster. Following a fast unloading within 10 ms, no signs of crystallinity were detected after 7 ms (Fig. 2 a).

The tensile impact tests clearly showed that the typical time scales of deformation in real rubber parts are too short to let the structure reach equilibrium.

This was proven in a second kind of test. Cyclic dynamic tensile tests with a frequency of 1 Hz are routinely performed to study the fatigue properties of rubber. Using a self-made tensile testing machine we carried out these experiments *in situ* (Fig. 2b, c). The crystallinity was recorded with a time resolution of 20 ms to resolve each deformation cycle individually as well as to follow the evolution over several cycles. We showed that the crystallinity under dynamic conditions was significantly suppressed as compared to the quasistatic level. Under fully relaxing conditions (minimum cyclic strain = 0), the maximum crystallinity is suppressed by more than one half. Under non-relaxing conditions, the crystallinity is much higher, but still below the quasistatic level.

These findings can give the structural explanation to the long known observation that in strain-crystallizing elastomers, under relaxing conditions cracks grow faster despite the smaller work of deformation.

Contact: Karsten Brüning, bruening@ipfdd.de

Authors

Karsten Brüning[1,2], Konrad Schneider[1], Stephan V. Roth[3], Gert Heinrich[1,2]

1. Leibniz-Institut für Polymerforschung, Hohe Str. 6, 01069 Dresden, Germany
2. Institut für Werkstoffwissenschaft, TU Dresden, Helmholtzstr. 7, 01062 Dresden, Germany
3. Deutsches Elektronen Synchrotron DESY, Notkestr. 85, D-22607 Hamburg, Germany

Original publication

"Kinetics of Strain-Induced Crystallization in Natural Rubber Studied by WAXD: Dynamic and Impact Tensile Experiments", Macromolecules 45, 7914–7919 (2012).

References

1. **H.P. Zhang, J. Niemczura, G. Dennis, K. Ravi-Chandar, M. Marder, "Toughening effect of strain-induced crystallites in natural rubber", Physical Review Letters 102, 245503 (2009).**
2. **S. Toki, I. Sics, S. Ran, L. Liu, B.S. Hsiao, S. Murakami, K. Senoo, S. Kohjiya, "New insights into structural development in natural rubber during uniaxial deformation by in situ synchrotron X-ray diffraction", Macromolecules 35, 6578 (2002).**
3. **B. Huneau, "Strain-induced crystallization of natural rubber: A review of X-ray diffraction investigations", Rubber Chemistry and Technology 84, 425-452 (2011).**
4. **M. Tosaka, K. Senoo, K. Sato, M. Noda, N. Ohta, "Detection of fast and slow crystallization processes in instantaneously-strained samples of cis-1,4-polyisoprene", Polymer 53, 864 872 (2012).**

The chemistry behind Van Gogh's discolouring flowers.

Cadmium yellow degradation mechanisms

The study and analysis of degrading painting materials by means of synchrotron radiation is considered as an important topic within the field of cultural heritage science as the unsolicited reactions that take place at the (sub-) micron level are causing significant changes in the appearance of many key works of art. Moreover, these detrimental phenomena often jeopardise the preservation of the affected paintings for future generations as the paint layers are rendered brittle and flaky. In this work, the formation mechanism of a disturbing greyish crust that had formed on the bright cadmium yellow paint strokes of a painting by Van Gogh was explained by combining a number of complimentary species-selective analytical techniques (μ-XRF/μ-XRD, μ-XRF/μ-XANES and μ-FTIR).

At the end of the nineteenth century, the avant-garde painters (e.g. the impressionists) refused adopting the prevailing way of painting that was traditionally taught at the art academies. As this transition was accompanied by drastic stylistic changes, it is often forgotten that this evolution was facilitated by rather technical innovations: (a) the invention of the collapsible metal paint tube allowing outdoor 'plein air' painting and (b) the development of a range of new and bright synthetic pigments by the emerging chemical industry. These pure chemical compounds soon found their way to the paint boxes of progressive artists and supplemented their set of conventional pigments of mainly mineral origin [1].

However, the inclusion of innovative but untested pigments in paintings at the expense of time-honoured materials with proven durability holds some risks. Nowadays, it becomes clear that a number of these colouring substances can become chemically unstable on the long term. One of these pigments is cadmium yellow (CdS), a bright yellow pigment that was initially thought to be highly durable in oil paint and watercolours. As a consequence, prominent painters such as Monet, Seurat and Cézanne frequently made use of cadmium yellow. However, in spite of its excellent reputation, alteration of CdS paint layers was recently reported [2].

In the past, the authors demonstrated how the UV radiation in ambient daylight instigated the oxidisation of bright yellow cadmium sulphide to colourless cadmium sulphate on a painting by James Ensor ('Still life with coffeepot, cabbages and mask', ca. 1920, Kröller-Müller Museum) [2]. For the Van Gogh painting that is discussed here ('Flowers in a blue vase', 1887, Kröller-Müller Museum), the morphology of the degraded cadmium paint layer was substantially different. Here, an opaque greyish crust obscures the yellow colour, as illustrated in Fig. 1. In addition, the Van Gogh case was rendered more complex due to the presence of a varnish coating that was applied on top of the paint during a previous conservation treatment, most probably in an attempt to consolidate the affected paint.

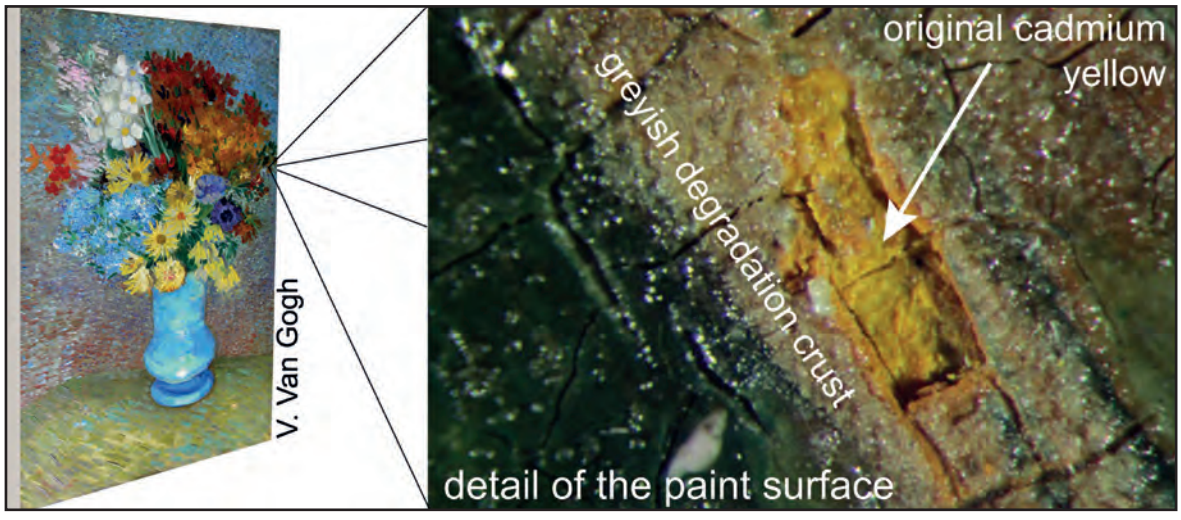

Figure 1
Left: 'Flowers in a blue vase' painted by Vincent Van Gogh in Paris in 1887. Right: detail of the paint surface.
A greyish degradation crust is obscuring the original warm yellow cadmium sulphide paint.

A few minute samples were extracted from the paint layer and analysed both at the P06 beamline of PETRA and at beamline ID21 of the European Synchrotron Radiation Facility (ESRF, Grenoble, France) with a combination of various analytical techniques. In particular, the X-ray diffraction maps collected at P06 and displayed in Fig. 2, revealed the presence of a thin (< 10 µm) film at the interface between the CdS paint and the varnish, containing cadmium oxalate, cadmium carbonate and lead sulphate. The identification of these compounds on the micron level allowed explaining the chemical pathway that leads to the discoloration phenomenon observed at the macroscopic level.

In spite of its divergent appearance, we concluded that the alteration on the Van Gogh still life was initially caused by oxidation of the original CdS pigment, similar as for the Ensor case. However, secondary reactions took place between (a) the primary degradation product ($CdSO_4$) and (b) lead- and oxalate- ions present in the varnish. Upon its application, the solvent rich varnish would have dissolved the highly-soluble $CdSO_4$ and dispersed this degradation product throughout the coating. It appears that the freed Cd^{2+} ions reprecipated out with $C_2O_4^{2-}$ instead of SO_4^{2-}. Oxalate ions are commonly observed in cultural heritage materials and are in this case believed to be a degradation product of the varnish/paint medium. The sulphate anions, for their part, found a suitable reaction partner in lead ions which resulted in the formation of grey opaque anglesite ($PbSO_4$) crystals. Most probably, the Pb^{2+} ions were supplied by a lead-based drier, a hypothesis that was corroborated by the fact that anglesite ($PbSO_4$) was identified in the Ensor case as well [3].

The origin of the encountered cadmium carbonate was less unequivocal. It may have been formed as a secondary degradation product following the primary photo-degradation of CdS as well, perhaps by the capture of atmospheric CO_2, as suggested by Mass et al. [4]. Alternatively, a tertiary process involving the further breakdown of cadmium oxalate into cadmium carbonate cannot be excluded while finally its presence might also be explained as simply a residue of the original raw material used for the industrial production of CdS.

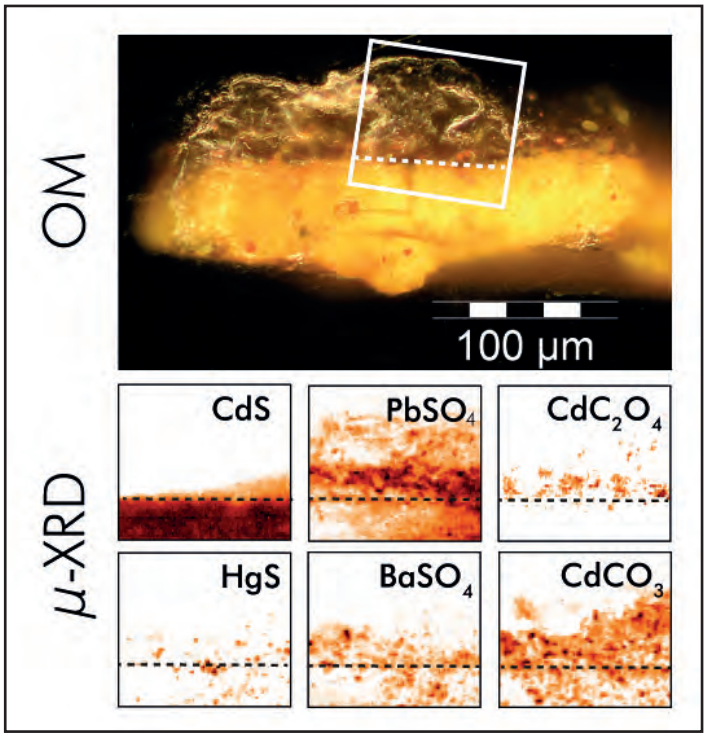

Figure 2

Top: microphotograph of a cross-sectioned sample extracted from the affected paint layer. The white rectangle indicates the area where the XRD maps were recorded. Bottom: corresponding X-ray diffraction maps collected at the P06 beamline of PETRA III.

In conclusion, this study showed how the primary degradation process, i.e. the oxidation of the original cadmium sulphide to colourless cadmium sulphate, was followed by secondary reactions after the application of a varnish film. This coating did not only dissolve the highly soluble cadmium sulphate, it supplied reaction partners (i.e. oxalate and lead ions) for the resulting Cd^{2+} and SO_4^{2-} ions as well. In this way, the application of what was once assumed to be a protective coating eventually lead to the formation of a disfiguring opaque-grey film at the paint/varnish interface instead.

Contact: Geert Van der Snickt, geert.vandersnickt@ua.ac.be

Authors

Geert Van der Snickt[1], Koen Janssens[1], Joris Dik[2], Wout de Nolf[1], Frederik Vanmeert[1], Jacub Jaroszewicz[1], Marine Cotte[3, 4], Gerald Falkenberg[5], and Luuk Van der Loeff[6]

1. Antwerp X-ray Instrumentation and Imaging Laboratory, Department of Chemistry, University of Antwerp, Groenenborgerlaan 171, B-2020 Antwerp, Belgium.
2. Department of Materials Science and Engineering, Delft University of Technology, Mekelweg 2, NL-2628 CD Delft, The Netherlands.
3. Laboratoire du Centre de Recherche et de Restauration des Musées de France, CNRS UMR 171, Palais du Louvre, Porte des Lions, 14, Quai François Mitterand, F-75001 Paris, France.
4. European Synchrotron Radiation Facility, Polygone Scientifique Louis Néel, 6, Rue Jules Horowitz, F-38000 Grenoble, France.
5. Deutsches Elektronen-Synchrotron DESY, Notkestrasse 85, D-22607 Hamburg, Germany.
6. Conservation Department, Kröller-Müller Museum, Houtkampweg 6, NL-6731 AW Otterlo, The Netherlands.

Original publication

"Combined use of Synchrotron Radiation Based Micro-X-ray Fluorescence, Micro-X-ray Diffraction, Micro-X-ray Absorption Near-Edge, and Micro-Fourier Transform Infrared Spectroscopy for Revealing an Alternative Degradation Pathway of the Pigment Cadmium Yellow in a Painting by Van Gogh", Analytical Chemistry, accepted August 30, 2012.

References

1. **G. Van der Snickt, et al. "James Ensor's pigment use: artistic and material evolution studied by means of portable X-ray fluorescence spectrometry", X-ray Spectrometry 39, 103-111 (2010).**
2. **G. Van der Snickt, et al. "Characterization of a Degraded Cadmium Yellow (CdS) Pigment in an Oil Painting by Means of Synchrotron Radiation Based X-ray Techniques", Analytical Chemistry 81, 2600-2610 (2009).**
3. **G. Van der Snickt, et al. "Combined use of Synchrotron Radiation Based Micro-X-ray Fluorescence, Micro-X-ray Diffraction, Micro-X-ray Absorption Near-Edge, and Micro-Fourier Transform Infrared Spectroscopy for Revealing an Alternative Degradation Pathway of the Pigment Cadmium Yellow in a Painting by Van Gogh", Analytical Chemistry, accepted August 30, DOI: 10.1021/ac3015627. 2012.**
4. **Jennifer Mass. Personal communication, July 2012.**

Hard X-ray scanning microscopy with coherent radiation.

Towards X-ray imaging with nanometer resolution

X-ray scanning coherent diffraction microscopy also known as ptychography is a new mode of operation for hard X-ray scanning microscopes. At beamline P06 at PETRA III, we have reached a record spatial resolution of 10 nm with this technique, clearly exceeding the spatial resolution limits of conventional hard X-ray microscopy. Unlike in conventional full-field imaging, the resolution in ptychography varies with the shape of the features in the object. In addition, the spatial resolution increases with increasing fluence on the sample. Therefore, the optimal ptychographic scanning microscope makes use of the brightest possible X-ray source and focuses the beam down to the smallest focus to generate the optimal probe beam.

Due to the large penetration depth of hard X-rays in matter, X-ray imaging offers unique ways to investigate the interior of an object without destructive sample preparation. In particular, X-rays can penetrate special sample environments, making *in situ* studies of various processes possible, e. g., electromigration in a functioning electronic device or the activity of small catalyst particles inside a chemical reactor. In both examples, spatial resolutions of at least a few ten nanometers are required. In full-field and in scanning X-ray microscopy, the spatial resolution is limited by the performance of the X-ray optics. In the hard X-ray range, the best conventional microscopes reach spatial resolutions slightly below 50 nm.

Scanning coherent X-ray diffraction imaging, also known as ptychography, can overcome this limit [1-4]. It has been developed over the last few years. In this microscopy technique, the sample is scanned through a confined coherent beam, recording at each position of the scan a far-field diffraction pattern. From these data, the attenuation as well as the phase shift induced by refraction inside of the sample can be reconstructed by iterative phase retrieval algorithms. While in conventional scanning microscopy the spatial resolution is limited by the lateral extension of the probe, the spatial resolution of ptychography can be significantly higher.

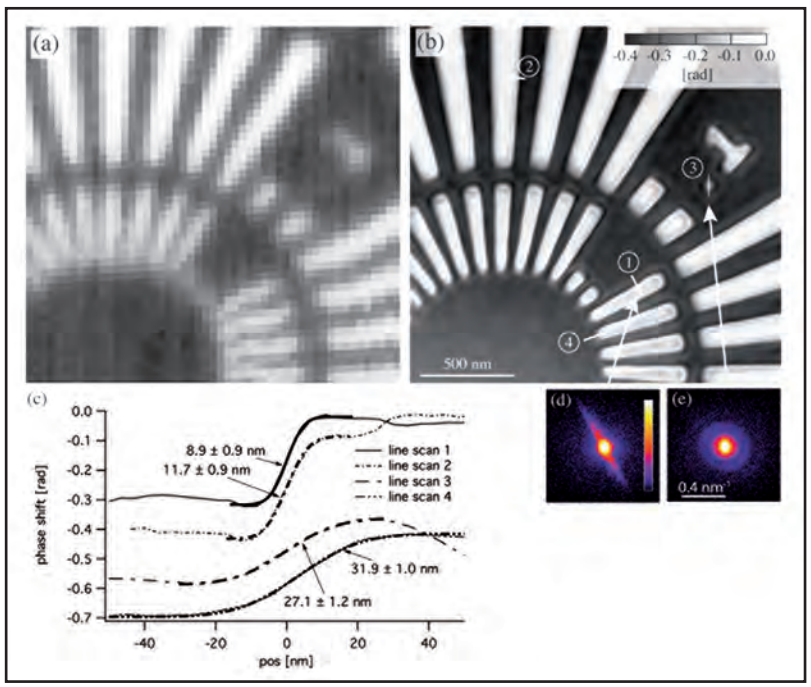

Figure 1

X-ray scanning micrograph of a test structure made of tantalum (NTT-AT). (a) Ta fluorescence map recorded over a field of view of 2 × 2 μm² in steps of 40 nm. (b) reconstructed ptychogram recorded simultaneously with the fluorescence data. (c) Line spread measured at different positions in (b). An error function is fitted to the line scans, and the FWHM spread is given for each. (d) Far-field diffraction pattern recorded on the edge of a spoke near line scan 1 in (b), (e) similar diffraction pattern recorded at the position of the dot in line scan 3.

Fig. 1(a) shows a conventional scanning micrograph of a test object made of tantalum that was recorded in fluorescence mode (pixel size 40 nm) with the hard X-ray scanning microscope at beamline P06 at PETRA III [4, 5]. The resolution in this image is determined by the size of the probing beam, which in this particular case has a lateral extension of about 80 nm at 15.25 keV. Therefore, the smallest features in the test object of about 50 nm lines and spaces can just about be resolved. Fig. 1(b) shows the ptychographic image of the test object that was recorded in parallel to the element map in Fig. 1(a). The image shows the quantitative phase shift induced by the test object with a spatial resolution that is about one order of

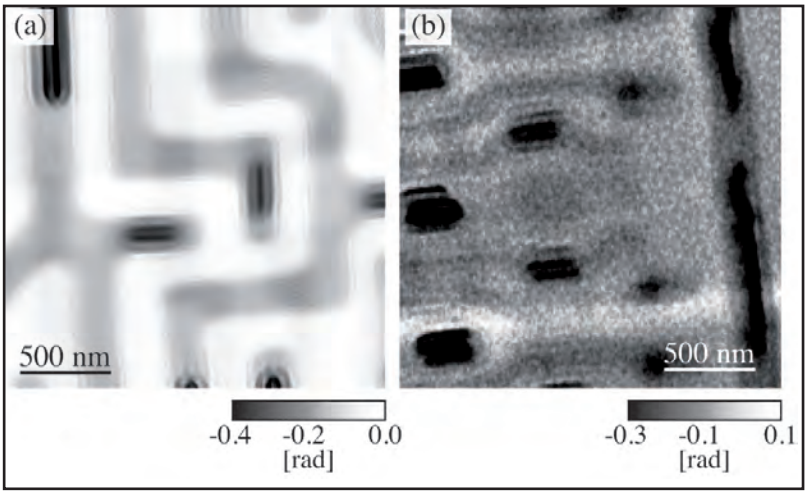

Figure 2
Ptychographic images of a front-end processed and passivated microchip [3,4]. (a) Ptychogram recorded with a detected fluence of 6700 ph/s, (b) ptychogram of another field of view with a detected fluence of 390 ph/s. Reprinted with permission from [4] (Copyright American Institute of Physics, 2012).

magnitude better than that of the fluorescence map. This increase in spatial resolution is obtained from the nano-scale information that is encoded in the far-field diffraction patterns. A detailed analysis shows that different features in the object are reconstructed with different resolution [4]. Fig. 1(c) shows line scans through different features, giving spatial resolutions between 9 nm and 30 nm, exceeding clearly that of conventional X-ray microscopy.

Ptychography is no longer limited by the resolution of X-ray optics but rather by the signal in the far-field diffraction patterns. For features with large diffraction amplitudes at large diffraction angles, the resolution is high. This can be seen, for example, for the diffraction at the sharp edge marked by the line scan 1 in Fig. 1(b). The diffraction pattern of this feature (see Fig. 1(d)) has a strong streak perpendicular to the sharp edge, extending to large diffraction angles (high momentum transfer q). Therefore, the resolution of this feature is high, i. e., about 9 nm. In contrast to that, the diffraction pattern of the dot marked by the line scan 3 in Fig. 1(b) has a circular symmetric diffraction pattern that decays quickly with increasing diffraction angle (Fig. 1(e)). As a result, the resolution of this feature is reduced to about 27 nm. This shows that the resolution varies with the shape of a given feature, depending on its structure factor. Independently of the shape of a particular feature, we can increase the diffraction signal by increasing the fluence on the sample. The optimal ptychographic microscope should thus be installed at one of the most brilliant X-ray sources, such as PETRA III. In addition, the coherent flux should be efficiently focused to the smallest possible spot on the sample. Thus the optimal ptychographic microscope will provide at the same time the best conventional scanning micrographs [4].

The effect of the fluence on the image quality is illustrated in Fig. 2, where two ptychograms of a microchip are compared [3, 4]. The image in Fig. 2(a) was recorded with 6700 ph/nm^2 while that in Fig. 2(b) was exposed with a 17 times lower fluence, i. e., 390 ph/nm^2. The quality of the ptychogram in Fig. 2(a) is superior to that in Fig. 2(b) in two ways: firstly, the spatial resolution is about a factor two higher in accord with the approximate power-law behavior of q^{-4} of the intensity in the diffraction patterns. Secondly, the signal-to-noise ratio is significantly improved, making visible also features with low contrast.

In the future, the X-ray scanning microscope at P06 will be optimized for ptychographic imaging with high sensitivity and high spatial resolution. By optimizing the focusing optics, the coherent flux density on the sample can be increased further by several orders of magnitude. This will improve both the resolution and the sensitivity of the technique. We hope that ptychography will find broad application in many fields of science, ranging from nanotechnology, physics and chemistry (e. g., catalysis) to bio-medical, earth and environmental science.

Contact: Christian Schroer, christian.schroer@tu-dresden.de

Authors

A. Schropp[1], R. Hoppe[1], J. Patommel[1], D. Samberg[1], F. Seiboth[1], S. Stephan[1], G. Wellenreuther[2], G. Falkenberg[2], and C.G. Schroer[1]

1. Institute of Structural Physics, Technische Universität Dresden, D-01062 Dresden, Germany
2. Deutsches Elektronen-Synchrotron DESY, D-22607 Hamburg, Germany

Original publication

"Hard X-ray scanning microscopy with coherent radiation: Beyond the resolution of conventional X-ray microscopes", Applied Physics Letters 100, 254112 (2012).

References

1. J.M. Rodenburg and H.M.L. Faulkner, Appl. Phys. Lett. 85, 4795 (2004).
2. P. Thibault et al., Science 321, 379 (2008).
3. A. Schropp et al., J. Microscopy 241, 9 (2011).
4. A. Schropp et al., Appl. Phys. Lett. 100, 253112 (2012).
5. C.G. Schroer et al., Nucl. Instrum. Meth. A 616, 93 (2010).

Making the invisible visible with coherent X-rays.

3D structure of a single colloidal crystal grain

High-resolution 3D imaging of the internal structure of mesoscopic materials, such as colloidal crystals, is a challenging problem. Development of new imaging approaches based on coherent X-ray scattering methods is quite important for understanding the internal structure of these novel materials. Self-organized colloidal crystals can be used as the basis for new functional materials such as photonic crystals. For many applications, crystal quality is crucial and monitoring the defect structure of these real colloidal crystals is essential. We performed a coherent X-ray diffraction imaging (CXDI) experiment on a single colloidal crystal grain and revealed the presence of plane defects in our sample.

Sayre was the first to propose to phase crystallographic data by measuring information between the Bragg peaks in reciprocal space [1]. The first experimental demonstration [2] showed its potential to reveal the structure of a non-periodic, finite-sized sample illuminated by coherent radiation through applying iterative phase retrieval algorithms [3]. Measuring diffraction patterns from a coherently illuminated, finite-sized crystalline sample locally around a selected Bragg peak (so-called Bragg CXDI) gives information about the shape and a uniform distribution of strain in this particle [4]. This method was recently extended to image a finite region of a two-dimensional (2D) colloidal crystal [5] where the position of individual scatterers (colloidal spheres in this case) as well as the core structure of the defects in the sample were revealed. Here, we extend these findings to a single 3D grain of a colloidal crystal illuminated by coherent X-rays. The coherent X-ray scattering experiment was performed at the Coherence Beamline P10 of the PETRA III facility with an incident energy of the X-rays of 7.9 keV in order to map several Bragg peaks onto a single 2D detector. The scattering geometry of the experiment is shown in Fig. 1. The colloidal crystal grain was mounted on a goniometer, which allows rotation of the sample around the vertical axis. In total 180 diffraction patterns were measured for each sample, in one degree increments covering the entire reciprocal space. Typical diffraction patterns

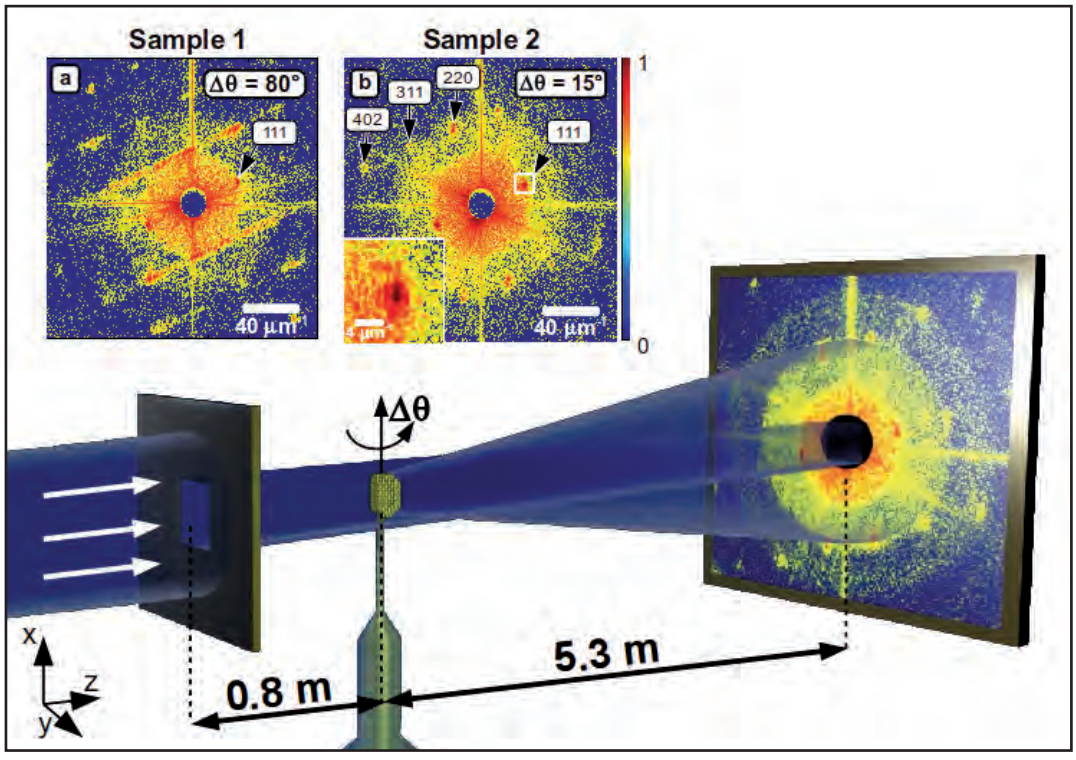

Figure 1

Schematic view of the CXDI experiment showing the guard slits, the colloidal sample and the detector. (a, b) Selected diffraction patterns measured at different relative angles Δθ of the azimuthal rotation for two colloidal grains. The inset in panel (b) presents a magnified view of the region around the Bragg peak shown by the white square.

measured at different relative azimuthal angles of rotation $\Delta\theta$ from the two colloidal crystal grains are shown in Fig. 1(a, b). Several Bragg peaks as well as fringes in the region around them due to the finite size and internal structure of the crystal grains are clearly visible in these diffraction patterns.

We investigated in detail a few grains. For one grain, we saw strong streaks through the Bragg peaks at a relative rotation angle of $\Delta\theta = 80°$ (Fig. 1(a)). At the same time, no streaks were observed in the diffraction patterns during the entire scan for the other grain (Fig. 1(b)). Such streaks are an indication of defects in the crystalline sample [5]. From this result, the conclusion may be made that the first grain contains structural defects and the second one does not. However, such a conclusion deduced only from the analysis of the 2D diffraction patterns can be misleading.

We combined 2D diffraction patterns measured from the second grain into a 3D data set shown in Fig. 2(a). To our surprise, in the 3D representation of the coherent scattering from the second grain, the streaks became visible indicating the presence of a defect in this sample as well. The additional features in the 3D diffraction pattern have the shape of thin rods passing through the 111 Bragg peaks, which is a clear indication that this particular colloidal grain contains a plane defect, a stacking fault in our case, in the (111) plane.

In order to confirm these observations, we performed simulations based on a model of a colloidal sample similar to that used in the experiment. The model, in the form of an ellipsoidal particle, was composed from colloidal spheres made from silicate with a diameter of 230 nm arranged in an fcc crystal lattice (see inset in Fig. 2(b)). A single defect in the form of a stacking fault was introduced inside our model grain particle. We simulated 2D diffraction patterns from this structure for different angles of azimuthal rotation $\Delta\theta$ from 0° to 180° and combined them into a 3D data set (see Fig. 2(b)). Around each Bragg peak we see strong fringes due to coherent scattering from the finite size crystalline particle. In addition, six parallel streaks going through the set of 111 Bragg peaks can be observed, which originate from the scattering from the stacking fault introduced in our model that is similar to the experimental data. This gives us confidence that we have indeed observed a defect in the form of a stacking fault in a single grain of a colloidal particle in our experiment. For reconstruction a set of the simulated data with 180 diffraction planes in total with one degree rotational increment similar to the conditions of our experiment was used. In Fig. 2(c, d) the results of the reconstruction after 2700 iterations are presented. The crystallinity of the sample and, importantly, the stacking fault (see Fig. 2(d)) are clearly resolved.

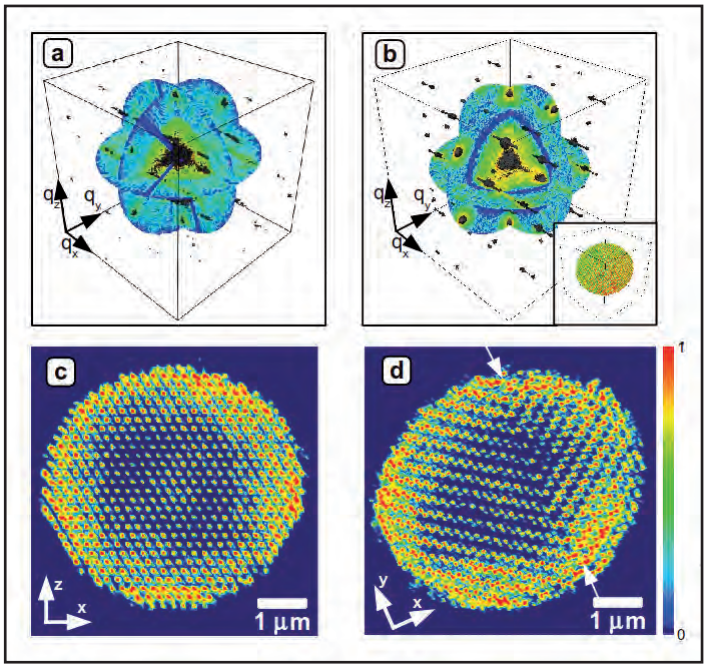

Figure 2

A 3D representation of the measured (a) and simulated (b) scattered intensities showing three orthogonal planes and an isosurface. The length of the arrows along the coordinate axes corresponds to 30 μm^{-1}. An inset in (b) shows the model colloidal sample used in simulations. (c, d) Two orthogonal cuts through the reconstructed object. The arrows in (d) point to the defect in the colloidal grain.

We foresee that this new methodology of studying mesoscopic materials by a combination of conventional small angle scattering CXDI and Bragg CXDI opens new opportunities to determine the structure of these important materials. Potential applications of this technique lie well beyond colloidal crystals and can be applied to various nanostructured materials such as assemblies of block copolymers, micelles, nanoporous materials, or nanoparticles that are on the forefront of modern research at the nanoscale.

Contact: Ivan Vartaniants, Ivan.Vartaniants@desy.de

Authors

J. Gulden[1], O.M. Yefanov[1], A.P. Mancuso[1,2], R. Dronyak[1], A. Singer[1], V. Bernátová[1,3], A. Burkhardt[1], O. Polozhentsev[1,4], A. Soldatov[4], M. Sprung[1], and I.A. Vartanyants[1,5]

1. Deutsches Elektronen-Synchrotron DESY, Notkestraße 85, D-22607 Hamburg, Germany
2. European XFEL GmbH, Albert-Einstein-Ring 19, 22761, Hamburg, Germany
3. Faculty of Science, University of Pavol Jozef Šafárik, Šrobárova 2, 04180 Košice, Slovakia
4. Southern Federal University, Zorge str. 5, 344090 Rostov-Don, Russia
5. National Research Nuclear University, "MEPhI", 115409 Moscow, Russia

Original publication

"Three-dimensional structure of a single colloidal crystal grain studied by coherent X-ray diffraction", Optics Express 20, 4039–4049 (2012).

References

1. **D. Sayre, "The squaring method: a new method for phase determination", Acta Crystallogr. 5, 60–65 (1952).**
2. **J. Miao, P. Charalambous, J. Kirz, and D. Sayre, "Extending the methodology of X-ray crystallography to allow imaging of micrometre-sized non-crystalline specimens", Nature 400, 342–344 (1999).**
3. **J.R. Fienup, "Phase retrieval algorithms: a comparison", Appl. Opt. 21, 2758–2769 (1982).**
4. **M.A. Pfeifer, G.J. Williams, I.A. Vartanyants, R. Harder, and I.K. Robinson, "Three-dimensional mapping of a deformation field inside a nanocrystal", Nature 442, 63–66 (2006).**
5. **J. Gulden, O.M. Yefanov, A.P. Mancuso, V.V. Abramova, J. Hilhorst, D. Byelov, I. Snigireva, A. Snigirev, A.V. Petukhov, and I.A. Vartanyants, "Coherent X-ray imaging of defects in colloidal crystals", Phys. Rev. B 81, 224105 (2010).**

Serial femtosecond crystallography.

Atomic-resolution diffraction before destruction with an X-ray FEL

A series of experiments carried out at the Linac Coherent Light Source (LCLS) at the SLAC National Accelerator Center, California, have demonstrated the unique advantages of hard X-ray free-electron lasers for high-resolution structural studies, especially of biological macromolecules. In recent experiments the methodology of "diffraction before destruction" has been confirmed to atomic resolution by solving the structure of lysozyme, a well-characterized model protein, from snap-shot diffraction patterns of a stream of hydrated room-temperature crystals intersecting the X-ray FEL beam. The studies are already beginning to demonstrate the promise of X-ray FELs to overcome bottlenecks in protein structure determination that are caused by the need for large, well-diffracting protein crystals and pave the way for time-resolved structures of difficult systems.

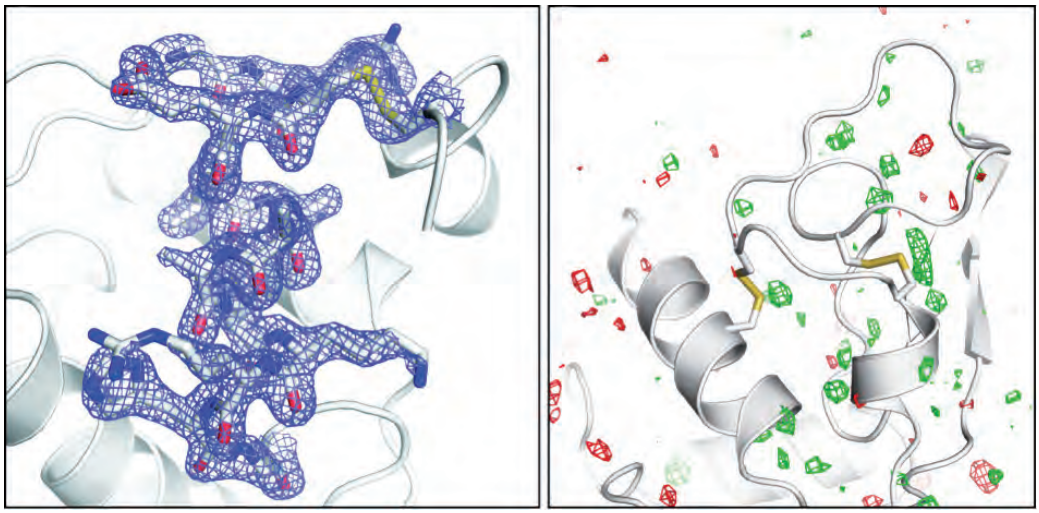

Figure 1

Left: The refined electron density map of lysozyme at 1.9 Å resolution, contoured to 1.5σ, obtained from thousands of individual snapshot diffraction patterns of microcrystals in a flowing jet, with 9 keV 40-fs X-ray pulses from the LCLS. The dose to the room-temperature sample was 33 MGy per crystal. Right: The map generated from the difference of structure factors measured at LCLS and the SLS synchrotron source, contoured at +3σ (green) and -3σ (red). No interpretable features are apparent (reproduced from [1]).

X-ray FELs produce pulses that are up to ten orders of magnitude higher in peak brightness than storage ring sources, with pulse durations of tens of femtoseconds or shorter and up to 10^{13} photons per pulse. When focused to micron dimensions, the power density is high enough to turn any sample into a plasma. The resulting explosion can easily be seen in an optical microscope trained on the interaction area, where the visible plasma glow can be visualized. This glow, however, is the after effect of the interaction of the X-ray pulse with the sample that happens after the pulse has passed through the sample and is propagating on towards the detector where the diffraction pattern is recorded. The structural information encoded within the diffraction pattern arises only from the time that the pulse interacts with the sample. Although photoionisation is rapid, the atomic displacements that result from Coulomb forces are limited by the pulse duration and the atoms' inertia. If the pulse terminates before structural changes take place at the length scale measured in the diffraction pattern then that pattern represents the undamaged structure.

As part of a large international collaboration we have developed the general technique of serial femtosecond-pulse crystallography, or SFX. Our study of lysozyme shows that room-temperature structures collected in the explosive "diffraction before destruction" regime give structures that are indistinguishable from those measured at very low doses with synchrotron radiation and a rotating anode source [1] (Fig. 1).

The LCLS measurements on micrometre-sized lysozyme crystals at room temperature showed diffraction extending beyond 1.9 Å resolution with pulses of 30 to 70 fs duration with about 7×10^{11} photons of 9 keV energy, focused to an area of 10 μm^2. This corresponded to a dose of 33 MGy per pulse, which is similar to the tolerable dose achievable with conventional sources with crystals at cryogenic temperatures. The dose is about 30 times higher than tolerable for room temperature samples. This dose was simply limited by the beamline configuration, and with tighter focusing that is now coming on line at the

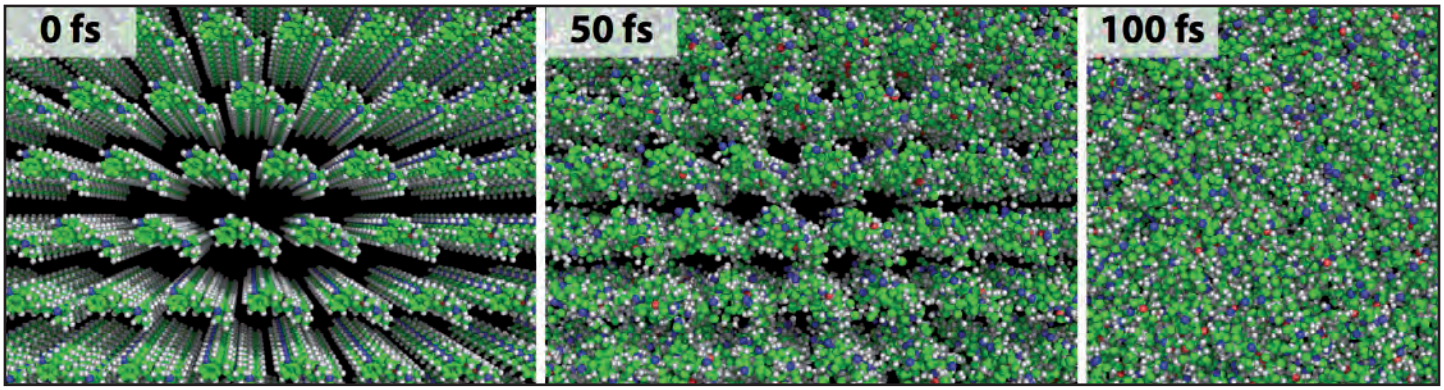

Figure 2

Plasma physics simulations of the explosion of a protein crystal induced by illumination with an intense X-ray pulse of 100 fs duration. Individual atoms are displaced according to displacements calculated using the Cretin code (see [2] for details). Correlation from unit cell to unit cell is initially lost at the shortest length scales and progresses to lower resolution over the time of the pulse. Only the initial part of the pulse contributes to Bragg diffraction (reproduced from [2]).

Coherent X-ray Imaging (CXI) instrument at LCLS, the dose per pulse may exceed 10 GGy. In fact, the highest doses to samples in SFX experiments were 3 GGy, at 2 keV photon energy [7]. In those measurements the 6 Å wavelength and maximum angular extent of the detector limited the resolution to 7.5 Å, not the excessive X-ray dose.

We have developed SFX to record diffraction from hundreds of thousands of microcrystals. Since a single X-ray pulse destroys a crystal, the sample must be continuously refreshed. This is achieved by flowing the sample in a liquid jet across the path of the X-ray beam. The liquid is the native buffer of the crystalline sample and acts as a conveyer belt to bring crystals into the focus of the beam with micron precision. In order to minimize noise in the diffraction pattern due to scatter from the water, jets of diameters from a few micrometres to less than 1 µm are used, formed by a unique design of gas focusing [8]. The jet flows into vacuum, but the sheath gas and short time of flight from the nozzle to the interaction point maintains the temperature of the sample. At present, the crystals are not synchronized with the arrival of an X-ray pulse, so the probability of striking a crystal is proportional to the particle density in the stream, with typical rates of 10 to 30% of pulses recording crystal diffraction. Even without this synchronization, the measurement time is determined by the X-ray pulse, making accurate time-resolved measurement possible by timing an optical pump pulse to the X-ray probe pulse. Since the sample is destroyed by the X-ray pulse anyway, it is feasible to measure irreversible reactions, as demonstrated by Aquila et al. [6].

Whether a pulse hits a crystal or not, the full detector frame is read out every pulse, at 120 Hz at LCLS, and processed off line to detect crystal diffraction patterns. Each detected pattern, originating from a crystal in a random and unknown orientation, is then processed using the CrystFEL software suite [9]. Since the crystal certainly does not oscillate during the exposure, spots in the diffraction pattern do not represent fully integrated Bragg intensities, but are partial reflections. The software passes the patterns through autoindexing routines in an unsupervised manner and determines the partial intensities at all indexed spots in the pattern. By processing tens of thousands of patterns we obtain a high redundancy of observations of every indexed Bragg peak in three-dimensional reciprocal space. By summing up all these intensities we perform a Monte Carlo integration that sums over the 3D volume of the Bragg peak, over variations in crystal size and fluctuations in the pulse fluence and wavelength. The summation is akin to that carried out by integrating the counts in Debye-Scherrer rings of a powder diffraction pattern, except that here the full 3D orientation is preserved. The result is a list of 3D structure factors that are equivalent to a full dataset collected from a high-quality single crystal, without the complications of radiation damage. Almost 60000 indexed patterns are required for this Monte Carlo approach to achieve a 5% convergence of the diffraction intensities.

To validate SFX at atomic resolution several diffraction datasets of lysozyme crystals were measured at the LCLS, the Swiss Light Source, and with a rotating anode X-ray setup. The crystals were prepared at the Max-Planck-Institut für Medizinische Forschung where the in-house data were also collected. The LCLS data were collected with pulses of 40 fs duration and 5 fs. As seen in Fig. 1, difference Fourier maps between these LCLS datasets showed no interpretable features, showing that outrunning radiation damage at 40 fs is just as effective as at 5 fs. Similarly, the difference Fourier electron density map between the 40 fs LCLS data and synchrotron data showed no features. The synchrotron data were collected at a low dose of 24 kGy at room temperature at 12.4 keV photon energy.

We have explained the remarkable agreement between these datasets, and the high dose tolerance for protein crystal diffraction with X-ray FEL pulses, by a self-termination effect of the diffraction [2]. At the extreme X-ray intensities achievable of 10^{20} W/cm^2, corresponding to about 10^4 photons/Å^2/fs, every atom in the entire crystal will be photoionised. At these and lower intensities the ionisation will occur in a random sequence leading to different atomic trajectories from unit cell to unit cell. That is, order will be lost between the repeating units of the crystal. Indeed, when the root-mean-square (RMS) displacement of atoms reaches a value of $\sigma = d / (2\pi)$, the condition of constructive

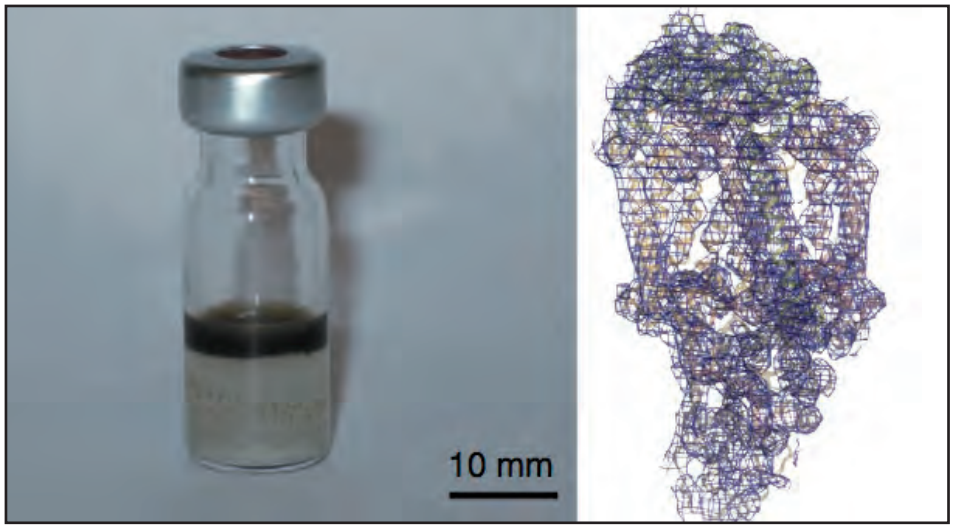

Figure 3

Left: A batch crystallisation setup with the lipidic sponge phase containing microcrystals of reaction centre from Blastochloris viridis floating on top. Right: The refined electron density map of the new crystal form determined by SFX at 8.2 Å resolution (reproduced from [3]).

interference, that supplies the huge gain in diffractive efficiency at Bragg peaks, is lost. In short, the crystal only gives rise to the measured Bragg diffraction while it is a crystal and long-range order exists, as can be easily visualized in Fig. 2. Only the first part of the pulse contributes to the measured Bragg diffraction, and the rapid termination of Bragg peaks is driven by displacements of the fastest atoms—the light atoms. Plasma physics simulations, using the Cretin code, predict that the RMS displacement accelerates during the interaction of the pulse. The high resolution peaks will terminate first, and the explosion will progress to the lower resolutions, if the X-ray pulse is long enough. To explore the dynamics of the explosion we examined SFX protein diffraction at doses above 1 GGy, achieved using long wavelengths where photoabsorption is higher. We measured the diffraction efficiency of photosystem I nanocrystals as a function of resolution and pulse duration, and found that the efficiency decreased with resolution (with a functional form distinctly different to the well-known Debye-Waller temperature effect) and with increasing pulse duration. The behaviour was in excellent agreement with predictions and showed that high-resolution diffraction terminated after about 30 fs. From these studies we see that the explosion progresses faster when the pulse intensity is increased, causing a faster gate to the pulse, but this decrease in the Bragg lifetime is more than compensated by the increase of photons during this time. That is, higher pulse intensities give stronger diffraction patterns.

The SFX technique promises to extend protein crystallography to samples that are challenging or impossible to solve using conventional methods. The intense X-ray pulses enable diffraction to be recorded from crystals as small as 100 nm, and perhaps even smaller. Crystallization attempts usually produce microcrystals that either cannot be improved upon or which take many months or years of efforts to yield large-enough well-diffracting crystals. Such time-consuming optimization can be bypassed, and the resolution achievable from any crystals should be improved with X-ray FEL pulses since the beam need only intersect a well-ordered 100-nm domain in the crystal. Some of the most challenging samples in protein crystallography are integral membrane proteins, which are notoriously difficult to crystallize. These proteins play vital roles in respiration, photosynthesis, cell signalling, and cell trafficking. Over 30% of human genes code for membrane proteins and 60% of all drugs target them. Out of the almost 80000 structures in the protein databank, less than 300 unique membrane protein structures are known at present.

Lipidic cubic phase crystallization is a generic method developed to mimic the natural lipid bilayer of membrane proteins, but it leads to a viscous solution that does not flow fast in the jet. We carried out SFX measurements of photosynthetic reaction centre from Blastochloris viridis that were crystallized in the closely related lipidic sponge phase technique by collaborators at Gothenburg University [3]. The sponge phase is low-density, separates from water, and was found to flow in the gas-focused jet. In a short proof-of-principle experiment carried out at the Atomic and Molecular Optics (AMO) beamline of the LCLS, at 2 keV photon energy, we collected over a thousand diffraction patterns from this sample. This gave a sufficiently complete dataset to yield a molecular replacement structure of a new crystal form of the reaction centre to 8.2 Å resolution (Fig. 3).

A very intriguing and novel approach to crystallisation is the spontaneous *in vivo* growth of crystals in cells. Protein crystallisation does occur as a native process in some specific cases such as in the storage of proteins in seeds and the compartmentalisation within secretory granules of the cell. Also, on infecting Sf9 insect cells, the baculovirus produces a protein called polyhedrin that crystallizes and encases the virion inside. This virus is used as a vector to over express proteins of interest, by replacing the polyhedrin gene with that of the protein to be produced. Surprisingly, the over expression of the enzyme cathepsin B by this method at the University of Tübingen produced stable intact needle-like crystals that were 10 to 15 µm in length and 0.5 to 1 µm wide [4], as shown in Fig. 4. The enzyme is a protease from *Trypanosoma brucei*, the parasite that causes African sleeping sickness. After isolating these crystals by lysis of the cells and differential centrifugation, we crushed them into smaller pieces for SFX measurements at LCLS. These were again carried out at the AMO station at 2 keV photon energy, yielding diffraction to 7.5 Å resolution which could be merged into a set of 3D structure factors.

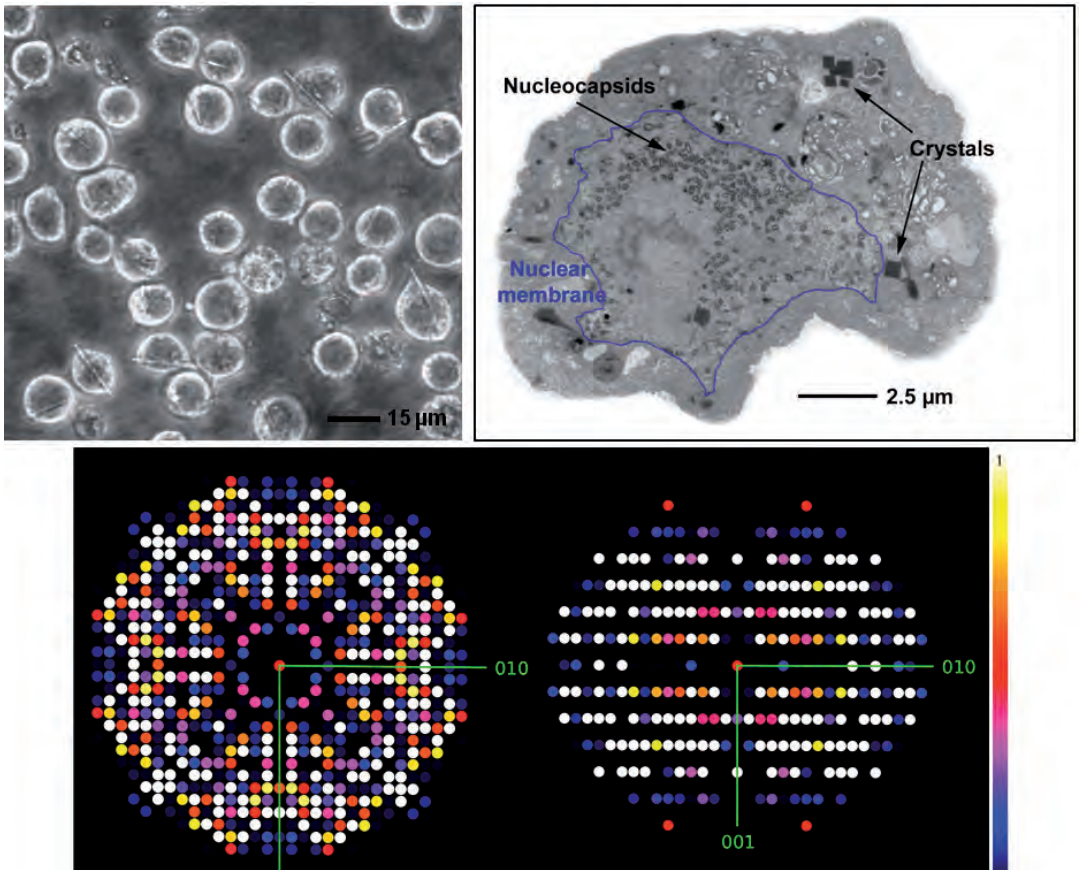

Figure 4

Left: Light micrograph of Sf9 cells infected with *Trypanosoma brucei* cathepsin B expressing virus 90 hours after infection. Right: A transmission electron micrograph of a sectioned Sf9 cell shows the cross-sections of crystals, in groups. Bottom: Precession-style image of the [001] zone for TbCatB, obtained by merging SFX data from 328 in vivo crystal patterns indexed with unit cell constraints (reproduced from [4]).

As an alternative approach to bring a constantly replenishing beam of particles into the X-ray focus we also use aerodynamic-focused beams of aerosols. These were utilised in the first single-particle imaging experiments at FLASH [10], virus imaging experiments at LCLS [11], and most recently to obtain structural information of single particles of soot in aerosols [5,12]. These particles play important roles in a wide range of fields from toxicology to climate science, but their properties are surprisingly difficult to measure. Visible light does not provide the necessary resolution, X-ray sources are usually not bright enough to image single particles, and for electron microscopy particles have to be collected onto a substrate, which potentially alters their structure and encourages agglomeration. In an experiment led by the PULSE Institute at SLAC, single coherent coherent diffraction patterns were collected, with LCLS pulses of 1 nm wavelength, from hundreds of particles which could be reconstructed to give images of 13 nm (full period) resolution. From the patterns we extracted the fractal dimension of the soot structure. At a mean value of 2.3 fractal dimension, the particles were more compact than expected, suggesting that restructuring was taking place in the airborne particles. In another methodological advance, ion time-of-flight spectra were recorded for each hit allowing the correlation of composition with the structural information.

Contact: Anton Barty, anton.barty@desy.de
Thomas White, thomas.white@desy.de
Henry Chapman, henry.chapman@desy.de

Original publications

1. S. Boutet et al. “High-resolution protein structure determination by serial femtosecond crystallography”, Science 337, 362–364 (2012).
2. A. Barty et al. “Self-terminating diffraction gates femtosecond x-ray nanocrystallography measurements”, Nature Photonics 6, 35–40 (2012).
3. L.C. Johansson et al. “Lipidic phase membrane protein serial femtosecond crystallography”, Nature Methods 9, 263–265 (2012).
4. R. Koopmann et al. “In vivo protein crystallization opens new routes in structural biology”, Nature Methods 9, 259–262 (2012).
5. N.D. Loh et al. “Fractal morphology, imaging and mass spectrometry of single aerosol particles in flight”, Nature 486, 513–517 (2012).
6. A. Aquila et al., “Time-resolved protein nanocrystallography using an X-ray free-electron laser”, Optics Express 20, 2706–2716 (2012).

Further references

7. H.N. Chapman et al., “Femtosecond X-ray protein nanocrystallography”, Nature 470, 73–77 (2011).
8. D.P. DePonte, U. Weierstall, K. Schmidt, J. Warner, D. Starodub, J.C.H. Spence, and R.B. Doak, “Gas dynamic virtual nozzle for generation of microscopic droplet streams”, Journal of Physics D: Applied Physics 41, 195505 (2008).
9. T.A. White, R.A. Kirian, A.V. Martin, A. Aquila, K. Nass, A. Barty, and H.N. Chapman, “CrystFEL: a software suite for snapshot serial crystallography”, Journal of Applied Crystallography 45, 335–341 (2012).
10. M.J. Bogan et al., “Single particle x-ray diffractive imaging”, Nano Letters 8, 310–316 (2008).
11. M.M. Seibert et al, “Single Mimivirus particles intercepted and imaged with an X-ray laser”, Nature 470, 78–81 (2011).
12. M.V. Martin et al., “Femtosecond dark-field imaging with an x-ray free electron laser”, Optics Express 20, 13501–13512 (2012).

Femtosecond images of magnetic order.

Holography experiments allow recording real space images of magnetic domains with single LCLS pulses

X-ray free-electron lasers (XFEL) promise real-space imaging of magnetic structures with femtosecond time resolution. Single-shot imaging will be an essential technique for studying transient magnetic and electronic states during stochastic ultrafast dynamics on the nanoscale. Employing resonant X-ray holography at the LCLS we measured for the first time real space images from ferromagnetic nanoscale spin order with single femtosecond pulses. Our results demonstrate that X-ray induced dynamics can be avoided with pulses shorter than 80 fs and fluence levels below 25 mJ/cm^2.

The advent of X-ray free-electron laser sources has opened the door for imaging atomic, electronic and magnetic structures of matter on their intrinsic atomic length and femtosecond time scales [1]. The main goal of single-shot X-ray imaging is to capture an image before manifestation of radiation damage. This concept has been shown to hold for nanoscale and atomic systems [2]. We address here when and if this carries over to the more quickly responding and fragile valence electronic and spin structures [3].

We recorded single shot diffraction patterns from a magnetic sample with an integrated holographic mask (Fig.1) [4]. The magnetic film samples studied were sputter deposited Co/Pd films on silicon nitride membranes. The samples show a ferromagnetic labyrinth-like nanoscale domain pattern with domain sizes of 100 nm in width and perpendicular magnetic anisotropy. An 800 nm thick Au film, opaque to soft X-rays, is sputtered on the back side of the membrane. A focused ion beam has been used to mill a 1.45 µm sample aperture and up to fifteen 100 nm diameter reference holes through the entire sample forming the holographic mask.

By tuning the LCLS X-ray pulses to the Co L_3 absorption resonance, the spin orientation in the ferromagnetic domains is resolved through the X-ray magnetic circular dichroism effect. X-ray pulses of up to 1.87 mJ are sent through a grating monochromator to select photons of 778.8 eV energy with an energy resolution of 0.5 eV. As the LCLS produces linearly polarized X-rays only, an in-plane Co magnetic thin film polarizer is used to generate circular polarization [5]. The unfocused monochromatic beam is therefore sent through the polarizer at 60 degrees to the incident X-rays producing up to 10^9 photons per pulse with 58 % polarization. At the sample position a spot size of 10 by 30 µm is achieved by focusing the beam with bendable mirrors. Finally, the hologram is recorded with a CCD camera. The holographic mask contains multiple reference holes, each of which produces a snapshot of the sample [5]. As the phase information is encoded in the hologram via the sample-reference interference, a single Fourier inversion of the diffraction pattern recovers the real space image.

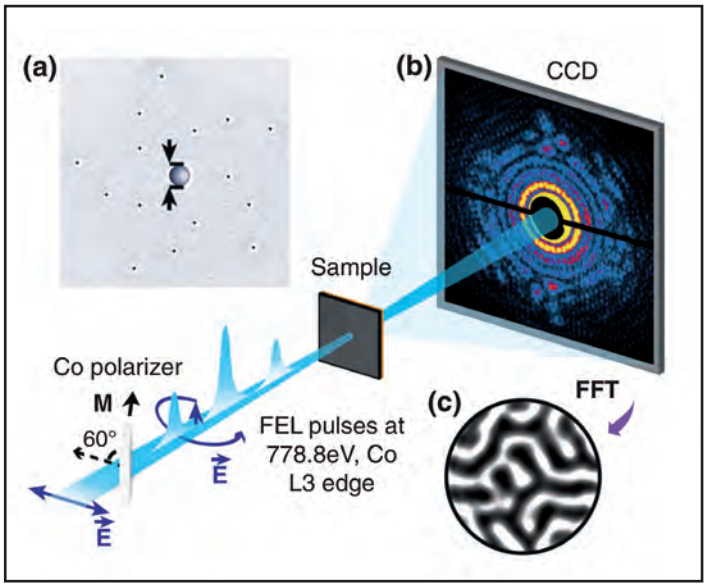

Figure 1

(a) The experimental setup of the single pulse X-ray holography experiment. (b) A CCD camera records the X-ray hologram. (c) Reconstruction of the magnetic domain state.

Fig. 2(a) shows a single-shot diffraction pattern from an 80 fs long pulse. With circularly polarized X-rays, the pattern forms due to charge-magnetic interference of the sample and reference waves. In Fig. 2(b) and Fig. 2(c) the strategic placement of the reference holes produces well-separated images of the spin-resolved electronic structure in the autocorrelation image after Fourier inversion. Each reference generates an independent reconstruction. The summation over all independent reconstructions significantly improves the image quality, increasing the signal-to-noise ratio by up to a factor of 4. The combination of resonantly enhanced scattering with spatially multiplexed X-ray

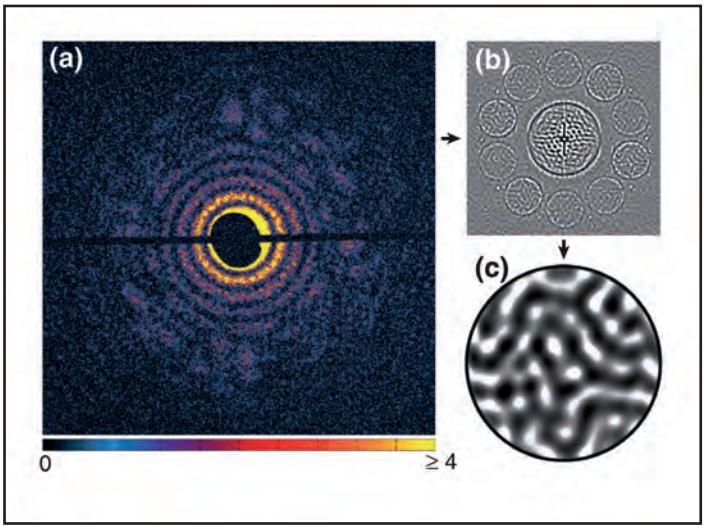

Figure 2

Single shot reconstruction of the nanoscale ferromagnetic order in a Co/Pd thin film. (a) X-ray hologram containing 1.5 x 10^5 detected photons from an 80 fs pulse. (b) Real space magnitude of the complex autocorrelation function after Fourier transform of (a). (c) Final averaged single-shot reconstruction with a resolution of 80 nm, limited due to the size of the reference holes.

holography operates at photon fluences two orders of magnitude less than phase retrieval methods, mitigating possible damage during and after the XFEL pulse. Here, we determined an imaging threshold of 5 mJ/cm^2 for our multilayer system. The stochastic SASE based intensity jitter at LCLS leads to successful reconstruction for half of the X-ray pulses.

Ultrafast pump-probe spectroscopy by sequential imaging at destructive fluences will be limited to the accuracy of cloning solid state targets with confined object regions and reproducible positioning in the X-ray beam. Therefore it is desirable for a single specimen to withstand the aftereffects caused by picosecond-scale thermal heating. The feasibility of non-destructive, sequential single-shot imaging is demonstrated in our experiments. Back-to-back snapshots produce highly correlated images with minor fluctuations along the domain borders near the 25 mJ/cm^2 fluence boundary which leads to an average temperature within the sample of 1100 K. Beyond this fluence a new domain configuration is formed upon cooling that is visible in the real space images. The nanoscale domain periodicity suggests also irreversible thermal damage caused by interstitial diffusion across the Co/Pd interfaces and subsequent anisotropy softening. Thus, the key to non-destructive sequential imaging is to utilize the regime between minimum imaging and thermal damage thresholds.

In summary, our study demonstrates the feasibility of highly efficient non-destructive single-shot imaging of magnetic nanostructures. This technique constitutes a very attractive tool for time-resolved studies of nanoscale femtosecond dynamics.

Contact: Christian Gutt, christian.gutt@desy.de

Authors

Tianhan Wang[1,2], Diling Zhu[3,4], Benny Wu[2,4], Catherine Graves[2,4], Stefan Schaffert[5], Torbjörn Rander[5], Leonard Müller[6], Boris Vodungbo[7], Cédric Baumier[8,9], David P. Bernstein[2,4], Björn Bräuer[2], Vincent Cros[10], Sanne de Jong[3], Renaud Delaunay[8], Andreas Fognini[11], Roopali Kukreja[1,2], Sooheyong Lee[3], Víctor López-Flores[12], Jyoti Mohanty[5], Bastian Pfau[13,5], Horia Popescu[9], Maurizio Sacchi[9,14], Anna B. Sardinha[7,15], Fausto Sirotti[9], Philippe Zeitoun[7], Marc Messerschmidt[3], Joshua J. Turner[3], William F. Schlotter[3], Olav Hellwig[16], Richard Mattana[10], Nicolas Jaouen[9], Franck Fortuna[17], Yves Acremann[11], Christian Gutt[6], Hermann A. Dürr[2], Eric Beaurepaire[12], Christine Boeglin[12], Stefan Eisebitt[13,5], Gerhard Grübel[6], Jan Lüning[8,9], Joachim Stöhr[2,3], and Andreas O. Scherz[2]

1. Department of Materials Science and Engineering, Stanford University, Stanford, California 94035, USA
2. Stanford Institute for Materials & Energy Science (SIMES), SLAC National Accelerator Laboratory, 2575 Sand Hill Road, Menlo Park, California, 94025, USA
3. Linac Coherent Light Source, SLAC National Accelerator Laboratory, 2575 Sand Hill Road, Menlo Park, California 94025, USA
4. Department of Applied Physics, Stanford University, Stanford, California 94035, USA
5. Institut für Optik und Atomare Physik, Technische Universität Berlin, Straße des 17. Juni 135, 10623 Berlin, Germany
6. Deutsches Elektronen-Synchrotron DESY, Notkestraße 85, 22607 Hamburg, Germany
7. Laboratoire d'Optique Appliquée, ENSTA ParisTech - CNRS UMR 7639 - École Polytechnique, Chemin de la Hunière, 91761 Palaiseau, France
8. Laboratoire de Chimie Physique - Matière et Rayonnement, Université Pierre et Marie Curie - CNRS UMR 7614, 11 rue Pierre et Marie Curie, 75005 Paris, France
9. Synchrotron SOLEIL, L'Orme des Merisiers, Saint-Aubin, BP 48, 91192 Gif-sur-Yvette Cedex, France
10. Unité Mixte de Physique CNRS/Thales, 1 ave A. Fresnel, 91767 Palaiseau, France and Université Paris-Sud, 91405 Orsay, France
11. Laboratorium f. Festkörperphysik, ETH Zürich, 8093 Zürich, Switzerland
12. Institut de Physique et de Chimie des Matériaux de Strasbourg, UMR7504, CNRS et Universitié de Strasbourg, 23 rue du Loess, 67034 Strasbourg, France
13. Helmholtz-Zentrum Berlin für Materialien und Energie GmbH, Hahn-Meitner-Platz 1, 14109 Berlin, Germany
14. Institut des NanoSciences de Paris, UPMC, CNRS UMR 7588, 4 Place Jussieu, 75005 Paris, France
15. Grupo de Lasers e Plasmas - Instituto de Plasmas e Fusão Nuclear, Instituto Superior Técnico, Av. Rovisco Pais, 1049-001 Lisbon, Portugal
16. San Jose Research Center, HGST, a Western Digital Company, 3403 Yerba Buena Road, San Jose, California 95135, USA
17. Centre de Spectrométrie Nucléaire et de Spectrométrie de Masse, CNRS/IN2P3, Université Paris-Sud, UMR 8609, 91405 Orsay, France

Original publication

"Femtosecond Single-Shot Imaging of Nanoscale Ferromagnetic Order in Co/Pd Multilayers Using Resonant X-ray Holography", Physical Review Letters 108, 267403 (2012).

References

1. **S. Eisebitt, J. Lüning, W.F. Schlotter, M. Lörgen, O. Hellwig, W. Eberhardt, and J. Stöhr, "Lensless imaging of magnetic nanostructures by X-ray spectro-holography", Nature 432, 885 (2004).**
2. **H.N. Chapman et al., "Femtosecond X-ray protein nano-crystallography", Nature 470, 73 (2011)**
3. **C. Gutt et al. "Single pulse resonant magnetic scattering using a soft X-ray free-electron laser", Phys.Rev.B. 81, 100401 (2010)**
4. **W.F. Schlotter et al. „Multiple reference Fourier transform holography with soft X-rays", Applied Physics Letters 89, 163112 (2006)**
5. **B. Pfau et al. "Magnetic imaging at linearly polarized X-ray sources", Optics Express 18, 13608 (2010)**

Pushing the frontiers of pulsed burst-mode amplifiers.

High-power burst-mode thin-disk laser amplifier

Sub-picosecond laser amplifiers with high output pulse energy at high repetition rate are of tremendous importance for many applications in the field of laser physics. For example, materials processing strongly benefits from a high repetition rate in terms of processing speed and a short pulse duration for ablation of the material. This type of amplifier is also used as a pump amplifier for optical parametric chirped-pulse amplification. For applications at free-electron lasers, a burst operation mode amplifier running at the repetition rate of the accelerator is needed for seeding and as a pump-probe laser for time-resolved studies. We present the development of a Yb:YAG thin-disk amplifier in burst-mode operation with up to 4.45 kW intra-burst output power at 100 kHz repetition rate.

Diode pumped solid-state lasers (DPSSLs) have been developed in the last decades to provide average output powers in the kilowatt range. Three main techniques have proven promising as high-power DPSSL concepts: Fiber, Innoslab and thin-disk amplifiers. Fiber lasers have been pushed to average output powers approaching 1 kW with MHz repetition rates [1]. Due to high nonlinear phase shift accumulated in passing the fiber medium, the output energy is restricted. With Innoslab laser technology [2], the output power and energy can be increased to >1 kW with high repetition rate. Output pulse energies of more than 20 mJ with 12.5 kHz repetition rate have already been shown [3]. The stability of these systems is better than 0.5 % rms. But the output energy of this amplifier type is limited due to a small seed beam diameter in the amplification medium. To increase the pulse energy, the implementation of thin-disk amplifier technology is the most promising. Pulse energies of more than 25 mJ have been reported for repetition rates of 3 kHz with a regenerative thin-disk amplifier [4]. Further increase in repetition rate with high output pulse energy is possible by using the thin-disk amplifier in a multipass setup.

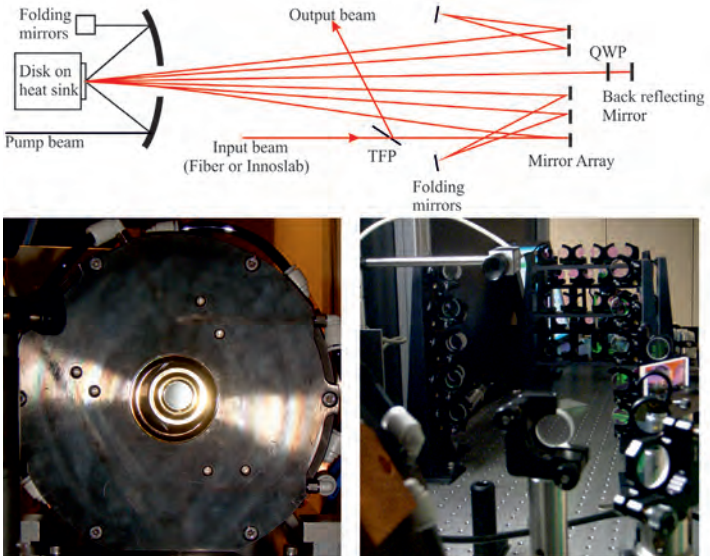

Figure 1

Top: Schematic of the thin-disk setup, QWP: quarter-wave plate, TFP: thin-film polarizer. Bottom: Photographs of thin-disk module (left) and multipass setup (right).

A schematic of the setup of the thin-disk multipass amplifier is shown in Fig. 1. A commercial pump head provided by Trumpf Laser GmbH is used for pumping the thin-disk gain medium (Yb:YAG disk with a thickness of 360 µm) with 24 pump passes. The pump light is emitted by laser diode stacks with a total average power of 10 kW and an emission wavelength of 941 nm in continuous operation. In burst-mode operation, the current of the pumping diodes can be exceeded, leading to a total pump power of 12.4 kW. The pump pulse duration is set to 1.3 ms at 10 Hz. The seed multipass is formed by 30 mirrors in a mirror array, yielding a total of 15 seed passes on the disk. Projection of the beam to a new beam path after every pass on the gain medium is achieved by folding mirrors. These are partly defocusing (radius of curvature of 8 m) to counteract the focusing effect of the thin disk (radius of curvature of 20 m). The number of passes can be increased to up to 30 by re-tracing of the multipass setup with a quarter-wave plate and a thin-film polarizer.

An important parasitic amplification effect in the thin-disk gain medium is the evolution of amplified spontaneous emission (ASE) at high pump powers. There are two different mode types, ring-type and radial modes [5]. To suppress these modes, different approaches can be used: Reduction of the pump spot size leads to suppression of ring-type modes, and bevelling the disk boundaries leads to suppression of the transversal modes. A third approach is to increase the power of the seed laser to reduce the population inversion available for ASE.

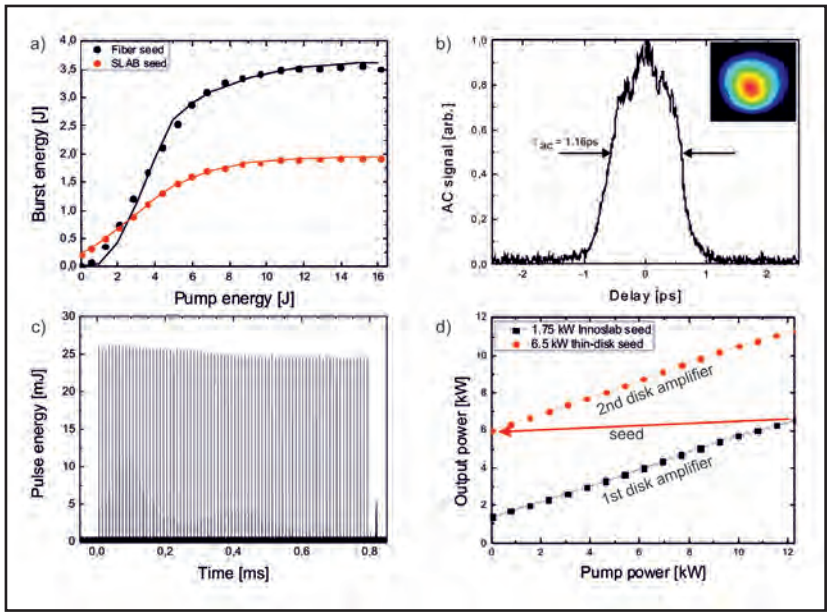

Figure 2

a) Energetics of the thin disk amplifier with a fiber seed (black dots) and a 500 W Innoslab seed (red dots). The results of the simulations are shown as lines.

b) Autocorrelation trace of the amplified and compressed pulses. The measured autocorrelation width yields a pulse duration of 820 fs. The Inset shows the spatial beam profile of the amplified beam. c) Profile of the amplified burst. d) Results of the analytical simulation for 1.75 kW Innoslab seed (black) and for a 6.5 kW seed resulting from the first stage of the thin-disk amplifier cascade (red). The maximum achievable output power in the burst is 11.3 kW.

The experimental results of the thin-disk amplifier are shown in Fig. 2. After suppression of the ASE modes by decreasing the pump spot diameter and bevelling the disk boundaries, a maximum of 4.45 kW output power in the burst mode operation could be achieved with a 50 W seed beam from a fiber amplifier system (Fig. 2a, black dots). The single pass gain was measured to be 1.17 per pass. An increase of the seed power of the thin-disk amplifier was performed by the use of a 500 W Innoslab amplifier. To improve the stability of the system, the number of passes was reduced to 10 (Fig. 2a, red dots). The single pass gain was measured to be 1.17, which is the same as for the seed beam from a fiber amplifier system. This shows that the single pass gain is saturated and ASE could be successfully suppressed. The pulses were then compressed to 820 fs FWHM pulse duration. The corresponding autocorrelation trace is shown in Fig. 2b. An example of the output burst with 25 mJ average pulse energy at 100 kHz repetition rate is shown in Fig. 2c. An improvement of the burst shape can be achieved by shaping of the pump pulse in the thin-disk amplifier and adjustment of the pre-pumping time.

Analytical simulations have been performed for both types of seed beams. A 1-dimensional code is used to simulate the dynamics of the thin-disk amplifier in burst-mode operation. It includes a pre-pumping phase and a main amplification phase. The effects of ASE are combined to one radial mode in the gain medium with absorption losses in the unpumped region of the disk and reflection losses at the disk boundaries. A comparison of the simulated results with the experiment is shown in Fig. 2a (black and red lines). Additionally, this code was used for a design concept to estimate the maximum output power of the thin-disk amplifier in burst operation mode with a two stage cascaded amplifier seeded by a 1.75 kW Innoslab seeder. An output power of 11.3 kW in the burst operation seems feasible (Fig. 2d).

We have proven the capabilities of a Yb:YAG thin-disk amplifier as a high-power amplification system in burst operation mode. Measures for suppressing parasitic modes in the amplifier medium have been successfully implemented. Analytical simulations show that this type of amplifier is suitable to attain output powers beyond 10 kW in burst operation mode, which makes such an amplifier attractive for applications at free-electron lasers.

Contact: Michael Schulz, mi.schulz@desy.de

Authors

M. Schulz[1,2,3], R. Riedel[2,3], A. Willner[1,2,3], S. Düsterer[1], M. J. Prandolini[3], J. Feldhaus[1], B. Faatz[1], J. Rossbach[2,4], M. Drescher[2,4] and F. Tavella[3]

1. Deutsches Elektronen-Synchrotron DESY, Notkestraße 85, 22607 Hamburg, Germany
2. Universität Hamburg, Luruper Chaussee 149, 22761 Hamburg, Germany
3. Helmholtz-Institute Jena, Max-Wien-Platz 1, 07743 Jena, Germany
4. Center for Free-Electron Laser Science, Luruper Chaussee 149, 22761 Hamburg, Germany

Original publication

"Pulsed operation of a high average power Yb:YAG thin-disk multipass amplifier", Optics Express 20, No. 5, 5038–5043 (2012).

References

1. **T. Eidam, S. Hanf, E. Seise, T. V. Andersen, T. Gabler, C. Wirth, T. Schreiber, J. Limpert, A. Tünnermann, "Femtosecond fiber CPA system emitting 830 W average output power", Opt. Lett. 35, 94–96 (2010).**
2. **P. Russbueldt, T. Mans, J. Weitenberg, H. D. Hoffmann, R. Poprawe "Compact diode-pumped 1.1 kW Yb:YAG Innoslab amplifier", Opt. Lett. 35, 4169-4171 (2010).**
3. **M. Schulz et al., "Yb:YAG Innoslab amplifier: efficient high repetition rate sub-ps pumping system for optical parametric chirped pulse amplification", Opt. Lett. 36, 2456–2458 (2011).**
4. **T. Metzger, A. Schwarz, C. Y. Teisset, D. Sutter, A. Killi, R. Kienberger, F. Krausz, "High-repetition-rate picosecond pump laser based on a Yb:YAG disk amplifier for optical parametric amplification", Opt. Lett. 34, 2123–2125 (2009).**
5. **A. Antognini et al., "Thin-Disk Yb:YAG Oscillator-Amplifier Laser, ASE, and Effective Yb:YAG Lifetime" IEEE J. Quantum Electron. 45, 993–1005 (2009).**

Optical flywheels with attosecond jitter.

The interest in timing and synchronization

Femtosecond laser pulses are used for optical timing distribution in next generation accelerators and light sources like FLASH and the European X-ray Free-Electron Laser, because of its ultralow timing jitter properties. Just how low can the jitter of such lasers be? By measuring the timing error between phase-locked optical pulse trains emitted from two oscillators, nearly identical 10-fs Ti:Sapphire lasers, we observed a record low integrated timing jitter of less than 13 attoseconds (1 as = 10^{-18} s) over the full dynamical bandwidth up to the Nyquist frequency. Such a highly uniform train of pulses will enable synchronization of pump-probe experiments which measure evolution dynamics of chemical and atomic processes evolving on femtosecond and attosecond timescales.

Free-electron lasers like FLASH or the future European XFEL, produce extremely short and intense flashes of ultraviolet or X-ray radiation. With this short-wavelength light pulses, it is possible to take flash photos of single molecules and atoms. However, the intense energy of each light pulse destroys the sample. Therefore, the slow-motion movie production of a molecular process requires the repetition of the same process with a fresh sample and each picture is taken a bit later. But how is it possible to reliably postpone the exposures by the same interval from shot to shot? This is achieved with optical lasers used as clock generators. Within these lasers a light pulse oscillates between two mirrors or circulates in a ring cavity, with part of the pulse being partially transmitted through one of the mirrors. As with any clock generator, in the case of a femtosecond laser, where pulse position in the laser resonator is the clock signal, this signal is perturbed or kicked by field fluctuations, which results in timing jitter of the emitted pulse stream from the cavity, see Fig. 1. Because the optical laser pulse is oscillating so steadily within the laser cavity, it is often termed an optical flywheel. In mechanics, flywheels are used among other things to stabilize periodical movements. However, up to now it was unclear, how accurate these optical flywheels are running. This can only be measured directly with a more precise instrument than currently available and by comparison with a second, identical pulsed laser. The fluctuations are fundamental and cannot be minimized beyond those required by the fluctuation-dissipation theorem, which ties it to the cavity losses compensated by gain, causing spontaneous emission noise that drives the random walk of the pulse position. The diffusion rate of the pulse position fluctuations is proportional to the noise power injected into the cavity, which is proportional to the loss and therefore the cavity decay time. The diffusion rate is also inversely proportional to the energy stored in the cavity and further scales with the square of the pulse width [1]. Thus, pulse streams from short pulse, solid-state lasers with low loss cavities, high stored intracavity pulse energy and very short pulses are poised to show the lowest timing jitter possible. Therefore, we chose to measure the timing jitter of pulse trains from two 10-fs Ti:Sapphire lasers.

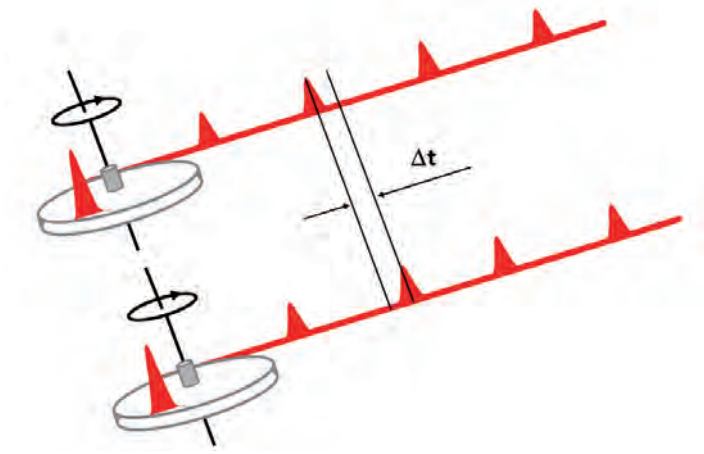

Figure 1

Femtosecond laser pulses as optical flywheels: Each ultrafast laser acts as an optical flywheel releasing optical pulses whenever it passes an output coupler. Highly constant circulation results in an extremely equidistant pulse stream.

The setup is shown schematically in Fig. 2. A balanced optical cross-correlator is based on sum-frequency generation (SFG) between orthogonally polarized pulses from the two Ti:Sapphire lasers. The difference in power of the up-converted signals is used as a measure for the temporal overlap between the two pulses [2]. The timing jitter spectrum, or equivalently the phase noise between the two pulse trains, is measured by dividing the balanced detector's output voltage spectrum by the slope

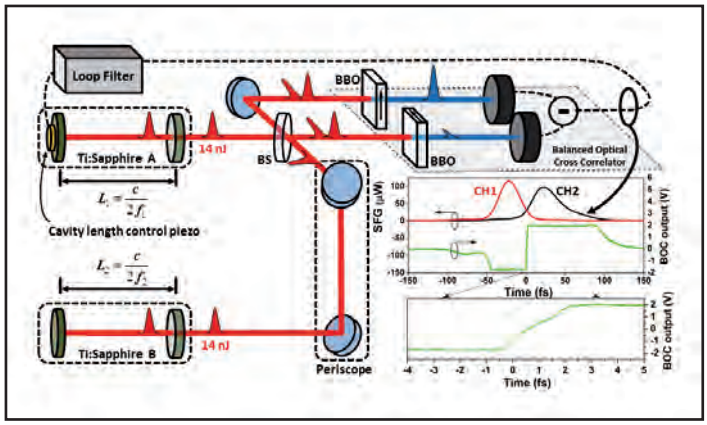

Figure 2

Experimental Apparatus: The output from two nearly identical Ti:Sapphire lasers, A and B, are combined using a beam splitter (BS). The polarization of one pulse train is rotated using a periscope composed of silver mirrors in front of the beam splitter. The resulting beams are composed of orthogonally polarized pulses from both lasers which are focused into two separate 400 μm long BBO crystals for type II second harmonic generation. Orthogonal orientation of the extraordinary axis of the two BBO crystals (indicated by arrows on crystals) ensures that equal up-conversion efficiency occurs only when the two pulses are exactly overlapped at the entrance to both crystals.

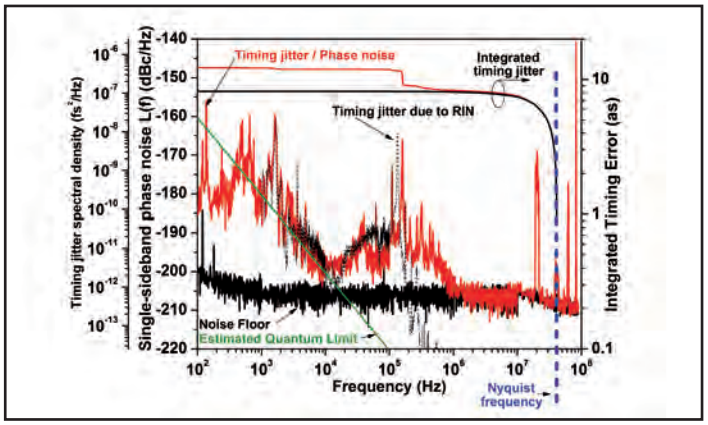

Figure 3

Timing jitter spectral density and rescaled single sideband phase noise between the phase-locked optical pulse trains from two mode-locked Ti:Sapphire lasers, as measured by the optical cross correlator: All traces have been scaled from the base 80 MHz pulse rate of the Ti:Sapphire lasers to 10 GHz as a common basis for comparison. The result of the optical cross correlator measurement is plotted in red, and the noise floor of the optical cross correlator measurement determined by measuring the output of the balanced detector when the input is blocked is plotted in black. The estimated contribution to the timing jitter spectrum due to pump laser relative intensity noise (RIN) is plotted using a dotted black line. The green line shows the estimated spontaneous emission-limited timing jitter for the lasers measured here.

of the balanced detector characteristic, converting voltage fluctuations to timing jitter or phase noise.

The measured residual timing jitter spectrum from the phase-locked pulse trains is plotted in Fig. 3, along with the integrated pulse arrival time error. The resulting integrated timing error is 12.3 ± 0.6 as, taking into account the entire frequency range up to the Nyquist frequency of 40 MHz for the 80 MHz pulse repetition rate lasers. Out of these roughly 13 as of jitter already 8.1 ± 0.4 as are due to the high-frequency noise floor. The dependence of timing jitter on pump laser noise was also investigated by modulating both pump lasers in turn and coherently detecting the resulting timing jitter using the cross correlator. In that way, it was proved, that the remaining timing jitter in the range 10 kHz – 1 MHz is due to pump power fluctuations and not the fundamental spontaneous emission noise. In fact, the calculated timing jitter due to spontaneous emission noise only, see green line in Fig. 3, is less than 1 as. Thus, the currently observed jitter is still completely dominated by pump laser noise rather than fundamental spontaneous emission noise. Recent results demonstrate that pump laser noise can be adequately suppressed by locking to an optical reference cavity [3] and, therefore, even further improvements are possible in the future. Low-jitter mode-locked lasers will benefit timing distribution and synchronization for next generation X-ray free-electron lasers such as seeded X-ray FELs in various ways. In such facilities, the critical laser systems for seed and probe generation are solid-state lasers very similar to those discussed here. The high frequency jitter result demonstrated here indicates that there are no fundamental limitations in the jitter of laser oscillators that may limit synchronization in the attosecond timing range. Such precision would make groundbreaking optical pump and X-ray-probe experiments possible measuring the evolution dynamics and structural changes of chemical and atomic processes evolving on femtosecond and potentially even attosecond timescales. The current measurement is only a first step into this direction. The jitter of optical timing distribution systems as well as drifts in the optical amplifier systems following the laser oscillators must be controlled to similar levels, both of which are formidable tasks.

Contact: Franz X. Kärtner, franz.kaertner@cfel.de

Authors

Andrew J. Benedick[1], James G. Fujimoto[1], and Franz X. Kärtner[1,2]

1. Department of Electrical Engineering and Computer Science and Research Laboratory of Electronics, Massachusetts Institute of Technology, 77 Massachusetts Ave, Cambridge, MA 02139
2. Center for Free-Electron Laser Science, DESY and Department of Physics, Hamburg University, Notkestraße 85, D-22607 Hamburg, Germany

Original publication

"Optical flywheels with attosecond jitter," Nature Photonics 6, 97-100 (2012).

References

1. **H.A. Haus and A. Mecozzi, "Noise of mode-locked lasers", IEEE Journal of Quantum Electronics, 29, 983-996 (1993).**
2. **T.R. Schibli et al., "Attosecond active synchronization of passively mode-locked lasers by balanced cross correlation", Opt. Lett. 28, 947-949 (2003).**
3. **T. M. Fortier et al., "Generation of ultrastable microwaves via optical frequency division", Nature Photonics 5, 425-429 (2011).**

Coming soon to a theatre near you: X-ray movies of electron motion.

Quantum connection between light and matter

To understand the functionality and dynamic behaviour of molecules, solids and complex biological systems, it is important to image the coherent motion of electrons in real-time and in real-space. The motion of atoms within molecules and solids that is associated with chemical transformations occurs on the femtosecond (1 fs = 10^{-15} s) timescale. The timescale of electronic motion can be even faster, on the order of attoseconds (1 as = 10^{-18} s) [1, 2]. Electrons are the glue that keeps the atoms in normal matter together, their dynamics playing a central role in the function and transformation of materials. The focus of our work was to answer an open question: How does an ultrashort X-ray pulse scatter from coherently moving electrons, and what information about the electron motion can be retrieved from the resulting scattering patterns?

X-rays are used to probe the atomic-level structure of molecules, solids and complex biomolecules. Methods for such tasks are being developed to more and more perfection, for instance at light sources like the PETRA III storage ring at DESY. But the images generated to date have been static: pictures resolve situations in real-space, but not real-time. Ultra-short, high-energy X-ray pulses from free-electron lasers, laser plasmas and high-harmonic generation promise to solve the problem in the near future, opening up a whole new world of exploration of matter in action.

The ultimate goal of the emerging field of time-resolved imaging (TRI) is to visualize electrons on an ultrafast timescale as they move in atoms, complex molecules or solids, such as occurs for instance during bond formation and breakage (see Fig. 1). But how does an ultrashort X-ray pulse interact with electrons in motion? How do we interpret a scattering picture of a dynamic system? To answer these questions we have calculated the interaction of X-rays and non-stationary matter and found that the obtained scattering patterns deviate substantially from the common notion of an image of the instantaneous electron density being encoded in the scattering pattern [1, 3]. In other words, measuring the scattering patterns does not merely provide an answer to the question of where the electrons are located at a particular instant of time. Instead, the patterns encode information on the electron motion directly.

In our work, we employed two distinct theoretical models of light for describing the scattering of X-rays from a dynamic electron system. We demonstrated that one of them, a quantum electrodynamics (QED) model, which describes light in terms of photons, is essential for correctly describing the scattering patterns, whereas a classical model, which describes light in terms of a wave, incorrectly predicts that the scattering patterns relate to the instantaneous positions of the electrons. Not only is this not the case, but the interpretation of the scattering patterns as encoding an instantaneous density would mislead the analysis of experimental data.

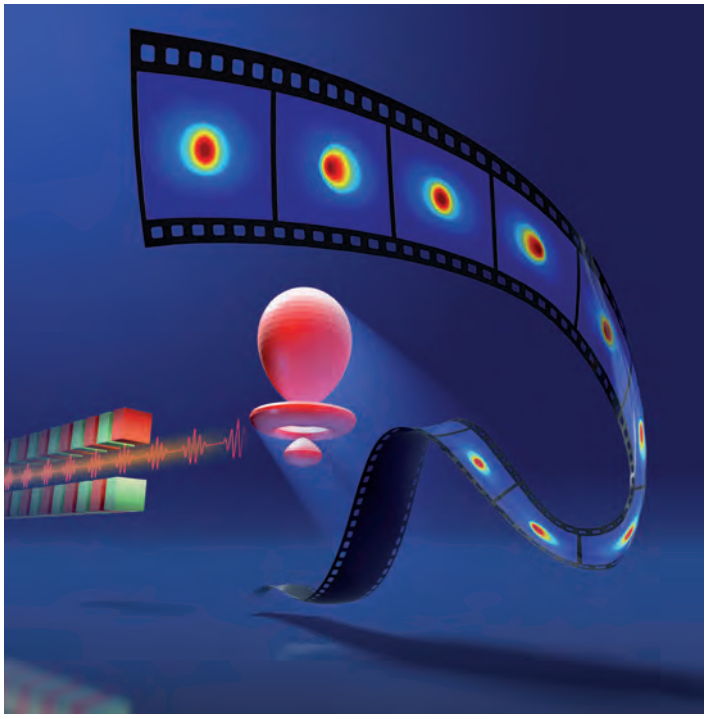

Figure 1

Schematic of the time-resolved X-ray imaging scenario. An electronic quantum wave packet is prepared by a pump pulse as a coherent superposition of energy eigenstates. The electronic dynamics of the quantum wave packet are probed by an ultrashort X-ray pulse. A series of scattering patterns, obtained by varying the pump-probe time-delay, may be stitched together to make a movie of the electronic quantum motion with atomic-scale spatial and temporal resolution.

In order to illustrate the general theory, we considered a situation in which a short pump pulse initiates the electronic motion in atomic hydrogen. This motion can be described by an electronic quantum wave packet. The quantum wave packet can be probed at various time intervals with an ultrashort X-ray pulse, producing

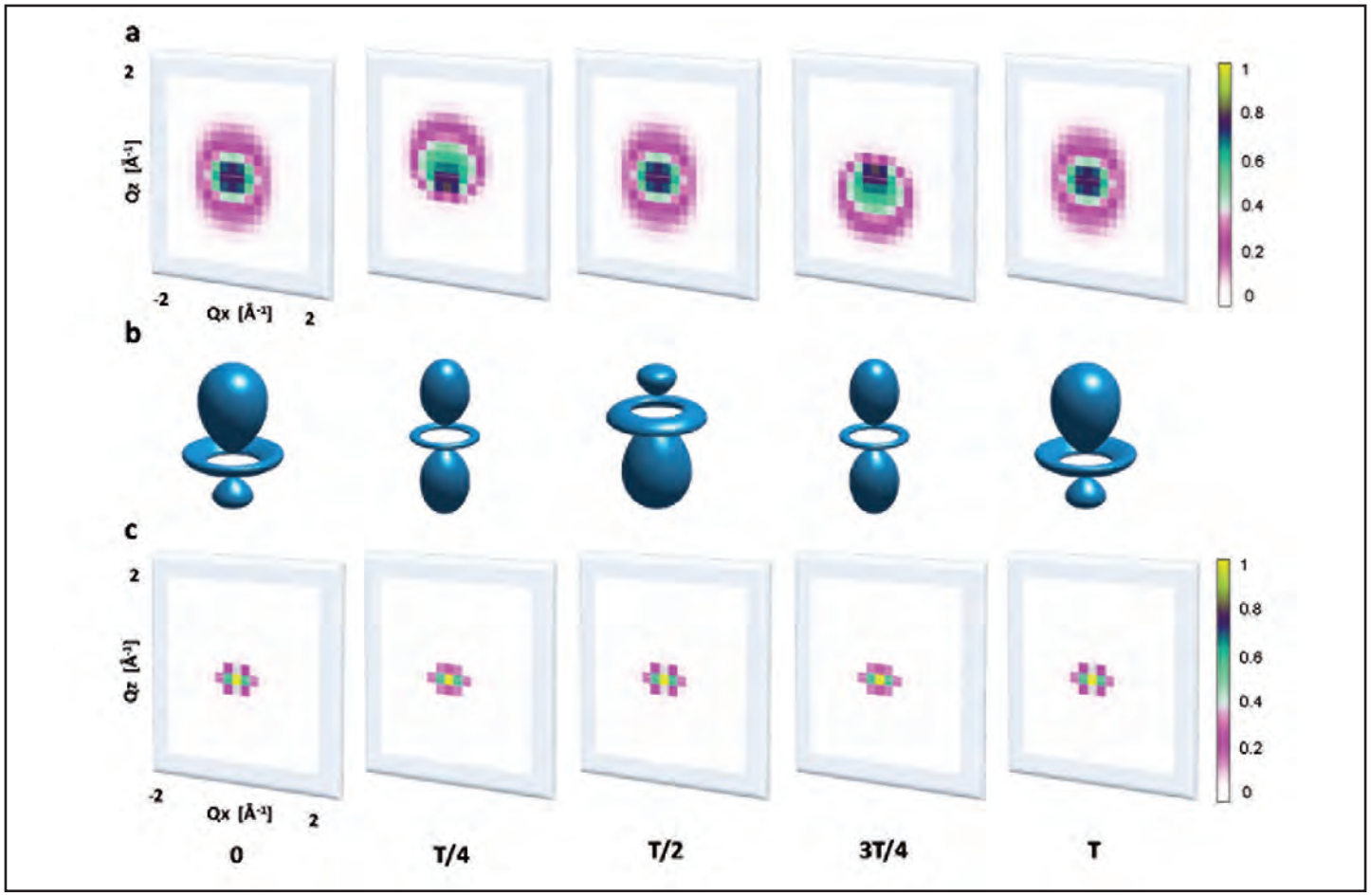

Figure 2

Scattering patterns and electronic charge distributions of the electronic quantum wave packet. (A) Scattering patterns obtained via the quantum electrodynamical description of X-rays, (B) electronic charge distributions and (C) scattering patterns obtained via the classical description of X-rays at pump-probe delay times 0, T⁄4, T⁄2, 3T⁄4, and T, where the oscillation period of the electronic quantum wave packet is T = 6.25 fs. The quantum wave packet is exposed to a 1 fs X-ray pulse with 4 keV photons. The figure is taken from [G. Dixit, O. Vendrell, and R. Santra, Proc. Natl. Acad. Sci USA 109, 11636 (2012)] © 2012 PNAS.

a distinctive scattering pattern that changes as the quantum wave packet evolves. Employing the QED model, we demonstrated that the scattering patterns for atomic hydrogen reflect the quantum motion of the electron, while accounting for eigenstate transitions that occur as a result of scattering. Note that a correct description of a TRI experiment requires both elastic and inelastic (Compton) scattering processes to be properly taken into account, which is only possible with a QED description of the X-rays. A classical description of light cannot accomplish this. A key point is that the observation of electron motion in the time domain requires X-ray pulses that are so short that, as a consequence of the energy-time uncertainty principle, a distinction between elastic and inelastic X-ray scattering can no longer be made. As a result, the obtained scattering patterns do not simply relate to a Fourier transform of the instantaneous electron density, and can be asymmetric under conditions for which the charge distribution is symmetric (see Fig. 2). The patterns also provide strikingly visual evidence of the quantum nature of light.

Our study suggests that X-ray TRI accesses the information on the motion of an electronic quantum wave packet with atomic-scale spatial and temporal resolution. Our result is counterintuitive as seen from the perspective of X-ray scattering from a stationary electronic system, as one would expect to access the instantaneous electronic density for sufficiently short pulses. Moreover, our present findings will help to solidify the conceptual foundations of the emerging field of TRI, where understanding the motion of electrons is key to understanding the functioning of complex molecular and biological systems.

Contact: Robin Santra, robin.santra@cfel.de

Authors

Gopal Dixit[1], Oriol Vendrell[1] and Robin Santra[1,2]

1. Center for Free-Electron Laser Science, DESY, Notkestrasse 85, D-22607 Hamburg, Germany
2. Department of Physics, University of Hamburg, D-20355 Hamburg, Germany

Original publication

"Imaging Electronic Quantum Motion with Light", Proc. Nat. Acad. Sci. U.S.A. 109, 11636-11640 (2012).

References

1. **F. Krausz and M. Ivanov, "Attosecond physics", Rev. Mod. Phys. 81, 163-234 (2009).**
2. **E. Goulielmakis et al., "Real-time observation of valence electron motion", Nature 466, 739-743 (2010).**
3. **H.C. Shao and A.F. Starace, "Detecting electron motion in atoms and molecules", Phys. Rev. Lett. 105, 263201 (2010).**

Research Platforms and Outstations.

Center for Free-Electron Laser Science CFEL.

Joining forces under a new roof

After more than three years of construction the new CFEL research building has been completed in August 2012 and handed over to the University of Hamburg by the Behörde für Wissenschaft und Forschung on 3 September 2012. On the following day, over 200 scientists from various locations started moving in. An official inauguration of the building will take place on the 17 June 2013.

The building, funded by the State of Hamburg and the Federal Government of Germany with 40 million Euros, will be home to about 400 scientists, students, technicians and administrative staff. It will also provide laboratory space for a wide range of activities, including laser and detector laboratories as well as chemistry, biochemistry, electron microscopy and clean room facilities.

In the large experimental hall, the CFEL-ASG Multi-Purpose (CAMP) instrument is now being re-assembled. This instrument came back to Hamburg from SLAC where it was used for over two years under the supervision of the CFEL MPG-ASG division for various successful experiments. For example, an experiment led by Daniel Rolles resulted in the observation of an ultra-efficient ionization of heavy atoms by intense X-ray FEL pulses (B. Rudek et al., *Nat. Photonics* advance online 2012). With a

Figure 1

View into the CFEL atrium from the third floor on 3 September 2012 (photo courtesy of Till Mundzeck).

Figure 2

Copter view on the CFEL building (photo courtesy of Jürgen Newger - www.flugkopter.de).

single 1.5 keV X-ray flash from LCLS, the researchers were able to kick out electrons with ionization energies far exceeding the photon energy. Up to 36 electrons were removed at once from a single xenon atom. These are significantly more than should be possible at this energy of the X-ray radiation. After reassembly, the CAMP instrument will be installed at FLASH and will be available to all users for future experiments.

The CFEL UHH-ASG recently reported results from FLASH where the group around Markus Drescher observed and probed the ultrafast explosion of iodine molecules (M. Krikunova et al., *Phys. Rev. A* 86 (2012) 043430). They used a strong 120 femtosecond near-infrared laser pulse to create in iodine a molecular wave packet with ultrafast dynamics and then probed it with a synchronized 13.4 nm, 35-fs extreme-ultraviolet pulse from FLASH. It turned out that the infrared pulse strips two outer (valence) electrons from the molecule within the central 75 femtoseconds around the pulse maximum. The chemical bond is disrupted and the now ionized molecule explodes. With FLASH, the scientists were able to record in real time how the remaining not localized valence electrons are distributed anew between both iodine atoms. This experiment was only possible because the X-ray pulses are absorbed from a completely different part of the atom than the IR pulse, thereby enabling to observe the system without disturbing the process.

The Coherent Imaging Division made large progress over the year in X-ray free-electron laser-based serial femtosecond crystallography (SFX) and single-particle diffractive imaging. Some highlights of this work, carried out with international collaborators, are described in “Serial femtosecond crystallography” in the “Research Highlights” section of this report. The work has continued from the first proof-of-principle experiments with a hard X-ray free-electron laser, carried out just over two years ago, to the confirmation of the “diffraction before destruction” principle to atomic resolution, the demonstration of time-resolved protein SFX experiments, and the application to various proteins. There was also a large progress in software development with the first public version of the software suite CrystFEL, which has been deployed on a 144-core computer cluster located in the DESY computer centre. New developments in phasing algorithms were applied to high-resolution coherent X-ray diffractive imaging of airborne soot particles. The improved understanding the microstructure of these particles has implications in human health and climate science.

The Ultrafast Optics and X-Rays Division started in 2011 and has grown to a group of 18 students, postdoctoral associates, senior researchers and technicians at DESY Campus complemented by a group of 21 additional researchers at MIT’s Research Laboratory of Electronics. Progress has been made in several

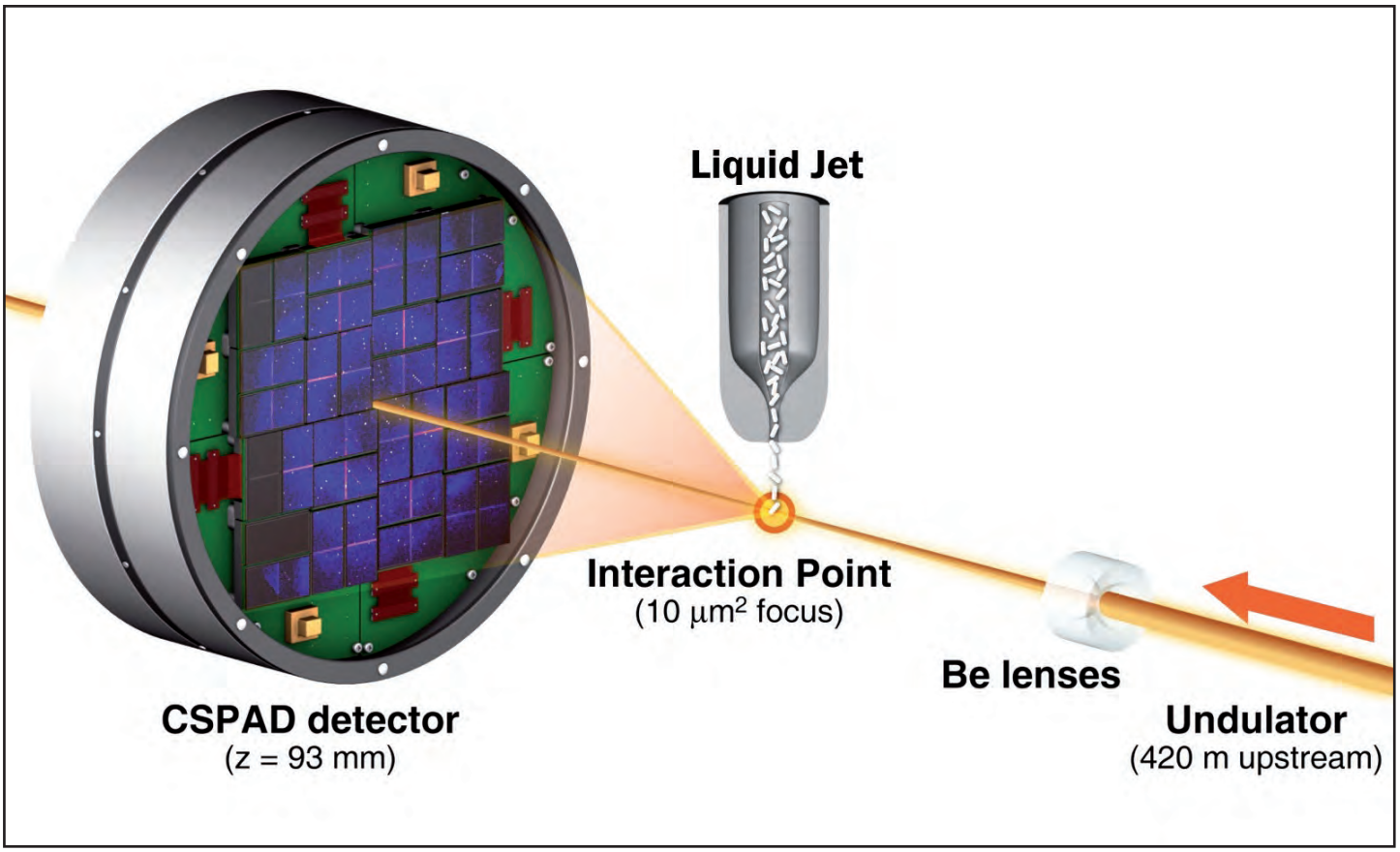

Figure 3

Experimental geometry for SFX at the Coherent X-Ray Imaging (CXI) instrument. Single-pulse diffraction patterns from single crystals flowing in a liquid jet are recorded on a CS-PAD at the 120-Hz repetition rate of LCLS. Each pulse was focused at the interaction point by using 9.4-keV X-rays. The sample-to-detector distance (z) was 93 mm.

areas important to next generation light sources: compact, coherent X-ray sources that can be used for seeding of large scale FELs (W. S. Graves et al., *Phys. Rev. Lett.* 108 (2012) 263904) as well as stand-alone source; demonstration of ultralow jitter femtosecond laser systems and polarization maintaining dispersion compensated fibre links – these systems enable large-scale timing distribution and synchronization in accelerators and light sources at the attosecond level (A. J. Benedick et al., *Nat. Photonics* 6 (2012) 97); record efficiency in THz radiation from Lithium-Niobate approaching 4% conversion from optical to THz wavelengths.

CFEL's Theory Division has been making scientific progress in several areas. The work on theoretical analysis of multiwavelength anomalous diffraction at high X-ray intensity points the way to solving the so-called phase problem in femtosecond nanocrystallography using X-ray FELs (S.-K. Son et al., *Phys. Rev. Lett. 107* (2011) 218102). The theoretical support for an experiment that demonstrated X-ray-induced broadening of an Auger-electron spectral line profile found first evidence for stimulated emission involving inner-shell electrons (E. P. Kanter et al., *Phys. Rev. Lett. 107* (2011) 233001). Clarification of the mechanisms underlying the molecular dynamic processes in ionized acetylene was achieved. This work explains observations that had been made in an experiment carried out at FLASH (M. Madjet et al., *Phys. Rev. Lett. 107* (2011) 263002). Finally, it was demonstrated that the scattering patterns obtained in ultrafast X-ray scattering from an electronic wave packet provide an unusually visual manifestation of the quantum nature of light (see the "Research Highlights" section of this report).

The Atomically Resolved Dynamics Division has now come online with three different ultrabright electron sources that provide distinctly different capabilities. The Relativistic Electron Gun for Atomic Exploration (REGAE) obtained its first diffraction results this year. The other source technology is based on RF pulse compression of nonrelativistic electrons. The first direct observation of molecular motions of weakly scattering organic systems discovered how chemistry maps so simply on to few key coordinates despite the innumerable different possible nuclear configurations possible. Finally, the simplest source based on a compact DC electron gun currently at 100 – 150 kV has shown the best diffraction yet based on a simple modification in detector design. This source allows new developments in nanofluidics that have enabled real space imaging with 1 nm resolution, sufficient to track nanoparticles and biomolecular dynamics *in situ*. In addition, a self-assembly method was introduced for creating megapixel arrays of nano to micron protein crystals that solved the solid target problem to enable high throughput structure determination with XFELs (A. Zarrine-Afsar et al., *Anal. Chem. 83* (2011) 767 & *Acta Crystallogr.* D 68 (2012) 321).

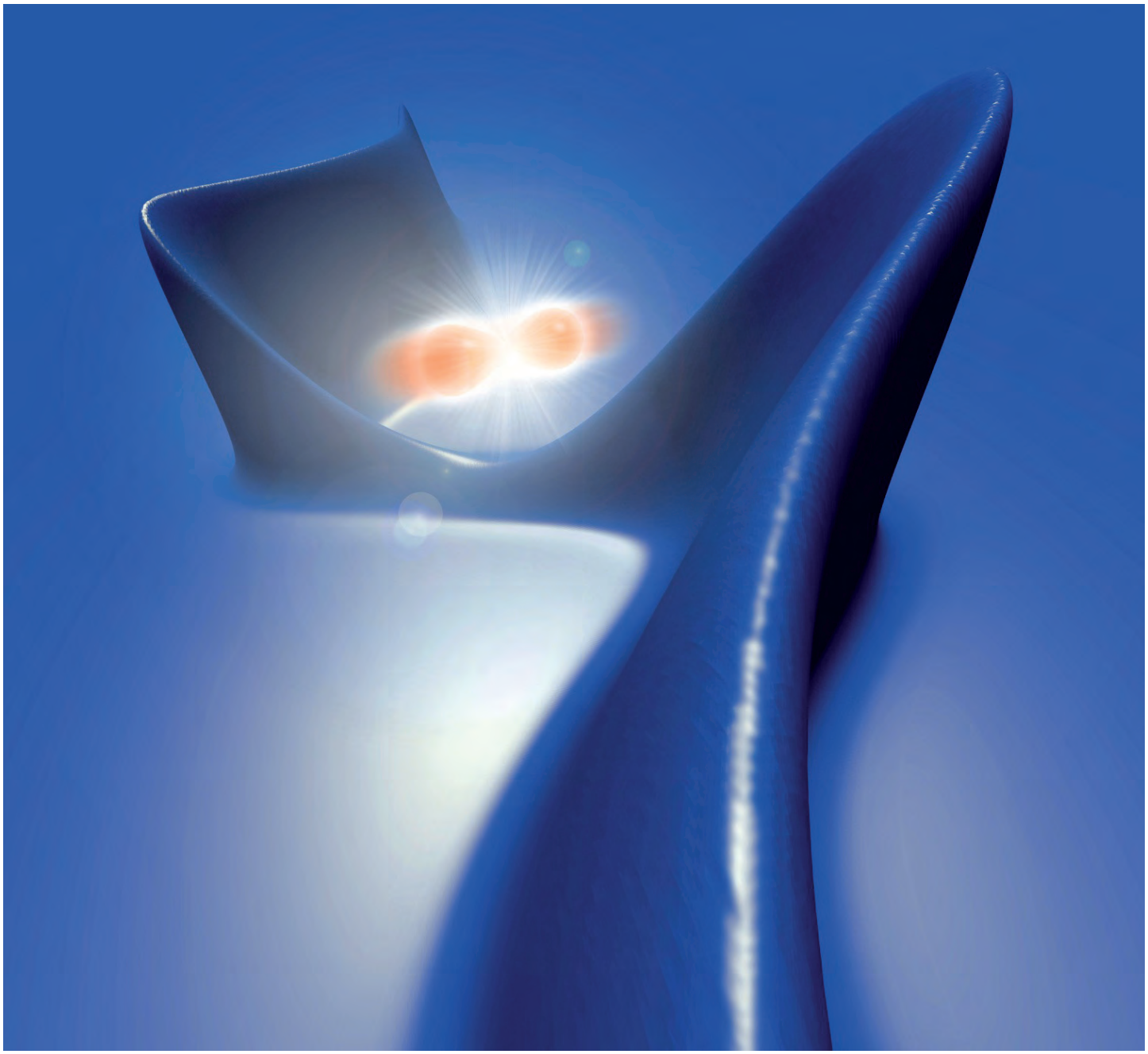

Figure 4

A single-cycle terahertz field accelerates photoelectrons emitted from neon atoms irradiated by an X-ray free-electron laser. In this way, the X-ray pulse temporal profile and arrival time are uniquely retrieved on a pulse-to-pulse basis with femtosecond precision.

In the past year, the Condensed Matter Division continued on its work on the structure and dynamics of complex oxides. Nonlinear THz dynamics in superconducting Josephson plasmons have been studied in detail, as well as studies of nonlinear lattice dynamics and light induced superconductivity in underdoped cuprates. On the FEL science front, a collaboration with the Coherent Imaging Division has developed a new class of experiments in the area of complex oxides nanocrystallography. A joint LCLS beamtime has investigated micro and nanocrystalline powers of magnetoresistive manganites, which were flown in a 200-K jet to acquire diffraction patterns. Better structural refinement compared to wide-beam powder diffraction is feasible and is the goal of this project. This would shine new light onto the microscopic details of charge order in materials that exhibit strong phase separation, potentially revolutionizing materials research. Adrian Cavalieri has developed a measurement technique that provides complete temporal characterization of individual FEL pulses at FLASH, ultimately allowing for complete characterization of their time of arrival and shape. As reported in Nature Photonics, this technique greatly supersedes all previous measurement, opening the way to X-ray pulse shaping at these unique light sources (I. Grguraš et al., *Nature Photonics*, 2012 / doi:10.1038/nphoton.2012.276).

Contact: Ralf Köhn, ralf.koehn@cfel.de

DESY NanoLab.

Small is beautiful!

To cope with today's challenges in nanoscience and nanotechnology, a large portfolio of different techniques is required. DESY is therefore setting up the NanoLab as a facility providing methods which are complementary to the advanced X-ray techniques available at DESY. The DESY nanolaboratory (NanoLab) is planned as a user facility providing access to advanced nano-characterization, nano-structuring and nano-synthesis techniques on-site, in combination with approved beamtimes at one of the DESY photon sources PETRA III and FLASH. The operation of the DESY NanoLab is embedded in the Photon Science research group "X-ray physics and nanoscience". The DESY NanoLab will be located in the new Photon Science Building (Fig. 1), to be constructed close to the PETRA III storage ring, Max von Laue Hall, allowing easy and fast access to the PETRA III beamlines. The new building will host low vibration laboratories, as well as standard labs and office space. In addition to the DESY NanoLab and its in-house research activities, several other Photon Science research groups and the Engineering Materials Science Centre (EMSC) of the Helmholtz-Zentrum Geesthacht will be located in the new building. The architect selection will take place until the end of 2012.

Figure 1

Architect's view of the new Photon Science Building's interior. The atrium will be used as meeting point and event location. The galleries will host offices, conference rooms and standard labs, while low vibration laboratories will be installed in the basement. (figure courtesy of REINER BECKER ARCHITEKTEN)

Construction work will start in autumn 2013 and the building will be finally completed in 2015. The scientific instrumentation of the DESY NanoLab will be implemented in a two-step process: an existing ultrahigh vacuum setup for surface preparation and nanoparticle growth will be extended by additional surface science techniques such as scanning tunnelling and atomic force microscopy as well as X-ray photoemission spectroscopy, which will be available on a collaborative basis end of 2013. In addition, an X-ray diffraction laboratory is currently being set up, which will allow specular reflectivity and grazing incidence X-ray diffraction measurements on a routine basis using a sealed tube Mo X-ray source and parabolic multilayer optics.

The NanoLab large scale instrumentation will be implemented in close discussion with the DESY photon science users; a satellite workshop at the Photon Science Users' meeting in January 2013 will address the users' needs and suggestions. Currently, a state-of-the art charge compensated scanning electron microscope with energy dispersive X-ray spectroscopy for nanostructure and compositional analysis is under discussion. For specimen preparation and nano-structuring a dual focussed ion beam is envisaged. In addition, e-beam or He ion beam lithography instrumentation is planned for the on-site fabrication of nanostructured samples. Optical microscopes as well as methods for the characterization of magnetic samples are under discussion. A chemistry laboratory for the preparation of nanoparticles by wet chemical methods and polymer films is foreseen. The aim of the NanoLab is to fully exploit the synergies between advanced X-ray techniques at large scale facilities and the enormous capabilities of state-of-the art nanoscience laboratory instrumentation.

Contact: Andreas Stierle, andreas.stierle@desy.de

Centre for Structural Systems Biology CSSB.

Widening competences

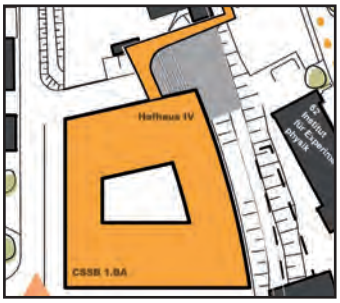

Figure 1

Site diagram (above) and Architect's view of the new CSSB building (figures courtesy of hammeskrause architekten).

The "Centre for Structural Systems Biology", a new interdisciplinary centre on the DESY campus dedicated to infection research, is taking form in many respects.
The result of an agreement among leading research institutions in Northern Germany, the CSSB will unite scientists from different disciplines under one roof, enabling close cooperation focused on key processes during the early stages of an infection. A new building will offer office and laboratory space to about 180 scientific and technical staff. Within this collaboration, DESY will provide direct and fast access to experimental facilities at PETRA III.
By fostering strategic co-operations and networking between universities and non-university research institutions, CSSB will be able to fully exploit existing resources and drive synergies in interdisciplinary approaches. Both its concept and infrastructure will make CSSB a highly innovative alliance institute, enabling it to rapidly gain visibility at national and international levels and develop into a leading research centre in the field.

The involved institutions are:

- Helmholtz-Zentrum für Infektionsforschung Braunschweig HZI
- Universität Hamburg UHH
- Universitätsklinikum Hamburg Eppendorf UKE
- Forschungszentrum Jülich FZJ
- Heinrich Pette Institut Hamburg HPI
- Bernhard Nocht Institut Hamburg BNI
- Medizinische Hochschule Hannover MHH
- European Molecular Biology Laboratory EMBL
- Deutsches Elektronen-Synchrotron DESY

DESY acts as host institution for the other eight partners and is responsible for the construction and, later on, for the operation of the CSSB building. Moreover, DESY will establish its own research group, thus extending its research activities to structural biology. It is expected that in view of a future use of the European XFEL by structural biologists CSSB and the Centre for Free-Electron Laser Studies (CFEL) will play a key role.
One young researcher group established by HZI is already active; another one, funded by the Swedish Research Council in the framework of the Röntgen-Ångstrom-Cluster RAC, is starting soon; a W2 protein crystallographer has been appointed by FZJ, as well as a W1 position for bio informatics by MHH.
In a first hiring phase three W3 professorships are to be appointed at CSSB: one by the UKE for "Structural and Systems Biology of Bacteria", one by the UHH together with HPI for "Structural Biology of Viruses" and one by the UHH together with BNI for "Cellular Biology of Human Parasites".

The realisation of the new building is also progressing: following a call for tender for detailed architectural planning, in which well-known architect's offices participated, a very attractive project was chosen, schematically illustrated in Fig. 1. The selected architects have now started detailed planning, and construction is expected to start in summer 2013.
In the meantime DESY will help to accommodate the new CSSB groups offering provisional laboratory and office space.

Contact: Edgar Weckert, edgar.weckert@desy.de

EMBL Hamburg Unit.

Integrated Structural Biology Services and Research with Synchrotron Radiation

The EMBL Hamburg Unit is a major provider of research services in structural biology, specifically for synchrotron radiation beamlines, preparation and crystallization facilities for biological samples, and the provision of computational services. Details of the quantity of our services are listed in Tab. 1.

Table 1: Research Services		Jan-Dec 2011	Jan-Sep 2012
EMBL beamlines	No. of user visits	361	230
	No. of projects	316	115
	No. of external research groups	207	89
EMBL software	No. of users	5266	5671
	No. of external research groups	2527	2586
EMBL crystallisation	No. of users	46	26*
	No. of crystallisation plates	513	260*

*HTX facility was not operational between April-August 2012

In 2011-2012, activities were focused on completing the construction, commissioning and operational start-up of EMBL's integrated research facilities at the PETRA III synchrotron on the DESY campus. EMBL operates three beamlines at the PETRA III ring – P12 for Small-angle X-ray Scattering for biological applications, and P13 and P14 for Macromolecular Crystallography (Fig. 1).

On the BioSAXS beamline P12, commissioning was combined with a limited "friendly user" operation, and in the final commissioning step in August-September 2012, focusing optics were also implemented. With the focusing bimorph mirrors installed, the beamline can toggle between two modes of operation: a monochromatic, unfocused mode with a straight beam and a focused mode with a deflected beam demanding a second beam branch due to the large mirror-to-sample distance. With this instalment P12 became fully operational and ready to take over all biological SAXS users upon the shutdown of DORIS. The beam quality on P12 reached the projected specifications, with accurate images collected in subsecond exposure time and the sample amount required under 5 µl (for DORIS beamline X33, 2 minutes and 50 µl were required, respectively). With the automated sample changer of P12, the full operational cycle is below 1 minute allowing a throughput of about 60 samples per hour (on X33, about 12 samples per hour could be measured). A new chromatography system coupled with refractometry, light scattering and UV absorption characterization was installed for the on-line purification and multi-method characterization of macromolecular solutions. The system significantly improves the sample quality and permits the characterization of equilibrium oligomeric systems and transient complexes.

During 2011-2012 the commissioning work also continued on both crystallography beamlines. The high-precision goniostat on P14 has surpassed the expectations in terms of mechanical precision with a sphere of confusion of less than 100 nm. Using the unfocussed beam from the U29 undulator, many data sets of high quality were collected allowing the determination of more than 20 crystal structures by molecular replacement. External user groups with accepted proposals were invited to use the beamline from May 2012. A major success of this year was the funding, delivery and commissioning of two large-area pixel-detectors (PILATUS 6M) for the two MX beamlines. The super-polished vertical focusing mirror of the P14 microfocus beamline has also been put into operation delivering a line focus of a few micron size. On P13, data collection using energies around and below 6 keV was explored. At these energies the beamline offers a high flux of photons on the order of 10^{13} photons per second. Using Sulfur-SAD (Single Anomalous Diffraction) data collected at 6 keV, the first unknown structure – a protein of 65 kDA molecular weight – was solved in September 2012.

The sample preparation and characterization (SPC) facility has started an international visitor program to help non-experts in the preparation of macromolecular samples for structural studies. Access to the program is supported by FP7 infrastructure grants P-cube and Biostruct-X. A visit involves crystallization, sample

Figure 1
Entrance to the control hutch area of the EMBL beamlines at PETRA III.

Figure 2
Course tutors and participants at the 8th PEPC course.

quality control and optimization and directly links to the BioSAXS and crystallography beamlines at PETRA III. In the near future, a comprehensive characterization combining light scattering and SAXS will be offered on the BioSAXS beamline. The facility was further equipped with a circular dichroism instrument, capable of determining secondary protein structure in the ultraviolet range. The quality of the spectra is similar to those obtained from circular dichroism beamlines.

EMBL is also engaged in providing additional support to external users through the so-called I3 scheme from the European Commission. Since September 2011 EMBL Hamburg is the coordinator of BioStruct-X focusing on X-ray based methods in structural biology. Scientists are encouraged to apply for access to European synchrotron radiation installations through an online BioStruct-X portal and during the first year almost 500 project proposals were received. Following the evaluation procedure after the first application deadline in March 2012, 334 projects were supported, reflecting a high level of scientific quality overall. BioStruct-X also works closely with other I3 projects and the ESFRI project INSTRUCT to coordinate relevant future projects in structural biology.

EMBL is a partner of the future Centre for Structural Systems Biology (CSSB) and is actively involved in the centre's task force. The goal of EMBL is to integrate current key infrastructures into the future CSSB infrastructures and to ensure that the centre will reach the level of international excellence originally envisaged. EMBL is planning to recruit a CSSB group leader in 2013.

EMBL has also continued to be involved in future XFEL activities in life sciences in 2012. Following the signing of a Memorandum of Understanding between European XFEL GmbH and EMBL in September 2011, EMBL presented a project proposing to construct, commission and operate a Biology Infrastructure Life Science Facility (XBI) at the European XFEL site to facilitate the preparation, analysis and interpretation of biological experiments in immediate proximity to the XFEL instruments. The proposal was positively received by the XFEL scientific advisory committee and EMBL was encouraged to submit a full XBI proposal which was done in March 2012.

EMBL's dedication to providing high quality advanced training to scientists at all levels continued in 2011 – 2012. EMBL Hamburg hosted a record number of courses this year for students from across the globe: the EMBL Advanced Course on Hybrid Structural Biology Approaches in June 2012, run for the first time; in September the successful biannual EMBO funded Practical Course on Protein Expression Purification and Characterisation now in its 8th year (Fig. 2); the successful Solution Scattering from Biological Macromolecules workshop also funded by EMBO in October, and the first European School for Macromolecular Crystallography jointly run by EMBL and CCP4 (Collaborative Computational Project No. 4 – Software for Macromolecular X-ray Crystallography) which will run in November 2012. Building on the success of last year, EMBL Hamburg joined forces with colleagues at EMBL EBI (European Bioinformatics Institute) again to run the annual EMBO Practical Course on Computational aspects of protein structure determination and analysis: from data to structure to function, held at the EBI. The 2013 course will be run in Hamburg in April. A major event in 2013 will be the 11th International Conference on Biology and Synchrotron Radiation organized by EMBL Hamburg in September 2013.

The EMBL Hamburg group has also been strong on research publications in 2012 with highlights including SAXS studies of allosteric competitive inactivation of a human CSF-1 protein by the viral protein BARF1 (Nature Molecular Structural Biology, see: **www.embl-hamburg.de/research/research_highlights/2012/120820_Hamburg/index.html**) and determination of an unusually irregular 42-mer protein assembly of the catalytic core of an archaeal 2-oxoacid dehydrogenase multienzyme (cover page of FEBS Journal, volume 279(5)). Crystallographic highlights include studies of the molecular requirements for peroxisomal targeting of alanine-glyoxylate aminotransferase (see: **www.embl-hamburg.de/research/research_highlights/2012/120501_Hamburg/index.html**) and the superhelical architecture of the myosin filament-linking protein myomesin published in PLoS Biology and detailed in the Research-Highlights Section of this report.

For further news see: **http://www.embl-hamburg.de/research/research_highlights/index.html**.

Contact: Matthias Wilmanns, matthias.wilmanns@embl-hamburg.de

Helmholtz-Zentrum Geesthacht Outstation at DESY.

GEMS is growing

In 2012, the outstation of the Helmholtz-Zentrum Geesthacht (HZG) has seen a considerable growth in staff (presently about 35) and in terms of research possibilities. It is part of HZG's German Engineering Materials Science Centre (GEMS), with the aim of providing highly brilliant synchrotron radiation for engineering materials science. As agreed with DESY, HZG has now become responsible for the respective project review panel rating proposals for PETRA III instruments.

One of the reasons for the expansion of GEMS on the DESY site is the successful acquisition of third-party funding. Our membership in the German Collaborative Research Centre SFB 986, coordinated by the TU Hamburg-Harburg, with a central project serves as an excellent example. The scattering and imaging techniques offered by GEMS are considered as indispensable tools to characterise and improve the tailored hierarchically structured functional materials with novel mechanical, optical and electric properties synthesised within the SFB. We can offer customised support to the SFB by two experienced postdocs. GEMS is a member of the Helmholtz Virtual Institute "New X-ray analytic methods in materials science" (VI-NXMM, coordinated by KIT) and contributes to the test, optimisation and implementation of novel X-ray optics. Two projects within the Röntgen-Ångström-Cluster, a Swedish-German initiative to foster scientific collaborations based on synchrotron radiation and neutrons, have been initiated by GEMS scientists and are based at GEMS beamlines. They focus on the microscopic origin of efficient joint lubrication and on *in situ* sputtering of hard metal coatings on tools, respectively. Within the EU project Science Link (DESY-coordinated multilateral cooperation) GEMS employs an Industrial Liaison Officer coordinating industrial projects, in particular from companies in the Baltic Sea region. Projects in the Kiel based SFB 677, in the Helmholtz Initiative "Energy Storage" and in the Helmholtz portfolio topic "Detector Technologies and Systems" complement our broad portfolio of third-party funded materials science research.

The GEMS beamlines at DESY have all entered "user mode" in 2012, in line with the GEMS commitment to support external scientists in their experiments.

The last user shifts of the *HARWI II* beamline before the shutdown of DORIS III included several diffraction user experiments concerning texture and structure analyses, including dilatometer

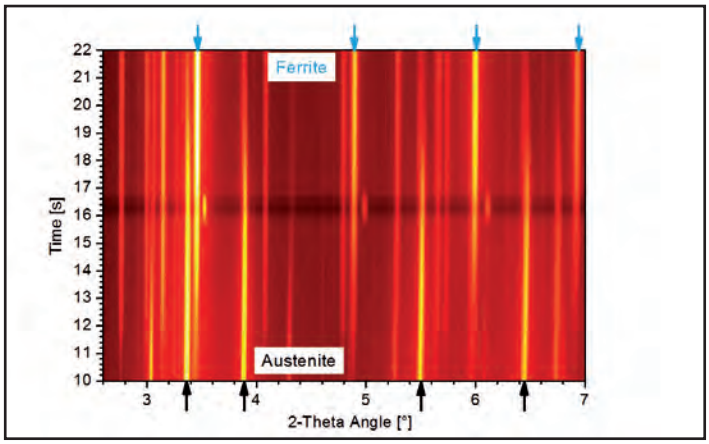

Figure 1

Phase transition in a fixed gauge volume during *in situ* friction stir welding of steel at HEMS. The process has been followed with 10 Hz image rate under real conditions (feed rate 1 mm/s). The background is due to the Ti backing plate.

experiments. Many groups will continue their experimental work at GEMS beamlines at PETRA III. For those particularly interested in the use of "pink" radiation, the planned "HARWI III" station at the damping wiggler of the PETRA extension beamline P61 is an experimental setup to look forward to. The long-term tomography users at HARWI II and BW2 (DORIS III) are facing a similar situation. Many successful experiments were still carried out thanks to the efficient support by the HZG "tomography team". At PETRA III, the Imaging Beamline (IBL) and the tomography station at HEMS greatly improve the spatial resolution in imaging applications (see below) whereas larger samples will use a planned new instrument and the new capabilities at the PETRA extension beamline P21. Phase-contrast techniques are being continuously improved within the VI-NXMM mentioned above.

The High-Energy Materials Science Beamline (*HEMS*, P07 at PETRA III) for research with high-brilliance high-energy X-rays has been in regular user mode for more than a year now. HEMS is one of the PETRA III beamlines with the highest overbooking. For all experimental hutches fast detectors (15 Hz maximum read-out frequency) have been integrated. The high-precision sample rotation axis and the X-ray optical tables of the 3D-XRD grain mapper were installed. Commissioning with samples and

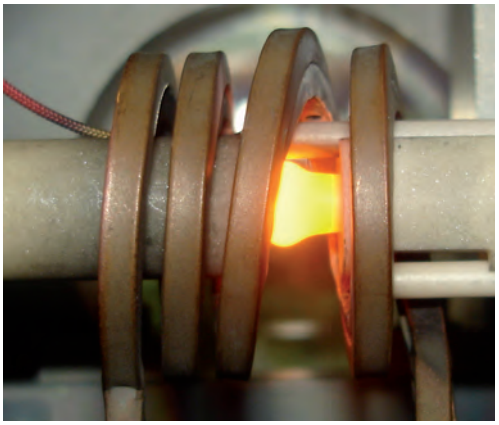

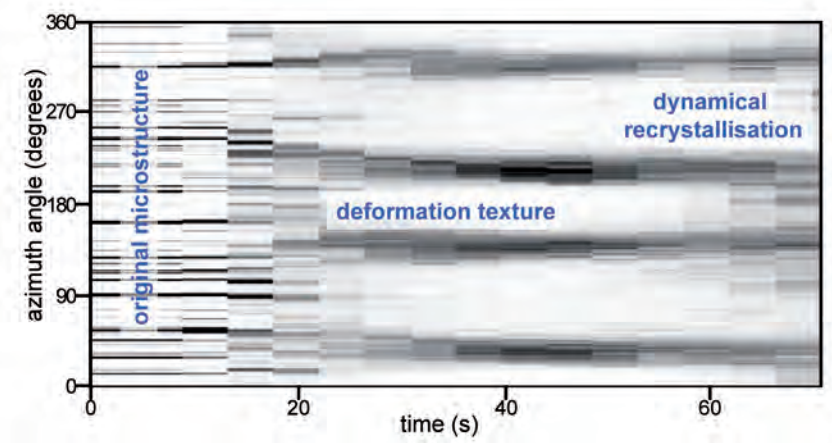

Figure 2

In situ forging of a novel γ-TiAl based alloy in the HZG dilatometer. The evolution of deformation textures has been measured by taking high-energy X-ray diffraction diagrams in real-time at HEMS. The azimuthal intensity distribution on a diffraction ring shows the development of a strong deformation texture followed by dynamical recrystallisation reducing the texture. All post-processing effects can be excluded in this way .

temporary detector setups is scheduled for spring 2013. The HEMS side station continues to be an extremely valuable experimental station for HZG in-house research in the areas of texture and residual stress measurements as well as for *in situ* phase analysis with the popular HZG dilatometer (see below).

An important strength of GEMS is the measurement of engineering materials processing i*n situ* under real conditions, now exploiting the full potential of PETRA III at HEMS. From numerous successful user experiments in this area, two examples shall be highlighted here. The combination of high brilliance and a fast detector allowed for a real-time observation of structural changes in a fixed gauge volume during friction stir welding (Fig. 1). The recently commissioned deformation unit of the dilatometer makes forging in the X-ray beam possible, with an *in situ* measurement of texture changes (Fig. 2). Still in 2012, a first *in situ* laser beam welding experiment will open up new possibilities to study fast processes in real time.

In December 2011, a group from KIT in collaboration with HZG performed an *in situ* X-ray diffraction analysis experiment on the mechanical stress evolution during laser surface hardening of steel at the Imaging Beamline (*IBL*, P05). IBL was chosen due to the available space in the experimental hutch before the complete installation of the imaging setup. In the first half of 2012, the installation of the nano tomography endstation at IBL was completed (Fig. 3). A vacuum tank for pre-focusing lenses was installed in the optics hutch as well as the rest of the experimental equipment in the nano tomography endstation. Initial tests with sub-micron resolution were successfully performed, further commissioning of the nano tomography with higher-resolving X-ray optics started in October 2012. In the micro tomography endstation the installation was finished, followed by a commissioning phase of the standard micro CT setup. User operation at the micro tomography station started early in October 2012.

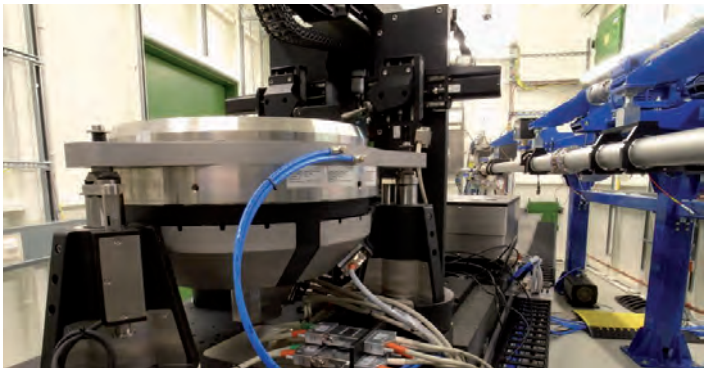

Figure 3

The nano tomography station at IBL is fully operational now.

BioSAXS (P12, operated by EMBL together with HZG) started user operation in May 2012 using an unfocused beam. A typical measurement cycle (automatic sample loading, data collecting, washing and drying of the sample container) only takes 40 seconds per sample. First user experiments were performed on the influence of metal ions and nanoparticles on structural changes of biological macromolecules. Focusing mirrors were installed in August and decrease the beam size down to 110 x 200 μm^2. The commissioning of a stopped-flow apparatus for time-resolved measurements has been started.

In 2012, the provisional GEMS office space has been continuously filling up with scientists and students, creating a very fruitful and lively atmosphere, ideal for productive scientific work. Still, we are looking very much forward to moving into a new building, jointly built with DESY, in particular in view of the currently limited laboratory space. The decision on the architectural concept has already been taken; construction will start by the end of 2013.

Contact: Martin Müller, martin.mueller@hzg.de
Andreas Schreyer, andreas.schreyer@hzg.de

University of Hamburg on the DESY site.

University and DESY – Strong partners for Photon Science

Research in Photon Science is one of the key science areas of the University of Hamburg. DESY and the University of Hamburg collaborate within **PIER** – a **P**artnership for **I**nnovation, **E**ducation and **R**esearch. In 2012 the first PIER innovation projects were selected. Two out of the three projects selected – "Nanoparticle growth studied by *in situ* high energy X-ray diffraction" and "Pulse Shaping of Accelerator-based THz Radiation" – expand the links between the University of Hamburg and DESY in the areas of Nanoscience and Photon Science and are based on research with accelerator driven light sources. Complementing the research activities a PIER Helmholtz Graduate School was established in 2012 which will form the overall structure for an excellent PhD training for candidates at DESY and University of Hamburg in the PIER research fields Particle- and Astroparticle Physics, Nanoscience, Life Sciences and Photon Science. In the framework of the graduate school additional PhD scholarships for outstanding students are granted by the private Joachim Herz Foundation.

With the final photons from DORIS III in October 2012 a highly successful example for the joint development of Photon Science between DESY and the University of Hamburg on the Bahrenfeld Campus has ended. From the very beginning of synchrotron radiation research at DESY to the foundation of HASYLAB and the later transition of DORIS to a dedicated synchrotron radiation facility, members of the Institute of Experimental Physics have played an important role in the shaping of Photon Science on the DESY campus. This chapter in the joint history of DESY and the University of Hamburg has been very nicely summarized in the recent booklet by Christof Kunz (Speaker since 1974 and Head of HASYLAB 1979-1985), which was issued at the occasion of the "last photon"-party on 22 October (Fig. 1).

However, despite the recent end of research at DORIS, the collaboration between the university and DESY in Photon Science is growing stronger every year. Groups from the university are actively involved in development of and research with accelerator based light sources at DESY. Focus areas are endstations at PETRA III and new innovative instrumentation for research at FLASH in the framework of the BMBF Verbundforschung. The

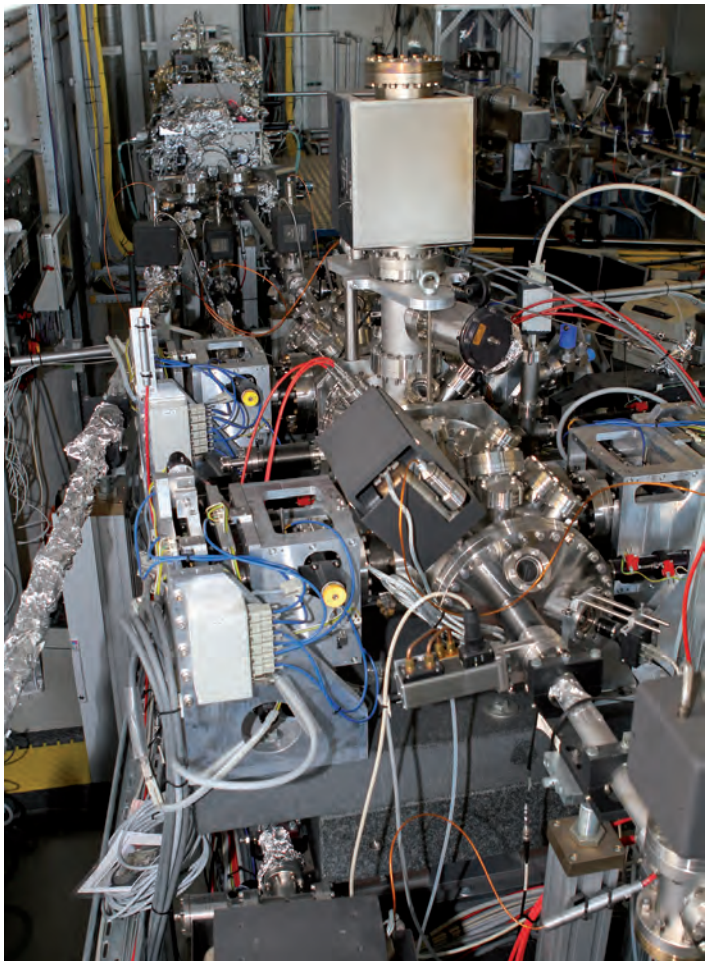

Figure 2

Plane grating monochromator beamline in the FLASH experimental hall with integrated XUV split- and delay unit. This setup serves a variety of advanced spectroscopies and time resolved pump-probe experiments, enabling ultrafast dynamic studies on chemical reactions and magnetical phenomena.

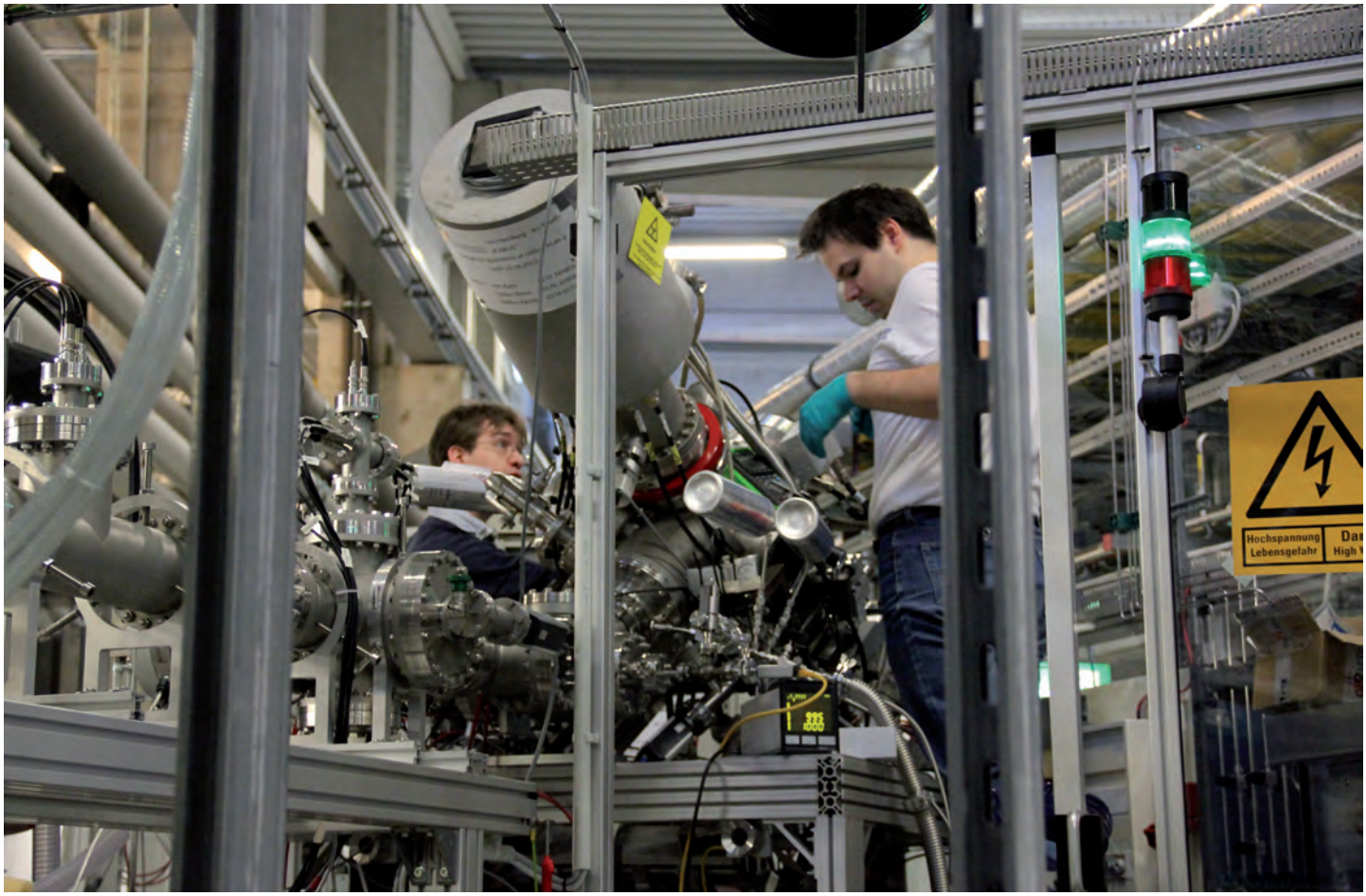

Figure 3

PhD students from the Hamburg University working at a cluster source in the PETRA hall.

new endstations for time-resolved spectroscopy, X-ray magnetic circular dichroism in strong magnetic fields and ion spectroscopy have seen first light at the XUV beamline P04 at PETRA III. University groups are major partners in the BMBF priority program (Forschungsschwerpunkt) FSP-301 “FLASH: Matter in the Light of Ultra Short and Extremely Intense X-ray Pulses” coordinated by Wilfried Wurth. As one of the highlights in this area the seeding experiment “sFLASH” (Markus Drescher and Jörg Roßbach) has demonstrated first successful seeding of the FLASH pulses with a HHG laser this year.
The member groups of the Center for Free-Electron Laser Science (CFEL), which was founded by the University of Hamburg together with DESY and the Max-Planck Society, have moved into the new building in September. Complementing CFEL will be the new Centre for Structural Systems Biology (CSSB) in the area of Life Sciences as well as the University (Center for Hybrid Nanostructures – CHyN) and DESY activities (NanoLab) in Nanoscience.

Based on these activities, on the strong commitment to excellence in Photon Science, Life Sciences and Nanoscience of the University of Hamburg and DESY and on the partnership with the Max-Planck Society and EMBL, the application for the foundation of a Cluster of Excellence – “Hamburg Center for Ultrafast Imaging (CUI): Structure, Dynamics and Control of Materials on the Atomic Scale” (speakers: Dwayne Miller, Klaus Sengstock and Horst Weller) – was successful within the framework of the Federal and State Excellence Initiative. The new centre, which ensures a bright future for the cooperation of University of Hamburg and DESY and their partners, started its operation in November 2012.

Figure 1

The cover illustration shows the first Rowland-spectrometer which was used at DESY. The spectrometer is now an exhibition piece close to the main entrance of the DESY campus.

Contact: Wilfried Wurth, wilfried.wurth@desy.de

Light Sources.

DORIS III.

The final year

Until the final end of operation, the demand for beamtime at DORIS III beamlines remained high. Experiments were carried out literally up to the last minute although in view of the facility shutdown in October 2012 no further call for proposals had been published in 2012. The performance of the storage ring during this last year (Fig. 1) reached the established level yielding a total of 4640 h for synchrotron radiation resulting in an availability of 95.1 %.

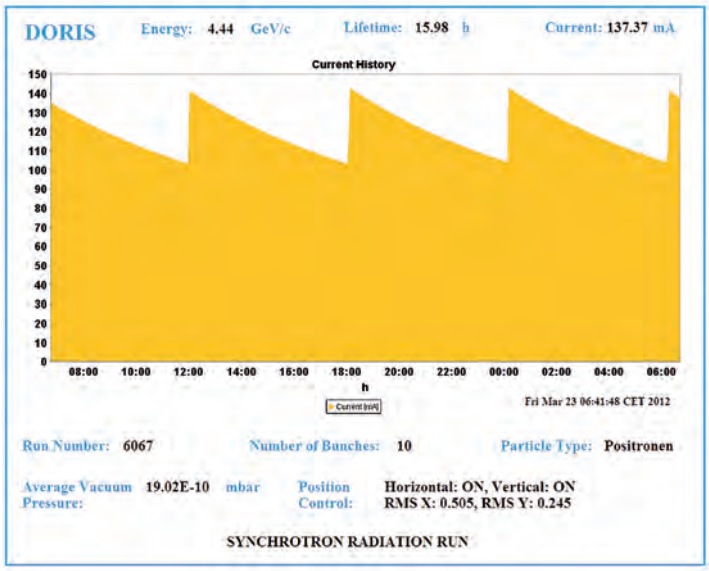

Figure 1

Recent status display of DORIS III showing a nicely performing machine.

The user operation at the X-ray powder diffraction beamline B2 ended already in mid-September because its double-crystal monochromator was taken out for heatload tests at undulator beamline BW1, in preparation for the use of this monochromator type at some of the new mini-undulator beamlines at PETRA III extension. All other beamlines were kept in operation for user experiments up to the end. As in previous years, a number of interesting and high-impact publications resulted from experiments performed at DORIS III instruments, examples of which are presented in the Research Highlights section of this report. On Monday 22 October at 08:00, the stored beam was finally dumped ending the era of synchrotron radiation research at DORIS (Fig. 2). In the afternoon of the same day, we all said

"Tschüüüs" (i.e. the Hamburg way to say "goodbye") to DORIS, celebrating the "old lady" with a special farewell party. About 350 users and long standing friends, including many of the pioneers of synchrotron radiation research at DESY, came to Hamburg and enjoyed a very nice 'family reunion'.
Without mourning but with a little melancholy, we looked back over so many years of hard and dedicated work, failures and successes, fruitful collaboration with wonderful colleagues, exciting and sometimes pioneering science.

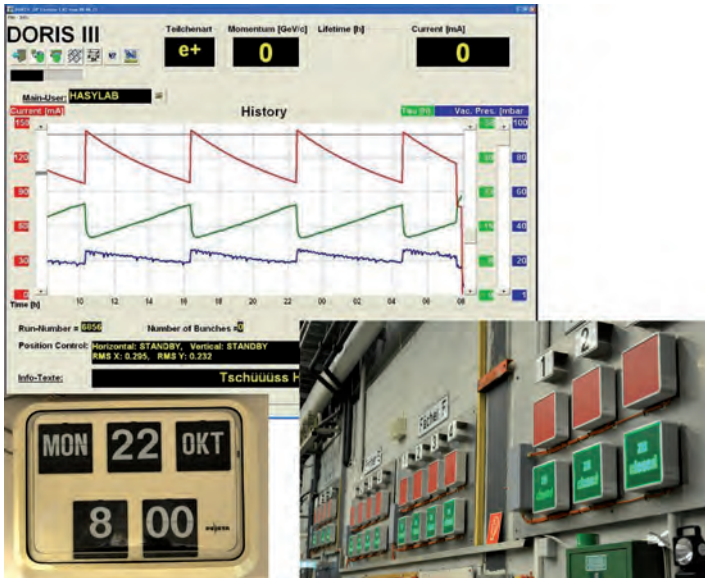

Figure 2

On 22 October 2012 at 08:00 synchrotron radiation research at DORIS III ended. All beam shutters remain closed.

After the final shutdown, there was little time to relax for the DORIS beamline staff because the new project – PETRA III extension – is already in full swing. Dismantling of instrumentation and beamlines in the DORIS halls had started right away to make room for new activities such as the assembly of instrumentation for the upcoming new PETRA III beamlines (Fig. 3).

Figure 3

Right after the shutdown, beamlines and instrumentation at DORIS are being dismantled and removed.

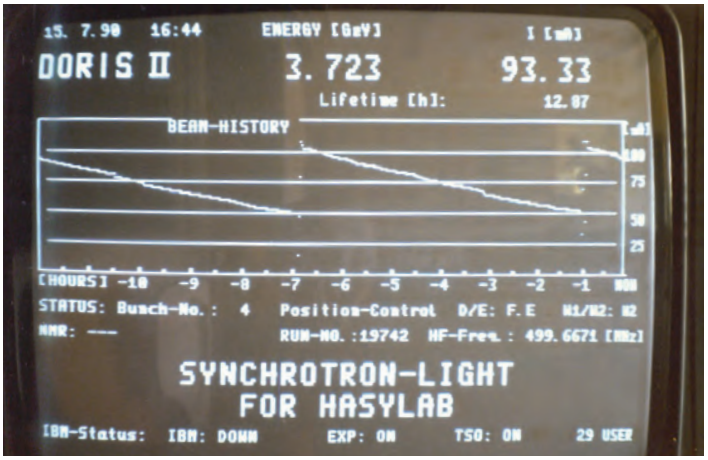

Figure 4

Status display of DORIS II showing a dedicated HASYLAB run at 3.7 GeV (July 1990).

The DORIS storage ring

Memories of 38 years of synchrotron radiation research

In 1964 the first synchrotron radiation beam became available at DESY for experiments in the spectral range of the VUV. Supported by the Deutsche Forschungsgemeinschaft pioneering work on the characterization and understanding of the radiation itself and in spectroscopy was performed. Only six years later, in 1971, the first hard X-ray experiment was done with the aim to solve a problem in structural biology. This early success triggered the decision to incorporate two synchrotron radiation beamlines into the design of the new storage ring DORIS, one for the VUV and one for hard X-rays with focus on biological applications, which became the nucleus of the EMBL Outstation at DESY founded in 1974. Compared to the conditions at the DESY synchrotron, much more intense and stable synchrotron radiation beams could be expected at DORIS. However, the commissioning of the new facility turned out to be very difficult and the concept of the storage ring had to be changed. Despite this, only about six years after approval of the project, the first synchrotron radiation experiments could be performed at DORIS in 1974.

These 10 years of early synchrotron radiation research have probably shaped the spirit of the synchrotron radiation activities on the DESY campus. Embedded in the open DESY atmosphere typical for particle physics laboratories and closely linked to the University of Hamburg, the work was driven by scientific curiosity and based on technical competence. The technical staff was very supportive to all users, especially to the many students. Moreover, the laboratory was able to attract outstanding scientists from universities and research institutions in Germany and abroad, who were fascinated by the unique and unexplored potential of synchrotron radiation research for science and accepted the challenges to be overcome before reaching their goals. With institutional flexibility and by keeping the level of administrative effort low, very effective collaborations were established, even for the construction and operation of big instruments. The generous funding of these collaborations by the German Federal Ministry of Education and Research through the so-called “Verbundforschung” was one key to success. Prominent user representatives helped in the discussions with the DESY directors who, at the end, were very supportive of the further development of the photon facilities. After intense discussions with and within the user community, a recommendation was made in 1977 to build a further storage ring for VUV and soft X-ray experiments in Berlin, BESSY, and to operate DORIS predominantly for hard X-ray experiments with considerably improved working conditions. Additional support by the funding bodies was provided and the “HAmburger SYnchrotronstrahlungsLABor” HASYLAB with 25 beamlines at the DORIS storage ring could be inaugurated in 1981.

At that time, DESY’s prime mission was particle physics research and the construction of DORIS was justified with the needs of colliding beam experiments. Here, the figure of merit is the integrated luminosity at the two interaction points of electrons and positrons, and fluctuations of the particle beams in the bends of the storage ring are not critical. However, this is where synchrotron radiation is produced and a fluctuating beam position leads to strong intensity and energy variations of the X-ray beam, as well as in the position of the focus at the experiment. Such instabilities often made it impossible for the X-ray users to perform the approved experiments. Obviously, the requirements

Figure 5

“Paving the way” in the DORIS II ring tunnel to accommodate the “bypass” (Fall 1990).

of the two communities were quite different. The DESY machine group made big efforts to improve the performance of DORIS, and over the years significant progress was accomplished. For a number of years, the particle physics experiment ARGUS and HASYLAB shared the DORIS ring and performed their research very successfully (Fig. 4). Nevertheless, it was a permanent challenge to balance the needs of the particle physics and the synchrotron radiation communities. In 1993, almost 20 years after the first beam in DORIS, the ARGUS detector stopped data taking and the ring became a dedicated synchrotron radiation facility.

In January 1988, the construction of the European Synchrotron Radiation Facility ESRF started, a 6 GeV low emittance storage ring dedicated to the production of high-brilliance synchrotron radiation beams. In the 1980s, a number of DESY scientists were strongly involved in the design of this new facility and they were aware of the upcoming competition. Therefore they proposed to modify the straight section of DORIS opposite to the ARGUS detector, still in operation for particle physics, and to install 6 wiggler and 1 undulator beamlines. The project was approved and funded and construction started in summer of 1990 (Fig. 5). At the end of 1991, first measurements could be performed at the new insertion device beamlines BW1, BW2 and BW3. Officially inaugurated in 1992, "DORIS III" started to provide hard X-ray beams of very high intensity for 20 years, serving 36 beamlines with 45 instruments. Many technical issues in handling the high power beams had to be solved and the success stimulated some of the progress made with the modern storage ring facilities later. The number of DORIS III users, many of them coming more than once per year, have been increasing even after the ESRF started its user operation and since 1998 reached an average number of 2000 p.a., 500 of them using the beamlines of the EMBL Outstation and the Max-Planck beamline (Fig. 6).

Haldor Topsøe in Lyngby, DK:

HALDOR TOPSØE
CATALYZING YOUR BUSINESS

A company devoted to catalysis as an example for collaboration with industry

Employees at Haldor Topsøe A/S have successfully used the DORIS synchrotron, in collaboration with HASYLAB staff, for several decades. The use of synchrotron radiation has given us unprecedented insight in the structure-activity relationships of many catalytic systems. Many different techniques such as XAFS, SAXS, XRD and X-ray tomography have been used over the years and they have contributed to a fundamental understanding of our catalysts and processes. The development of new and combined techniques, such as the combination of XAFS and XRD to obtain short- and long-range structural information simultaneously, the use of quick-scanning-XAFS time-resolved spectroscopy and the development of reaction cells and detectors have added significantly to knowledge in the field of catalyst characterization. The use of XAFS has given us valuable input for development of new catalysts for a.o. hydrotreating of oil. It has also given us insight in the dynamic shape changes of Cu/ZnO-containing methanol catalysts, the active phases in high-temperature shift catalysts and alloy composition in reforming catalysts close to industrial operating conditions.
Bjerne S. Clausen, CEO, Haldor Topsoe A/S

Box 1

Selection of methodological breakthroughs at DORIS adopted by other facilities

1970 Diffraction data from muscles
1973 X-ray topography with synchrotron radiation
1975 Tests of X-ray lithography
1975 Angle-resolved photo electron emission spectra using synchrotron radiation
1976 Imaging of living cells using an X-ray microscope and synchrotron radiation
1983 X-ray standing waves for localization of atoms on surfaces
1984 Mößbauer-Spectroscopy with synchrotron radiation
1986 Phonon spectra determined by high resolution inelastic X-ray scattering
1986 Study of osteoporose as an example for element specific 3d tomography
1986 Grazing incidence X-ray scattering from liquid surfaces
1987 Circular dichroism as a powerful tool for studies of magnetic properties of matter
1988 Quick scanning EXAFS for time resolved measurement of absorption spectra
1989 Time resolved X-ray diffraction to study the dynamics of biological macromolecules
1989 Shock-freezing of crystals for mitigating radiation damage in protein crystallography
1991 Diffraction of high energy synchrotron radiation as a complement to neutron scattering
1995 Hard X-ray photoelectron spectroscopy
2002 Large study on human intravenous coronary angiography with synchrotron radiation
2008 Colour reconstruction of hidden paintings for visualizing lost masterpieces

Box 2

The DORIS user community was very successful in many different fields of science and published a large number of papers, many of them in high-profile journals. Support of industrial research either by companies themselves or through collaboration with university groups has always been of high priority [Box 1]. Some of the methodological breakthroughs achieved at DORIS have subsequently been realized at other facilities [Box 2], and we counted 33 scientific awards granted to DORIS users [Box 3]. Most prominent is the 2009 Nobel Prize in Chemistry awarded to Prof. Ada Yonath (Weizmann Institute, Rehovot, Israel) for studies of the structure and function of the ribosome. She had been leading the Max-Planck Ribosomal Structure Group at DESY from 1986 to 2004.

DESY is proud of the success of the DORIS facility having made possible many outstanding scientific results over the last 38 years (Fig. 7). We are very grateful for the continuous support of our Photon Science user community who is now looking forward to continuing their research at PETRA III which will be extended by ten more beamlines in the next years

Contact: Wolfgang Drube, wolfgang.drube@desy.de

Special thanks to Jochen R. Schneider for looking back at the DORIS history.

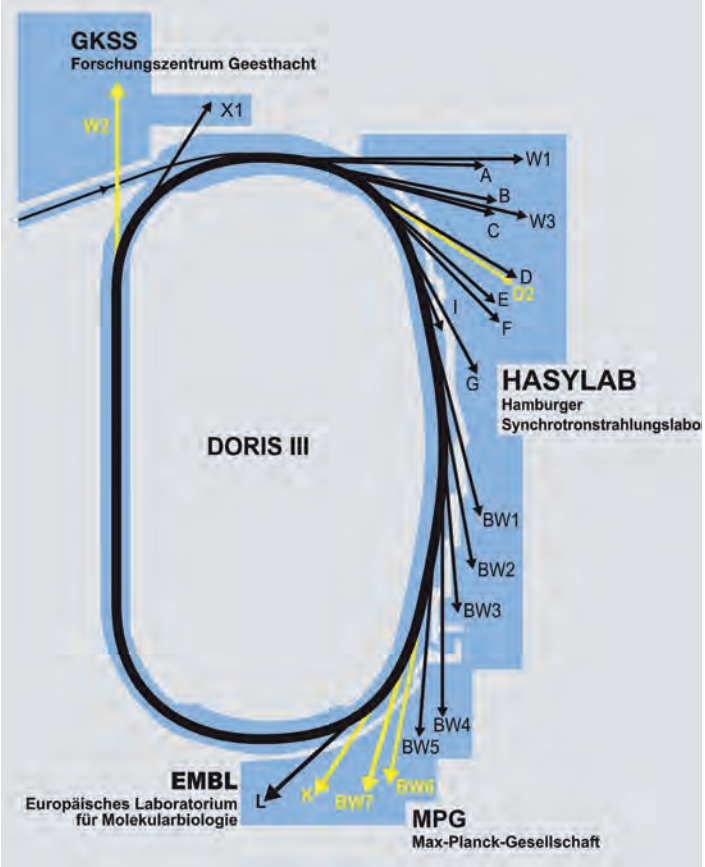

Figure 6

Sketch of DORIS III and its beamlines after the completion of the bypass.

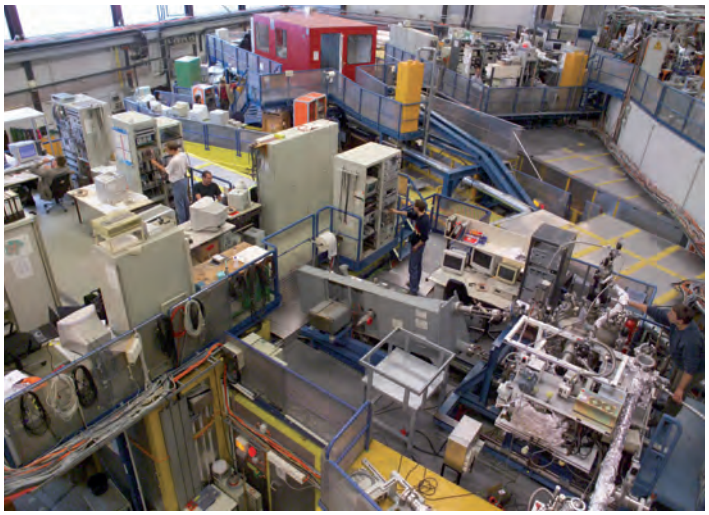

Figure 7

View of the well-known "HASYLAB hall" at DORIS, which has been the centre of activities for many years.

Selection of awards granted to DORIS users

Jens Als-Nielsen (Niels Bohr Institute, University of Kopenhagen, DK)
1985 Hewlett Packard Europhysics Prize

Ulrich Bonse (Technische Universität Dortmund)
2002 Röntgenplakette der Stadt Remscheid

Birger Dittrich (Freie Universität Berlin)
2006 Max von Laue Preis der Deutschen Gesellschaft für Kristallographie

Helmut Dosch (DESY, Hamburg)
2010 Röntgenplakette der Stadt Remscheid

Helmut Ehrenberg (KIT, Karlsruhe)
2001 Max von Laue Preis der Deutschen Gesellschaft für Kristallographie

Alexandra Friedrich (Goethe Universität Frankfurt)
2011 Max von Laue Preis der Deutschen Gesellschaft für Kristallographie

Walter Graeff (DESY, Hamburg)
1988 Röntgenpreis der Universität Gießen

Erich Gerdau (Universität Hamburg)
1988 Stern-Gerlach-Preis der Deutschen Physikalischen Gesellschaft

Jan-Dirk Grunwald (KIT Karlsruhe)
2006 Jochen-Block-Preis der Deutschen Gesellschaft für Katalyse in der DECHEMA

Kenneth C. Holmes (Max-Planck Institut für Medizinische Forschung, Heidelberg)
1997 Gabor Medal of the Royal Society of London

Karsten Knorr (Christian-Albrechts-Universität zu Kiel)
2003 Max von Laue Preis der Deutschen Gesellschaft für Kristallographie

Eckhard and Eva-Maria Mandelkow
2009 MetLife Award for Medical Research

Gerhard Materlik (Diamond, Oxford, UK)
2002 Röntgen Preis der Universität Würzburg

Dirk Meyer (TU Bergakademie Freiberg)
2004 Max von Laue Preis der Deutschen Gesellschaft für Kristallographie

Ilme Schlichting (Max-Planck Institut für Medizinische Forschung, Heidelberg)
2000 Gottfried Wilhelm Leibniz Preis der Deutschen Forschungsgemeinschaft

Jochen R. Schneider (DESY, Hamburg)
2001 Second European Crystallography Prize

Gisela Schütz (Max-Planck Institut für Metallforschung, Stuttgart)
2000 Agilent Technologies Europhysics Prize

Edgar Weckert (DESY, Hamburg)
1996 Max von Laue Preis der Deutschen Gesellschaft für Kristallographie

Max Wilke (HZP Deutsches GeoForschungsZentrum, Potsdam)
2009 Medal for Research Excellence, European Mineralogical Union

Ada Yonath (Weizmann Institute, Rehovot, Israel)
2000 First European Crystallography Prize
2009 Nobel Prize in Chemistry

Box 3

FLASH.

Rapid progress of the FLASH II project

The fourth user period at FLASH started in March 2012 and will finish mid-February 2013. It is encased between two shutdowns of the facility, one required for civil construction of the FLASH2 tunnel in fall/winter 2011/12, the other for connecting the existing FLASH accelerator to the new FLASH2 undulator beamline in 2013. Six beamtime blocks with a total of 178 12-hour shifts were allocated to the 20 projects that were selected by the international project review panel in October 2011. The third block, originally scheduled in June/July 2012, had to be shifted to January 2013 because the electron gun had to be exchanged. After two years of operation it suddenly exhibited a very high trip rate, accompanied by dark current, and could not be processed any more to operate at high gradients. It was found that damage had occurred in the cathode area, obviously caused by an exceptionally strong RF spark. The gun was replaced by one that had previously operated at PITZ in Zeuthen and was therefore well conditioned.

The first four beamtime blocks which were scheduled between 19 March and 6 November 2012, included in total 2213 hours of beamtime. 260 hours of this time were lost due to technical problems, i.e. the uptime of the FLASH accelerator during the user runs was 88.3 %. Another 308 hours of the remaining time (13.9 % of the scheduled 2213 h) were used for set-up and tuning of the machine. This time is needed because a large number of different beam parameters are requested for the different experiments. In particular, a significant fraction of experiments asks for very short pulses (< 50 fs) for which a suitable online photon diagnostics is not yet available. Sometimes the best result is achieved by optimising the machine settings using a signal from the experiment. In total, 1645 hours of FEL radiation were actually delivered to the users. The first two and a half months of 2012 as well as the time between user blocks was used for FEL and accelerator studies (in total 3659 hours) and for commissioning (832 hours). The replacement of the electron gun and other work in the tunnel needed 551 hours of shutdown, regular maintenance another 194 hours (see Fig. 1).

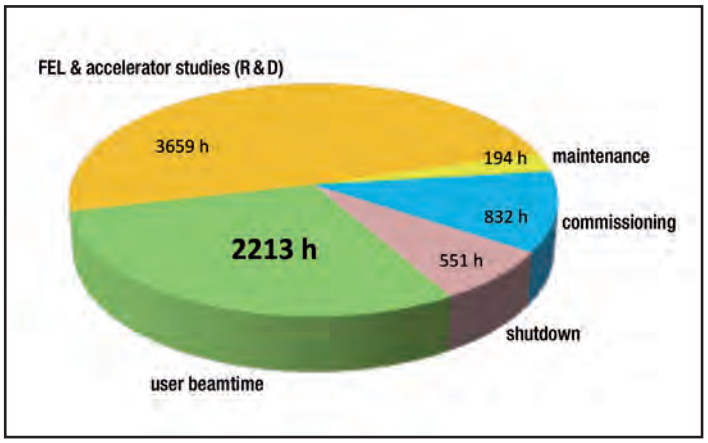

Figure 1

FLASH operation during the time period 1st January – 6th November 2012. The last user beamtime block in 2012 with ~700 hours of scheduled beamtime is not included.

After commissioning and first pioneering experiments on the THz/BL3 beamline during previous beamtime periods, this beamline has now been modified such that it can also be used for experiments, which require their own specialised end stations (Fig. 2). In addition, a solid hutch was built with optical tables to facilitate THz diagnostics and the use of optical laser radiation. The combination of THz and XUV radiation is worldwide unique and attractive for various applications. For example, the strong electromagnetic field of the THz pulses up to 1 MV/cm can be

__FLASH__ is the existing __FEL facility at DESY,__ which is currently being doubled via the __FLASH II project__. This expansion project includes the construction and establishment of an additional __FEL undulator line (FLASH2)__ in a separate tunnel, and a new experimental hall. Thus the future FLASH facility at DESY will comprise two separate and almost independent FEL sources.

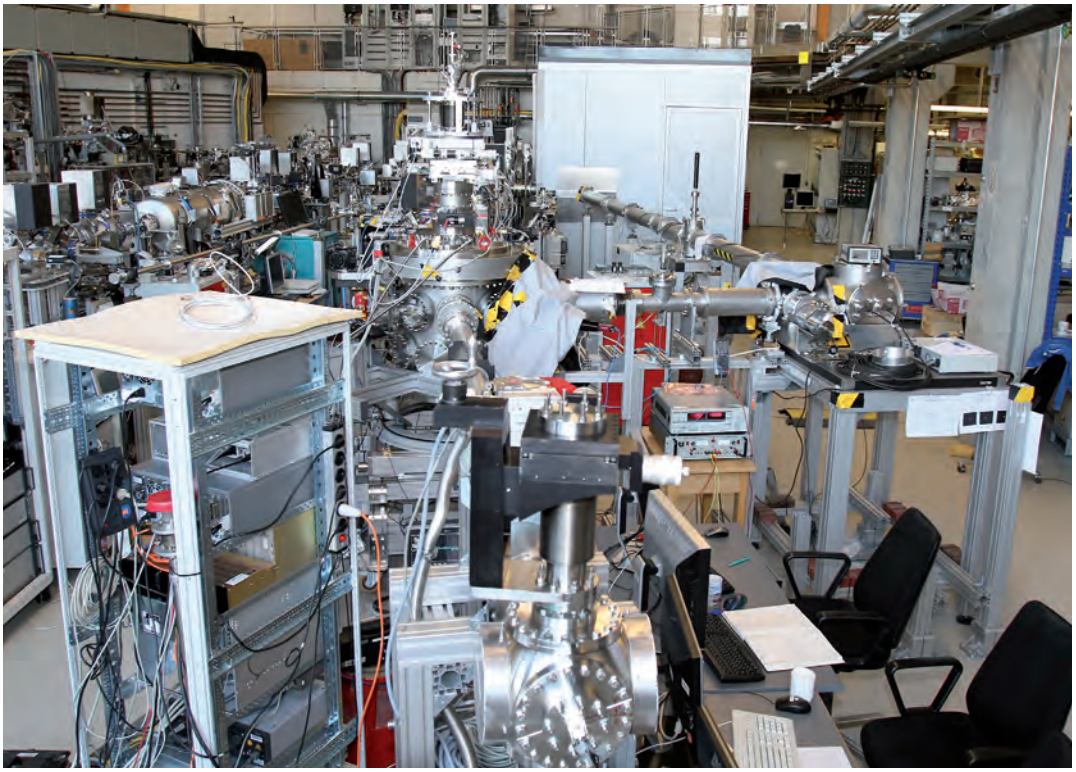

Figure 2

The new THz beamline extension with the new THz diagnostics and laser hutch in the background. The extension allows using different user end stations of considerable size for time-resolved THz pump – XUV probe experiments.

used to excite electrons, or to streak photoelectrons in order to achieve extremely high time resolution on the order of 10 fs. The wavelength can also be tuned to initiate specific collective excitations such as phonons or magnons and then probe the excited system time-resolved with the subsequent XUV FEL pulse.

In order to meet the increasing demands of the user community, the FLASH facility is undergoing a major extension through the FLASH II project. It includes a new undulator line FLASH2 in a separate tunnel and a new experimental hall, which doubles the capacity for experimental stations. The design builds on experience gained during years of user operation. It aims at optimal transmission of the beam transport to the experiment for the entire wavelength range (4 to 60 nm at the fundamental) including harmonic radiation down to ~1 nm. The FLASH2 FEL will also be complemented by a THz undulator, similar to FLASH1, but at a 3° angle with respect to the FEL undulator in order to facilitate beam separation and transport. The design of the new THz undulator and beamline for pump-probe experiments has started in collaboration with the Budker Institute in Novosibirsk.

Figure 3

The civil construction of the FLASH2 tunnel under progress (November 2012).

The main part of the FLASH2 tunnel building is now under construction (Fig. 3) and the construction of the experimental hall will soon follow. Installation of the infrastructure in the new tunnel will start at the beginning of 2013, after which the beamline components will be mounted. The connection to the FLASH accelerator is planned for spring 2013. Commissioning of the accelerator and the FLASH1 beamline will start right after the shutdown in July 2013 to ensure that user operation at FLASH1 can continue in October. This beamtime period – the fifth user period at FLASH – is planned to finish at the end of 2014. The new undulator beamline FLASH2 will be commissioned during the remainder of the year 2013 and part of 2014. A significant part of the R&D time between beamtime blocks will be reserved for this task, and during user operation the commissioning can continue parasitically.

Contact: Josef Feldhaus, josef.feldhaus@desy.de (FLASH)
Elke Plönjes, elke.ploenjes@desy.de (FLASH)
Bart Faatz, bart.faatz@desy.de (FLASH II)

PETRA III.

A growing facility

In 2012 PETRA III was running in stable user mode throughout the operation period. All beamlines were serving users, 12 out of 14 on the basis of reviewed proposals. The remaining two beamlines had been used by a number of friendly user groups distributed over the year.
In parallel, the commissioning of further instruments enlarging the scope of the facility continued. For example, at P01 a high energy-resolution instrument was installed while at P02 a high angular-resolution instrument was added.
On 19 September the PETRA III experimental hall was dedicated to Max von Laue. In a big event with participation of the Federal Chancellor Angela Merkel, the First Mayor of the City of Hamburg, Olaf Scholz, the Nobel Prize Laureate Ada Yonath, and representatives of Max von Laue's family the hall was named after the founder of X-ray crystallography (Fig. 1).

Storage ring

The operation for users started in the second half of March 2012, after a long winter shut-down to allow for construction work preparing the crossing of the FLASH II beam pipe. This loss of operation time was compensated by cancelling the usual summer shut-down. In total, 4944 hours of user beamtime have been scheduled, thus the goal of 5000 hours was almost achieved. The average availability remained at a value of 94.5 %, similar to the performance in 2011. A power failure (black-out) on the DESY campus and a vacuum problem in the cavity section were the most prominent reasons for down times. On the positive side we recorded an uninterrupted top-up run of 13 days end of August. The weekly uptime availablility of the machine in 2012 is summarised in Fig. 2.

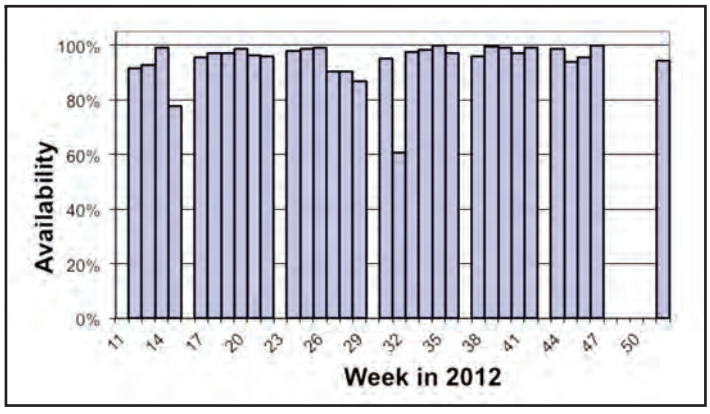

Figure 2
Uptime availability of PETRA III in 2012. The last bar on the right indicates the average which amounts to 94.5 %.

The high degree of beam stability achieved toward the end of 2011 could be maintained in 2012. In all frequency ranges vibrations of the positron beam remained well below the specifications. Only after service weeks beam position offsets at the beamlines of the order of 100 µm had to be corrected. The option to change the value of the beta-function during a service week was further explored in fall 2012. In sector 5 (P07) a test run with low-beta settings (standard was high-beta) was used to characterise the beam at the experiment. All measured parameters fitted very nicely to the expectations calculated on the basis of the electron optics.
As planned, the bunch pattern delivered covered 50 % "timing" mode with 60 and 40 equally spaced bunches and the "continuous" mode with 240 or 320 bunches. Some tests were performed during machine shifts to increase the bunch number to 480.

The commissioning of the APPLE II undulator at P04 with full current beam was continued using the newly developed diagnostics tool. Up to now, due to limitations in the cooling of the optics, the device can only be used in circular polarized mode. Additional modes will be available after the upgrade of the cooling system scheduled for the shutdown period in 2013.

Beamlines and experiments

All 14 PETRA III beamlines have served users in 2012. In total, 390 user experiments have been performed based on rated proposals. On top of that, we had about 200 commissioning, in-house research, and 'friendly user' experiments. Almost 2000 user visits from 33 countries were counted. The number of proposals submitted by the user community showed a further increase to 614 active proposals after the first call in 2012. In addition, 164 proposals were submitted for beamtime at the EMBL life science instruments. Figure 3 shows the development of the active proposals numbers over the last 2.5 years together with the number of user experiments performed. In the last calls approximately 35% of the submitted proposals were awarded beamtime.

Figure 1

Main entrance to the PETRA III experimental hall now named after Max von Laue.

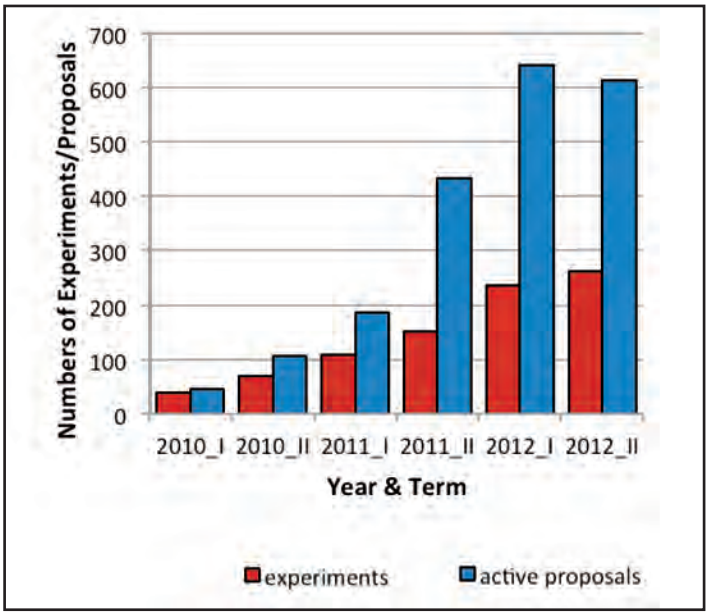

Figure 3

Number of active PETRA III proposals in comparison with the number of experiments performed based on these proposals. Each active proposal is valid for one year and allows the user to apply for beamtime over a period of 2 terms. The discrepancy of active proposals and experiments reveals the high demand for beamtime. EMBL proposals and experiments are not included in this figure.

Further progress has been made in the delivery of nanometre sized beams. Four beamlines (P03, P06, P10, and P11) have achieved spot sizes well below one micrometre, even down to some 10 nm. These beams are now routinely made available to users. An X-ray microscope with a resolution of about 50 nm is now also available at beamline P04 in the soft X-ray regime.

Some highlights from the experiments like the dynamics of crystallization behaviour in natural rubber upon cyclic load on the time scale of seconds or below, the structure determination of single colloidal crystal grains or experiments on the stability of van Gogh paintings disentangling the aging processes of pigments will be detailed in the Research Highlights section of this report.

Contact: Hermann Franz, hermann.franz@desy.de
Alexander Kling, alexander.kling@desy.de

PETRA III Extension

After the end of the synchrotron radiation era at DORIS III on 22 October 2012 the work focusing on the planning and realization of the PETRA III extension has intensified considerably. Within the scope of this project, new experimental halls on either side (North and East) of the experimental hall Max von Laue will be built (Fig. 4), allowing using the respective long straight sections and part of the adjacent arcs for the implementation of a total of ten new beamlines. The northern straight section already accommodates a 40 m long damping wiggler array producing an extremely hard and powerful X-ray beam which will be the source for one of the beamlines. The long straight in the east – not used so far – will be available for additional insertion devices.

In each of the arc sections, about 60 m of the machine lattice will be modified to replace long dipole magnets by two double-bent achromat (DBA) cells, each providing a 5 m long straight section. Following the present PETRA III beamline concept, a canting dipole deflecting the beam by 20 mrad will be used to divide each DBA cell into two 2 m straight segments allowing separate insertion devices for two independent beamlines. The modified lattice therefore provides additional eight 2m long straight sections in the arcs with high-β source properties similar to PETRA III today which make them very suitable for the use of undulators.

East of the Max-von-Laue hall, the construction situation is rather complex because the PETRA III tunnel is partly underground and the new experimental hall PETRA III East (PXE) is closely surrounded by other buildings. Different from previous planning, the front section of the storage ring tunnel where the photon beamlines are located will be completely removed. It will later be rebuilt together with the monolithic plate of the experimental floor, similar to the scenario in the current PETRA III hall. The rear tunnel section will stay intact and will remain outside the experimental hall.

Hall East will accommodate beamlines P21-P25, where several insertion devices in the long straight section provide brilliant high-energy X-rays for the Swedish materials science beamline (P21). Using a canted undulator scheme also in this straight section, it is planned to add an independent side station to the beamline.

Beamline P22 will be built with funding from the India-DESY collaboration and will focus on nano-spectroscopy applications. The second beamline (P23) in this sector is funded by Federal Ministry of Education and Research (BMBF) within a German-Russian collaboration and will be designed for nano-diffraction experiments in close coordination with the Russian partners. Both beamlines will use 2 m long undulators and cryo-cooled monochromators.

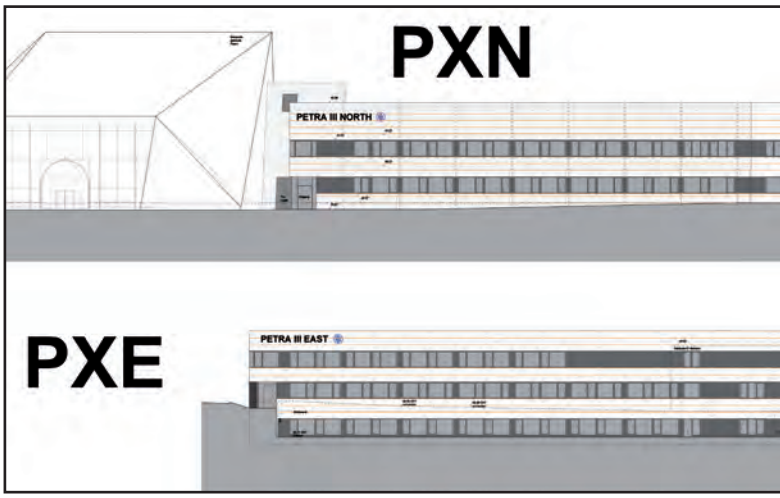

Figure 4

Architect's view of the experimental halls in the North (PXN) and in the East (PXE). (figure courtesy of Architekturbüro Renner Hainke Wirth)

The third sector consists of two short-undulator beamlines using water-cooled "CEMO-type" double-crystal monochromators, which were developed for DORIS III bending magnet beamlines and had been very well-performing for many years. In order to study their performance in a more intense short-undulator beam, a test was conducted at undulator beamline BW1 of DORIS III shortly before the facility shutdown. Beamline P24 is being designed for chemical crystallography methods and will receive two different instruments in separate experiment hutches. A beamline dedicated for education, training and testing purposes (P25) will be realized at later stage depending on the available funding.

Hall PETRA III North (PXN) is located adjacent to the FLASH facility and will accommodate beamlines P61-65 (Fig. 6). The powerful beam generated by the damping wiggler array in the northern long straight section will be used for high X-ray energy materials science applications. This beamline (P61) provides

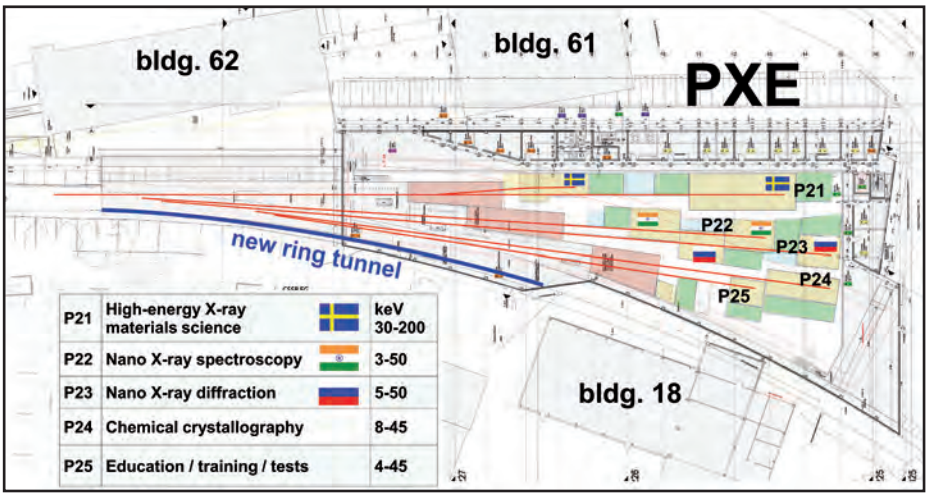

Figure 5

Layout of the experimental hall and beamlines in the East. The construction situation is complex due to surrounding buildings and the tunnel being underground. The section of the ring tunnel which will be completely removed and rebuilt is indicated by the blue line. (figure courtesy of Architekturbüro Renner Hainke Wirth)

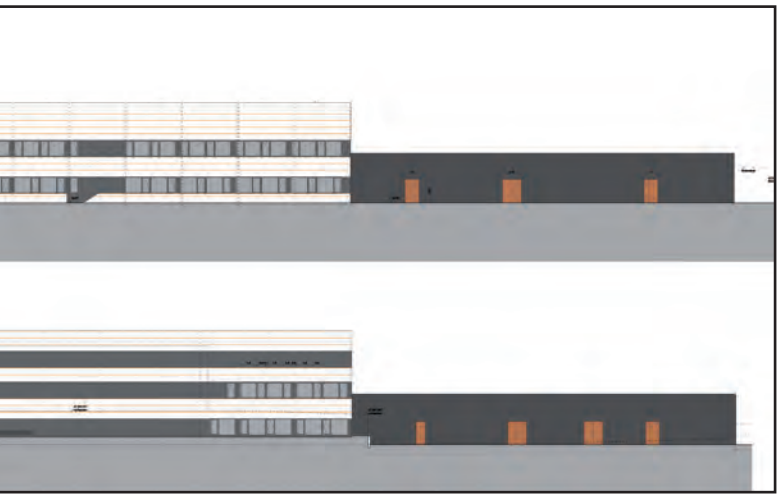

monochromatic as well as pink beams in the range 50 – 200 keV for experiments in two in-line hutches. The instrumentation in the first hutch will allow continuation of the engineering materials science activities of Helmholtz-Zentrum Geesthacht (HZG) which were located at the HARWI II station of DORIS III. Experiments in the downstream hutch will be focusing on extreme conditions research using a new large volume press. This instrument will be operated by DESY.

In the arc section of the storage ring, short-undulator beamlines for small angle X-ray scattering (P62), X-ray μ-fluorescence (P63) and *in situ* X-ray absorption spectroscopy (P65) will be built. A second XAFS beamline (P64) has been designed for flux hungry applications such as time-resolved absorption studies (QEXAFS), bioXAFS and investigation of diluted systems and will be using cryo-cooled monochromators and a 2 m long insertion device. The technical design report for the phase I beamlines (XAFS beamlines P64 and P65) has been completed and discussed with an international advisory committee and users. Corresponding reports for phase II beamlines are currently being prepared.

The civil construction of the PETRA III extension is planned to start in Summer 2013. The exact timing is currently being iterated because it strongly interacts with many other activities on the DESY site (Fig. 7). In the course of the civil construction, the modified part of the storage ring will be installed as soon as the re-built sections of the ring tunnel in the North and East are completed. After the machine restart, the completion of the experimental halls will continue in parallel to the user operation in the Max-von-Laue hall. During the long shutdown starting in 2013, the beamline frontends of the first beamlines P64 and P65 will also be installed. The implementation of the remaining frontends may require additional short shutdowns in the following years. It is expected that the new beamlines for X-ray absorption spectroscopy in PETRA III North will be available for users at the end of 2014.

Contact: Wolfgang Drube, wolfgang.drube@desy.de
Michael Bieler, michael.bieler@desy.de

Figure 7

The road to the side entrance passing by the future Eastern Hall has already been relocated in October 2012 to make room for the new PXE building.

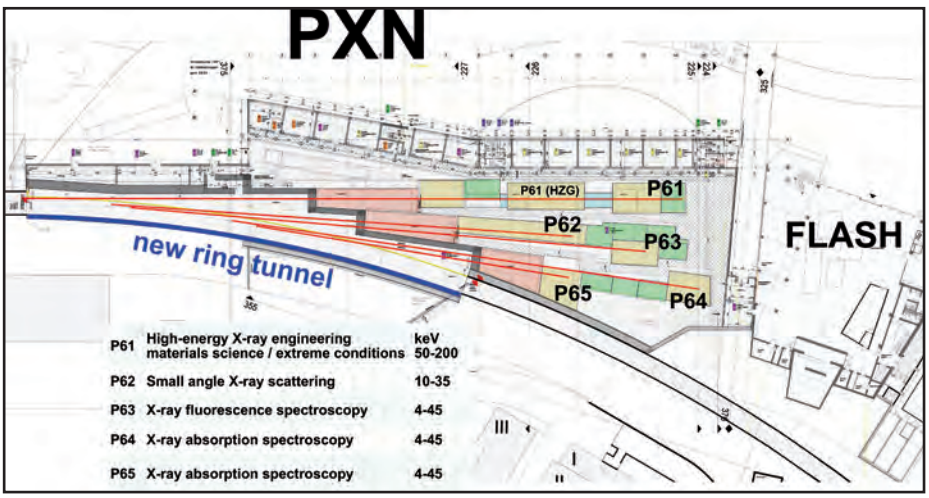

Figure 6

Corresponding layout of the experimental hall and beamlines in the North. This new hall will be adjacent to the FLASH building. (figure courtesy of Architekturbüro Renner Hainke Wirth)

European XFEL.

Milestone reached on the way to build the world's brightest light source

In 2012, both civil construction and the scientific development at European XFEL made considerable progress.
A major milestone was reached with the successful completion of tunnel construction, which was a major challenging task in the civil construction process. On 29 February, the tunnel boring machine TULA ("**TU**nnel **F**or **L**aser") reached its target destination, thus completing the construction of the more than 2 kilometre long accelerator tunnel of the new research facility. Work on this tunnel had started in January 2011 at the construction shaft on the Osdorfer Born site. To build the tunnel wall, more than 8000 precast segments were inserted. The tunnel then was equipped with a flat floor made of concrete elements, which will later provide space for cables and technical infrastructure distribution. At the end of February, the construction company ARGE Tunnel XFEL officially handed over the tunnel to DESY, which is acting as the building contractor on behalf of European XFEL. Currently, the tunnels are equipped with the technical infrastructure and safety devices. First sets of specialized 'pulse' cables to later power the super-conducting accelerator have been laid (Fig. 1).

A few months later, construction of the five photon tunnels between Osdorfer Born and Schenefeld also was successfully completed. In June, the second tunnel boring machine AMELI (Am Ende Licht, German for "At the end there will be light") reached its last target destination near Schenefeld and was dismantled and removed. At a festive event on 14 June 2012, more than 400 participants — including guests from politics and science as well as staff from collaborating companies — celebrated the completion of tunnel construction. AMELI's mission had been especially difficult: Given the special layout of the tunnels, the 160 tons colossus had to be repeatedly relocated and brought back into action.

The network of tunnels for the European XFEL totals nearly 5.8 kilometres in length and extends 3.4 kilometres from Hamburg Bahrenfeld to Schenefeld in Schleswig-Holstein. Massimo Altarelli, Managing Director of European XFEL, said at the tunnel completion celebration he was glad that this very challenging task could be completed according to plan and that costs could be kept essentially within the tight budget targets set at the time the contract was awarded.

Also in summer 2012, research at Hamburg's deepest scientific workplace resumed: Three teams of researchers from European XFEL started to equip their laboratories in one of the former experiment buildings of the Hadron-Electron Ring Accelerator (HERA) that was switched off in 2007. The underground building complex of HERA South stretches over 8 floors and is more than 25 m deep. The centre of the complex, which offers 2000 square metres of test and laboratory area, hosts the more than 1000 square metres large experiment hall. HERA South provides a good infrastructure, steady and controllable conditions, and the possibility to work free of vibrations. About 25 European XFEL scientists and engineers will work in HERA South, mainly developing and testing equipment in the areas of X-ray beam guiding and controlling, X-ray diagnostics devices, instrumentation of the scientific end-stations, detectors, and data acquisition and processing. Renovation and preparation of the underground building lasted 12 months, during which more than 300 heavy concrete blocks had to be moved.

Progress had also been made on the technical parts of the X-ray free-electron laser itself. In the area of the electron accelerator and the technical infrastructure a majority of components is coming through in-kind contributions (IKC). To date, European XFEL has received proposals for 76 IKCs from 9 different countries for a total of 563 million Euro. In general, work on the IKCs progresses very well, several IKC have already been delivered and concluded, among them 125 magnets from Russia and Sweden (in July) and cryostats from Poland for cryogenic tests (in August and November). Based on a design by DESY, the 125 magnets were custom-built by the Budker Institute of

Figure 2
The undulator hall with three magnetic measurement laboratories in October 2012 (© European XFEL).

Figure 1
Pulse cables were pulled into the accelerator tunnel in October 2012.

Nuclear Physics (BINP) in Novosibirsk. After production, they were measured and fiducialized (their magnetic centreline position being measured and marked on the magnets) at the Manne Siegbahn Laboratory at Stockholm University. The cryostat is a 5 tons, 4.5 metre high cylinder with complex inner workings. After installation in the Accelerator Module Test Facility (AMTF) it will be used to test the superconducting niobium cavities due to start after November 2012.

In the area of the X-ray systems in October 2012, the first undulator components from industrial production at companies in Germany and Spain were delivered to Hamburg. Before the 5.0 m long undulator segments will be installed inside the tunnels, the undulator group of European XFEL will extensively measure and tune their magnetic field properties to ensure correct adjustment. For this purpose, two large magnetic measurement benches have been commissioned in 2012. The European XFEL magnetic lab is now fully operational with three benches and ready for the high throughput necessary to keep pace with production and installation schedule (compare Fig. 2). For the next two years on average one undulator segment per week will be commissioned, measured, tuned and prepared for installation, which is planned to begin end of 2014.

In 2012, “self-seeding” was the buzzword for all scientists at FELs around the world. Based on a method developed in 2010 by Gianluca Geloni from European XFEL, Vitali Kocharyan and Evgeni Saldin, both DESY, researchers at the Linac Coherent Light Source (LCLS) at SLAC National Accelerator Laboratory in the US successfully implemented a self-seeding setting proposed by their colleagues in Germany. By inserting a thin diamond crystal, they selected a highly monochromatic part of the light generated from a first series of undulator segments and set it on top of the electron beam again. These X-rays seed the generation of very intense and coherent flashes in the following undulator segments – a procedure known as self-seeding – that can dramatically improve the quality of the X-ray flashes, generating more “laser-like” flashes with higher intensity. At European XFEL a working group studied ways to implement seeding at the European XFEL undulators. In its October 2012 meeting the European XFEL Council decided to proceed with the implementation of seeding and encouraged the project to secure additional funding.

Even without self-seeding, its more than 27 000 ultra-bright X-ray flashes per second will make the European XFEL unique among the world’s X-ray light sources. The new research facility, which is expected to deliver its first laser beam in 2015 and will start user operation in 2016, is one of the largest and most ambitious European research projects to date. The non-profit limited liability company European X-Ray Free-Electron Laser Facility GmbH (European XFEL GmbH) grew from 119 in December 2011 to 145 employees as of December 2012. At present, 12 countries are participating in the project: Denmark, France, Germany, Greece, Hungary, Italy, Poland, Russia, Slovakia, Spain, Sweden, and Switzerland. The governments of the partner countries designate shareholders who form the European XFEL Council, which decides on important issues related to the company and the project. The main shareholder is DESY. European XFEL and DESY closely cooperate on construction, commissioning, and operation of the facility on the basis of a long-term agreement.

Contact: Massimo Altarelli, massimo.altarelli@xfel.eu

New Technologies and Developments.

High-intensity optics.

Manipulating FLASH pulses with novel multilayer structures

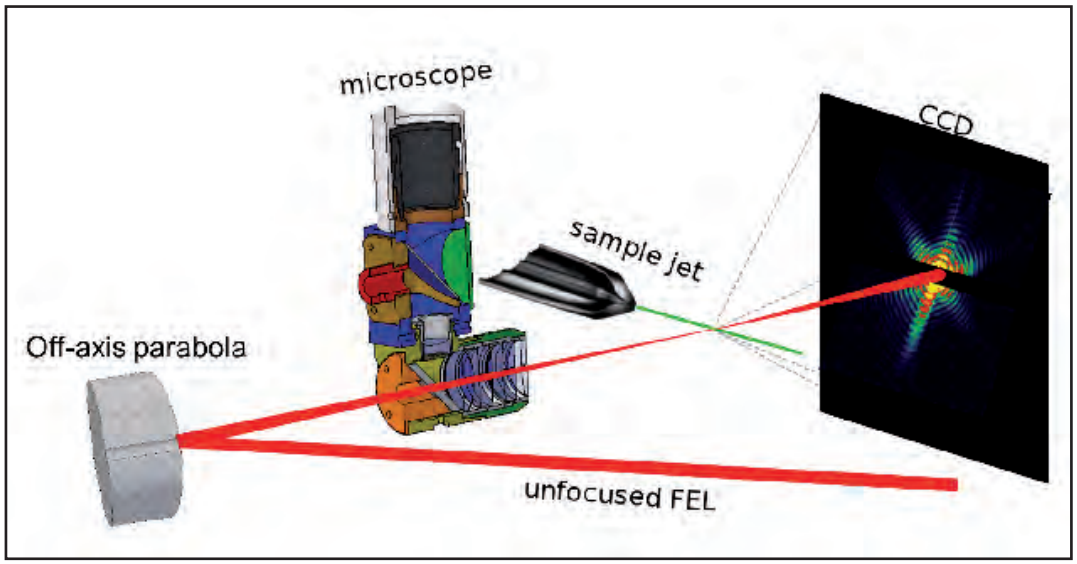

Figure 1

The experimental setup at the end of the unfocused branch of BL2 at FLASH. The imprints of the focused single-shot beam profile on PMMA samples were observed in real time with an in-vacuum microscope to find the best focus.

High-intensity coherent monochromatic femtosecond pulses from X-ray free-electron lasers (FELs) have opened up new science fields including nano-crystallography and single-particle diffractive imaging. To collect X-ray diffraction patterns from biological objects, such as nano-crystals, viruses, and cells, injected into the FEL beam [1] one requires a tightly focused beam. This is necessary to achieve a high enough X-ray intensity to acquire diffraction patterns of these extremely small and weakly scattering objects with the necessary signal to background ratio. We have produced some of the highest peak intensities at FLASH by using focusing mirrors coated with multilayer reflective films. For example, our off-axis parabola (OAP) enabled new research in warm dense matter studies [2] by providing a submicron focused beam [3, 4] with intensities > 10^{17} W/cm^2 at 13.5 nm wavelength. We have now extended this design to 6.8 nm wavelength.

The super-polished substrate of the OAP was coated with a Mo/B4C multilayer. We have chosen this material combination due to its high reflectivity and thermal stability [5]. The OAP was coated in our magnetron sputtering deposition system at DESY. After the coating the OAP was characterized by white light interferometry at the optical metrology lab (Helmholtz-Zentrum Berlin, HZB) and with an at-wavelength reflectometer at PTB (BESSY II). The white light interferometer measurements confirmed that the multilayer did not change the shape of the optic or roughened the substrate. By grading the multilayer period across the clear aperture of the mirror we obtained a uniform reflectivity of 21.5 % at a wavelength of 6.798 nm.

The experimental set-up is shown in Fig. 1. The unfocused beam at BL2 was focused by the OAP and the position and the size of the focus were observed in real time by viewing single-shot craters created on PMMA samples. A series of such craters obtained under known experimental conditions was characterised ex-situ with a Nomarski differential interference contrast microscope and an Atomic Force Microscope (AFM). A fluence series of crater shapes allowed us to reconstruct the beam profile and extract the intensities. One such crater, created close to the best focal position, is shown in Fig. 2. In collaboration with our colleagues from Academy of Sciences of the Czech Republic ASCR we estimated the smallest beam size to be < 0.8 µm in diameter with pulse intensities above 5 x 10^{17} W/cm^2.

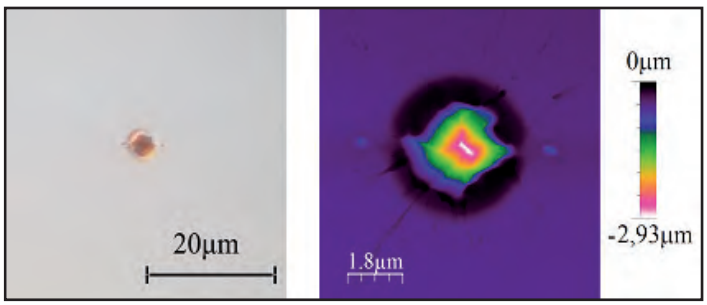

Figure 2

Optical and Nomarski differential interference contrast microscope image of a crater obtained close to the best focus.

One of the issues of using an optic in close proximity to the high-intensity X-ray interaction region with the sample is that the optic can be quickly contaminated. After a few experimental shifts we observed that the area of the mirror that was directly exposed to the FEL beam was visibly contaminated with a surface layer of carbon (Fig. 3). Although this leads to reduced reflectivity it does not affect the optical figure nor does it change the operating wavelength of the optic. In collaboration with the HZB team we demonstrated that this contamination can be cleaned off with oxygen plasma, without damaging the multilayer underneath. The accumulation rate of the contamination can also be reduced by a differential pumping scheme.

Figure 3

Carbon contaminated off-axis parabola.

We are also making progress in the development of novel X-ray optical elements [6] that will enhance the capabilities of FELs by focusing and/or dispersing pulses. Currently, certain time resolved studies are limited by how well the FEL pulses can be shaped and controlled in time. We have developed X-ray optical components for temporal and spatial control of FLASH pulses.

One such component is an asymmetrically cut multilayer. This device is prepared from a multilayer consisting of thousands of nanometre-thick layers. Preparing such structures requires a very good control of the thickness and stress of the deposited layers, as well as suppression of interface roughness. Further sample preparation and shaping, such as the asymmetric cut, need to be done with minimal damage to the original multilayer structure. Bragg reflection is a volume effect and as long as any increased surface roughness due to polishing is limited to the top surface the effect on the overall performance of such an optical element is small. As an example, an asymmetric-cut multilayer with an AFM image of the cut and polished side is shown in Fig. 4. Although the surface roughness exceeded 1 nm the difference in reflectivity from the top and side surface is only few per cent. Such asymmetric-cut multilayers act as perfect blazed gratings with grating periods much smaller than can be made lithographically or by ruling. For example, a 7-nm period multilayer, cut at a 8 degree angle gives a grating period of 20000 lines per mm. Such a grating has an extremely high angular dispersion, which can be used to build a grating pulse compressor, for example [6].

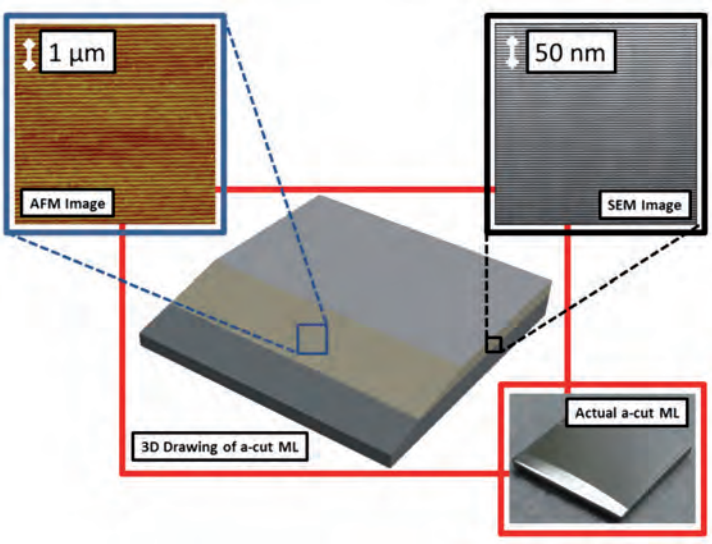

Figure 4

Asymmetric cut multilayer.

To minimize or outrun the radiation damage of large biomolecules and protein nano-crystals during X-ray coherent imaging one would like to work with the highest intensity and the shortest pulse beam. In principle, this can be achieved by compressing longer intense pulses with a pulse compressor. We proposed a pulse compressor based on two asymmetric-cut multilayers (reflection geometry) or two cross sectioned thick multilayers (transmission geometry) [6]. Development of such a pulse compressor and its testing are planned in the near future.

Contact: Saša Bajt; sasa.bajt@desy.de

References

1. H. N. Chapman et al., Nature 470, 73-77 (2011)
2. B. Nagler et al., Nature phys. 5, 693-696 (2009)
3. A. J. Nelson et al., Opt. Exp. 17, 18271 (2009)
4. S. Bajt et al., SPIE 7361 (2009).
5. M. Barthelmess and S. Bajt, Appl. Opt. 50, 1610 (2011)
6. S. Bajt et al., JOSA A 20, 216-230 (2012)

Detectors for dynamics.

The MAXIPIX 2x2 and the Mythen detector for coherent scattering experiments

When coherent photons are scattered by a disordered sample, a typical interference pattern is created, a so called speckle pattern. When the sample shows dynamics the speckle pattern is changing. In order to detect these changes the detector system must then be able to capture speckle patterns faster than the dynamical processes of the investigated sample system change it. These changes of the speckle pattern are analysed in an X-ray photon spectroscopy experiment (XPCS), which allows to investigate dynamical processes of the sample system.
To investigate faster dynamical processes, point detectors in combination with hardware auto-correlators are frequently used. To be able to probe a range of momentum transfers simultaneously, we investigated the performance of two novel detectors for XPCS experiments:
The MAXIPIX 2x2 detector, which is able to collect data with framing rates of a few hundred hertz, making it thus possible to investigate dynamical processes in the sub-second time regime, and the Mythen detector, which offers the advantage of a maximum frame rate in the kilohertz regime.

The Mythen detector is a single photon counting, high framing rate, 1D detector developed by Paul Scherrer Institute, Switzerland [2,3]. The sensor consists of 1280 strips with a pitch between neighbouring channels of 50 µm. To be able to resolve speckles, a slit in front of the Mythen detector was used to decrease the strip length of 8 mm down to 50 µm, resulting in an apparent square pixel size. The dynamic range of the detector can be set in between 4 to 24 bit. The usage of the lowest dynamic range of 4 bits allows framing rates of up to 2000 Hz, which allows to extend the time window of multi-speckle XPCS experiments.
The MAXIPIX 2x2 [4] is a photon-counting 2D Pixel Array Detector developed by the ESRF. It is based on the MEDIPIX2/TIMEPIX [5] readout Application Specific Integrated Circuits (ASICs) developed by CERN and the MEDIPIX2 collaboration. The MAXIPIX detector has a pixel size of 55 x 55 µm². It consists of 2 x 2 modules with a total pixel number of 516 x 516 pixels.

We tested both detectors, together with an avalanche photo diode (APD, point detector) as a reference at the Coherence Beamline P10 at PETRA III. The three detector systems were placed on the same translation stage at a distance of approximately 5 m downstream of the sample position. The experiments were carried out in Small Angle X-ray Scattering geometry. A beam of 200 µm in the vertical and 100 µm in the horizontal was focused by a set of compound refractive lenses to a beam-size of approximately 3 x 5 µm (V x H).

The investigated sample was a model colloidal system of spherical particles suspended in polypropylene glycol. The colloidal SiO_2 particles were coated with a polymer, resulting in a system interacting via a hard-sphere like potential.

Fig. 1, top, shows a series of typical speckle pattern recorded with the MAXIPIX 2x2 detector. The figure shows always the same quadrant of the MAXIPIX detector – starting from the left to the right the figure displays the mean scattering intensity for 0.2, 2, 30 and 525 seconds of total acquisition time. With increasing acquisition time, and thus increasing movements of the scatterers in the sample, the typical grainy appearance washes out.
To control the Mythen detector, a device server has been implemented using the Tango control system. As an additional feature, this Tango device server allows for the automatic merging of individual frames taken by the Mythen detector in a continuous

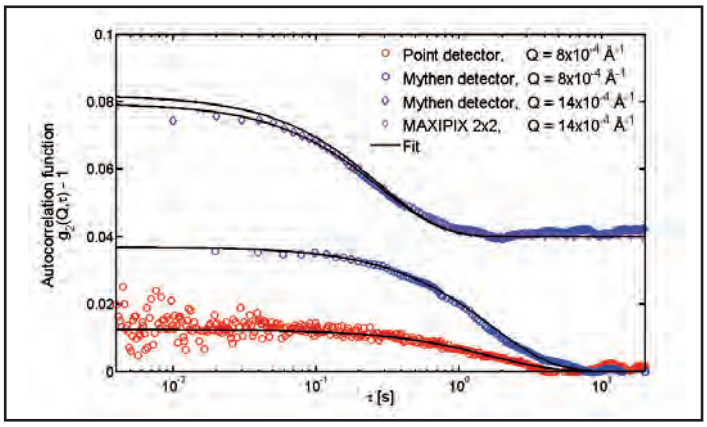

Figure 2

Intensity autocorrelation functions taken with a point detector, the Mythen detector and the MAXIPIX 2 x 2. The curves measured at Q=14x10^{-4} Å^{-1} are shifted vertically for better clarity.

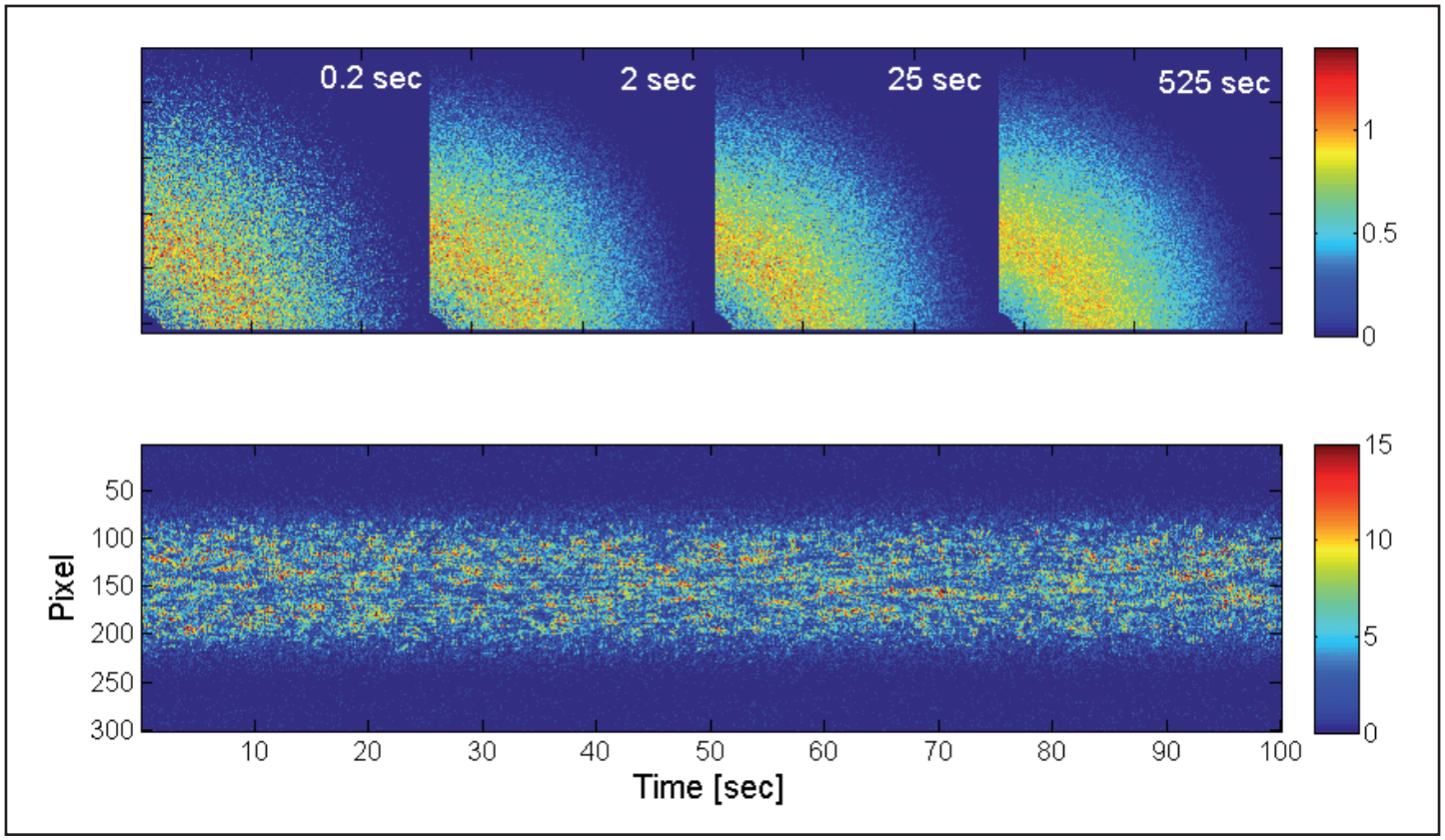

Figure 1

Top: The mean of four scattering 2D pattern series with acquisition times of 0.2, 2, 25 and 525 seconds. Bottom: 20000 frames (1D pattern) taken with the Mythen detector. Both show the temporal evolution of the speckle pattern of a colloidal sample.

series. The merged frames are stored as a 2D matrix. The Mythen detector is equipped with an additional 128 MB RAM memory buffer, making it possible to store data in RAM without having to wait for data transfer. In fig. 1, bottom, a typical merged frame series taken with the Mythen detector for a frame series consisting out of 20000 individual acquisitions is displayed. The individual strips of the Mythen detector are displayed in the vertical, while in the horizontal the individual frames are shown. The changing of the intensity for a given Q (and thus a certain strip) can be clearly seen from the changes in the pattern.

In an XPCS experiment, the dynamics of a sample are analyzed by means of the normalized intensity autocorrelation function g_2 (Q,t) at a given momentum transfer Q. 10000 frames have been measured with a frame rate of 100 Hz for both the Mythen and the MAXIPIX 2x2 detector, resulting in a total exposure time of 100 seconds, while the APD was accumulating data for a period of 300 seconds. The comparison between APD, Mythen and MAXIPIX 2x2 is shown in fig. 2.

All resulting intensity autocorrelation functions show a single exponential decay. The displayed autocorrelation functions have been measured at two momentum transfers, a single exponential fit to the data results in identical relaxation rates for all three detectors. The different visibility of the autocorrelation functions is a result of the different effective pixel sizes of the detectors at the respective momentum transfer.

As expected, both detection systems, the Mythen and the MAXIPIX 2x2 offer the possibility to measure the dynamics of a sample in the millisecond time-window for a range of momentum transfers simultaneously and are two suitable for XPCS experiments.

Contact: Fabian Westermeier, fabian.westermeier@desy.de

Authors

Fabian Westermeier, Alexander Schavkan, Michael Lohmann, Andrea Parenti, Alexey Zozulya, Sergej Bondarenko, Gerhard Grübel, Christian Schroer and Michael Sprung

References

1. G. Grübel and F. Zontone "Correlation Spectroscopy with Coherent Photons" Journal of Alloys and Compounds 362, 3-11 (2004).
2. B. Schmitt, C. Brönnimann, E. Eikenberry, F. Gozzo, C. Hörmann, R. Horisberger, and B. Patterson "Mythen Detector System", Nuclear Instruments & Methods in Physics Research Section A 501, 267-272 (2003).
3. A. Bergamaschi, C. Brönnimann, R. Dinapoli, E. Eikenberry, F. Gozzo, B. Henrich, M. Kobas, P. Kraft, B. Patterson and B. Schmitt "Performance of a single photon counting microstrip detector for strip pitches down to 10 µm" Nuclear Instruments & Methods in Physics Research Section A 591, 163-166 (2008).
4. C. Ponchut, J.M. Rigal, J. Clément, E. Papillon, A. Homs, and S. Petitdemange "MAXIPIX, a fast readout photon-counting X-ray area detector for synchrotron applications" Journal of Instrumentation 6, C01069 (2011).
5. X. Llopart, M. Campbell, D.S. Segundo, E. Pernigotti, and R. Dinapoli "Medipix2: a 64-k Pixel Readout Chip With 55-mm Square Elements Working in Single Photon Counting Mode" IEEE Transactions on Nuclear Science 49, 2279-2283 (2002).

“Transparent” photon diagnostics.

Using angle resolved electron time-of-flight spectroscopy as an online photon characterization tool

The quest for the utmost brilliance was one of the stimulating factors for the continuous development of X-ray sources based on charged particle acceleration. For the third generation storage rings which continue to be developed since decades, stability and reproducibility is a further equally important key factor. It is necessary because the ever increasing brilliance is utilized for higher spatial and/or energy resolution which requires a corresponding increase in stability.

Therefore photon diagnostic is becoming more important both for passive observation such as quality control as well as active feedback control in order to minimize effects of fluctuations. It is preferable if these diagnostics can be used in parallel with the anticipated use of the radiation by the actual experimental application. Especially the softer X-ray regime is difficult in this respect because here no “transparent” media exists, as it would be e.g. a thin diamond window in the case of hard X-rays (> 3 keV photon energy).

For the particular case of the Variable Polarization XUV Beamline P04 at PETRA III delivering photons in the range of about 200 – 3000 eV we developed a suitable diagnostic tool based on the requirements of the different user groups developing various instruments for this beamline. The required photon beam parameters are:

- Photon energy (calibration should be dE/E ≤ 1/10000),
- Photon flux (accuracy ≤ 1 % absolute, ≤ 0.1 % relative),
- Photon beam position (accuracy ≤ 10 µm),
- Degree of polarization (accuracy ≤ 1 %).

If possible all of these parameters should be determined independently and “online” while the user is acquiring the data.

In order to achieve these goals our diagnostic tool (Fig. 1) is based on a dilute gas phase target (about 10^{-5} hPa partial pressure) which absorbs typically less than 1 ppm of the radiation and also does not interfere with the wave-front of the radiation. In order to obtain a significant signal within a relatively short time period we decided to employ electron time-of-flight spectrometers which in principle allow detecting electrons of all kinetic energies simultaneously. In order to detect the electrons efficiently, several independent spectrometers should be used to cover a large solid angle and at the same time allow for precise angular distribution determination.

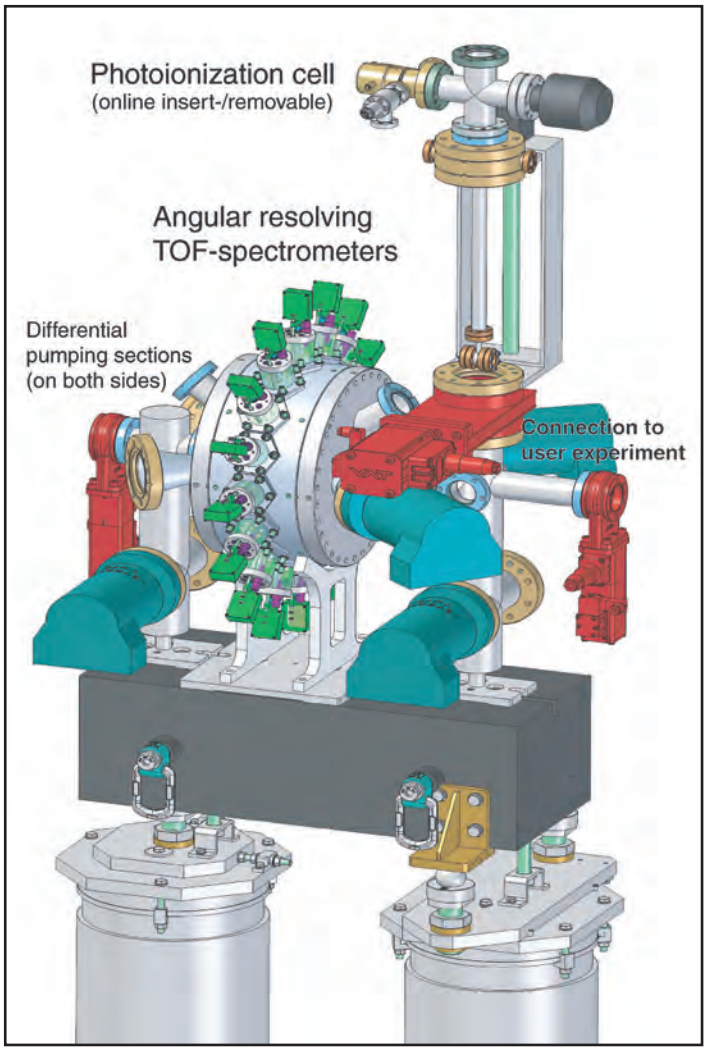

Figure 1

Sketch of the online diagnostic unit just in front of the user experiment at P04 of PETRA III.

It is obvious that the electron kinetic energy spectrum gives direct access to the photon energy spectrum. In the same sense there is a direct correlation between electron signal intensity and photon flux. The time-of-flight of the photoelectrons depends

Figure 2

View inside the diagnostic unit. German Chancellor Angela Merkel and DESY Director Helmut Dosch are inspecting the 16 independent drift tubes of the electron time-of-flight spectrometers.

also on the path length from the interaction region where the electrons are ionized up to the detector. Therefore variations in the beam position are reflected by a change of the location of the interaction region which will in turn lead to a correlated time-of-flight variation of the ejected photoelectrons. And last but not least the angular distribution of the photoelectrons is affected by the polarization of the ionizing radiation. Therefore the setup combines 16 spectrometers (Figure 2) with sufficient angular resolution (± 6.5°) and a quite large total solid acceptance angle (3.6 % of 4π) enabling us to record spectroscopic data based on inert gas targets over a very wide photon energy range up to the hard X-ray regime. Each spectrometer is mounted in a gold coated aluminium ring. The gold coating was found to be necessary to avoid patch fields on the surface of the aluminium ring. In the actual status, a single spectrometer consists of a flight tube divided into four independent potential sections terminated by a “micro channel plate” (MCP) based detector including the relevant cabling for applying the necessary high voltages and decoupling the output signal. The total length from the interaction region to the MCPs is ≈ 140 mm. The separate flight tube potentials allow tuning the electron trajectories for decelerating the electrons in order to improve the energy resolution and simultaneously keeping a good transmission efficiency for higher kinetic energies. All parts of each detector were under continuous development during the last years to increase the performance of the spectrometer setup. The peripherals of the setup as well as the whole chamber are carefully selected to be non-magnetic.

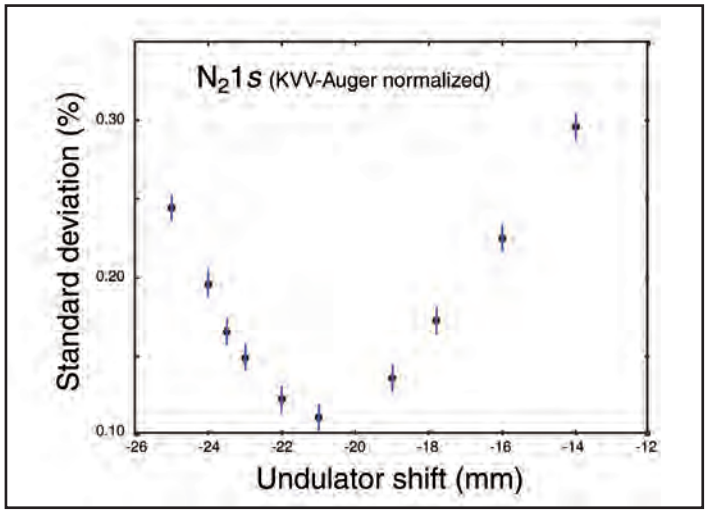

Figure 3

First test of the online diagnostic unit at P04 of PETRA III: Minimum standard deviation in the angular distribution of the N2 1s photoelectron line measured at hν = 500 eV coincides with the minimal degree of linear polarization which in turn implies maximum degree of circular polarization. Thereby the optimum shift of the APPLE-II-type undulator can be determined. Typical dwell time is 60 s.

Initial tests of the device have been performed at BW3 (DORIS III) and FLASH. First measurements at P04 at PETRA III were done in order to optimize the degree of circular polarization of the radiation provided by the APPLE-II-type undulator of P04 (Fig. 3). Altogether these tests have shown that the required parameters can be obtained with sufficient accuracy by the online diagnostic unit.

Contact: Frank Scholz, frank.scholz@desy.de
Leif Glaser, leif.glaser@desy.de
Markus Ilchen, markus.ilchen@desy.de
Jens Viefhaus, jens.viefhaus@desy.de

Light machines.

Recent undulator developments at DESY

1. Undulator design for FLASH II

Since the present fixed-gap undulator system for FLASH I and the new FLASH II-undulators will share the same electron beam accelerator, variable gap undulators are mandatory in order to provide radiation of different wavelengths to both experimental halls independently.
Each of the 12 undulator segments for FLASH II has a length of 2.5 m. The magnet structure is a hybrid design with a period length of 31.4 mm. It provides a maximum field of 0.98 T and thus a maximum K-value of 2.87 at a minimum magnetic gap of 9 mm. In comparison to the PETRA III magnet design, the width of the Vanadium Permendur poles has been downsized to 30 mm and the shape of NdFeB-magnets for FLASH II has been optimized in order to reduce the costs and the maximum magnetic forces acting on the support structure while preserving a good field region (with less than 1 ‰ horizontal field roll-off) which is more than ±2 mm wide.
The end poles are designed in a 1:¾:¼ configuration and have also been optimized for minimum gap dependence of the remaining field integrals using a recursive process in *Radia* [1]. In a first step, the impact on the gap dependent trajectory offset and slope was calculated for each of the parameters. These results were used for weighting the parameters during numerically minimizing the gap dependent trajectory changes in the second step of each iteration. The simulation of the electron trajectory in the undulator for different gaps shows a peak to peak deviation in the 2nd field integral of 4 Tmm^2 (see Fig. 1) at the end of the insertion device. For 1 GeV electrons this relates to a negligible displacement of less than 1.5 µm which can easily be compensated for by dedicated corrector coils. To allow for the correction of magnetic multipoles, there is a compact retainer for “magic finger” correctors attached to each end of the magnet structure.
To increase the lateral stiffness of the girders despite their increased length, their cross section was changed to 400×130 mm^2. Finite element calculations show that the maximum vertical deformation expected due to the changes of the magnetic load is 3.4 µm. Magnetic simulations yielded that the typical phase errors of 2° to 3° rms are only marginally compromised by this dynamic long scale girder deformation.

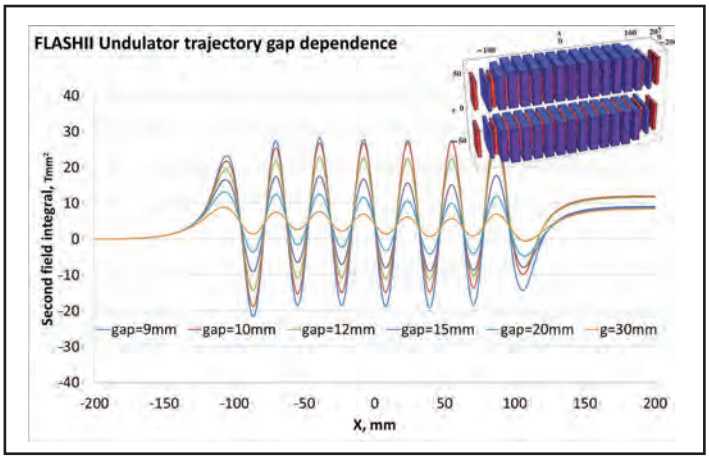

Figure 1

Simulation of the beam trajectory for different gaps and the model used for the endpole design (inset).

2. Shimming dynamic field integrals at the PETRA III Apple II-Undulator

The 5m-long Apple II-undulator UE65 which is operated since 2009 at PETRA III-beamline P04 was built in cooperation between Helmholtz-Zentrum Berlin and DESY Hamburg. Its magnetic field measurements proved the success of the careful mechanical design considering the exceedingly strong 3D forces of this device especially in the inclined operation mode. Therefore the spectral properties for the entire energy-range of 250 - 3000 eV are expected to be close to perfection in all operation modes. Though the positron energy of PETRA III is rather high the dynamic multipoles of the UE65 are expected to have some impact on the closed orbit and the linear optics of the machine and had to be shimmed with L-shaped Fe-shims [2]. To be compatible with top-up operation and allow for injection at closed gap it is crucial that only minimal multipoles remain within a transverse range of ±20 mm around the golden orbit. The dynamic field integrals were simulated in *Radia* [1] and an optimized L-shim quadrupole geometry and configuration consisting of one shim on each magnet row was determined from these results.

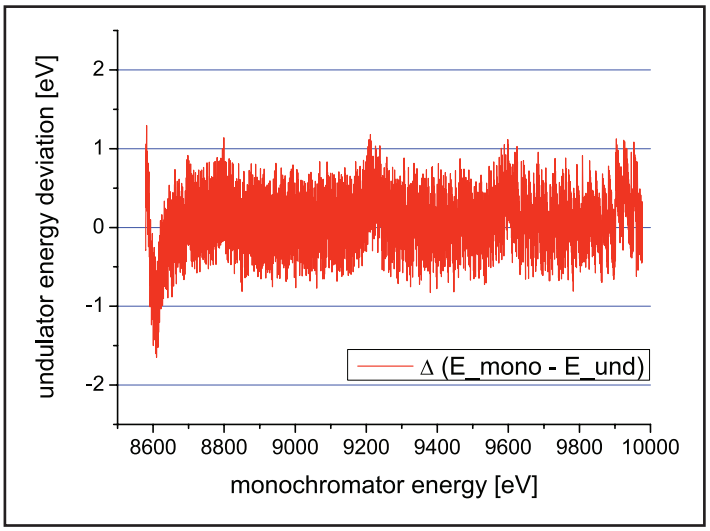

Figure 3

Deviation between the energy defined by the monochromator angle and the energy corresponding to the undulator gap during a scan over a range of 1400 eV done within 20 sec.

During machine studies the tune shift was measured as a function of the horizontal beam position in the undulator before and after the L-shims were applied (see Fig. 2). The results were in very good agreement with the simulations and showed that by application of the L-shims onto the magnet structure the remaining effects on the tune could be suppressed by more than a factor of three down to a level that presently does not need any further active compensation scheme.

3. Synchronizing undulator gap and monochromator movements

In order to fully exploit the high brilliance at modern synchrotron light sources like PETRA III it is essential to minimize the overhead caused by movement and settling times of motors. This problem becomes apparent especially in the case of energy scans for spectroscopy applications at undulator sources. To cover the energy range of about 1200 eV for a typical EXAFS scan on the fly, a synchronized movement of monochromator system and undulator gap is required. Although monochromator and undulator are each equipped with an elaborate motion control system, synchronization with external components is usually not foreseen.

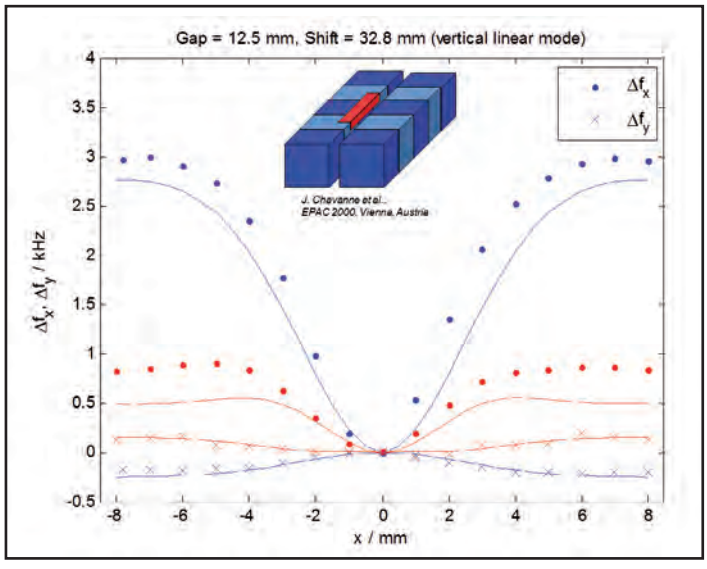

Figure 2

Horizontal (dots) and vertical (crosses) tune shift as a function of the horizontal beam position. The data is shown for the vertical linear operation mode of the Apple II-undulator before (red) and after (blue) installation of the L-shims (see sketch in inset). The solid lines show the calculated/theoretical values.

Therefore in the first tests that have been made at PETRA III beamline P06, the synchronization is done on the level of the beamline control system *Online* [3]. This has some convenient side effects since it allows for addressing both, the monochromator and the undulator, via their corresponding Tango-device on the energy scale. The desired scan-velocity for both devices is estimated beforehand. After starting a scan, the monochromator energy is regarded as a reference and the undulator gap velocity is adjusted accordingly on the fly. Current undulator position and velocity setpoints are updated with a rate of up to 10 Hz. By these means a position jitter of ±1 eV was achieved (see Fig. 3) which is well below the line-width of the undulator and therefore is sufficient for the needs concerning the intensity stability of a spectroscopy beamline. These results could be improved further by implementing a combined monochromator/undulator TANGO device for energy scans or a synchronisation done by the undulator control system.

Contact: Andreas Schöps, andreas.schoeps@desy.de

Authors

A. Schöps[1], M. Tischer[1] and P. Vagin[1] (on behalf of DESY FS-US), T. Ramm[1], J. Bahrdt[2], J. Keil[1], T. Kracht[1] and G. Wellenreuter[1].

1. Deutsches Elektronen-Synchrotron DESY, Notkestr. 85, 22607 Hamburg, Germany.
2. Helmholtz-Zentrum Berlin, Albert-Einstein-Str. 15, 12489 Berlin, Germany.

References

1. **O. Chubar, P. Elleaume, and J. Chavanne, "A three-dimensional magnetostatics computer code for insertion devices", *J. Synchrot. Radiat.* 5, 481-484 (1998).**
2. **J. Bahrdt *et al., Proc. of IPAC2011, San Sebastián, Spain*, pp 3254-3256 (2011).**
3. **M. Alfaro *et al., Proc. of ICALEPCS2011, Grenoble, France*, pp 44-46 (2011).**

Catching the wavelength for each pulse.

Online Photoionization Spectrometer at FLASH.

Processes of light interaction with matter are strongly defined by the radiation properties like wavelength, intensity, polarisation and pulse duration. Since these properties determine the way the system under investigation evolves, most experimenters want to have stable conditions in that respect. At Free-Electron Laser facilities, however, the FEL radiation parameters vary continuously due to the stochastic nature of the Self-Amplifying Spontaneous Emission (SASE) process. Some user experiments can even benefit from these fluctuations, for example if they can make use of slight intensity or wavelength changes which they get for free. Nevertheless, the properties of the light have to be known and hence measured for a decent data analysis of the experiment. In the ideal case parameters are constantly monitored for each individual light pulse without interfering with the user experiment.

Regarding the FEL wavelength there are spectrometers in the FLASH accelerator tunnel and in the PG monochromator beamline serving particularly as diagnostic tools for setting up SASE operation. However, they block the photon beam when enabled and therefore cannot be used to measure the wavelength while running user experiments at the same time. To go towards online monitoring of the spectral distribution, the photon diagnostics group at FLASH established a variable line spacing grating spectrometer (VLS) for the BL beamlines without monochromator [1]. This device uses only a small fraction (5 - 10 %) of the light in the 1st diffraction order for the wavelength determination whereas most of the intensity is passed in 0th order to the user experiment. Restrictions are currently the acquisition rate of 10 Hz (single-bunch mode capability) and a short wavelength limit at 5.4 nm in the first diffraction order.

A different approach is used for the online photoionization spectrometer (OPIS) [2] which was designed and tested by the FLASH photon diagnostics group during the last years and has been installed in the photon diagnostics section in the FLASH tunnel (Fig. 1). The wavelength determination with this device is based on single photoionization processes of gas phase targets, for which the relevant quantities of the ionization process like binding energies and photoionization cross sections are well-known from literature. Typical target gas pressures are in the range of 10^{-7} hPa which allows a photon transmission to the user experiment of essentially 100 %.

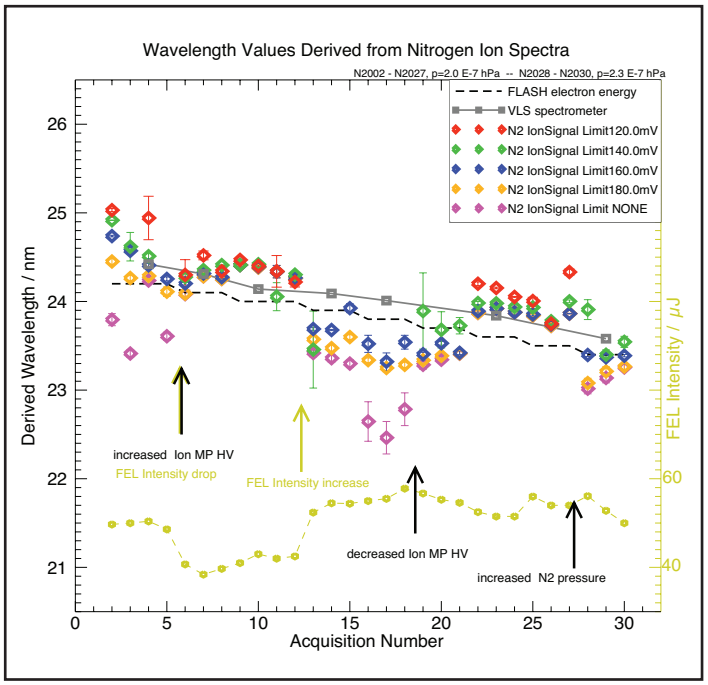

Figure 2

Results of a measurement run in which the FLASH nominal wavelength (dashed black line) was scanned over 0.8 nm by changing the electron energy. Wavelength values determined by the OPIS (coloured diamonds for different signal strengths to investigate saturation effects) are compared to those derived from the VLS (grey squares). The FLASH pulse energy is shown in lower part of the panel referring to the right y-axis. Changes on some operation parameters which may have an effect on the derived wavelength value are indicated.

The OPIS device comprises a set of time-of-flight spectrometers for detection of photoions and photoelectrons, respectively. Fast digitizers record the spectrometer detector signals on a shot-to-shot basis within full bunch trains of FLASH. Thus it is possible to have a monitor for single bunch resolved determination of the spectral distribution.The advantages of this device make the OPIS a promising complement to the existing optical dispersive spectrometers.

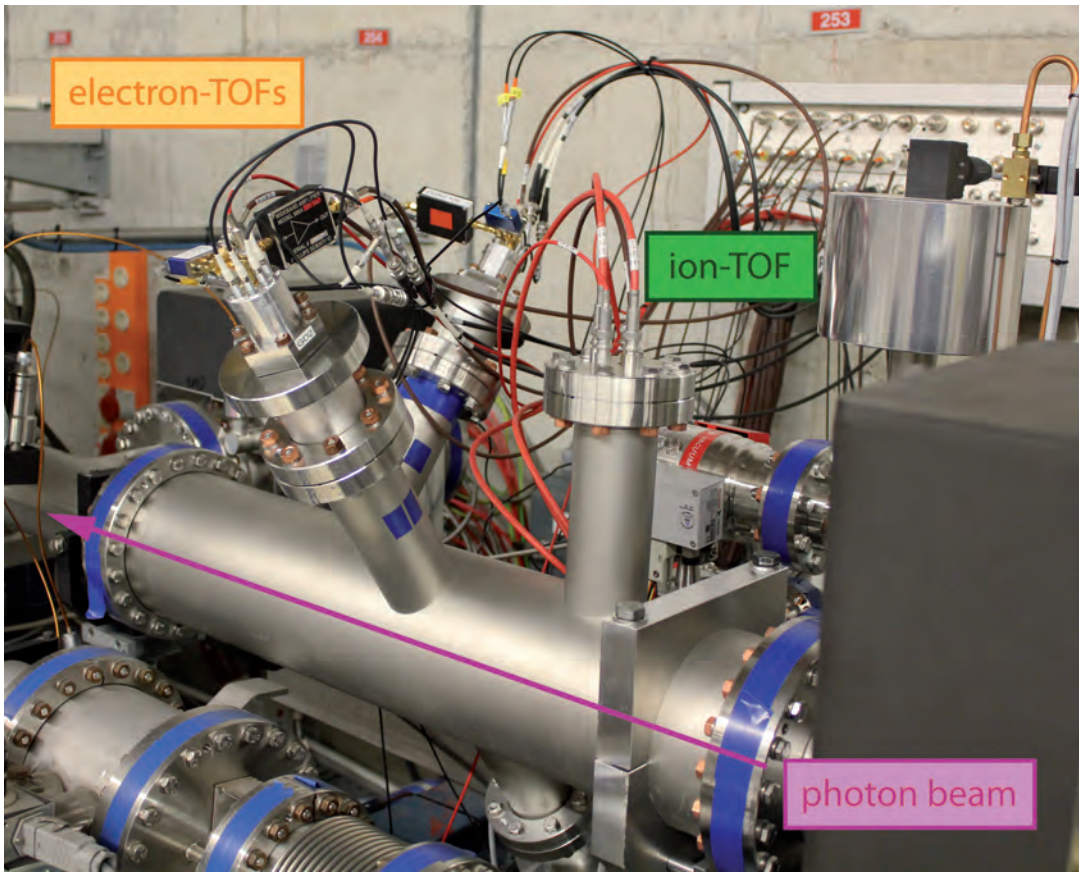

Figure 1

Photograph of the OPIS μ-metal chamber with one ion and three electron time-of-flight spectrometers mounted in the photon diagnostics section in the FLASH accelerator tunnel.

The ion spectrometer is used to measure the intensities of different charge states of the created photoions. Since the partial cross sections of the different charge states evolve differently with increasing photon energy, the ratios of the according intensities are a unique measure of the photon wavelength in a certain wavelength interval. Literature data of partial cross sections for the different charge states of various rare gas species cover basically the full wavelength range of FLASH. The major advantages of the ion spectrometer are the high signal intensity due to the extraction fields collecting all ions created by the radiation and its insensitivity against beam position changes.

In the electron time-of-flight spectra the arrival times of the photoelectrons reflect directly their kinetic energy. The only information needed for the wavelength determination are the values of the electron binding energy of the orbitals the photoelectrons were emitted from. Hence, with only a few well-known constant quantities the FEL wavelength can be derived over the full wavelength range which is the main advantage compared to the ion method described above. In addition, further spectral information like higher harmonics contribution or the number of FEL modes can be in principle deduced as well [4]. On the other hand the electron signal intensity is lower compared to the ion spectrometer due to limited apex angles and it is sensitive to external magnetic and electric fields.

Most recently, test and cross-calibration measurements have been performed in a campaign over several FLASH studies periods together with the VLS spectrometer and the compact spectrometer using the PG beamline spectrometer as a reference [3]. In several studies shifts the FLASH machine operators managed to maintain the SASE pulse energy level while tuning the electron energy stepwise by several 10 MeV and accordingly shifting the nominal FEL wavelength by about 1 nm (Fig. 2). This was extremely useful to compare wavelength values derived from different spectrometers and in order to optimize important operation parameters of the OPIS. These test runs will also help to establish an automatized procedure for online analysis of the recorded electron and ion detector traces that will be implemented in the DOOCS system for a routine operation at FLASH and FLASH II.

Contact: Markus Braune, markus.braune@desy.de
Kai Tiedtke, kai.tiedtke@desy.de

References

1. G. Brenner et al., „First results from from the online variable line spacing grating spectrometer at FLASH“,Nucl. Instr. and Meth. A 635, S99-S103 (2011).
2. P. N. Juranic et al., “Using I-TOF spectrometry to measure photon energies at FELs”, J. Instr. 4, P09011 (2009).
3. F. Frassetto et al., “Compact spectrometer for photon diagnostics of the extreme-ultraviolet free-electron-laser radiation”, Nucl. Instr. and Meth. A 635, S94-S98 (2011).
4. M. Wellhöfer et al., “Photoelectron spectroscopy as a non-invasive method to monitor SASE-FEL spectra”, J. Instr. 3, P02003 (2008).

Hot science at the diamond tip.

Laser-heating at the Extreme Conditions Beamline P02.2

Investigations of materials at high pressure find its application in ever growing scientific disciplines, ranging from chemistry and physics to material science, geophysics and biology. By adding temperature to the system one opens up the largely unexplored pressure-temperature phase space.

Because of the tiny nature of the samples (order of several tens of micrometres in lateral dimensions, few micrometres in thickness), and the proximity of highly thermally conductive diamonds, reaching temperatures above 2000 K requires powerful lasers focused to a spot size of about 15 - 20 µm. Alternatively, resistive heating up to 2000 K is available at the beamline.

To study matter *in situ* at high pressure and temperatures in diamond anvil cells (DAC), online laser heating systems have been set up at the Extreme Conditions Beamline P02.2 at PETRA III [1]. "*Off-axis*" and "*on-axis*" systems utilize Ytterbium fibre lasers (1070 nm) for heating of optically opaque materials. In future, also a CO_2 laser with a wavelength suitable for absorption in transparent samples is foreseen to operate at the beamline (Fig. 1).

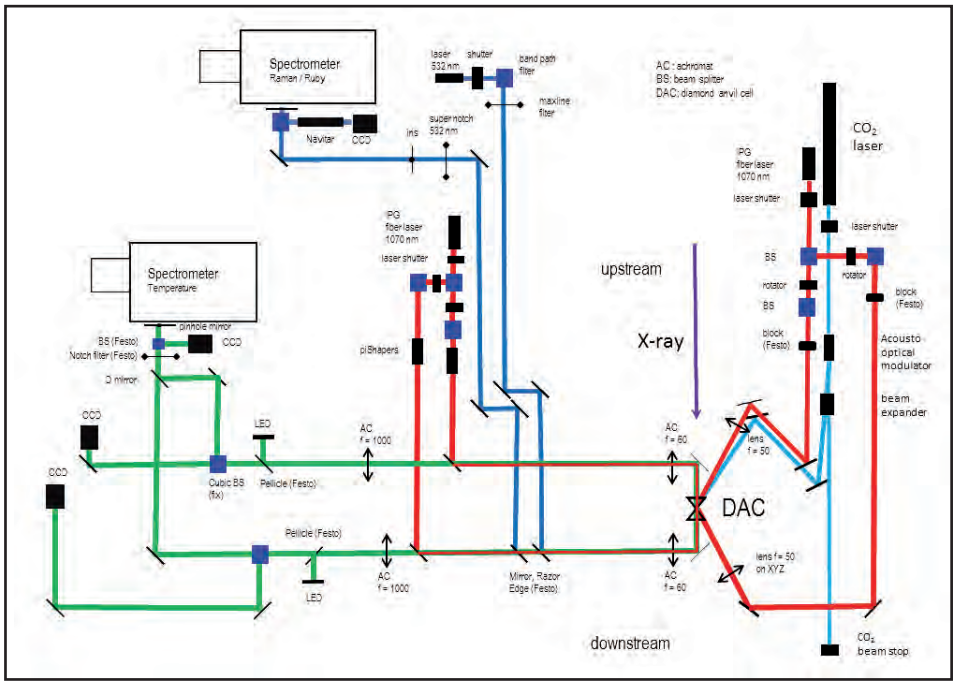

Figure 1

Layout of beam paths in the Laser Heating System at the Extreme Conditions Beamline P02.2.

For the *off-axis* laser heating, one 100 W Ytterbium fibre laser is split into two beams and focused onto the sample at an angle of about 25 degrees relative to the X-ray beam (Fig. 1 and Fig. 2). The laser power is controlled by rotating λ/2 waveplates between polarizing beamsplitter cubes. Since the laser and optical paths are disentangled, no optical elements remain in the path of the X-ray beam.

Due to the laser focusing, the heated area of the sample exhibit large temperature gradients. To minimize this effect, the hot-spot is probed by an even smaller but very bright X-ray beam (typical size of 2 x 2 μm^2 (FWHM) and 6 x 10^{10} ph/sec in the focal spot, at 42.8 keV photon energy). The temperature of the sample is determined by fitting Planck's function to the thermal radiation originating from the glowing sample. The irradiated light is collected through a modular optical system and guided to a spectrometer that analyses light in the wavelength range of 600 – 800 nm. The temperature measurements are performed simultaneously on the up- and downstream side of the DAC using different regions of the intensified CCD camera separated by a double pinhole positioned at the entrance of the spectrograph.

For the *on-axis* laser heating, a 200 W Ytterbium fibre laser is split into two paths and later introduced into the optical inspection pathway; hence the heating is performed parallel to the X-ray beam. The advantage of this system is the possibility to heat samples at megabars pressures where the seat openings become smaller and inaccessible by the off-axis laser beams. The optical system comprises a second spectrometer and green laser (532 nm, 2mW) for the online pressure determination, see Fig. 1.

In the past two years several high pressure, high temperature powder X-ray diffraction experiments were performed to investigate the structure of matter, such as melting of mantle minerals, drawing high P-T phase diagrams or inducing chemical reactions which can lead to novel compounds with unusual structural features.

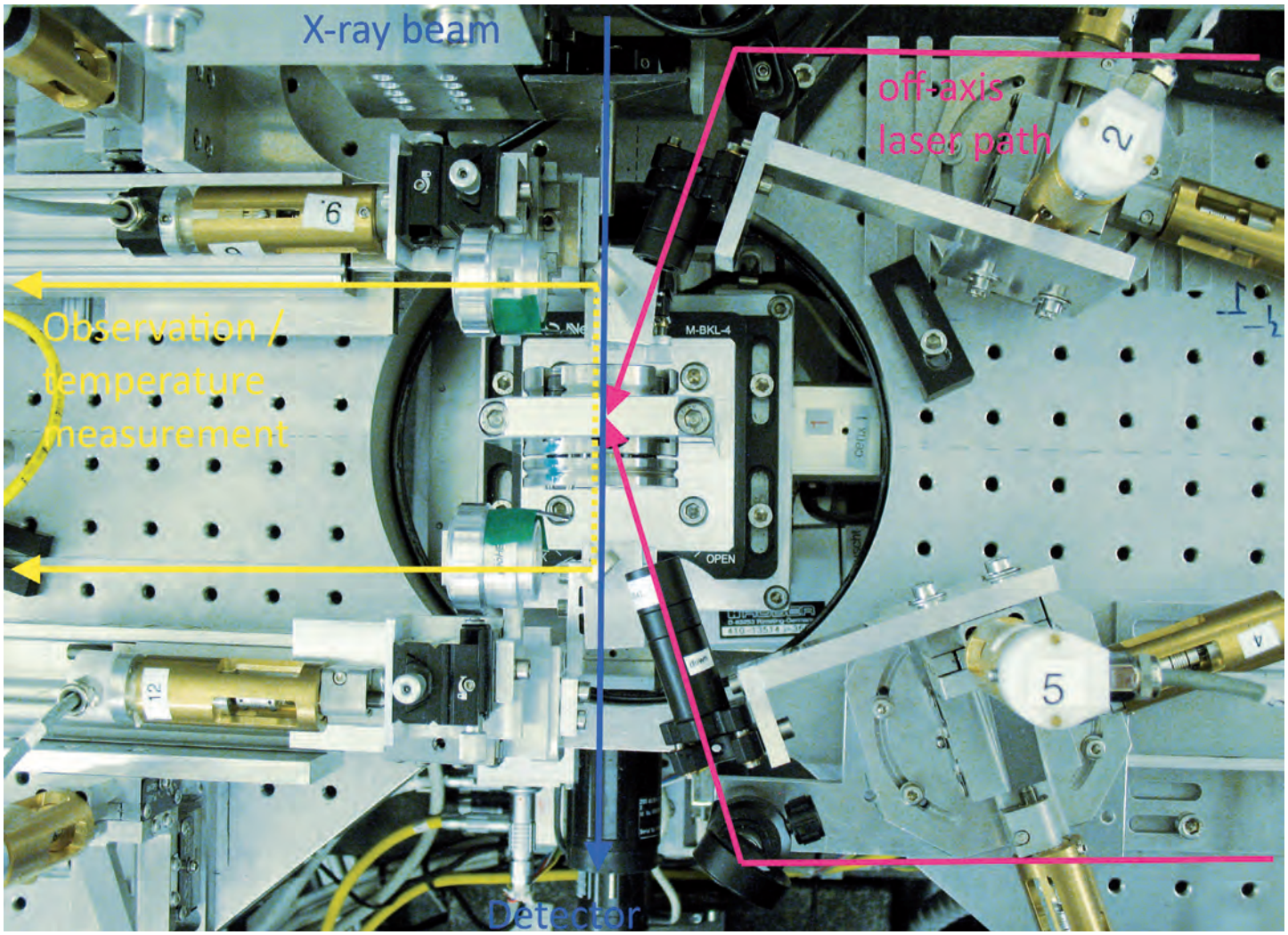

Figure 2

Beam paths in the Laser Heating System at the Extreme Conditions Beamline P02.2. Red: *off-axis* fibre laser for heating, yellow: observation, temperature measurement and *on-axis* laser heating, blue: X-rays to detector.

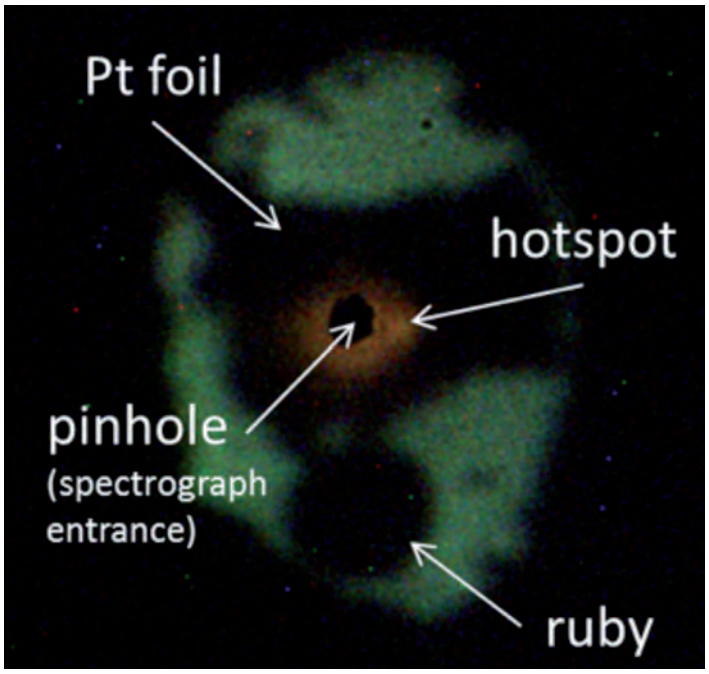

Figure 3

Sample (Pt foil) in the diamond anvil cell. Orange area: glowing hotspot, the dark circle in its centre is the entrance to the spectrograph. Image is taken at the pinhole-entrance mirror in front of the spectrometer.

Contact: Zuzana Konôpková, zuzana.konopkova@desy.de
Hanns-Peter Liermann, hanns-peter.liermann@desy.de
Wolfgang Morgenroth (Universität Frankfurt), wolfgang.morgenroth@desy.de

References

1. **H.-P. Liermann et al., "The Extreme Conditions Beamline at PETRA III, DESY: Possibilities to conduct time resolved monochromatic diffraction experiments in dynamic and laser heated DAC", J. Phys.: Conf. Ser. 215, 012029 (2010).**

Liquids in two dimensions.

A nano gap cell for confined liquids investigated with X-rays

Polymer and liquid films with thicknesses of a few molecular diameters are a topic of theoretical and experimental studies since a long time [1-6]. The investigations show that soft matter confined in the range of the molecular size behaves in a completely different way compare to bulk materials. The confinement influences strongly the mobility of the molecules and therefore e.g. the glass transition behaviour and the melting temperature are affected [1]. Here, the authors introduce a "confined phase" within the phase diagram depending significantly on the shape and the size of the confining object. Liquids confined between two parallel substrates (confined film in slit) arrange as molecular layers parallel to the interface, the so-called layering. Theoretical studies and computer simulation experiments suggest that the liquid in the gap may be partially crystalized and/or is in-plane organized in clusters (solidification of the liquid phase) [2]. The confinement effects show up in liquid films with thicknesses as large as ten times the molecular dimensions.

For confined liquid films in slit geometry previous studies have shown that the X-ray reflectivity is perfectly suited to investigate molecular layering along the surface normal [3], as it is sensitive to the averaged electron density profile. For reflectivity the spatial accuracy is usually better than 0.1 nm and the sensitivity to the contrast (density changes in the profile) is in the range of a few per cent. However, reflectivity cannot monitor in-plane ordering of molecules. For this reason grazing incidence diffraction (GID) and/or small angle scattering (SAXS) is mandatory to extract the in-plane information.

The great challenge is to design and construct sample environments that enable measurements of confined liquids in slit geometry. This requires two extremely flat surfaces which can be aligned exactly parallel with tuneable gap sizes in the nanometre range. First very successful attempts have been achieved in the groups of Israelachvili, Granick, van der Veen, and others [4, 5, 6]. Israelachvili developed the surface force apparatus with crossed cylinders as first gap-defining device [4]. The groups of Granick and van der Veen built environments for X-ray methods, however with fairly large gaps of micrometre size mostly using colloids as a model fluid. Even in the last works based on the surface force apparatus a full structural analysis of confined soft matter has not been achieved [5, 6] due to problems with the sample geometry.

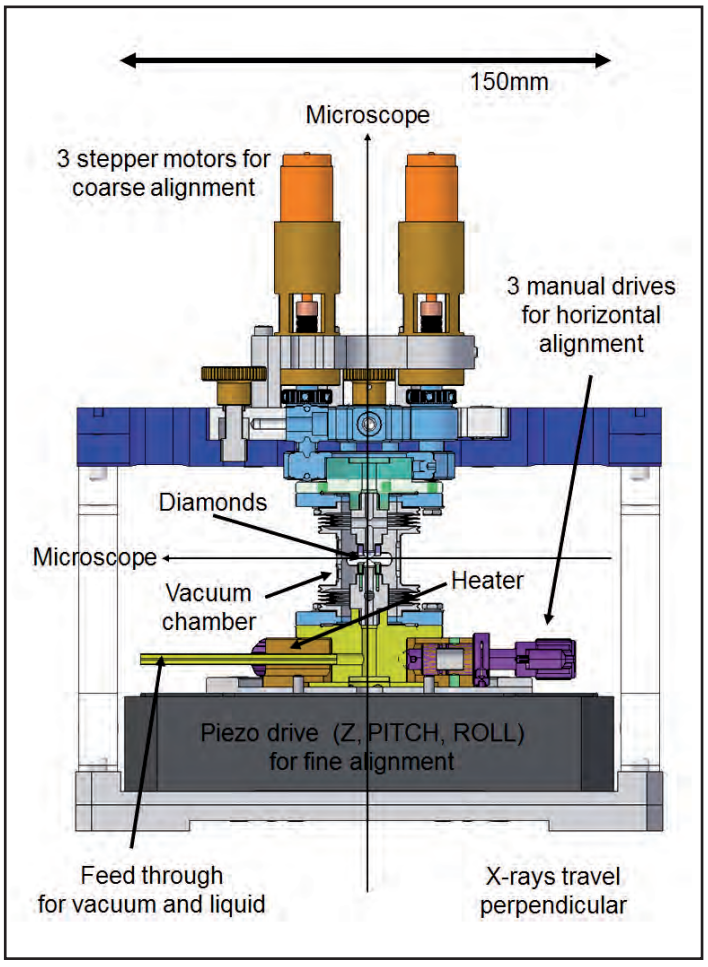

Figure 1

The liquid confinement cell. The diamonds are the two substrates to confine the liquid.

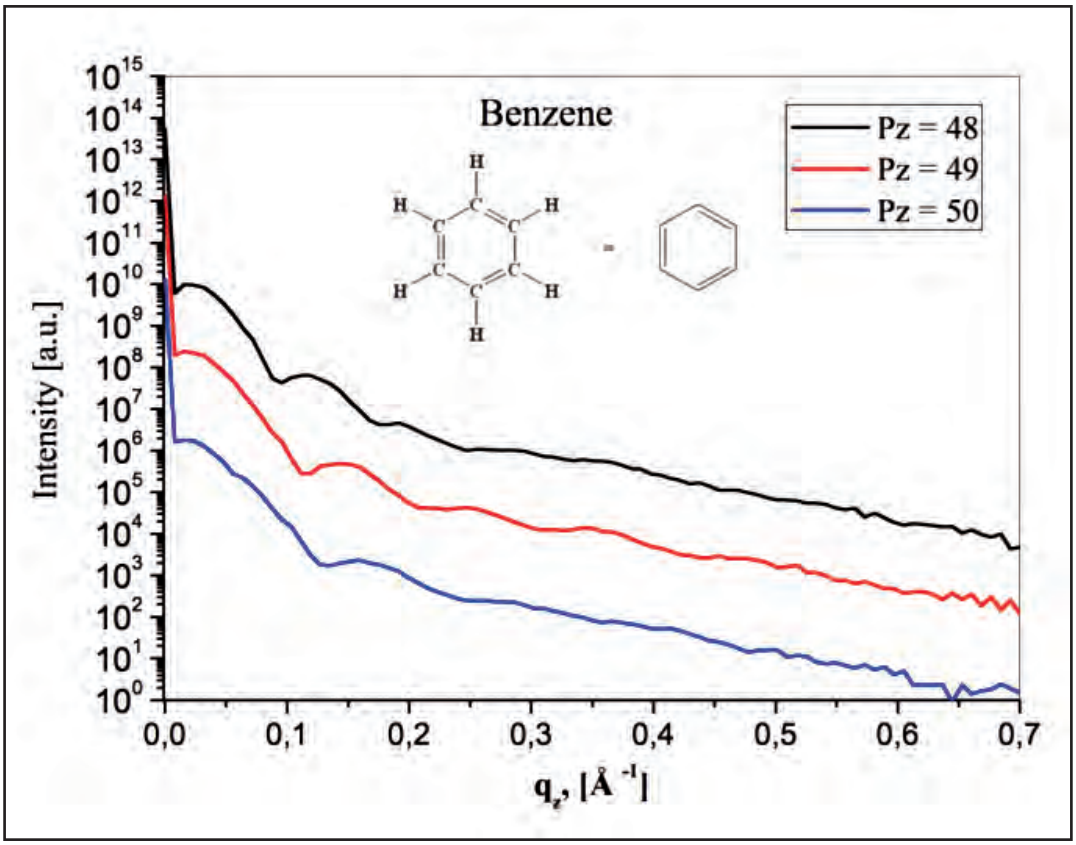

Figure 2

Reflectivity curves of a confined benzene film. Pz notes the position of the vertical travel of the piezo device. The measurements were performed at beamline P08 (PETRA III) with 18 keV and beam size of 200 x 30 µm (horizontal × vertical).

Our approach for an X-ray nano gap cell is based on diamond anvil cells. Two diamond crystals with a diameter of 4 mm, height of 3 mm and 200 µm culet size acting as confinement areas are used as substrates. The quality of the surface has been checked by atom force microscopy and X-ray reflectivity measurements. The mounting and the coarse alignment of the diamonds has also been done in the clean room, using optical microscopes from the top and the side (see Fig 1). The final alignment of the substrates and the tuning of the gap size are conducted by a piezo stage (PI P-518K024) at the bottom of the cell. The stage is able to align the diamonds with an accuracy of 0.001° and has a translation in vertical direction with max. 100 µm ± 1 nm.

The liquid is injected into the bottom part of the sample cell and then heated from below with the gap open at 20 µm. The liquid evaporates and condenses at the surface of the colder top diamond. The presence of the liquid can be monitored from the top and from the side by microscopes. Then the gap is closed and reflectivity curves of the confined liquid film are measured to determine the gap size and the density profile. Fig. 2 shows examples of measured reflectivities with different gap sizes (see the distance of the fringes). The refinement of the curves confirms that gap sizes of 50 Å to 70 Å have been achieved. The molecular diameter of benzene is 4.96 Å so that even the smallest gap is still approximately ten times larger than the molecular size. Therefore, more effort has to be done in preparing smoother and cleaner surfaces. However, the experiment has verified that the setup can be used for confinement of liquids down to molecular levels. In-plane and out-off-plane X-ray measurements are possible.

Contact: Milena Lippmann, milena.lippman@desy.de
Anita Ehnes, anita.ehnes@desy.de
Oliver Seeck, oliver.seeck@desy.de

References

1. Y. Xia, G. Dosseh, D. Morineau, and Ch. Alba-Simionesco, “Phase diagram and glass transition of confined Benzene”, J. Phys. Chem. B 110, 19735 (2006).
2. J. Klein and E. Kumacheva, “Confinement –induced phase transition in simple liquid”, Science 269, 816 (1995)
3. O. H. Seeck , Hyunjung Kim, D. R. Lee, D. Shu, I. D. Kaendler, J. Basu, and S. K. Sinha, “Observation of thickness quantization in liquid films confined to molecular dimension”, Europhys. Lett. 60, 376-382 (2002).
4. A. Dhinojwala, S. Chul Bae, and S. Granick, “Shear-induced dilation of confined liquid films”, Tribology Letters 9, 55 (2000).
5. J. N. Israelachvili, P. M. McGuiggan, and A. M. Homola, “Dynamic Properties of molecular thin liquid films”, Science 240, 189 (1988).
6. E. Perret, K. Nygard, D. K. Satapathy, T. E. Balmer, O. Bunk, M. Heuberger and J. F. van der Veen, “Molecular liquid under nanometer confinement: density profiles underlying oscillatory forces”, J. Phys.: Condensed Matter 22, 235102 (2010).

Tuning polarization.

Double phase-retarder set-ups for polarization control

At X-ray wavelengths, near Bragg diffraction, perfect crystals are birefringent and can be used to vary the polarization of incident X-rays. For a scattering plane at 45° from the synchrotron ring plane, the phase shift $\Phi_{\sigma\pi}$ produced between the two orthogonal components of the electric field of an incident horizontal plane wave propagating through the crystal is $\Phi_{\sigma\pi} = A^*t_{eff}/\Delta\theta$ with the angular offset $\Delta\theta$ from the Bragg angle and the effective thickness t_{eff} of the crystal. A is a coefficient that depends on the type of material used and the crystal planes (hkl) set in diffraction. The coefficient varies with the wavelength. If a phase shift of $\pm\pi$ [$\pm\pi/2$] is generated, the transmitted X-rays are linearly polarized in the vertical plane [circularly polarized] and the phase-retarding crystal is called a half-wave plate (1/2 WP) [quarter-wave plate (1/4 WP)]. Recent technical developments [1-3] have demonstrated that using two 1/4 WP in series in the antiparallel geometry generates X-rays with a much higher degree of linear polarization than using a single 1/2 WP. This is explained by two reasons. On one hand, the antiparallel geometry compensates for the phase shift spreads due to the divergence of the beam and due to the energy spread. On the other hand, depolarization effects are minimized when using a $\Delta\theta$ further away from total Bragg diffraction. In analogy, the degree of circular polarization is significantly enhanced by using two 1/8 WP in series.

The Resonant Scattering and Diffraction beamline P09 at PETRA III is equipped with a state-of-the-art double phase-retarder that generates linearly and circularly polarized X-rays in the energy range between 3.5 and 8.5 keV as yet. The double phase-retarder (HUBER Diffraktionstechnik GmbH & Co. KG, Rimsting, Germany) is shown in Fig. 1a. It consists of two separate identical 3-circle (θ, χ, 2θ) diffractometers sitting on independent Z and X stages to bring their centre of rotation onto the beam axis. The two χ circles are aligned parallel to each other better than 0.1°. A pitch and yaw rotation underneath further helps aligning the whole assembly along the beam axis. Rotating χ by 90°, the Bragg condition can be kept within ± 5” for the 2nd cradle while within ± 10” for the 1st cradle. The double phase-retarder sits in its own tank right after the high-heat-load monochromator and is part of the optics hutch vacuum implying that all its components are UHV compatible.

Diamond is the best material for phase retardation at X-ray energies above 3.1 keV due its low Z, its high single-crystallinity and due to the large structure factors of the (111) or (220) reflections that maximize the coefficient A i.e. the phase shift [4].

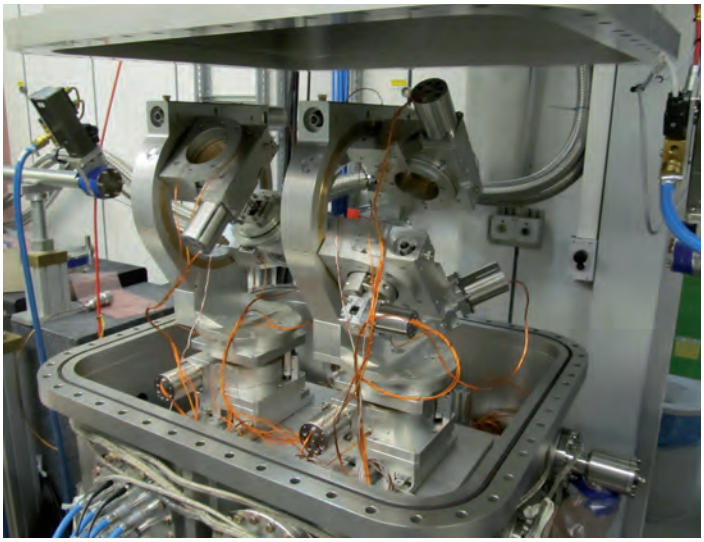

Figure 1a

Double phase-retarder set-up installed in the optics hutch of P09 (UHV tank opened).

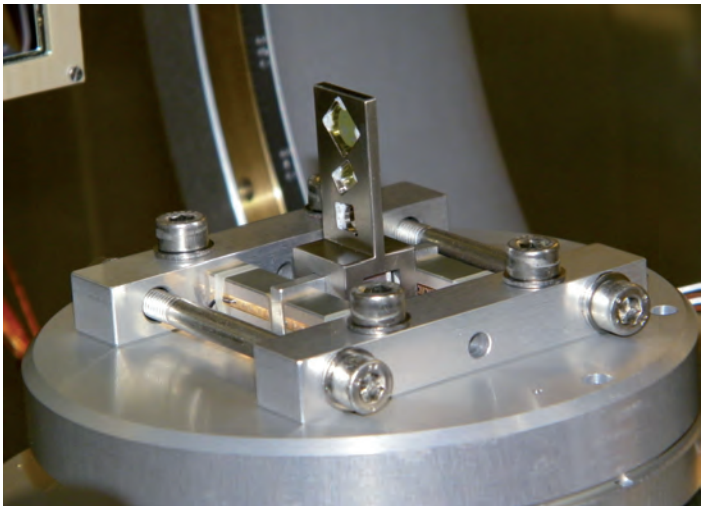

Figure 1b

Diamond plates holder and piezo-actuators underneath.

Currently two identical sets of three type Ib diamond plates are mounted on the two high resolution θ circles. An example of a plate holder is shown in Fig. 1b. The number of crystals per plate holder is limited to 3 due to a travel range of ± 10 mm of the Z translations on the θ stages and due to diamond plate have sizes larger than 4 x 4 mm^2. The top plate is a (100) diamond crystal 400 µm thick; the middle and bottom ones are (111) diamond plates, 200 and 100 µm thick. The crystals were oriented by

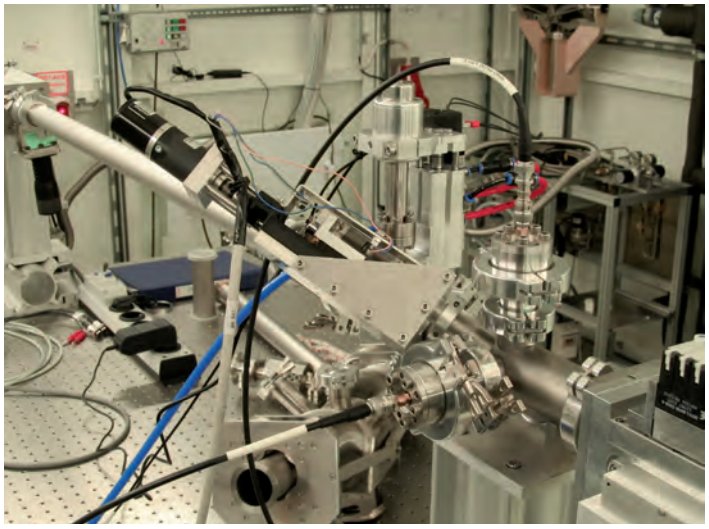

Figure 2

Double beam monitor installed in experimental hutch 1

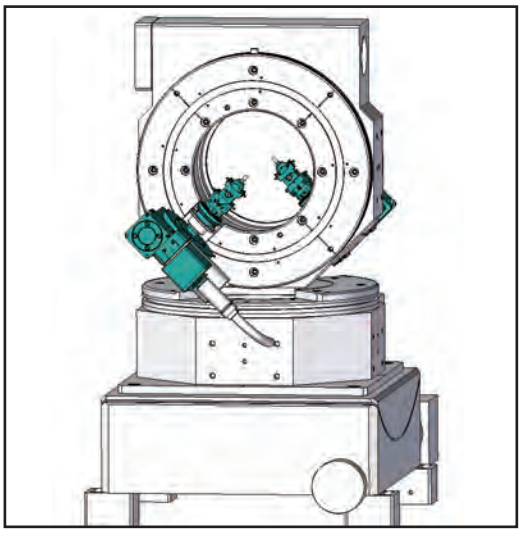

Figure 3

Double phase-retarder set-up foreseen for experimental hutch 1.

back-scattering Laue diffraction and mounted so that the (111), (11-1) and (220) reflections lie in the synchrotron ring plane within ± 2° when $\chi_1 = \chi_2 = 0$. This orientation allows extending the energy range of use for each plate owing to the several possible glancing angles onto the different diffracting planes [5]. The 400 µm plates are used between 6 and 8 keV and the 100 and 200 µm plates between 3 and 5.5 keV.

Commissioning time was dedicated to determine the Bragg angles for the (111) reflections as well as the angular offset for the 1/4 WP condition for the different plates and the different configurations as a function of energy. A good agreement between the experimental points and the expected theoretical curves was achieved [5]. A Tango server was programmed for each phase-retarder allowing to store the detailed information about the alignment of each plate and to compute the θ_1 and θ_2 positions for 1/2, 1/4 or 1/8 WP at any energy. Using the server, the plates can be rotated into position within a few thousandths of a degree without any further time consuming alignment. After positioning, 1/4 WP condition can be refined within 5" using the beam monitor shown in Fig. 2 that is located in EH1. The beam monitor is equipped with glassy carbon foils of different thicknesses that can be translated into the beam. The foils are rotated by 45° both vertically and horizontally. Two PIPS diodes positioned 90° apart are used to monitor the intensities scattered horizontally and vertically within an acceptance angle of about 10°. The 1/4 WP condition is determined by comparison of the intensity in the two PIPS diodes.

The double phase-retarder at P09 has been used successfully in the past four user runs. A major practical application is for linear polarization scans i.e. for the production of linearly polarized incident X-rays rotated by variable angle η about the X-ray beam and analysis of the dependence upon η of the Stokes parameters P_1' and P_2' of the scattered signal from a sample [2]. Using two 1/4 WP in series gives the highest degree of linear polarisation P_{LIN} with > 90 %. However P_{LIN} systematically degrades at values of $\Delta\theta$ lower than 40" and for those configurations requiring low glancing angles onto the crystal plates i.e. higher effective thicknesses [5]. This can be explained as follows: type Ib diamonds have more defects than type IIa diamonds; this combined with the large beam size at P09 at the double phase-retarder set-up location (e.g. 1.4 x 1.1 mm^2 FWHM at 10 keV) and the low glancing angles results into wider rocking curves. Therefore, angular offsets must be kept further away from total Bragg diffraction.

It is foreseen in the long shut-down of 2014 to replace the type Ib diamond plates at P09 with type IIa diamond plates. Polarization control will be further extended to 14 keV using plates of larger thickness and down to 2.7 keV using thin Si [6]. A double phase-retarder has been designed (shown in Fig. 3) that will be located in the 1st experimental hutch. It will operate in air and will be used instead of the double phase-retarder in the optics hutch at energies above 9 keV where X-ray absorption in air is less significant. Finally, a major practical application of the double phase-retarder at P09 is the fast switching between left and right circularly polarized light for the purpose of XMCD experiments. The two θ stages of the double phase-retarder in the optics hutch have been equipped with piezo-actuators operating at 40 Hz. Those piezo-actuators will be commissioned during 2014.

Contact: Sonia Francoual, sonia.francoual@desy.de
Jörg Strempfer, joerg.strempfer@desy.de
David Reuther, david.reuther@desy.de

References

1. K. Okitsu et al., J. Synchrotron Rad. 8, 33-37 (2001) and, Acta Cryst. A. 58, 146-54 (2002).
2. V. Scagnoli et al., J. Synchrotron Rad. 16, 778-787 (2009).
3. J. Lang et al., APS Annual Report (2005) 148-149.
4. C. Giles et al., Nucl. Instrum. Methods A 349, 622-625 (1994).
5. S. Francoual et al., submitted
6. J. Goulon et al., J. Synchrotron Rad. 3, 272 (1996) and L. Bouchenoire et al., Appl. Phys. Lett. 101, 064107 (2012).

More photons for surface scattering.

Optics for studying liquid surfaces with photon energies above 50 keV

For scattering experiments on surfaces the sample is rotated towards the incident beam to scan the angle of incidence. This is not feasible for liquids, since gravity holds the surface parallel to the ground. Here the incident beam has to be rotated with respect to the sample to scan the angle of incidence. The solution for this problem was already found a long time ago employing an additional monochromator [1]:

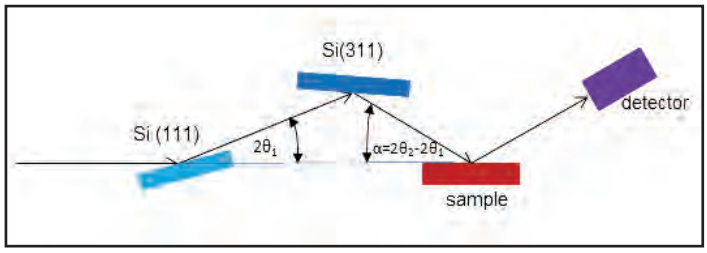

Figure 1

Schematic view of the crystal configuration from the side. χ is at 90°, the maximum incident angle α is reached.

The optics as shown in Fig. 1 consisting of two crystals C1 and C2 with different lattice spacing placed on a common rotation axis χ allows to keep the beam position on the sample while varying the incident angle α of the beam onto a sample surface from 0 to $(2\theta_2 - 2\theta_1)$, where θ_i is the Bragg angle of the crystal Ci:

$$\sin(\alpha) = \sin(\chi)\sin(2\theta_2 - 2\theta_1)$$

The aim is to bring reliably as many photons as possible onto the sample. For scattering on liquids the requirements concerning the angular width of the beam are moderate. It can be easily afforded to use crystals with a broad acceptance comparable to the acceptance of the first monochromator. Therefore, gradient crystals with adaptable angular width and high reflectivity used in Laue geometry are employed at P07 [2].

This crystal configuration could preserve the source properties, if the two crystals are set up non-dispersive and close to each other. It is not the case here, since the first crystal is a composition gradient $Si_{1-x}Ge_x$ (111) and the second a thermal gradient Si (311) crystal. Thus, a broadening of the beam in the diffraction plane of the optics is expected. An additional broadening is expected due to the penetrated crystal thickness $t_{crystal}$.

The beam height t is proportional to the size of the footprint F on the sample surface, which varies with the angle of incidence α:

$$F = \frac{t}{\sin\alpha}$$

Since the beam, and therefore also the beam profile, is rotated by the optics, as shown in Fig. 2, the beam height depends on its rotation angle χ:

$$t = t_h \sin\chi + t_v \cos\chi \rightarrow F = \frac{t_h \sin\chi + t_v \cos\chi}{\sin\chi \sin(2\theta_2 - 2\theta_1)}$$

with t_h the horizontal and t_v the vertical beam width of the beam at $\chi = 0$.

The incident beam is focused at the sample position by compound refractive Al-lenses, placed 4 m in front of the optics, to 2.5 µm x 40 µm in height and width, respectively.

By changing the gradient of the crystals, the angular acceptance can be adapted. For the $Si_{1-x}Ge_x$ gradient crystal with a gradient perpendicular to the incident beam the angular acceptance can be changed by translating the crystal in the beam. The crystal was positioned in the beam for broadest angular acceptance, about two times the angular divergence of the incident beam. In this way, only half of the crystal contributed to the scattering of the incident beam, thus decreasing the effective thickness

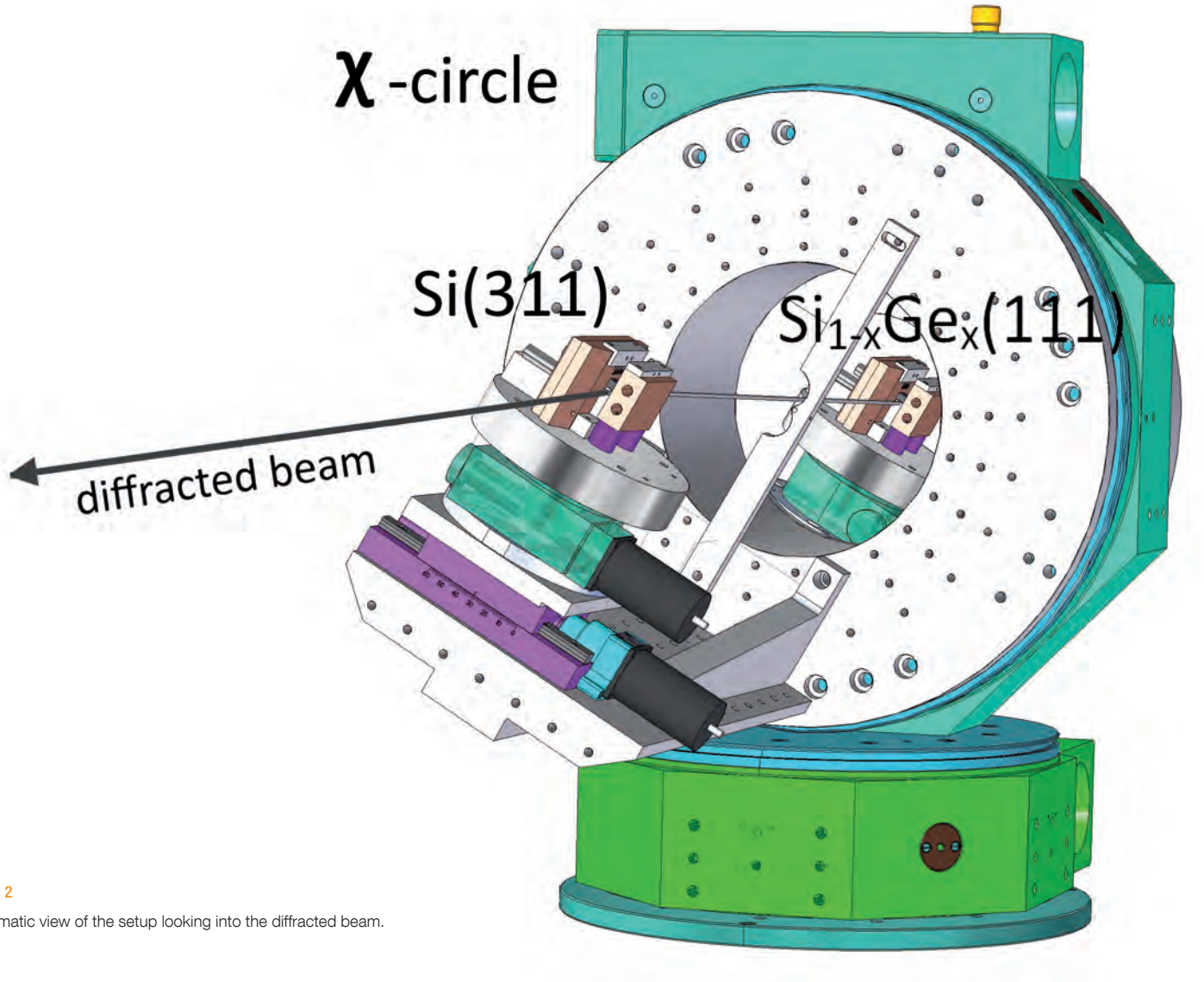

Figure 2

Schematic view of the setup looking into the diffracted beam.

of the crystal. The angular acceptance of the second crystal is tuned to optimize beam width and flux. The latter can be varied by the applied temperature gradient, which is chosen to be 75 K/cm, see Fig. 3. The reflectivity in this case is still higher than 80 % [2].

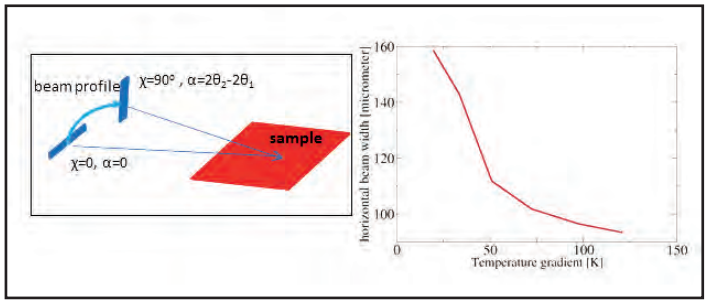

Figure 3

On the left, a sketch of the change of the beam profile with the rotation χ. On the right, the dependence of the horizontal beam width with the temperature gradient on the second crystal.

The sample sizes have usually a minimum size of 10 mm in diameter, therefore the footprint of the beam should be smaller than this value. At $\alpha = 0$, the footprint is infinite. The scattering of interest is at angles larger than the critical angle, which is usually larger than 0.02°. With $t_h = 100$ µm and $t_v = 2.5$ µm, the effective footprint at $\alpha = 0.02°$ is about 9.5 mm.

The overall decrease in flux on the sample due to this optics is a factor of three, but because of the broad acceptance of the crystals, the stability of the beam intensity is better than 1% during the rotation of χ.

Contact: Uta Rütt, uta.ruett@desy.de
Olof Gutowski, olof.gutowski@desy.de
Martin von Zimmermann, martin.v.zimmermann@desy.de

References

1. **V. Honkimaki, H. Reichert, J. S. Okasinski et al. "X-ray optics for liquid surface/interface spectrometers"J. of Syn. Rad., 13 426, (2006).**
2. **U. Rütt, H. Schulte-Schrepping, J. Heuer and M. v. Zimmermann, "Thermal gradient crystals as tuneable monochromator for high energy X-rays", SRI 2009, Conference Proceedings, Vol. 1234, pp. 748 (2010).**

Highly automated sputter equipment (HASE).

A new flexible device to investigate deposition processes with Grazing Incidence X-ray Scattering using synchrotron radiation

In thin-film processing technology, sputter deposition often is a crucial step on the way towards creation of micro- and nano-structures for tailoring devices with desired properties. For better control of sputter deposition and optimization of the deposition parameters, it is necessary to understand the kinetics involved in structure formation in thin films. Today, this is possible with *in situ* X-ray scattering techniques thanks to highly brilliant third generation synchrotron sources like PETRA III. Synchrotron radiation is a powerful tool for *in situ* and real-time measurements of kinetic processes [3,4,5]. In order to use the excellent beam properties of PETRA III beamlines to investigate the growth of thin films during sputter deposition, we designed and constructed a sputter system called Highly Automated Sputter Equipment (HASE) and integrated this instrument into the micro-focus X-ray scattering beamline P03 at PETRA III [1,2].

Central part of HASE is an ultra-high vacuum chamber (see in Fig. 1, Pos.3), which is able to reach a base pressure below 5 x 10^{-8} mbar. Such low pressures are required to protect the sample from contamination. On the other hand, the vacuum system of HASE is also able to provide high-pressure sputtering conditions larger than 10^{-1} mbar if required. To enable the deposition of organic and inorganic materials (metals, alloys, plastics, ceramics), two independent radio frequency (RF) sputter guns are installed on a rotable flange (see Fig.1, Pos.1). This arrangement allows for changing the sputter gun in operation without breaking the vacuum and thus for subsequent depositing different materials on the same substrate (multi-layer). The arrangement also provides adjustment of the sputtering angle in a range from α = 46° to 90° relative to the sample surface (Fig. 1). Thus, different sputter scenarios are feasible, like glancing angle deposition (GLAD) or co-sputtering experiments. During deposition, the temperature of the substrate can be controlled in a range from -20 °C to 200 °C.

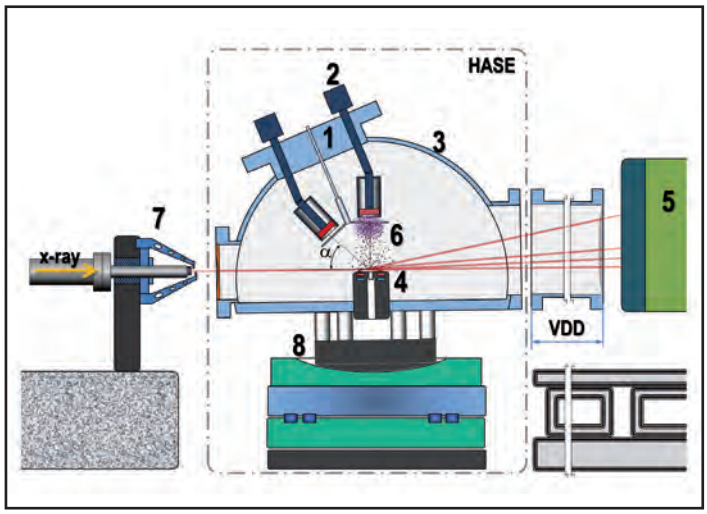

Figure 1

Schematic drawing of the *in situ* GIXS measurements during sputter deposition with: (1) rotatable flange, (2) RF- sputter guns, (3) vacuum deposition chamber, (4) sample stage, (5) X-ray detector, (6) plasma, (7) beam defining slit system, variable distance to detector (VDD) (0.1 m – 10 m), (α) angle for GLAD sputter options (46° – 90°) and (8) sample positioning stage. The components in the marked area belong to the HASE-Device.

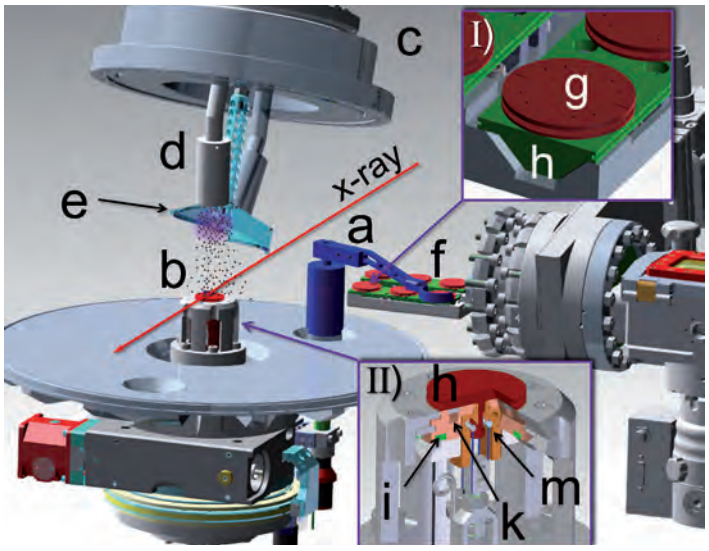

Figure 2

View of the inner parts of the sputter chamber, of the transfer system and of the installed sample change robot with (a) pick- and place robot, (b) sample stage, (c) rotatable flange, (d) sputter guns, (e) automated shutter and (f) transfer arm.
I) Enlarged view of the sample transfer arm with: (g) sample holder, (h) sample carrier.
II) Enlarged view of the sample stage and the patented clamping device with: (h) Sample holder, (i) ceramic heating element, (k) cooling channel and (m) clamping device. The sample stage is mounted on a rotation feed-through which enables a free rotation of ± 180°.

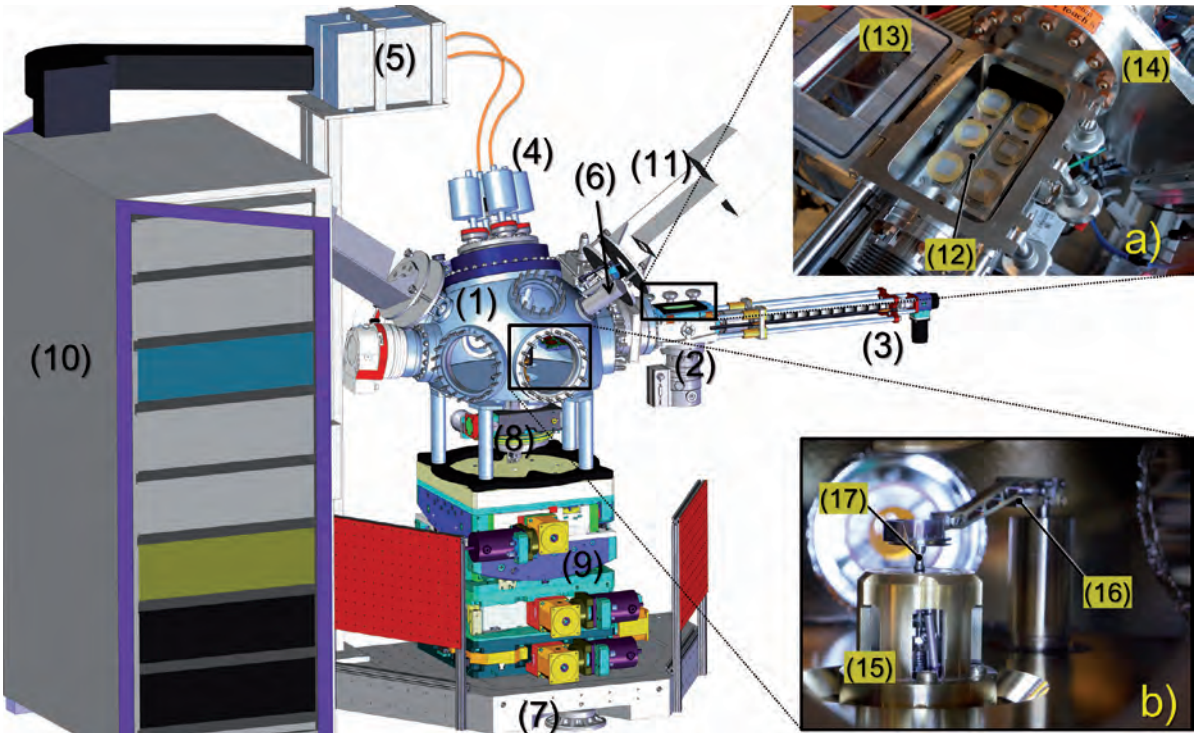

Figure 3

Overview of the highly automated sputter equipment with (1) sputter deposition chamber, (2) transfer chamber with load lock and (3) sample transfer system, (4) sputter guns, (5) power supplies, (6) gas inlet valve, (7) air pads to move the system, (8) sample rotation stage, (9) sample positioning stage and (10) control-electronics rack.

(a) Photograph of the transfer chamber with: (12) transfer arm, (13) load lock and (14) transfer valve.

(b) Photograph of the inner part of the chamber with: (15) sample stage, (16) pick- and paste robot and (17) sample holder. The photograph shows the robot just before setting the sample holder into the sample stage.

The sample stage is positioned in the centre of the sputter chamber. The sample surface is in line with the windows for the incident X-ray beam and the scattered radiation and with the intersection of the plasma cones of the sputter guns (Fig. 1). The sample holder is fixed by a patented clamping device [6], which allows for changing the sample automatically (Fig. 2). Moreover, HASE is equipped with a separate transfer chamber containing the load lock system. This consists of two sample carriers, a gate valve, a motorized sample transfer system, a quick-access door and an observation window. Each sample carrier can be loaded with three sample holders. The transfer system is able to lock in the carriers into the sputter chamber without breaking the vacuum. This enables the HASE system to change the sample with a pick- and place robot within less than 4 minutes.

The control and power electronic components are mounted in a 19” electronic rack and can be moved together with the sputter chamber. This simplifies the transport and the setting up at the beamline (see Fig. 3). The whole system is controlled by a programmable logic controller (PLC), which manages all functions and all input and output channels. A self-developed control program based on TwinCat® handles all logical interconnections, the safety conditions of the vacuum system, the numerical control of the stepper motors and the sample change procedure. Furthermore, the program gates the output power of the sputter sources and triggers the sputtering time. A graphical user Interface (GUI) has access to all functions of the PLC. HASE is an independent, transportable and extendable instrument, which can be operated off-line in the laboratory to deposit thin films and run tests. Furthermore, it allows for an easy integration into a beamline, for example P03, to use grazing incidence X-ray scattering (GIXS) methods to obtain structure information from the surface and near surface regions of the sample during deposition processes [1,2].

HASE has been successfully commissioned. The sample change works smoothly. First *in situ* investigations, using HASE in μ(GI)WAXS, μ(GI)SAXS, and μ(GI)USAXS geometry, have been successfully performed at beamline P03. The modular construction of the sample stage makes the integration of different sample environments possible. A high temperature stage as well as a magnetic field stage is under development. Further developments, like GLAD-Sputter experiments under very small deposition angles (typically of $\alpha = 10°$) and *in situ* imaging ellipsometry are planned.

Contact: Ralph Döhrmann, ralph.doehrmann@desy.de

Authors

R. Döhrmann, S. Botta, A. Buffet, G. Santoro, S.V. Roth
Deutsches Elektronen-Synchrotron DESY, Notkestr. 85, D-22607 Hamburg, Germany

References

1. A. Buffet et al., J. Synchrotron Rad. 19, 647 (2012)
2. S. V. Roth et al., J. Phys: Cond. Matter 23, 254208 (2011)
3. G. Kaune et al., ACS Appl. Mater. Interfaces 3, 1055 (2011)
4. G Kaune et al., ACS Appl. Mater. Interfaces 1, 353 (2009)
5. M. Metwalli et al., Langmuir 24, 4265 (2008)
6. R. Döhrmann, PCT/EP2010/006052 (DESY 2011)

Nanopositioning.

High precision mechanics for nanobeams

The PETRA III storage ring provides a beam with a very low emittance of 1 nmrad. This allows focusing a large number of photons into a spot of only nanometre size. Especially nano-beam applications require extremely stable and precise mechanics. They should ideally enable large travel ranges with single nanometre digit precision and high mechanical stiffness. To achieve nano-positioning of samples and beamline components, we developed for the crystallography endstation at beamline P11 a new approach with nanometre accuracy and high scan speed. In contrast to stepper motors, piezoelectric motors offer significantly higher resolution combined with a small size. For the positioning of samples as well as beamline components, we use in-house developed flexure and linear bearing based positioning stages with piezoelectric motors and optical incremental encoder feedback with up to 0.2 nm resolution (Fig. 2). Closed loop control is achieved with a VME MaxV type motion controller card, which in its turn is controlled via a Tango server. Motors and encoders are also available in UHV compatible versions.

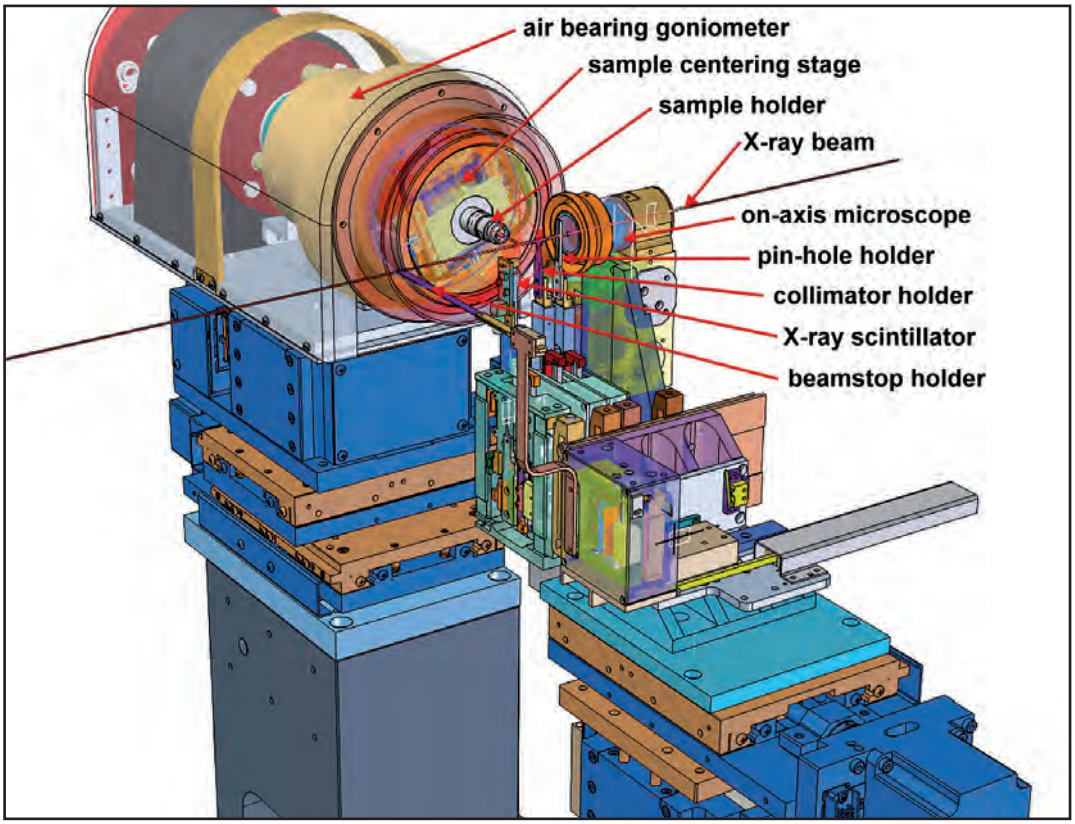

Figure 1

The Crystallography endstation at beamline P11 at PETRA III is equipped with different nanopositioning piezo-stages for crystal centring, the selection of different pinholes, and the movement of the collimator and the beamstop.

The piezo motors are controlled using custom designed driver electronics with linear amplifiers and on-board interpolation (up to 100,000 times). Each driver card controls two motors and features connectors for the motors, limits switches and optical encoders. Up to four cards can be accommodated into a housing, allowing the control of eight motors corresponding to the eight channels of one MaxV card. The backplane is directly connected to the MaxV card with two SCSI connectors. The travel speed is dependent on the stage and the accuracy requirements, and can be varied between 1 µm/s and 2000 µm/s.

Depending on the load, there are several sizes of motors available with a stall force from 6 N to 450 N. The piezo motors are used for different applications at PETRA III.

For positioning of e.g. pinholes, collimators and attenuators, we have developed a compact positioning stage with 30 mm of vertical and 4 mm of horizontal travel range (Fig. 1). A magnetic mount on stage allows an easy exchange of the tools. The same stage, although not specifically designed for this purpose, has been successfully used to carry the optical elements of a

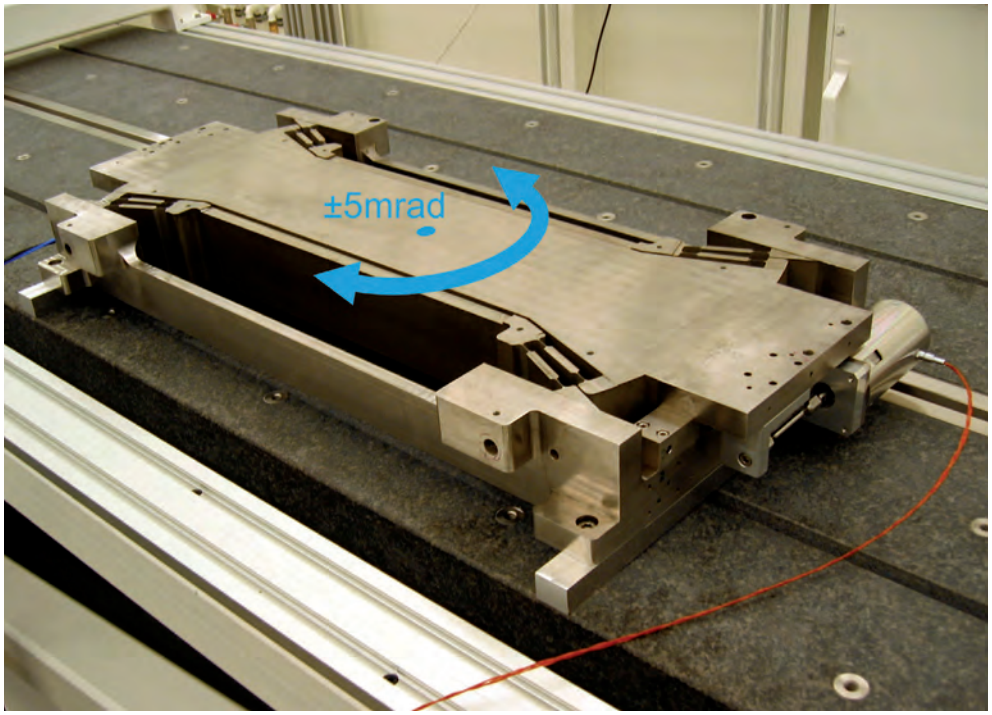

Figure 3

Piezo-motor driven theta rotation stage with a load capacity of 50 kg and an angular precision better than 5 nrad.

full-field microscope which achieved a resolution of 50 nm. This stage can be also used in-vacuum e.g. for the positioning of XBPMs (X-Ray Beam Position Monitors). This eliminates long-term drift of the beam by controlling the reflecting angles of the X-ray mirrors. Other experimental setups at the beamline may require X-ray beam to be moved at the experiment. The accurate in-vacuum positioning stage of the XBPM allows us to steer the beam by moving the XBPM.
For the centring of protein crystals, we have developed a two-axis stage equipped using compact Schneeberger linear bearings. The stage is extremely compact with a height of only 28 mm, diameter of 100 mm and a weight of only 400 g. Each axis is powered by a 20 N strong piezo motor and provides a travel range of 5 mm. The positioning accuracy of this device is a few nanometres.

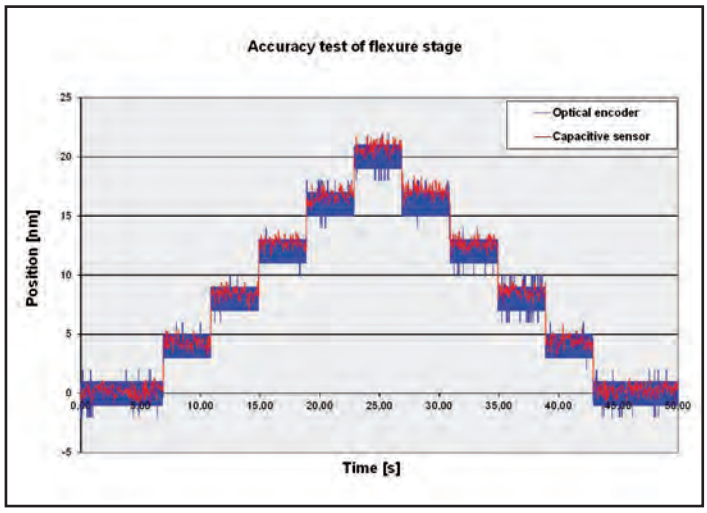

Figure 2

Accuracy of a 2-axis flexure based centring stage for micro-tomography. The signal of the optical encoder used for the feedback is shown in blue. As an independent measure, the signal of a second capacitive sensor is shown in red.

With a distance of 30 metres between the optics hutch and the experiment a precise angular adjustment of the glancing angle is required to control the beam position at the experiment. This angular control of the horizontal mirror under UHV conditions is accomplished using a 800 mm long monolithic flexure based rotation stage with 200 µm thin flexural hinges with a load capacity (mirror and mirror bender) of 50 kg and +/- 5 mrad movement (Fig. 3). The stage is equipped with a larger piezo-electric motor (450 N stall force) with optical encoder feedback and optional capacitive sensor feedback. The capacitive sensor is especially suited for UHV applications due to its extremely low power consumption and high radiation resistance. These optics are now operating for more than one year without interruption and have proven to be extremely reliable, stable and high performing.

With this setup, we have achieved an angular positioning accuracy of better than 5 nrad, this allows to control the beam position in the experimental hutch (30 m away) with sub-micron precision.

Contact: Alke Meents, alke.meents@desy.de

Authors

Pontus Fischer, pontus.fischer@desy,de
Alke Meents, alke.meents@desy.de
Jan Meyer, jan.meyer@desy.de
Tim Pakendorf, tim.pakendorf@desy.de
Bernd Reime, bernd.reime@desy.de
Nicolas Stuebe, nicolas.stuebe@desy,de

Facts and Numbers.

Light source characteristics.

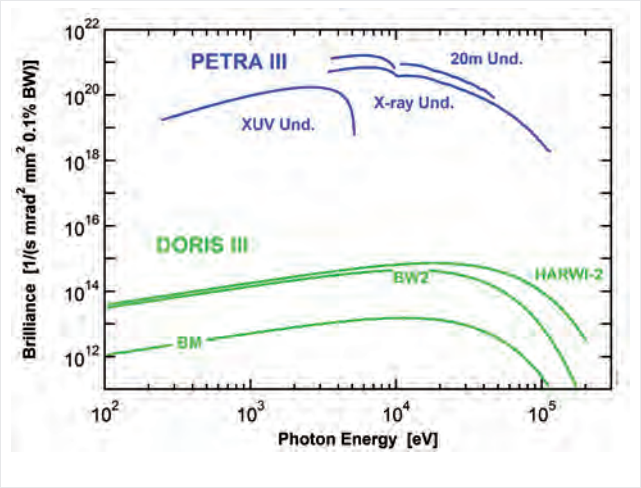

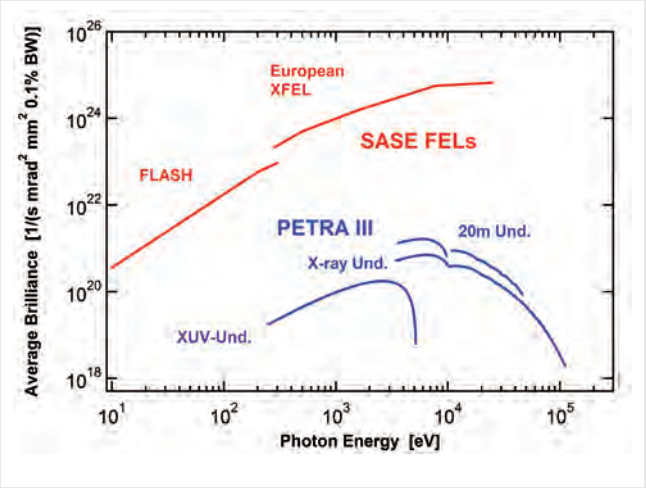

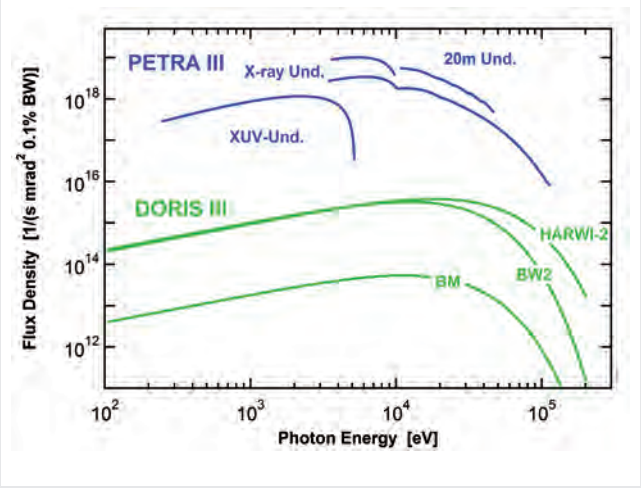

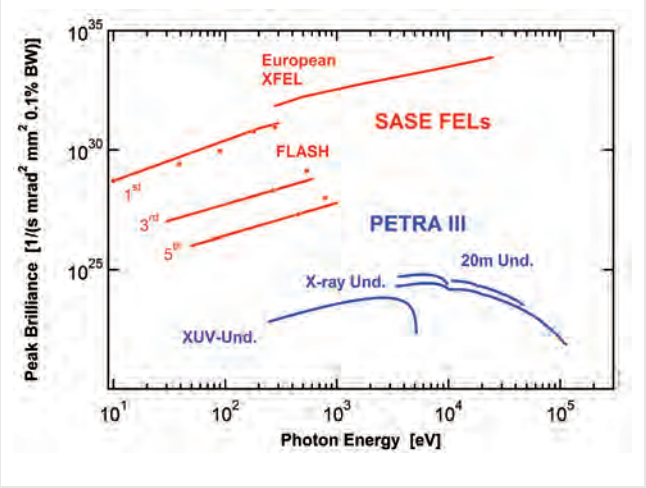

Storage ring sources

Brilliance and Flux Density values are given for machine conditions in the usual user operation mode, i.e. in case of PETRA 1 nm rad horizontal emittance with 1% coupling. In machine shifts, a vertical emittance of 2.5 pm rad can be achieved routinely which corresponds to nearly four times larger brilliance values.

Free-electron laser sources (in comparison with PETRA III)

Peak Brilliance values for European XFEL are given for the optimum bunch charge at each photon energy. Dots correspond to experimentally measured values at FLASH.

Beamtime statistics 2012.

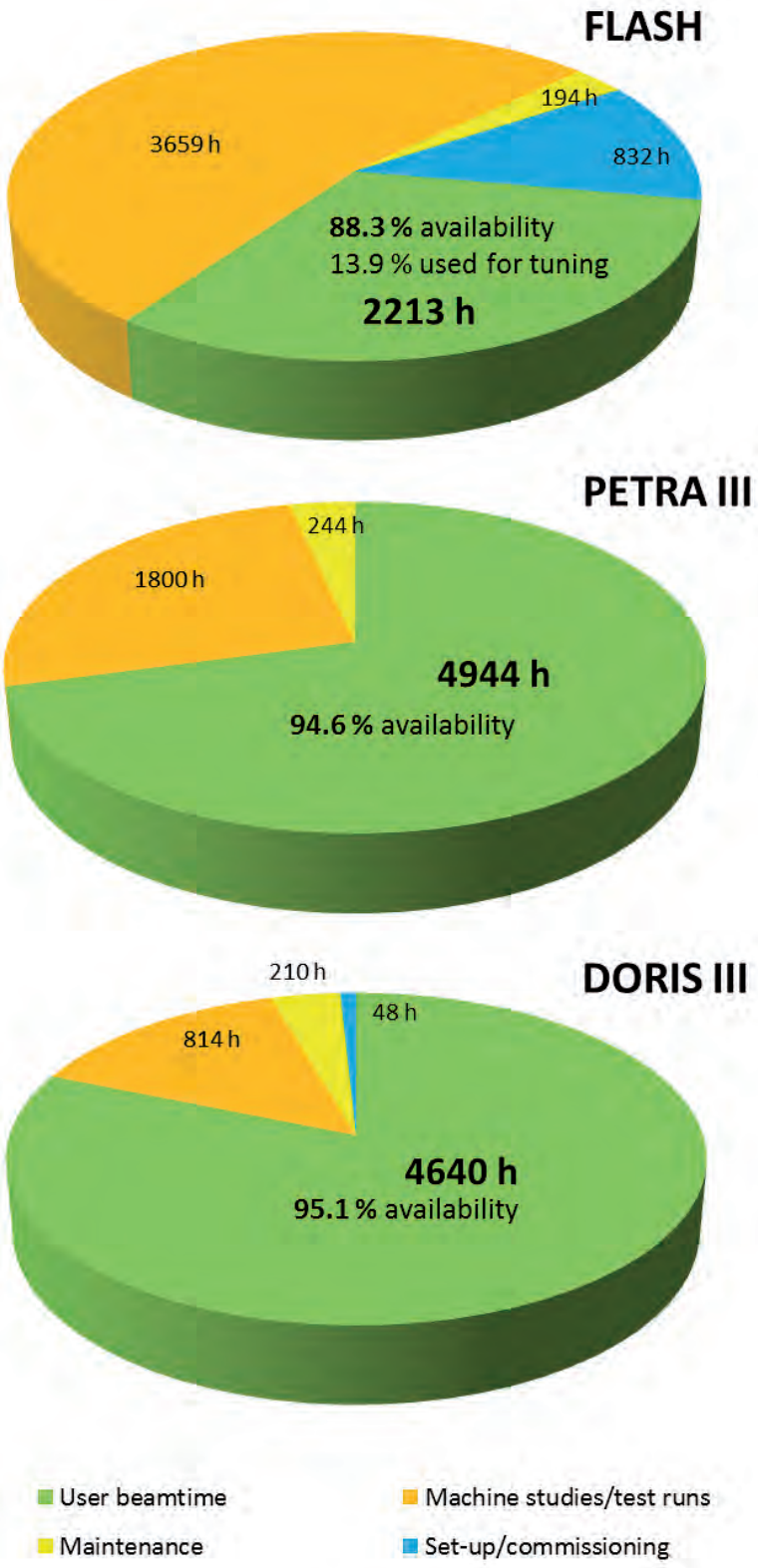

Operation periods 2012

FLASH	2012: 02.01.-06.11.
PETRA III	1/2012: 19.03.-23.07.
	2/2012: 30.07.-18.12.
DORIS III	1/2012: 27.02.-23.07.
	2/2011: 30.07.-22.10.

FLASH.

Beamlines and parameters

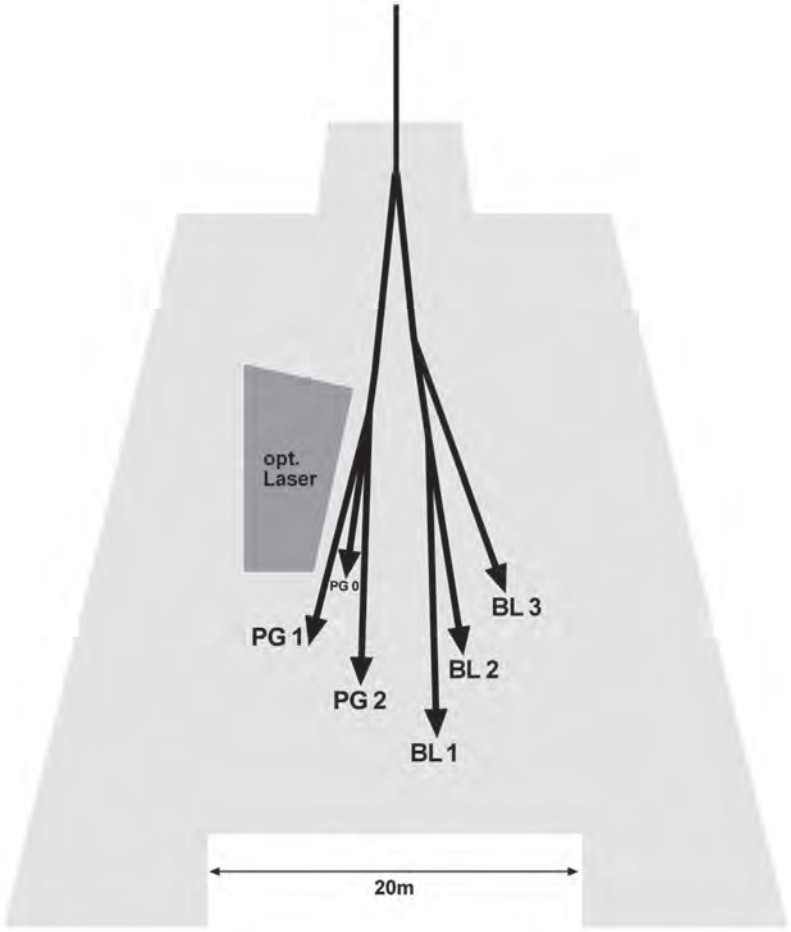

Machine parameters FLASH

Electron energy (max.)	1.25 GeV
Length of the facility	315 m
Normalized emittance	1.5 mm mrad (rms)
Emittance	0.6 nm rad (rms)
Bunch charge	0.1 – 1 nC
Peak current	1 – 2 kA
Bunches per second (typ. and max.)	300 and 6000

Lasing parameters

Photon energy (max.)	301 eV (fundamental)
Wavelength (min.)	4.12 nm (fundamental)
Pulse duration (FWHM)	50 – 200 fs
Peak power	1 – 3 GW
Bunch energy (average)	up to 500 μJ
Photons per bunch	$10^{11} – 10^{13}$
Average brilliance	$10^{17} – 10^{21}$ photons/sec/mm^2/mrad^2/0.1%
Peak brilliance	$10^{29} – 10^{31}$ photons/sec/mm^2/mrad^2/0.1%

FLASH beamlines and user instruments
(including instrumentation provided by university groups and funded by the BMBF „Verbundforschung“)

BL1

Focused FEL beam, 100 µm spot size	DESY
Instrumentation for the preparation of and electron and ion spectroscopy on mass-selected clusters	U Rostock
Pump-probe setup for the study of transient response of melting/ablating solids	U Duisburg-Essen
Setup for resonant soft X-ray scattering	CFEL U Oxford
Experimental system for the spectroscopic study of molecular desorption from surfaces of solids	U Münster
Single-shot cross-correlator	U Hamburg

BL2

Focused FEL beam, 20 µm spot size or unfocused beam	DESY
Instrumentation for two-colour pump probe experiments of atoms and molecules	DESY DCU Dublin European XFEL
Reaction microscope for the study of multiple ionization processes of atoms and molecules	MPI-K Heidelberg
Velocity map imaging spectrometer (electrons and ions) for atoms and molecules in strong fields	MBI Berlin AMOLF Amsterdam
Setup for angle-resolved photoelectron spectroscopy (ARPES) of atoms and molecules	FHI Berlin
Station for spectroscopy of rare gas clusters and nanoparticles	TU Berlin
Single-shot single-particle (time-resolved) diffraction imaging of nanostructures and biological samples	CFEL DESY LLNL Livermore U Uppsala
Setup for Thomson scattering spectroscopy to probe plasma dynamics in a liquid hydrogen jet	DESY LLNL Livermore U Oxford U Rostock
Instrumentation for measuring damage thresholds and optical properties of solid samples	ASCR Prague DESY IFPAS Warsaw LLNL Livermore
Setup for electron and ion spectroscopy to study multi-photon processes in gases	DESY PTB Berlin U Hamburg
XUV beam splitter with variable delay for photon diagnostics and time-resolved experiments (permanent installation)	DESY HZB U Münster
Magnetic X-ray diffraction imaging and holography	DESY HZB TU Berlin

FLASH beamlines and user instruments

BL3		
	Focused FEL beam, 20 µm spot size or unfocused beam + THz undulator radiation	DESY
	Magneto-optical trap & reaction microscope to study ultra-cold plasmas	MPI-K Heidelberg
	Setup with multilayer optics for sub-micron focusing to create and study plasmas and warm dense matter	U Belfast CFEL DESY U Oxford
	System for angle-resolved photoelectron spectroscopy (ARPES) and ion spectroscopy of metal vapors	DESY U Hamburg
	Microfocus setup for spectrometry of multi-photon processes in rare gases at extreme power densities	DESY PTB Berlin
	Split multilayer-mirror & reaction microscope for time-resolved spectroscopy of small molecules	MPI-K Heidelberg
	Microfocus setup for time-resolved imaging of rare gas clusters	TU Berlin
	Experimental station for pump-probe experiments combining μJ-level, few-cycle THz and XUV FEL pulses	DESY U Hamburg
	THz pump X-ray photo-emission probe (Mott-Detector) setup for magnetic measurements	CFEL DESY U Hamburg HZB
	Molecular beam setup to study femtochemistry via pump-probe photoelectron-spectroscopy	DESY HZB CFEL FU Berlin
PG1		
	Plane grating monochromator, microfocus (5 µm spot size)	DESY, U Hamburg
	High-resolution two-stage spectrometer for inelastic (Raman) scattering (permanent installation)	DESY U Hamburg
PG2		
	Plane grating monochromator (50 µm focus)	DESY, U Hamburg
	Setup for resonant inelastic X-ray scattering (RIXS) and photoelectron spectroscopy of solids	U Hamburg
	Electron beam ion trap (EBIT) for high-resolution spectroscopy of highly charged ions	MPI-K Heidelberg
	Ion source and trap for spectroscopic studies of the photo-fragmentation of molecular ions and radicals (permanent installation)	U Aarhus MPI-K Heidelberg
	System for angle-resolved photoelectron spectroscopy (ARPES) of solids and surfaces	U Kiel
	Setup for the study of fs-dynamics of magnetic materials	U Hamburg HZB
	XUV beamsplitter with variable delay for time resolved experiments (permanent installation)	U Hamburg
	Soft X-ray diffraction imaging system for magnetic materials and nanostructures	DESY U Hamburg U Heidelberg HZB FH Koblenz
	Spin-polarized photo-emission (Mott-Detector) chamber for the investigation of laser induced ultrafast demagnetization processes	ETH Zürich HZB DESY U Hamburg SLAC

Note: instruments are non-permanent installations unless noted otherwise

PETRA III.

Beamlines and parameters

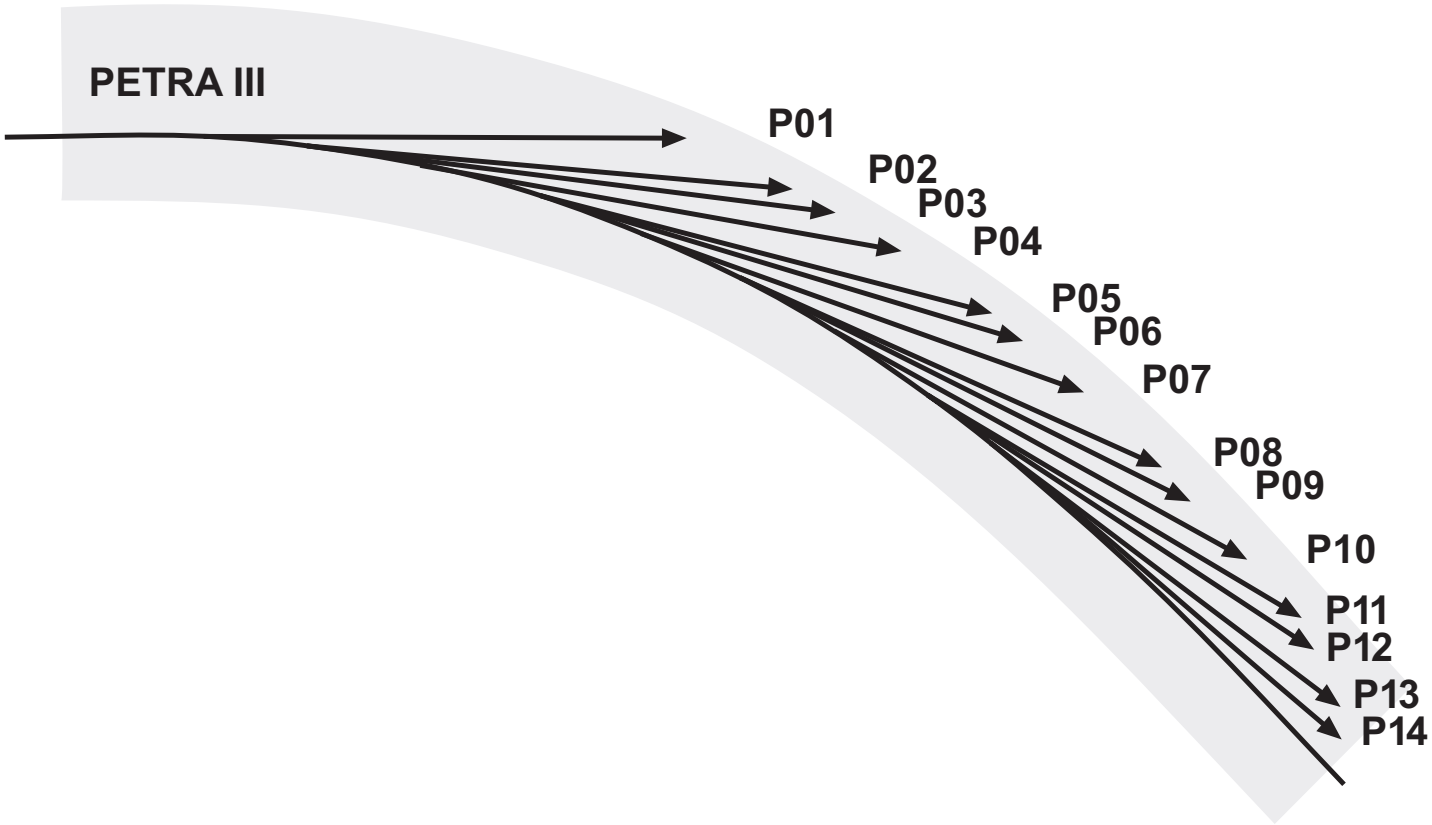

Machine parameters PETRA III

Positron energy	6.08 GeV
Circumference of the storage ring	2304 m
Number of buckets	3840
Number of bunches	320, 240, 60, and 40
Bunch separation	24 ns, 32 ns, 128 ns, and 192 ns
Positron beam current	100 (80) mA (top-up)
Horizontal positron beam emittance	1.0 nmrad (rms)
Coupling factor	0.7%
Vertical positron beam emittance	0.007 nmrad (rms)
Positron beam energy spread	0.1% (rms)
Horizontal x vertical beam size at 5 m undulator (high β section)	141.5 x 4.9 μm
Horizontal x vertical beam size at 5 m undulator (low β section)	34.6 x 6.3 μm

PETRA III beamlines and instruments
(including instrumentation provided by university groups and funded by the BMBF „Verbundforschung“)

P01 Inelastic and Nuclear Resonant Scattering			
	10 m undulator (U32), high-ß		
	Hutch1 Nuclear resonant scattering setup Nuclear lighthouse effect spectrometer	6 – 40 keV	DESY
	Hutch2 Spectrometer for inelastic scattering with nanobeam	6 – 40 keV	DESY, TU Dortmund
	Hutch3 Nuclear resonant scattering with special sample environments: Extreme conditions and UHV	6 – 40 keV	DESY TU Kaisersl.
P02 Hard X-Ray Diffraction			
	2 m undulator (U23), high-ß		
	Hutch1 Powder diffraction side station High-resolution powder diffractometer	60 keV	DESY TU Dresden
	Hutch2 Station for diffraction experiments under extreme conditions (high p, high T) Laser heating for the extreme conditions station	8 – 100 keV	DESY U Frankfurt
P03 Micro- and Nanobeam Wide and Small Angle X-ray Scattering (MINAXS)			
	2 m undulator (U29), high-ß		
	Hutch1 General Purpose µSAXS/WAXS station Setup for in-situ deposition experiments, AFM µGISAXS option with ellipsometer	8 – 23 keV	DESY U Hamburg TU München
	Hutch2 Setup for nanobeam Scanning-Experiments (SAXS/WAXS, GISAXS) Nanofocus endstation including in-situ deformation experiments	8 – 23 keV	DESY U Kiel
P04 Variable Polarization Soft X-rays			
	5 m APPLE undulator (UE65), high-ß		DESY
	UHV-diffractometer for elastic and inelastic resonant XUV scattering	0.2 - 3.0 keV	U Köln
	Ultra-high resolution XUV photoelectron spectrometer for in-situ real-time investigation of dynamic processes in nano structures	0.2 - 3.0 keV	U Kiel U Würzburg
	PIPE: instrument for flexible two-beam experiments to investigate mass selected ions (atoms to nano particles) with photons	0.2 - 3.0 keV	U Giessen U Hamburg FU Berlin U Frankfurt
	Soft X-ray absorption spectrometer with variable polarization at 30 mK	0.2 - 3.0 keV	U Hamburg U München
	Nano focus apparatus for spatial and time resolving spectroscopy	0.2 - 3.0 keV	U Hamburg FH Koblenz
P05 Imaging beamline			
	2 m undulator (U29), low-ß		
	Hutch1 Micro tomography setup for absorption, phase enhanced and phase contrast tomography	5 – 50 keV	HZG
	Hutch2 Nano tomography instrument combining hard X-ray microscopy and tomography	5 – 50 keV	HZG
P06 Hard X-ray Micro/Nano-Probe			
	2 m undulator (U32), low-ß		
	Hutch1 Instrument for imaging at (sub-)micrometer spatial resolution applying X-ray fluorescence, X-ray absorption and X-ray diffraction techniques	2.4 - 100 keV	DESY
	Hutch2 Instrument for imaging by coherent X-ray diffraction and X-ray fluorescence with nanoscopic resolution	5 – 50 keV	DESY KIT Karlsruhe TU Dresden

P07 High Energy Materials Science (HEMS)		
2 m undulator (U29), high/low-ß		
Hutch1 Test facility	53 / 87 keV (fixed)	HZG
Hutch2 Multi purpose diffractometer for bulk and interfaces	50 – 250 keV	DESY
Hutch3 Heavy-load (1t) diffractometer	50 – 250 keV	HZG
Hutch4 3D-XRD strain and stress mapper instrument for microtomography	50 – 250 keV	HZG
P08 High-resolution diffraction		
2 m undulator (U29), high-ß		
Hutch1 High-resolution diffractometer X-ray diffractometer for liquid interfaces studies	5.4 – 30 keV	DESY U Kiel
P09 Resonant scattering / diffraction		
2 m undulator (U32), high-ß		
Hutch1 High precision diffractometer for resonant scattering and diffraction	2.4 – 50 keV	DESY
Hutch2 Heavy load diffractometer for resonant scattering and diffraction, high magnetic fields	2.4 – 50 keV	DESY
Hutch3 High-resolution hard X-ray photoelectron spectroscopy instrument	2.4 – 15 keV	DESY U Mainz U Würzburg
P10 Coherence applications		
5 m undulator (U29), low-ß		
Hutch1 USAXS setup for coherent diffraction imaging (CDI) and X-ray photon correlation spectroscopy (XPCS) Instrument for XPCS and CDI at large angles (6-circle diffractometer) Rheology setup	4 – 25 keV	DESY
Hutch2 Instrument for XPCS and CDI in SAXS and wide angle geometry (horizontal scattering geometry) CDI setup for propagation imaging techniques	4 – 25 keV	DESY U Göttingen
P11 Biological imaging / diffraction		
2 m undulator (U32), high-ß		
Single-axis diffractometer for macromolecular crystallography Setup for imaging of biological systems	6 – 33 keV 3 – 12 keV	HZI/DESY MPG
P12 Biological small-angle X-ray scattering		
2 m undulator (U29), high-ß		
Instrument for biological SAXS on protein solutions and time resolved experiments, biomembrane related and soft matter research, tunable sample-detector distance	4 – 20 keV	EMBL HZG U Freiburg
P13 Macro molecular crystallography I		
2 m undulator (U29), high-ß		
Instrument for highly collimated beams and variable focus size, in crystallo spectroscopies	4 – 17 keV	EMBL
P14 Macro molecular crystallography II		
2 m undulator (U29), high-ß		
Protein micro-crystallography instrument	7 – 35 keV	EMBL

Note: for each undulator, high-ß and low-ß operation can be chosen freely.

DORIS III.

Beamlines and parameters

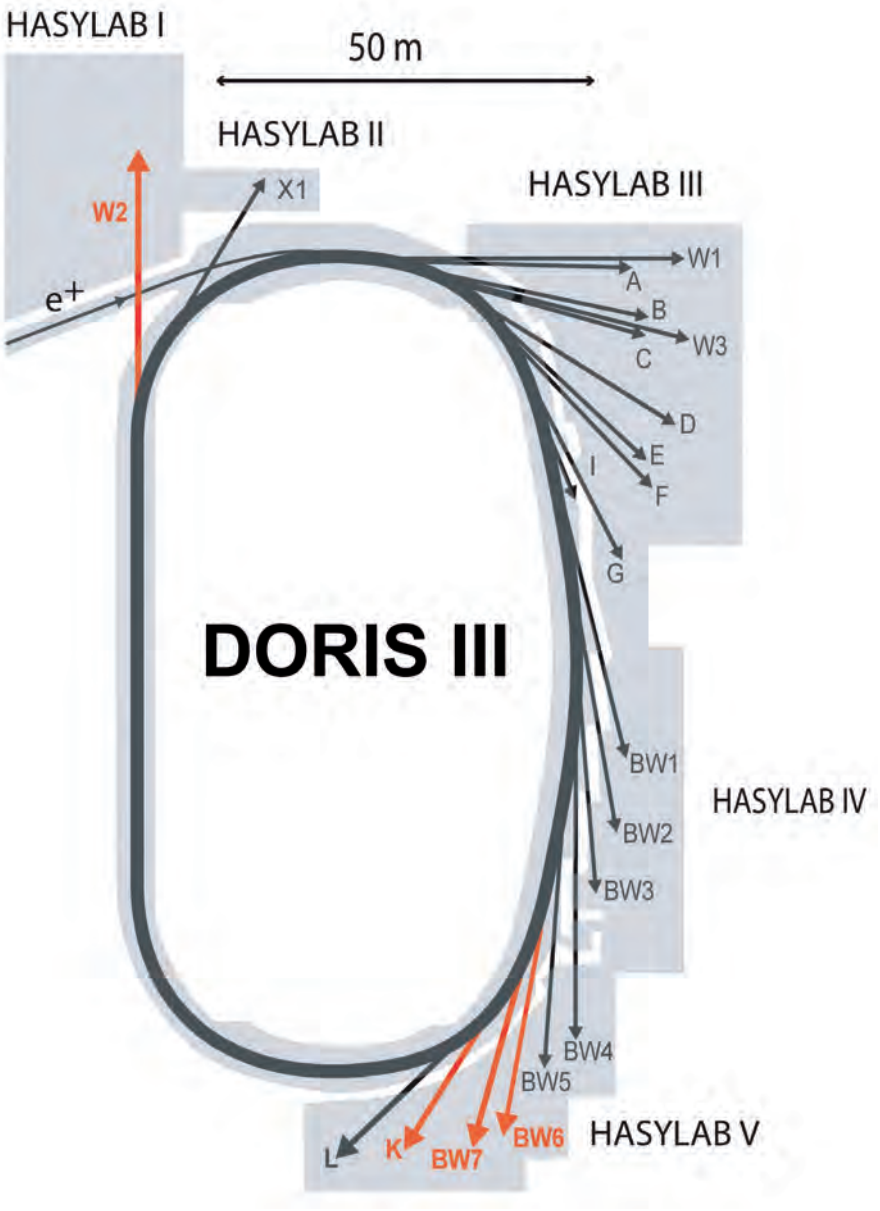

Machine parameters DORIS III

Positron energy	4.45 GeV
Circumference of the storage ring	289.2 m
Number of buckets	482
Number of bunches	1 (for tests), 2, and 5
Bunch separation (minimum)	964 ns (for tests), 480 ns, and 192 ns
Positron beam current	140 mA (5 bunches)
Horizontal positron beam emittance	410 nmrad (rms)
Coupling factor	3%
Vertical positron beam emittance	12 nmrad (rms)
Positron beam energy spread	0.11% (rms)
Curvature radius of bending magnets	12.18 m
Magnetic field of bending magnets	1.218 T
Critical photon energy from bending magnets	16.0 keV

DORIS III beamlines and instruments

A1 X-ray absorption spectroscopy		
Bending magnet (Ec = 16 keV)		
Instrument for in-situ XAFS including fast energy scanning	2.4 – 8 keV	DESY
A2 Small-angle X-ray scattering		
Bending magnet (Ec = 16 keV)		
Multi setup instrument for (simultaneous) small and wide angle scattering from soft matter samples	8 keV	DESY
B1 Anomalous small-angle X-ray scattering		
Bending magnet (Ec = 16 keV)		
Instrument for anomalous scattering (ASAXS)	5 – 35 keV	DESY
B2 X-ray powder diffraction		
Bending magnet (Ec = 16 keV)		
Heavy duty diffractometer including special setups for in-situ studies	5 – 44 keV	DESY
BW1 X-ray diffraction / scattering		
4 m X-ray undulator		
Horizontal diffractometer for liquid surface scattering	9.5 keV	DESY
UHV instrument for surface diffraction / standing waves including MBE sample preparation	2.4 – 12 keV	DESY U Bremen
Multi purpose heavy load 8-circle diffractometer	5 – 18 keV	DESY
Rheometer	9.9 keV	DESY
BW2 X-ray spectroscopy / diffraction / tomography		
4 m X-ray wiggler (Ec = 15.4 keV)		
UHV instrument for hard X-ray photoelectron spectroscopy	2.4 – 10 keV	DESY
X-ray micro-tomography setup	6 – 24 keV	HZG
Heavy load vertical diffractometer with CCD detector arm for grazing incidence diffraction	5 – 11 keV	DESY
BW3 Soft X-ray spectroscopy		
4 m XUV (double) undulator		
High-resolution SX-700 plane grating monochromator, beam port for user supplied instruments	50 – 1500 eV	DESY
BW4 Ultra small-angle X-ray scattering		
2.7 m X-ray wiggler (Ec = 15.4 keV)		
Flexible instrument for (ultra) small angle (grazing incidence) scattering experiments	6 – 14 keV	DESY
BW5 High-energy X-ray diffraction		
4 m X-ray wiggler (Ec = 26 keV)		
Triple axis diffractometer in horizontal Laue scattering geometry including high magnetic field (10 T) sample environment	60 – 250 keV	DESY

DORIS III beamlines and instruments

BW7A Macromolecular crystallography		
4 m X-ray wiggler (Ec = 15.4 keV)		
Crystallographic end-station with CCD detector, double multilayer optics, optimized for high-flux fast data collection	12.8 keV	EMBL
BW7B Macromolecular crystallography		
4 m X-ray wiggler (Ec = 15.4 keV)		
Crystallographic end-station with CCD detector, new high-precision Phi spindle, EMBL Hamburg robotic sample changer (MARVIN)	14.7 keV	EMBL
C X-ray absorption spectroscopy / diffraction		
Bending magnet (Ec = 16 keV)		
Setup for high-energy XAFS in-situ studies including fast energy scanning	5 – 44 keV	DESY
Vertical diffractometer for grazing incidence X-ray diffraction	5 – 44 keV	DESY
D1 (X33) Small-angle X-ray scattering		
Bending magnet (Ec = 16 keV)		
Instrument optimized for automated solution scattering studies of biological macromolecules	8 keV	EMBL
D3 Chemical crystallography		
Bending magnet (Ec = 16 keV)		
4-circle diffractometer	8 – 50 keV	DESY
D4 Grazing incidence X-ray scattering		
Bending magnet (Ec = 16 keV)		
2-circle diffractometer, horizontal scattering plane	5 – 20 keV	DESY
E1 (Flipper2) Soft X-ray spectroscopy		
Bending magnet (Ec = 16 keV)		
UHV instrument for soft X-ray photoelectron spectroscopy	10 – 150 eV	U Hamburg
E2 X-ray reflectometry / grazing incidence diffraction		
Bending magnet (Ec = 16 keV)		
6-circle diffractometer for reflectometry & high-resolution diffraction	4 – 35 keV	DESY / RWTH Aachen
F1 Chemical crystallography		
Bending magnet (Ec = 16 keV)		
Kappa-diffractometer for low/high-temperature / high-pressure single-crystal diffraction	5 – 41 keV white beam	U Hamburg
F2 X-ray diffraction / VUV spectroscopy		
Bending magnet (Ec = 16 keV)		
Hutch1 MAX80 Multi-Anvil-X-ray apparatus for high pressure X-ray diffraction	5 – 80 keV white beam	GFZ
Hutch2 UHV instrument for angle-resolved UV photoelectron spectroscopy	5 – 41 eV	U Hamburg
F3 Energy dispersive scattering		
Bending magnet (Ec = 16 keV)		
Horizontal diffractometer with heavy load sample stage	white beam	DESY U Kiel

F4 X-ray test beam		
Bending magnet (Ec = 16 keV)		
Used for detector characterization		DESY
G3 Diffraction X-ray imaging		
Bending magnet (Ec = 16 keV)		
4-circle diffractometer for position resolved diffraction	5.4 – 26 keV	DESY
I Superlumi) UV luminescence spectroscopy		
Bending magnet (Ec = 16 keV)		
Superlumi setup for luminescence analysis	3 – 40 eV	DESY
K1.1 (X11) Macromolecular crystallography		
Bending magnet (Ec = 16 keV)		
Crystallographic end-station with large surface area flat panel detector, cryoshutter, single horizontal axis of rotation	15.3 keV	EMBL
K1.2 (X12) Macromolecular crystallography		
Bending magnet (Ec = 16 keV)		
Crystallographic end-station with CCD and fluorescence detector, single axis of rotation, opt. for MAD and SAD	6 – 18 keV	EMBL
K1.3 (X13) Macromolecular crystallography		
Bending magnet (Ec = 16 keV)		
Crystallographic end-station with CCD detector, cryoshutter, micro-spectrophotometer, single horizontal axis of rotation, optimised for automated expert data collection	15.3 keV	EMBL
L X-ray micro probe		
Bending magnet (Ec = 16 keV)		
X-ray microprobe combining fluorescence analysis, absorption spectroscopy and diffraction	5 – 80 keV white beam	DESY
W1 X-ray spectoscopy / diffraction		
2 m X-ray wiggler (Ec = 8 keV)		
High-resolution fluorescence in vacuo spectrometer	4 – 11.5 keV	DESY
Heavy load diffractometer for grazing incidence diffraction in vertical or horizontal scattering geometry	4 – 11.5 keV	DESY
W2 (HARWI II) High-energy X-ray engineering materials science		
4 m X-ray wiggler (Ec = 26 keV)		
Hutch1 Materials Science Diffractometer (heavy load up to 600 kg) Micro-tomography setup (attenuation and phase contrast) Diffraction-tomography “DITO” instrument	60 – 250 keV 20 – 250 keV 20 – 150 keV	HZG HZG TU Dresden TU Berlin
Hutch2 MAX200x Multi-Anvil X-ray apparatus for high pressure and temperature conditions	white beam	GFZ
X1 X-ray absorption spectroscopy		
Bending magnet (Ec = 16 keV)		
Setup for high-energy fast-scanning XAFS for in-situ studies including chemistry lab	7 – 100 keV	DESY

Committees 2012.

Photon Science Committee PSC – advises the photon science management	
Colin Norris (chair until May 2012)	Diamond, CCLRC, UK
Simone Techert (vice chair until October 2012)	Max-Planck-Institut Göttingen, D
Melissa A. Denecke (vice chair since October 2012)	Karlsruhe Institute of Technology KIT, D
Markus Drescher (chair since October 2012)	Universität Hamburg, D
Michael Fröba (until October 2012)	Universität Hamburg, D
Roland Horisberger (until May 2012)	Paul-Scherrer-Institut, Villigen, CH
Koen Janssens (until May 2012)	University of Antwerp, B
Chi-Chang Kao	SSRL, SLAC, USA
Maya Kiskinova (since October 2012)	Sincrotrone Trieste, I
Franz Pfeiffer	Technische Universität München, D
Harald Reichert	ESRF, Grenoble, F
Jean-Pierre Samama	Synchrotron Soleil, F
Bernd Schmitt (since October 2012)	Paul-Scherrer-Institut, Villigen, CH
Philip J. Withers (until October 2012)	University of Manchester, UK
Lucia Incoccia-Hermes (PSC secretary)	DESY, Hamburg, D

Laser Advisory Committee LAC (shared between DESY and the European XFEL)	
Uwe Morgner (Chair)	Universität Hannover, D
Giulio Cerullo	Politecnico di Milano, I
Patrick Georges	CNRS, F
Alfred Leitenstorfer	Universität Konstanz, D
Robert Schoenlein	LBL, USA
William E. White	SLAC, USA

PRP1: VUV- and Soft X-Ray	
Jens Viefhaus (PRP Secretary)	DESY, Hamburg, D
Michael Meyer	European XFEL, Hamburg, D
Luc Patthey	PSI Villigen, CH
PRP2: X-Ray Spectroscopy	
Wolfgang Drube (PRP secretary)	DESY, Hamburg, D
Johannes Hendrik Bitter	Utrecht University, NL
Melissa A. Denecke	Karlsruhe Institute of Technology KIT, D
Thorsten Ressler	Technische Universität Berlin, D
Christina Streli	Technische Universität Wien, A
PRP3: X-Ray Diffraction/Scattering – Hard Condensed Matter	
Hermann Franz (PRP secretary)	DESY, Hamburg, D
Denis Andrault	University of Clermont-Ferrand, F
Lars Ehm	Stony Brook University, Stony Brook, NY, USA
Peter Hatton	University of Durham, UK
Helmut Klein	Universität Göttingen, D
Christian Kumpf	Karlsruhe Institute of Technology KIT, D
Ulrich Schwarz	MPG Dresden, D
Sergio Speziale	GFZ Potsdam, D

PRP4: X-Ray Diffraction/Scattering – Engineering Materials Science	
Martin Müller (PRP secretary)	HZG, D
Ralf Röhlsberger (DESY representative)	DESY, Hamburg, D
Walter Reimers	Technische Universität Berlin, D
Guilliermo Requena	Technische Universtität Wien, A
Jozef Keckes	Montanuniversität Leoben, A
Gerold Schneider	Technische Universität Hamburg-Harburg, D
Bernd Schönfeld	ETH Zürich, CH
PRP5: X-Ray Diffraction/Scattering – Soft Materials, Bulk	
Rainer Gehrke (PRP secretary)	DESY, Hamburg, D
Wim de Jeu	University of Massachusetts, Amherst, USA
Jochen S. Gutmann	Universität Mainz, D
Uwe Klemradt	RWTH Aachen, D
Beate Klösgen	University of Southern Denmark, DK
Yongfeng Men	Changchun Inst. of Applied Chemistry, CN
Christine M. Papadakis	Technische Universität München, D
Joachim Wagner	Universität Rostock, D
PRP6: X-Ray Diffraction/Scattering – Soft Materials, Surfaces and Interfaces	
Oliver Seeck (PRP Secretary)	DESY, Hamburg, D
Hyunjung Kim	Sogang University, Seoul, Korea
Moshe Deutsch	Bar-Ilan University, Ramat Gan, Israel
Thomas Gutsmann	Leibniz-Zentrum Borstel, D
Gerald Brezesinski	MPG, Potsdam, D
Mark Schlossmann	University of Illinois, Chicago IL, USA
PRP7: Imaging	
Karen Appel (PRP secretary)	DESY, Hamburg, D
Felix Beckmann	HZG, Geesthacht, D
Peter Cloetens	ESRF, Grenoble, F
Bert Müller	University Basel, CH
Michael Nickel	Friedrich-Schiller-Universität Jena, D
Stefan Vogt	APS, Argonne, USA
PRP8: Methods and Instrumentation	
Horst Schulte-Schrepping (PRP secretary)	DESY, Hamburg, D
Kawal Sawhney	Diamond Light Source, UK
Frank Siewert	HZB, Berlin, D
Anatoly Snigirev	ESRF, Grenoble, F
PRP11: Soft X-Ray – FEL Experiments (FLASH)	
Josef Feldhaus (PRP secretary)	DESY Hamburg, D
Massimo Altarelli	European XFEL, Hamburg, D
Chris Jacobsen	APS, Argonne, USA
Steven Johnson	ETH Zürich, CH
Maya Kiskinova	Sincrotrone Trieste, I
Jonathan Marangos	Imperial College London, UK
Ronald Redmer	Universität Rostock, D
Jan-Michael Rost	MPI, Dresden, D
Bernd Sonntag	Universität Hamburg, D
Urs Staub	PSI, Villigen, CH
Kiyoshi Ueda	Tohoku University, Sendai, J
Gwyn P. Williams	Jefferson Laboratory, Newport News VA, USA

HASYLAB User Committee HUC	
Peter Müller-Buschbaum (Chair)	Technische Universität München, D
Thomas Möller	Technische Universität Berlin, D
Markus Perbrandt	Universität Hamburg, D
Christian Schroer	Technische Universität Dresden, D
Joachim Wollschläger	Universität Osnabrück, D

Committee Forschung mit Synchrotronstrahlung KFS representative of the German synchrotron radiation and FEL user community	
Wilfried Wurth (chair)	Universität Hamburg
Christian Schroer (vice chair)	Technische Universität Dresden
Andreas Schreyer	Helmholtz-Zentrum Geesthacht
Stefan Eisebitt	Technische Universität Berlin
Peter Müller-Buschbaum	Technische Universität München
Irmgard Sinning	Universität Heidelberg
Claus M. Schneider	Forschungszentrum Jülich
Eckart Rühl	Freie Universität Berlin
Rainer Fink	Universität Erlangen-Nürnberg
Jan-Dierk Grunwaldt	Karlsruhe Institute of Technology KIT
Lutz Kipp	Universität Kiel
Dietmar Manstein	Medizinische Hochschule Hannover

Photographs and Graphics:
CFEL
Collection Kröller-Müller Museum, Otterlo, The Netherlands
DESY
EMBL
European XFEL
HZG
Heiner Müller-Elsner, Hamburg
Manfred Schulze-Alex
Marco Urban, Berlin
Universität Hamburg

Figures of the Research Highlights were reproduced by permission from authors or journals.

Acknowledgement
We would like to thank all authors and all those who helped in the creation of this annual report.

Imprint

Publishing and Contact:
Deutsches Elektronen-Synchrotron DESY
A Research Centre of the Helmholtz Association

Hamburg location:
Notkestr. 85, 22607 Hamburg, Germany
Tel.: +49 40 8998-0, Fax: +49 40 8998-3282
desyinfo@desy.de

Zeuthen location:
Platanenallee 6, 15738 Zeuthen, Germany
Tel.: +49 33762 7-70, Fax: +49 33762 7-7413
desyinfo.zeuthen@desy.de

Photon Science at DESY
Tel.: +49 40 8998-2304, Fax: +49 40 8998-4475
photon-science@desy.de
photon-science.desy.de

www.desy.de

ISBN 978-3-935702-70-6

Online version:
photon-science.desy.de/annual_report

Realisation:
Lucia Incoccia-Hermes, Tim Laarmann, Ralf Röhlsberger

Editing:
Karen Appel, Rainer Gehrke, Christian Gutt, Lucia Incoccia-Hermes, Tim Laarmann, Wolfgang Morgenroth, Ralf Röhlsberger, Horst Schulte-Schrepping, Ulla Vainio, Martin von Zimmermann

Layout: Britta Liebaug, Heike Becker

Printing: Heigener Europrint, Hamburg

Copy deadline: December 2012

HELMHOLTZ
ASSOCIATION

Deutsches Elektronen-Synchrotron
A Research Centre of the Helmholtz Association

The Helmholtz Association is a community of 18 scientific-technical and biological-medical research centres. These centres have been commissioned with pursuing long-term research goals on behalf of the state and society. The Association strives to gain insights and knowledge so that it can help to preserve and improve the foundations of human life. It does this by identifying and working on the grand challenges faced by society, science and industry. Helmholtz Centres perform top-class research in strategic programmes in six core fields: Energy, Earth and Environment, Health, Key Technologies, Structure of Matter, Aeronautics, Space and Transport.

www.helmholtz.de